" AERODYNAMICS AND INTERACTION OF SINGLE AND MULTIPLE JETS WITH ROTATION "

A Thesis submitted to the
University of Sheffield
for the degree of
Doctor of Philosophy
by

Roger Ashton Allen, B.Sc. (TECH.)

Department of Fuel Technology
and Chemical Engineering
University of Sheffield

April 1970

SUMMARY

The work contained within the body of this thesis is concerned with the isothermal aerodynamic study of multiple jet systems with special reference to flame interactions. The type of jets used were jets with or without recirculation (swirl) and simple flame interactions were shown to occur for the configurations studied. The main purpose of the study was to show the nature and degree of the aerodynamic interference and to relate these to the factors which govern flame length, stability and combustion intensity.

The thesis also contains a study of the turbulence and mean flow characteristics of a swirling jet of variable swirl.

The instrument used to measure the mean velocity and turbulence quantities was the hot wire anemometer, and since for the case of a strongly swirling jet each component of the mean velocity and the normal and shear stresses are significant, a technique was evolved capable of separating out each of the 9 individual terms associated with the above, namely $\bar{u}$, $\bar{v}$, $\bar{w}$, $\overline{u'v'}$, $\overline{u'w'}$, $\overline{v'w'}$, $\overline{u'^2}$, $\overline{v'^2}$, $\overline{w'^2}$. The method of analysis is based upon a new

velocity voltage relationship which is accurate for all types of probe and/or flow velocity range. Previous methods of analysis were restricted to low turbulence levels where typically the local turbulence intensity $(\overline{u'^2})^{\frac{1}{2}}/\overline{u}$ is not more than 20%. The new method is shown to be valid until the onset of flow reversal which depends upon the type of waveform that the fluctuations in velocity take. The magnitude of the measured quantities are shown to be independent of the type of waveform and assuming that the fluctuations closely resemble a triangular waveform the maximum turbulence levels measurable are 57%.

ACKNOWLEDGEMENTS

The Author wishes to thank Professor J.M. Beér who helped to initiate the research jointly with the Admiralty, and particularly Dr.N. Chigier under whose guidance the research was carried out.

Thanks are also due to the Admiralty for their helpful suggestions and financial support to the research programme.

The Author would also like to thank all the other members of staff and technical assistants in the Department who helped in any way, and to my wife for typing the thesis.

TABLE OF CONTENTS

LIST OF FIGURES

5.2 Comparative Axial $(I)_{max}$, $(\tilde{u}'/\bar{u}_o)_{max}$ $(\tilde{w}'/\bar{u}_o)_{max}$ $(\tilde{v}'/\bar{u}_o)_{max}$ values for a single swirling free jet of varialbe swirl

5.3 Axial 100 $(\frac{\overline{u'v'}}{\bar{u}^2})_{max}$, $\frac{Me}{M_o}$, $(r/D)_{\bar{u}_{max}}$, $\frac{\bar{w}_{max}}{\bar{u}_o}$ values for a Single Swirling Free Jet of variable Swirl

5.4 Radial fluctuating Velocity terms for a Strongly Swirling Jet (Normal Stress Terms)

5.5 Radial Shear Stress Terms for a Strongly Swirling Jet

5.6 Radial I distribution for a Single Free Swirling Jet

5.7 Relation between $\frac{-R}{\bar{u}_o} \cdot \frac{(d\bar{u})}{(dr)}$ and 100 $\frac{\overline{u'v'}}{\bar{u}_o^2}$ Distribution for a Non-Swirling and Strongly Swirling Jet

5.8 Radial variation of measured effective viscosity terms for a strongly swirling jet 4 diameters downstream

5.9 Radial $\overline{u'v'}/\bar{u}^2_{max}$, $\bar{u}/\bar{u}_{max}$, I_{loc} distribution for 3 Non-Swirling Jets 1.25 diameters apart (P=1.25)

5.10 Radial $\overline{u'v'}/\overline{u}^2_{max}$, $\overline{u}/\overline{u}_{max}$, I_{loc} distributions for 3 Non-Swirling Jets 2.0 diameters apart (P=2.0)

5.11 Deflection of outer jet axis for 3 Non-Swirling Jets 1.25 and 2.0 diameters apart.

5.12 Axial $\frac{\overline{u}_{max}}{\overline{u}_o}$ and $\tilde{u}'/\overline{u}_{max}$ for 3 Non-Swirling Jets (Values on centre line of central jet)

5.13 Typical ε/ν and l/D distribution for 3 Non-Swirling jets 1.25 diameters apart

5.14 Comparative $(\overline{u}_{max})$ $\left(\frac{\overline{u}_{max}}{\overline{u}_o}\right)$ cen. & edge, reg.

$\left((I)_{max}\right)$ cen. & edge, reg. vs Pitch (P) values for multiple non-swirling jets

5.15 $\left(\frac{100\ (\overline{u'v'})}{\overline{u}_o^2}\right)_{max}$ values (for the mixing region between jets) for multiple non-swirling jets.

5.16 Typical $\overline{u}/\overline{u}_o$, $\overline{w}/\overline{w}_o$, I_{loc} and I distributions for 3 swirling jets

5.17 Comparative $\left(\frac{\overline{u}_{max}}{\overline{u}_o}\right)$ cen. & edge reg. values vs Pitch (P) for multiple swirling jets 'in mesh' and 'out of mesh'

A.6.1 Spatial $\bar{u}/\bar{u}_o$ and I distribution for a single non-swirling jet

A.6.2 Spatial 100 $\overline{u'v'}/\bar{u}_o^2$ distribution for a single non-swirling jet

A.6.3 Spatial $\bar{u}/\bar{u}_o$ distribution for 3 non-swirling jets 1.25 and 2.0 diameters apart

A.6.4 Spatial I distribution for 3 non-swirling jets 1.25 and 2.0 diameters apart

A.6.5 Spatial 100 $\overline{u'v'}/\bar{u}_o^2$ distribution for 3 non-swirling jets

A.6.6 Spatial $\bar{u}/\bar{u}_o$ and I distribution for a single swirling jet

A.6.7 Spatial 100 $\overline{u'v'}/\bar{u}_o^2$ and $\bar{w}/\bar{u}_o$ distribution for a single swirling jet

A.6.8 Spatial $\bar{u}/\bar{u}_o$ distribution for 3 swirling jets 'out of mesh'

A.6.9 Spatial $\bar{u}/\bar{u}_o$ distribution for 3 swirling jets 'in mesh'

A.6.10 Spatial I distribution for 3 swirling jets 'out of mesh'

A.6.11 Spatial I distribution for 3 swirling jets 'in mesh'

LIST OF PLATES

PLATE No.	TITLE
P1.1	Typical Marine Type Boiler
~~P3.1~~	~~General View Of Apparatus~~
P5.1	3 Non-Swirling Jet Flames In A Stable Condition
P5.2	3 Non-Swirling Jet Flames Showing Blow-Off of Central Flame
P5.3	3 Swirling Jet Flames In A Stable Condition
P5.4	3 Swirling Jet Flames Showing Blow-Off Of Central Flame

NOMENCLATURE

a	Distance to apparent point origin of jet in diameters; Heat transfer coefficient
A,B,C	Wire calibration constants
A',B'	constants in equation (A1.3)
A",B"	Constants in equation (A1.4)
c_p	Specific heat of gas at constant pressure
D	Jet nozzle diameter
d	Wire diameter
E	Instantaneous voltage from anemometer; $\bar{E}$ Time mean average (D.C.) voltage; E' instantaneous fluctuating voltage from anemometer; $(\overline{E'^2})^{\frac{1}{2}} = \tilde{E}'$ r.m.s. fluctuating voltage; $\bar{E}_o$ zero flow voltage; E_w wire voltage; E_+ wire voltage defined in equation (A1.5)
e	Conversion constant (4.2 joules/calorie)
g	Acceleration due to gravity
G	$(=\bar{w}_{mo}/\bar{u}_{mo})$ ratio of tangential/axial velocity maximum at nozzle exit
G_x	Axial flux of linear momentum
G_ϕ	Axial flux of angular momentum
I	Relative turbulence intensity $= \left(\frac{\overline{u'^2} + \overline{v'^2} + \overline{w'^2}}{\bar{u}_o^2}\right)^{\frac{1}{2}}$
$I_{loc.}$	Local turbulence intensity $= \frac{(\overline{u'^2} + \overline{v'^2} + \overline{w'^2})^{\frac{1}{2}}}{(\bar{u}^2 + \bar{v}^2 + \bar{w}^2)^{\frac{1}{2}}}$

NOMENCLATURE - continued

I_w	Wire current
K	Factor to allow for cooling component along the wire(defined by equation A1.7) K_1 for wire (a) K_2 for wire (b), K_3 for wire (c)
	K_o total pressure coefficient (P_1-P_t/P_t-P_s)
	K_g heat conductivity of gas at temp θ_g
l	Prandtl mixing length defined by equation (2.7)
M,N	Constants in equation (A1.5); M_o original nozzle mass flowrate; M_T total mass flowrate at axial station considered; $M_e(=M_T-M_o)$ entrained mass flowrate
Nu	Nusselt No. $(=a.d/K_g)$
P	Pitch of jets (=distance between jet centres/D); P_s static pressure; P_t total pressure; $P_{1\rightarrow5}$ pressure tappings on 5-hole pitot probe; P_o atmospheric pressure
Pr	Prandtl No. $(=c_p\mu_g/K_g)$
R	Jet radius; R_w wire resistance
Re	Reynolds No. $(=\rho_g.\bar{U}.d/\mu_g)$
r	Radial distance from central jet axis
S	Swirl No. defined by equation (2.12)
t	Time
U	Total instantaneous velocity; $\bar{U}$ time mean average total velocity; U' total instantaneous fluctuating velocity; U_n total cooling velocity resolved normal to the wire; $(\overline{U'^2})^{\frac{1}{2}}=\tilde{U}'$ r.m.s. fluctuating total velocity

NOMENCLATURE - continued

u,v,w	Component velocity terms in the x,y,z axes respectively (u',ũ',ū etc.as with U terms above)
$\overline{u'v'}$	
$\overline{u'w'}$	Shear stress components
$\overline{v'w'}$	
$\tilde{u}',\tilde{v}',\tilde{w}'$	Normal stress components
V	Total velocity vector (used for pitot data)
x,y,z	The 3 mutually perpendicular axes (Cartesian co-ordinate system)
y,r,θ	Polar co-ordinates

GREEK SYMBOLS

ϕ	Angle defined by equation (A1.5); $\phi_{0.5}$ jet half angle
β	Pitch angle defined by Fig. (3.5)
θ	Yaw angle defined by Fig. (3.5); radial angle for polar co-ordinates; θ_g gas temperature θ_w wire temperature; θ_f film temperature $(=\frac{\theta_w+\theta_g}{2})$
ρ	Air density; ρ_a ambient fluid density; ρ_o original jet fluid density; ρ_g gas density at temperature θ_g

NOMENCLATURE - continued

GREEK SYMBOLS - continued

ε Boussinesq eddy viscosity defined by equation (2.6)

μ Viscosity of air; μ_{eff} effective viscosity defined by equations of type (2.21); μ_g absolute gas viscosity at temperature θ_g; μ_{lam} laminar viscosity at S.T.P.

τ Stress tensor; $\tau_{rr}, \tau_{\theta\theta}, \tau_{xx}, \tau_{r\theta}, \tau_{x\theta}, \tau_{rx}$ components of the stress tensor defined by equations (2.21)

ψ Stream function defined by equation (2.1)

ψ_T total value at particular axial station;

ψ_o value of ψ_T at nozzle exit

ν Kinematic viscosity

SUBSCRIPTS

$( )_{max}$ Maximum value at axial station considered

$( )_{loc}$ Local value (ie. non-dimensionalised w.r.t. local total velocity)

$( )_{\substack{cen \\ reg}}$ Values within the region between the central jet axis and the outer jet centre line, (ie. in the mixing and central regions)

$( )_{edge}$ Values outside of the outer jet centre line, (ie. in the outer region of a jet system)

CHAPTER 1

Summary Of Contents

Multiple adjacent fluid streams encountered in engineering practice are discussed in general, together with the particular application of multiple burner systems. Some of the phenomena experienced in practical systems, and reported as being considered due to the interaction effects of adjacent flames, are noted.

The objectives of the study are outlined showing the particular relevance to Marine Boiler practice together with the overall objectives more relevant to interaction of multiple jets in general.

CHAPTER 1

1.1 Statement Of The Problem And Objectives Of The Study

1.1 Statement Of The Problem

1.1.1 The Overall Picture

In many engineering practices conditions are experiencedwhere more than one individual fluid stream is used to achieve heat or mass transfer from one fluid to another fluid or solid surface. The individual streams may be formed by flow of the fluid over grids, tube banks, holes in a plate, or individual jets, depending upon the particular application. In general it is required to have high mixing rates of the individual streams whilst maintaining a uniform or stable condition which is under control for any variation in flow rates or number of individual fluid streams that may be required. In order to achieve the high rates of mixing and to be able to control and predict the results of the system, we need to know how adjacent fluid streams interact and to relate these to upstream fluid conditions, number and nozzle spacing characteristics, dimensions of the system or any relevant variable.

1.1.2. The Particular Application

A particular application of the above problem is

combustion with multiple burners in marine type boilers. The particular requirements of a marine boiler are a very high heat output for a small volume, which generally means a cubic type of combustion chamber with many burners positioned closely together on one wall firing directly into the chamber. A typical marine type boiler, showing the configuration of the burners is shown in plate (P1.1). Some of the methods used in firing of marine boilers are detailed in (Ref.1).

The Admiralty, who initially proposed the research topic (Ref.2 and 3), use air registers with swirlers which impart a rotational motion to the fluid, producing radial and axial pressure gradients within each jet. The resultant jet has a recirculation zone downstream of the swirler which gives stability to the flame by recirculation of hot combustion products, and relatively low velocities which prevent blow-off.

It has been reported (Ref.3) that when two identical burners are used close together the resultant visible flame length can be shorter than when only one burner is used. So it was found that doubling the heat input in the boiler by lighting another burner led to a decrease in the observed flame length. This mechanism is not fully understood.

On a purely aerodynamic basis one may at first assume that the resultant combined jet length would increase with the addition of another burner, the increase being a result of reduced entrainment of the surrounding air.

The close proximity of the burners in marine boilers causes interaction effects, the magnitude of which can be considerable, as indicated in the literature survey.

Some of these effects are mentioned in Ref.2 , and the important effects may take any of the following forms :-

(a) Low frequency oscillations within the combustion chamber which could be detrimental to the equipment.

(b) Flame switching, where the overall flame configuration may switch at random from one condition to another.

(c) Preferential crowding of the flames to one wall of the combustion chamber.

(d) Blow-off of one or more of the flames.

(e) Flame lengthening or shortening, giving bad heat distribution within the furnace.

(f) Poor mixing resulting in improper combustion.

1.2 Objectives Of The Study

It was considered that the aerodynamic interaction of the jets must play a major role in the overall interference

of multiple jet flames. It was decided to examine the principle factors which affect the interference of multiple jets under isothermal non-burning conditions and subsequently relate the results to multiple jet flames.

1.2.1 The Particular Objective

For the case of marine boilers where enclosed swirling jet flames are used, it was decided to study the turbulence characteristics of enclosed multiple swirling air jets having a strong swirl. From the results, the aerodynamic factors governing the choice of jet configurations which give jet stability, good mixing, and short flame lengths, were to be determined. The choice of the research is detailed in Chapter 2.

1.2.2. The Overall Objective

In order to be able to establish the extent of jet interference it was considered advantageous to study the turbulence characteristics of a single swirling jet of variable swirl. Since swirling jets are a particular case relevant to flame studies, and since many applications do not include the individual rotation of the fluid streams, a similar investigation of non-swirling multiple jets was also carried out.

REFERENCES - CHAPTER 1

(1) Hardcastle J.W.
"Downwards and Sideways Firing In A Naval Boiler"
Proc. Symposium On Combustion In Marine Boilers
Inst. Of Fuel (Jan. 1968).

(2) Mc.Nair E.G.
"Problems Of Multiple Burners"
D.G.S. (Admiralty) 1967.

(3) Hardcastle J.W.
"Combustion And Multiple Burners"
A.M.E.E. Report (1967).

CHAPTER 2

Summary Of Contents

The definitions of the terms used to express the mean flow, turbulence characteristics, regions and properties of swirling and non-swirling jets are detailed.

The equations of motion governing isothermal turbulent flow are quoted, noting their relevance to prediction procedures being developed for recirculating flow systems.

A short review of the relevant work quoted in the literature, and the justification of the choice of research is included.

The capabilities and choice of the measuring instruments is discussed and the chapter is concluded with an outline of the research programme.

CHAPTER 2

PRESENT STATE OF KNOWLEDGE, JUSTIFICATION OF CHOICE OF RESEARCH AND OUTLINE OF THE RESEARCH PROGRAMME.

2.1 Definition Of Terms Used

2.1.1 Regions And Properties Of A Non-Swirling Jet

Fig.(2.1) shows velocity profiles at 3 axial stations downstream of the nozzle exit for a non-swirling jet and subsequent interpretations of the regions associated. The fluid emerges from the nozzle and starts to mix with the surrounding fluid, a mixing region is formed which spreads outwards from the nozzle and towards the centre line of the jet forming the mixing region. Within this mixing region is the potential core of unmixed fluid which still has the properties of the upstream fluid of high velocity and low turbulence intensity. High shear and turbulence intensities are associated with the mixing region of the jet. The transition region extends from the end of the potential core to the beginning of the fully developed region. In the fully developed region the rate of spread of the jet becomes constant and the velocity profiles have a similar form. Dimensionless velocity distribution are independent of axial distance and a typical turbulence

intensity distribution is shown in Fig.(A.4.2) (Appendix 4). The flow patterns in the jet are dependant upon the total jet momentum and the distance from the apparent origin, which is the apparent source of the jet defined as the position from which the jet with finite momentum and infinite velocity may be considered to emanate. The apparent origin position may be determined by extrapolation of the spread of the jet in the fully developed region back into the nozzle.

The theory of turbulent jets is fully described in (Refs. 1 to 6).

2.1.2 Terminology Used To Describe Non-Swirling Jets

We assume that we can split any flow field into its 3 component average velocities $\bar{u},\bar{v},\bar{w}$, and instantaneous fluctuating velocities u',v',w', in the x,y,z, directions respectively such that $u = \bar{u}+u'$, $v = \bar{v} + v'$, $w = \bar{w} + w'$, hence $\overline{u^2} = \bar{u}^2 + \overline{u'^2}$; $\overline{v^2} = \bar{v}^2 + \overline{v'^2}$; $\overline{w^2} = \bar{w}^2 + \overline{w'^2}$, where bar ($^-$) terms denote time mean average terms.

In order to non-dimensionalise all the results plotted, the following terms are used :-

$\bar{u}$ - average axial velocity at point considered.

$\bar{u}_{max}$ - maximum axial velocity at the radial cross section downstream of the nozzle considered

$\bar{u}_o$ - maximum nozzle outlet velocity for non-swirling jet, (also used for swirling jets having the same total initial mass flowrate.

R - nozzle radius.

D - nozzle diameter.

The turbulence intensity quantities I, I_{loc} are defined as :-

I - relative turbulence intensity

$$= \frac{(\overline{u'^2} + \overline{v'^2} + \overline{w'^2})^{\frac{1}{2}}}{\bar{u}_o} \simeq \frac{(\overline{u'^2})^{\frac{1}{2}}}{\bar{u}_o}$$ For non-swirling jets

I_{loc} - local turbulence intensity

$$= \frac{(\overline{u'^2} + \overline{v'^2} + \overline{w'^2})^{\frac{1}{2}}}{(\bar{u}^2 + \bar{v}^2 + \bar{w}^2)^{\frac{1}{2}}} \simeq \frac{(\overline{u'^2})^{\frac{1}{2}}}{\bar{u}}$$ For non-swirling jets

Typical quantities plotted are :

$\bar{u}/_{u_{max}}$, $\bar{u}/_{u_o}$, $\bar{u}_{max}/_{u_o}$, I, I_{loc}, $\overline{u'v'}/_{u_{max}}$

$\overline{u'v'}/_{u_o}$, ψ/ψ_o, $R/_{u_o}$, $\frac{(d\bar{u})}{(dr)}$,

For a non-swirling jet the predominent quantities are $\bar{u}$, $\overline{u'^2}$, $\overline{u'v'}$ terms, but the above I, I_{loc} terms are plotted in order to compare them with those values obtained for swirling jets.

Streamlines are representatative of the average direction of particles within the jet. The stream function ψ may be defined as:-

$$\psi = \int \bar{u} . r . dr \quad ; \quad \psi_T = \int_0^\infty \bar{u} . r . dr . \qquad (2.1)$$

Where ψ_T = total stream function value.

The results are non-dimensionalised, by dividing by ψ_o, where ψ_o is the value of ψ_T evaluated at the nozzle exit, and plotted as ψ/ψ_o. The flow between any two stream lines is by definition constant and the $\psi/\psi_o = 1$ boundary contains within it the original axial mass flowrate from the nozzle.

Since the total axial mass flowrate at any cross section downstream of the nozzle exit may be defined as :

$$M_T = \int_0^\infty \rho . 2\pi . \bar{u} . r dr = 2\pi\rho\psi_T \qquad (2.2)$$

and also the original mass flowrate from the nozzle may be defined as :-

$$M_o = \int_o^r \rho . 2\pi . \bar{u}\, r dr = 2\pi\rho . \psi_o \qquad (2.3)$$

Hence relative total axial mass flowrate

$$M_T/M_o = \psi_T/\psi_o \qquad (2.4)$$

Also the amount of mass entrained downstream of the nozzle Me $= M_T - M_o$ and the relative mass entrained :

$$= \frac{M_T - M_o}{M_o} = \frac{\psi_T - \psi_o}{\psi_o} = \psi_T/\psi_o - 1 \qquad (2.5)$$

From $\overline{u'v'}$ and $d\bar{u}/dr$ values the effective Boussinesq eddy viscosity $\mathcal{E}$ and Prandtl mixing length l may be determined using the following equations :-

$$\mathcal{E} = - \overline{u'v'}/(d\bar{u}/dr) \qquad (2.6)$$

$$l^2 = - |\overline{u'v'}|^{\frac{1}{2}}/|d\bar{u}/dr| . (d\bar{u}/dr) \qquad (2.7)$$

Local kinetic energy of turbulence $(K\ E)_{loc}$ and relative kinetic energy of turbulence (KE) may be

defined as :-

$$(KE)_{loc\bar{c}} \qquad \frac{\overline{u'^2} + \overline{v'^2} + \overline{w'^2}}{\bar{u}^2 + \bar{v}^2 + \bar{w}^2} = I_{loc}^2$$

Which is the energy per unit volume contained by the fluctuating velocity divided by the energy contained by the mean velocity

$$(KE) = \frac{\overline{u'^2} + \overline{v'^2} + \overline{w'^2}}{\bar{u}_o^2} = I^2$$

which is that divided by the mean initial nozzle velocity.

Mean static pressure $\bar{p}$ within the jet is determined from the Reynolds equations of motion in the transverse direction, after applying the boundary layer assumptions and integration, from which :-

$$\bar{p} = \bar{p}_o - \rho \overline{v'^2} \quad \text{where } \bar{p}_o \text{ is the ambient pressure} \qquad (2.8)$$

and v' is the fluctuating component of velocity in the transverse direction.

Velocity ($\bar{u}_{max}$) on the axis of the jet may be related by the empirical equation :-

$$\frac{\bar{u}_{max}}{\bar{u}_o} = 6.8 \left(\frac{\rho_o}{\rho_a}\right)^{\frac{1}{2}} \cdot \frac{D}{x} \qquad (2.9)$$

Where x is the distance downstream of the nozzle, ρ_o is the nozzle fluid density and ρ_a that of the ambient fluid.

Transverse profiles may be represented empirically by:-

$$\frac{\bar{u}}{\bar{u}_{max}} = \exp\left(-92\left(\frac{r}{x+a}\right)^2\right) \qquad (2.10)$$

The entrainment rate $\left(\frac{M_e}{M_o}\right)$ is represented empirically by:-

$$\frac{M_T - M_o}{M_o} = 0.32\left(\rho_a/\rho_o\right)^{\frac{1}{2}} \frac{x}{D} = \frac{M_e}{M_o} \qquad (2.11)$$

2.1.3 Regions And Properties Of A Swirling Jet

Fig.(2.2) shows the axial velocity and tangential (swirl) velocity profiles for a strongly swirling jet. Very strong swirl is usually associated with a recirculation zone, on the axis of the jet and close to the nozzle exit.

The swirl is produced upstream in the nozzle by tangential introduction of the fluid into the swirl chamber, the resultant jet issuing from the nozzle exit has axial, radial and tangential velocity components. Due to the swirl velocity, radial and axial pressure gradients are set up and in the case of the strongly swirling jet are large enough to produce reversed flow along the axis of the jet. The reduced axial velocity on the axis continues until the start

of the similar velocity profile region, Refs.6.7.8.9.10 and 11 contain experimental and theoretical investigations of weakly to very strongly swirling jets.

In swirling jet flames the recirculation zone produces flame stability by the recirculation of hot combustion products and by acting as a direct heat supply. The velocities are sufficiently low in this region to prevent blow-off and the resultant jet flame is shorter, wider and more intense. Swirling flows may be of a free or forced vortex type according to the variation of the swirl velocity component with radial distance. In the forced vortex or solid body rotation flow region near to the jet axis the swirl velocity increases linearly with radial distance from the axis. In the free vortex flow region the swirl velocity decreases hyperbolically with radial distance.

2.1.4 Terminology Used To Describe Swirling Jets.

The degree of swirl may be characterised by the non-dimensional swirl number S (Ref.9).

$$S = G_{\phi} / G_x \cdot R \qquad (2.12)$$

Where G_{ϕ} and G_x are the axial flux of linear and angular momentum respectively. R is the jet radius.

The values G_ϕ and G_x for the case of a solid body rotation flow with a uniform distribution of the axial velocity at the orifice (when $\bar{w} = \bar{w}_{mo} \, (r/R)$ and $\bar{u} = \bar{u}_{mo}$) are determined as follows (Ref.9).

$$G_\phi = 2\pi\rho \int_o^R r^2 \, \bar{u}\bar{w} dr = \tfrac{1}{2} \pi \rho \, \bar{u}_{mo} \, \bar{w}_{mo} \, R^3 \qquad (2.13)$$

$$G_x = 2\pi\rho \int_o^R r \, (\bar{u}^2 - \tfrac{1}{2} \bar{w}^2) \, dr$$

$$= \pi \rho \, \bar{u}_{mo}^2 \, . \, R^2 \, (1 - G^2/4) \qquad (2.14)$$

where $G = \bar{w}_{mo} / \bar{u}_{mo}$

So $$S = G_\phi / G_x R = \frac{\frac{1}{2} G}{1 - G^2/4} \qquad (2.15)$$

Where subscripts m_o refer to maximum values at the orifice. Fig.(2.3) shows a plot of $\frac{1}{2}G / 1 - G^2/4$ and is considered valid up to G values of 0.4. For higher degrees of swirl the axial velocity distribution at the exit deviates from a uniform distribution and for these higher swirl values the plot of :-

$$S = \frac{\frac{1}{2} \cdot G}{1 - \frac{1}{2} \cdot G} \qquad (2.16)$$

fits the experimental data much better.

Axial velocity profiles in the similar velocity profile region may be characterised by the Gaussian error curve.

$$\bar{u}/\bar{u}_{max} = \exp(-k_u \xi^2) \quad \text{where } \xi = r/(x+a) \qquad (2.17)$$

The swirl velocity profiles, which display similarity for all degrees of swirl from about 2 diameters downstream, can be described by a third order polynomial:

$$\bar{w}/\bar{w}_{max} = C''\xi + D''\xi^2 + E''\xi^3 \qquad (2.18)$$

These empirical constants C'',D'',E'' are dependent upon the swirl number.

Axial velocity decays may be related by:

$$\frac{\bar{u}_{max}}{\bar{u}_{mo}} = K_1' \, D/(x+a) \, f_1^{\frac{1}{2}} \qquad (2.19)$$

and :-

$$\frac{\bar{w}_{max}}{\bar{w}_{mo}} = K_2' \left(D/(x+a) \right)^2 f_2^{-\frac{1}{2}} \qquad (2.20)$$

Where f_1 and f_2 are functions of the degree of swirl (Ref.9) and K_2 is a constant which varies with the swirl number.

The results of measurements performed on swirling

jets, are plotted in non-dimensional form similar to those described in section 2.1.2. for non-swirling jets, the terms $\overline{v'^2}$, $\overline{w'^2}$, $\bar{w}$, now being much greater and take a significant part in the I, I_{loc}, $\bar{w}/\bar{u}_o$ quantities.

The values of $\bar{u}_o$ and ρ_o are those evaluated for the case of a non-swirling jet having the same total mass flowrate (ie. volumetric flowrate) as the swirling jets.

2.1.5 Equations of Motion And Prediction Procedure For Isothermal Flow System

Equations which fully describe the flow of a viscous isothermal fluid in 3 dimensions may be derived (Refs.3,4,28) which contain velocity gradients, shear and normal stresses, effective viscosities, pressure and gravity terms. These equations may be used to predict flow situations knowing only the physical properties of the fluid and various assumptions about pressure, density and effective viscosity terms. Spalding et al (Ref.29) have initiated prediction procedures involving axially symmetrical systems including rotation and recirculation. The procedures become very complex and require a fast digital computer to evaluate the terms, which is performed by using a grid or mesh over the system similar to relaxation procedures, and

marching downstream from the fluid exit. Regions between the grid intersection points are interpolated and consequently the greater the number of points over a system the greater the accuracy. In order to check the results of the procedure, the predicted results are compared to known (measured) results on similar systems.

One of the main assumptions made in order to simplify the calculations is to assume that the viscosity remains constant throughout the system, however it is considered an over simplification, and effective viscosity terms obtained from measurements within a system show this to be so (see Fig.5.8)

Effective viscosities may be related to normal and shear stress terms, velocities and velocity gradients by the following equations in cylindrical co-ordinate systems. (Where θ is the angle, and for all symmetrical systems $\partial/\partial\theta = 0$, and using $\bar{v}$ and r for the radial direction $\bar{u}$ and x for the axial direction, and $\bar{w}$ and θ for the θ direction).

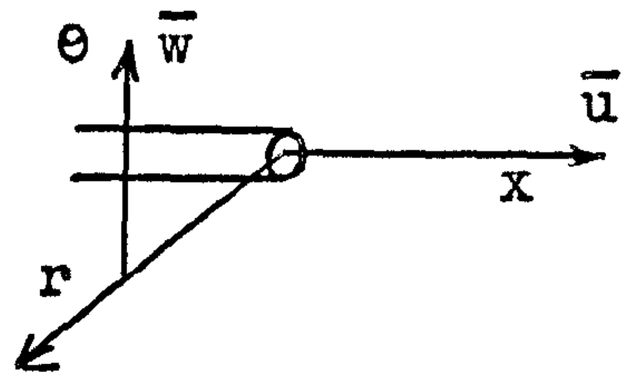

The components of the stress tensor in cylindrical co-ordinates:

$$\tau_{rr} = \rho\overline{v'^2} = -\mu_{eff(rr)}\left(2\frac{\partial\bar{v}}{\partial r} - \tfrac{2}{3}(\nabla\cdot V)\right)$$

$$\tau_{\theta\theta} = \rho\overline{w'^2} = -\mu_{eff(\theta\theta)}\left(2\left(\tfrac{1}{r}\frac{\partial\bar{w}}{\partial\theta} + \frac{\bar{v}}{r}\right) - \tfrac{2}{3}(\nabla\cdot V)\right)$$

$$\tau_{xx} = \rho\overline{u'^2} = -\mu_{eff(xx)}\left(2\frac{\partial\bar{u}}{\partial x} - \tfrac{2}{3}(\nabla\cdot v)\right)$$

$$\tau_{r\theta} = \rho\overline{v'w'} = -\mu_{eff(r\theta)}\left(r\,\partial/\partial r\cdot(\bar{w}/r) + \tfrac{1}{r}\frac{\partial\bar{v}}{\partial\theta}\right)$$

$$\tau_{x\theta} = \rho\overline{u'w'} = -\mu_{eff(x\theta)}\left(\frac{\partial\bar{w}}{\partial x} + \tfrac{1}{r}\cdot\frac{\partial\bar{u}}{\partial\theta}\right)$$

$$\tau_{rx} = \rho\overline{u'v'} = -\mu_{eff(rx)}\left(\frac{\partial\bar{u}}{\partial r} + \frac{\partial\bar{v}}{\partial x}\right) \qquad (2.21)$$

Where :-

$$(\nabla\cdot V) = \tfrac{1}{r}\cdot\partial/\partial r\cdot(r\cdot\bar{v}) + \tfrac{1}{r}\frac{\partial\bar{w}}{\partial\theta} + \frac{\partial\bar{u}}{\partial x} = 0$$

for incompressible flow.

These above equations may be used in conjunction with the equation of motion, (of which one, the r component is quoted below), to solve all the unknown quantities,

given expressions for the radial and axial velocity distribution within the system :

Equation of motion - r component.

$$\rho\left(\frac{\partial \bar{v}}{\partial t} + \bar{v}.\frac{\partial \bar{v}}{\partial r} + \frac{\bar{w}}{\bar{r}}.\frac{\partial \bar{v}}{\partial \theta} - \frac{\bar{w}^2}{r} + \bar{u}.\frac{\partial \bar{v}}{\partial x}\right)$$

$$= -\frac{\partial P}{\partial r} - \left(\frac{1}{r}\cdot\frac{\partial}{\partial r}(r.\gamma_{(rr)}) + \frac{1}{r}\frac{\partial}{\partial \theta}(\gamma r\theta) - \frac{\gamma\theta\theta}{r} + \frac{\partial \gamma rx}{\partial x}\right) + \rho gr \qquad (2.22)$$

Clearly if the effective viscosities are not constant throughout the system, it would be helpful if some relation could be found between the effective viscosity, and radial and axial position within the system. With the method of analysis outlined in Chapter 4, it is possible to measure all the quantities in equations (2.21) to evaluate the effective viscosity terms, and some of the measured effective viscosity distributions are quoted in Chapter 5.

2.1.6 The Relative Order Of Magnitude Of Terms

In order to simplify calculations, various terms may be neglected with respect to other terms which are typically an order of magnitude greater. For systems without rotation or recirculation the $\bar{u} \gg \bar{v}$, $\bar{w}$ and terms including $\bar{v}$, $\bar{w}$ are neglected. It is also possible to neglect

pressure terms, and for radially symmetrical systems $\partial/\partial\theta$ terms are zero. Pressure (eg. $\frac{\partial p}{\partial r}$) terms for non-rotating systems are usually neglected.

For systems with recirculation or rotation or both, few terms are negligible, depending upon the degree of rotation and position in the flow field. In such systems it is often necessary to evaluate each of the terms in the equations of motion. For the particular case of a strongly swirling jet one has to be about 8 diameters downstream before the radial ($\bar{v}$) and tangential ($\bar{w}$) velocity gradients may be neglected with respect to the axial ($\bar{u}$) velocity gradients.

For any incompressible fluid ($\nabla\cdot V$) terms may be neglected, and for simplicity the ($\nabla\cdot V$) terms are often neglected for compressible flow systems, with a resulting small error.

2.1.7 Some Methods Of Flame Stabilisation

Lewis and Von Elbe (ref.30) describe the phenomena associated with flame stability and conditions which give rise to "blow off" or "flash back" with reference to a single jet flame. Some methods of flame stabilisation and their relevance to this investigation of multiple jets are summarised below.

For a single non-swirling jet flame the flame is stabilised on the edge of the jet by the fact that the local velocity normal to the flame front is low enough for the particular flame speed of the combustable mixture. At high flowrates the local velocity becomes too high and the jet "blows off", which means the flame is extinguished. Any wall, duct or adjacent jet which interferes with this region of low velocity (and high mixing rates due to high shear stress, velocity gradients and local turbulence intensities) will seriously affect the stability of the jet and such a jet may be made to blow off as a direct result of this local interference.

Stable jet flames tend to become less stable as the flowrate increases, so that for jet flame systems where high velocity, flowrate or variable flowrate is required some other form or method of stabilising the flame is required. A common method to stabilise jet flames is to introduce a

disc or wedge within the nozzle exit of the flame. The disc has a zone of recirculating fuel/air and hot combustion products immediately downstream ~~share~~ where low velocities, high mixing rates and temperatures occur giving a position where the flame may 'sit' and hence provide stability to the flame as a whole. This recirculation zone is continuously fed with a fresh supply of combustable material and similarly continuously releases hot combustion products into the flame.

Another method of producing a recirculation zone within the jet flame is by rotation of the jet fluid, which produces axial and radial pressure gradients giving a region of low velocity or reversed flow on the axis of the jet flame depending upon the degree of swirl or rotation given to the jet. The swirl may be produced by tangential supply of the fluid to the jet, or by positioning of a swirler disc with vanes which imparts a ~~rotational~~ swirling motion to the fluid after hitting the disc.

The choice between a disc stabiliser or a swirler type is governed by the particular requirements of the system Briefly a disc type stabiliser is cheaper to manufacture but dearer to maintain due to carbon deposits forming on the disc, whereas a swirler will require a greater amount of energy (fan power) but will burn fuel at a greater rate

It is shown (Chapter 5) that there is an advantage to have adjacent swirling jets 'out of mesh' where the direction of the swirl velocity of adjacent jets is opposite rather than 'in mesh' from a stability and mixing rate point of view and consequently it is reasonable to assume that there will be similar advantages to have multiple jets swirling 'out of mesh' rather than having disc type stabilisers.

2.2 Survey Of Relevant Work

The amount of information on multiple jets in the literature is strictly limited. There are a few references to axial velocity measurements on 2 or more non-swirling jets, and 2 on local turbulence intensity measurements. The Author is not aware of any velocity or turbulence measurements for multiple swirling jets. There are a few references for velocity and turbulence intensity measurements on single swirling jets.

2.2.1 Multiple Non-Swirling Air Jets

Laurence and Benninghof (Ref.13) studied turbulence and mean flow characteristics for a system of four slotted nozzles positioned in line and of variable pitch, and for a 3 sector nozzle. The measurements were performed using a hot wire anemometer and showed that the turbulent mixing, that occurs when a jet exhausts into stationary air, is aided by dividing the flow into multiple interfering jets. The scale and intensity of turbulence are less in the common mixing zone of two interfering jets than in the mixing zone of a single jet. The maximum turbulence intensities occured at the outer fringes of the jets.

Miller and Comings (Ref.14) investigated the force momentum fields in dual jet flows issuing from a plane wall. They found that in the region of jet convergence near the nozzles that the structure of the flow in the core of either jet is similar to that of a single free jet allowing for the static pressure differences. A sub-atmospheric pressure region is set up between the jets which they say accounts for the fact that the two jets tend to converge. After convergence the jets combined to form a single jet symmetrical about the centre line, the combined jet behaving similarly to that of a single free jet. A portion of the flow reverses in the sub-atmospheric region and two stable contra-rotating vortices together with a free stagnation point on the centre plane were detected.

Corrsin (Ref.15) investigated the behaviour of parallel two dimensional jets issuing from the slots in a grid made up of a row of parallel rods with a grid density (solid area/ total area) of 0.83. The system was unstable and consisted of grouping together of adjacent jets immediately after their exit from the slots, which resulted in wildly eddying flow. Adjacent groups then joined together and the phenomenon was non-stationary and switched from one configuration to another. The flow was stabilized

PAGE
MISSING
IN
ORIGINAL

Knystantas (Ref.19) studied the flow formed by the turbulent jets issuing from a series of holes in line with a pitch (distance between jet centres/jet diameter) of 1.5 and 3. He measured the mean velocity profiles at 11 axial stations from the nozzle exit to 28 diameters downstream and compared these to the theoretical profiles. He was particularly interested in the formation of a quasi-two dimensional jet and gives some theory on the prediction of the start of the two dimensional region downstream of the row of individual jets.

Koestel and Austin (Ref.20) investigated the flow pattern from two closely spaced parallel air jets and derived equations for the maximum jet velocities at any distance from the nozzles, by the principle of addition of momentum.

Whaley (Ref.22) made a study of the flow characteristics in a multiple burner system where he showed that the main characteristics of axial velocity decay and recirculation of enclosed multiple jets can be related to those of enclosed single jets. When the jets are close together the region near to the jet exit can be treated as enclosed single jets, whereas further downstream the jets combine, and the combined jet may be treated as a single jet from a source along the common axis. Introduction of a wire mesh grid downstream increased the recirculation upstream.

2.2.2 Multiple Non-Swirling Jet Flames

Wright (Ref.23) reported on multiple flameholder arrays with special reference to flame interactions. With several flame-holders arranged in a single plane each holder operates nearly as though it were a single flame-holder in a small duct. The blow-off speeds for multiple non-swirling jets is reported to be lower, and said to be due to the high blockage of the flame-holder in each duct. Wright also reports that pinching of alternate flames in a row of multiple jets is observed with many flame-holder arrays, particularly for closely spaced flame-holders in conditions approaching blow-off. The configuration could switch to a

more uniform condition where all flames are of equal size whilst still under the same average flow conditions.

Miss M^{c}Nair (Ref.24) has summarised some of the problems associated with multiple burners and suggests that there should be an optimum pitching which will give the best conditions for rapid and complete combustion. It is stated that little is known about the desirable air distribution to individual burners when multiple burners are used and the possibilities of flow instabilities are mentioned due to the fact that each jet is trying to entrain its neighbour.

2.2.3 Swirling Jet Flames

Hardcastle (Ref.26) has reported various heat transfer characteristics within a marine type boiler and the effect upon these of the number of flames employed and total heat energy into the furnace. The swirling burners used gave rotation to each flame in the same sense, that is to say all the flames had the same direction of rotation. The terminology used in this thesis is that the jets were swirling "out of mesh". For alternate jets having different directions of rotation the system is defined as swirling "in mesh".

Miss McNair (Ref.24) suggests that there may be a substantial difference between the two types of meshing, and the above two reports form the basis upon which the investigation of multiple enclosed swirling jets was initiated.

Chigier and Chervinsky (Ref.33) performed an aerodynamic study of turbulent burning free jets with swirl. Velocity and temperature measurements were performed in premixed butane-air jets of variable swirl number. The decay of axial and tangential velocities was shown to be reduced in the flame as compared with cold swirling jets.

A theoretical analysis was put forward where the turbulent equations of motion, energy and state were integrated to obtain expressions for the decay along the axis of the maximum values of axial velocity, swirl velocity, and temperature. The radial distributions of velocity and temperature were described by Gaussain error curves.

2.3 Justification Of Choice Of Research

It is considered that aerodynamics play a major part in the overall interaction effects of multiple jet flames. The way in which the turbulent mixing of multiple fluid streams affect the stability, length and combustion intensity of the resultant overall flame has not to the Author's knowledge been reported in literature. With the above factors in mind an investigation was initiated in order to examine the extent of the aerodynamic interaction of multiple jet systems which would reproduce typical burner configurations, flow characteristics and combustion chamber dimensions. The regions which were considered of major interest were those between adjacent jets (mixing region and central region) and those on the outer edge of the jet system (outer region and edge - see Fig.2.4) particularly close to the nozzle exit.

Clearly the number of variables which may be encountered was prohibitive, and the main variables were restricted to number of jets, pitch of the jets, non-swirling jets and jets swirling "in mesh" and "out of mesh" with one strong degree of swirl.
(The particular requirements of the Admiralty are detailed in (Ref.25)).

In addition to multiple jet studies it was considered useful to find out whether effective viscosity terms are affected by the position within a flow field, with a view to aiding the prediction proceedure outlined in section 2.1.3. Turbulence and mean flow characteristics of a single free swirling jet of variable swirl number were studied to provide information not published in the literature.

In order to obtain as much information as possible about the turbulent mixing in a system it was considered desirable to have measurements of mean velocity, r.m.s. fluctuating velocity, and shear stress at each position, which meant developing a new method of analysis capable of separating out each of the 9 individual terms associated with the above. This was achieved and the results quoted were dependent upon the success of this method.

In order to understand how flames may interact, simple multiple flame studies were conducted where visible flame interactions occurred, and it was considered that these observations would aid the eventual interpretation of the results.

2.4 Capabilities And Choice Of Measuring Equipment

The 5 hole pitot probe is an instrument capable of measuring the magnitude and direction of the total average velocity vector, and static pressure within flow fields.

When used correctly the hot wire anemometer may measure average velocity, fluctuating velocity and shear stress within a flow field. The analysis of the signals obtained from a hot wire anemometer have been restricted for sometime to low turbulence intensities and flow-fields where there is a predominent flow direction, and where some of the component average and fluctuating velocities can be neglected with respect to the predominent ones. These assumptions greatly simplify the measuring techniques and analysis, and a typical example is measurement in the boundary layers formed by flow over flat surfaces.

For any system such as a strongly swirling jet we have conditions where all the average and fluctuating velocity terms may be of the same order of magnitude and the turbulence intensity typically as high as 60 per cent. Clearly no terms may be neglected with respect to others, and since no comprehensive analysis was known, or available to the Author, which was capable of separating out all the

individual average velocity, normal and shear stress terms, it was found necessary to develop a new technique to allow the research to be done.

The development of this new analysis is detailed in Chapter 4 and Appendix 1, and comparison of the results obtained to those quoted in the literature for a single non-swirling free jet are shown in Appendix 4.

The hot wire anemometer was chosen as the prime measuring instrument for this work and the 5 hole pitot probe was used for checking the accuracy of the velocity measurements obtained with the hot wire anemometer. Comparison of hot wire and pitot readings on a single swirling jet are included in Appendix 4.

2.5 Outline Of The Research Programme

The research programme may be split up into four main catagories concerned with the investigation of the turbulence characteristics of :-

(a) A single free swirling jet of variable swirl number (S) from zero to 0.6.

(b) Single and triple non-swirling enclosed jets of pitch 1.25 and 2.0 diameters.

(c) Single and triple swirling enclosed jets "in mesh" of swirl number 0.6 and pitch of 1.25 and 2.0 diameters.

(d) Single and triple swirling enclosed jets "out of mesh" of swirl number 0.6 and pitch of 1.25 and 2.0 diameters.

In addition to the above, flame interactions of double and triple, swirling and non-swirling flames were observed, and overall flow patterns within the system using a water modelling technique.

Calculations were made of effective viscosity distributions.

REFERENCES - CHAPTER 2

(1) Abramovich G.N.
"The Theory Of Turbulent Jets"
Mass. Inst. Of Tech. Press (1963)

(2) Prandtl L.
"Essentials Of Fluid Dynamics"
Blackie and Son, London 1954

(3) Hinze J.O.
"Turbulence"
McGraw Hill Book Co.

(4) Schlicting H
"Boundary Layer Theory"
McGraw Hill, New York 1965

(5) Ricou F.P. and Spalding D.B.
"Measurements Of Entrainment By Axisymmetrical Turbulent Jets"
Jnl.Fl.Mech. Vol.2 pt.1 (1961)

(6) Laurence J.C.
"Intensity Scale And Spectra Of Turbulence In Mixing Region Of Free Subsonic Jet"
N.A.C.A. T.N. 3561

REFERENCES - CHAPTER 2 Cont.

(7) Shao-Lin Lee
"Axisymmetrical Turbulent Swirling Jet"
Jnl.Appl.Mech, Trans A.S.M.E. (June 1965)

(8) Craya A and Darrigol M.
"Turbulent Swirling Jet"
Physics Of Fluids Supplement (1967)
Vol.10 pt.9.

(9) Chigier N.A. and Chervinsky A.
"Experimental Investigation Of Swirling Vortex Motion In Jets".
Jnl.Appl.Mech. (June 1967) Trans.A.S.M.E.

(10) Johansen O.H.
"Investigation Of The Flow-Pattern In An Oil Burner With Varying Degree Of Swirl On The Combustion Air"
Ph.D. Thesis Heat Eng.Lab. Mech.Dept. N.T.H. Trondheim (July 1967).

(11) Allen R.A.
"Interaction Of Multiple Jets"
Combustion Aerodynamics Report No.16
Dept.Of Fuel Tech. University Of Sheffield (Dec.196

REFERENCES - CHAPTER 2 Cont.

(12) Rose W.G.
"A Swirling Round Turbulent Jet"
Jnl.Appl.Mech. (Dec.1962)
Trans. A.S.M.E.

(13) Laurence J.C. and Benninghof J.M.
"Turbulence Measurements In Multiple Interfering Air Jets".
N.A.C.A. T.N. 4029 (1957).

(14) Miller D.R. and Coming E.W.
"Force And Momemtum Fields In Dual Jet Flows"
Jnl.Fluid Mech. V.7 pt.2 (Feb 1969).

(15) Corrsin S.
"Investigation Of The Behaviour Of Parallel Two Dimensional Air Jets".
N.A.C.A. W.R. 4H24 (1944)

(16) Von Bohl J.G.
"Das Verhalten Paraller Luftstrahlen"
Ing. Archiv. Bd.2 Heft 4 (1940)

REFERENCES - CHAPTER 2 Cont.

(17) Jung Von R.
"
"Grandzuge der Von Parallel Schlitzbrennern Ausgehenden Rauchgasstromung und Feuerranmen" Mitt der Vereinigung der Grosshesselbesitzer Heft 90 (June 1964)

(18) Brusdeylins Von G. and Tillmann W.
"Experimentelle Untersucking des Verhaltens Von Benachbarten, Teils Feststoffbeladenen Luftfreistrahlen".
Mitt der Vereinigung der Grosshesselbesitzer Heft 81 (Dec.1962)

(19) Knystautas R.
"The Turbulent Jet From A Series Of Holes In Line"
The Aeronautical Quarterly Vol.XV (Feb 1964)

(20) Koestel A and Austin J.B.
"Air Velocities In Two Parallel Ventilating Jets"
Heating Piping And Air Conditioning (Feb 1956)

REFERENCES - CHAPTER 2 Cont.

(22) Whaley H.
"A Fundamental Study Of Flow Characteristics And Heat Transfer In Multiple Burner Oil Fired Marine Boilers"
Ph.D Thesis - Sheffield University (June 1965)

(23) Wright F.H.
"Multiple Flameholder Arrays And Flame Interactions"
Jnl.Amer.Rocket Soc., 29 (1959)

(24) McNair E.G.
"Problems Of Multiple Burners"
D.G.S. (Admiralty) 1967.

(25) Allen R.A.
"Interaction Of Multiple Jets"
Combustion Aerodynamics Report No.13
Dept.Of Fuel Tech.Univ.Of Sheffield (Dec.1967)

(26) Hardcastle J.W.
"Combustion And Multiple Burners"
A.M.E.E. report 1967

(27) Allen R.A.
Combustion Aerodynamics Report No.14 (June 1968)

REFERENCES - CHAPTER 2 Cont.

(28) Bird R.B. Stewart W.E. Lightfoot E.N.
"Transport Phenomena"
J. Wiley and Son (1962)

(29) Spalding D.B. et.al.
"Heat And Mass Transfer In Recirculating Flows"
Dept. of Mech. Eng., Imperial College, London
(Dec. 1968).

(30) LEWIS B. VON ELBE G.
"COMBUSTION FLAMES & EXPLOSION OF GASES"
ACC. PRESS 1961

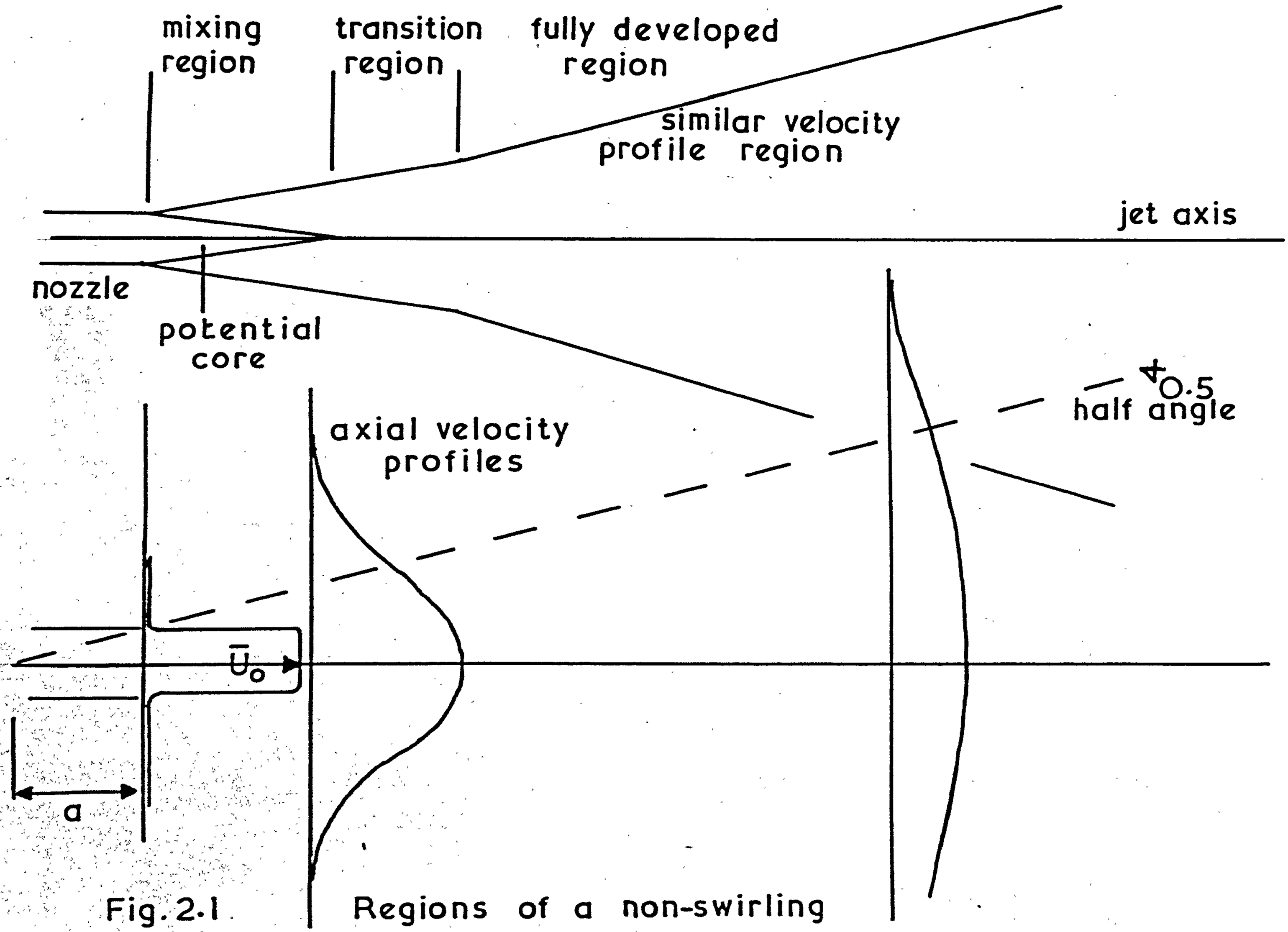

Fig. 2.1 Regions of a non-swirling turbulent jet

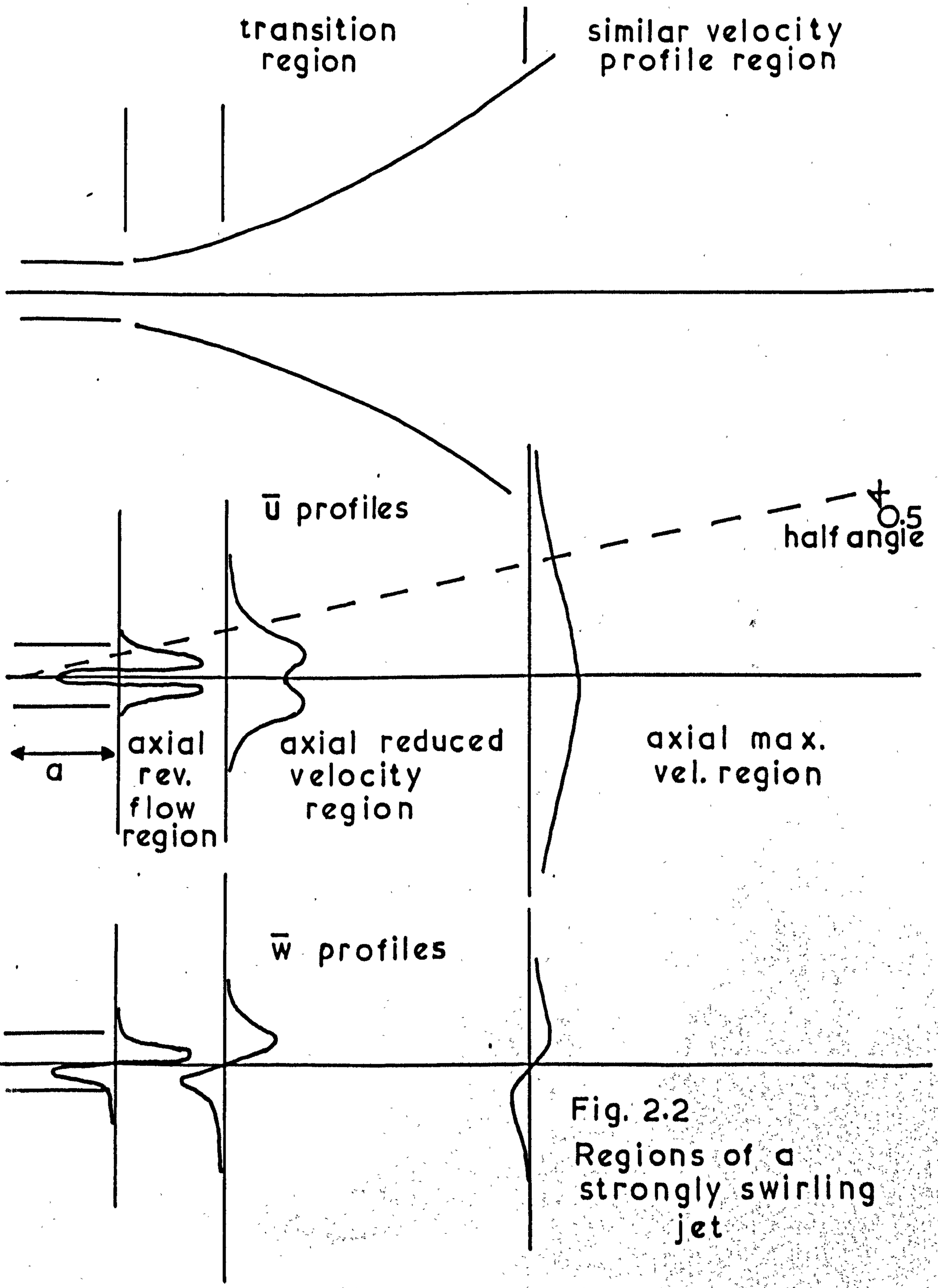

Fig. 2.2
Regions of a strongly swirling jet

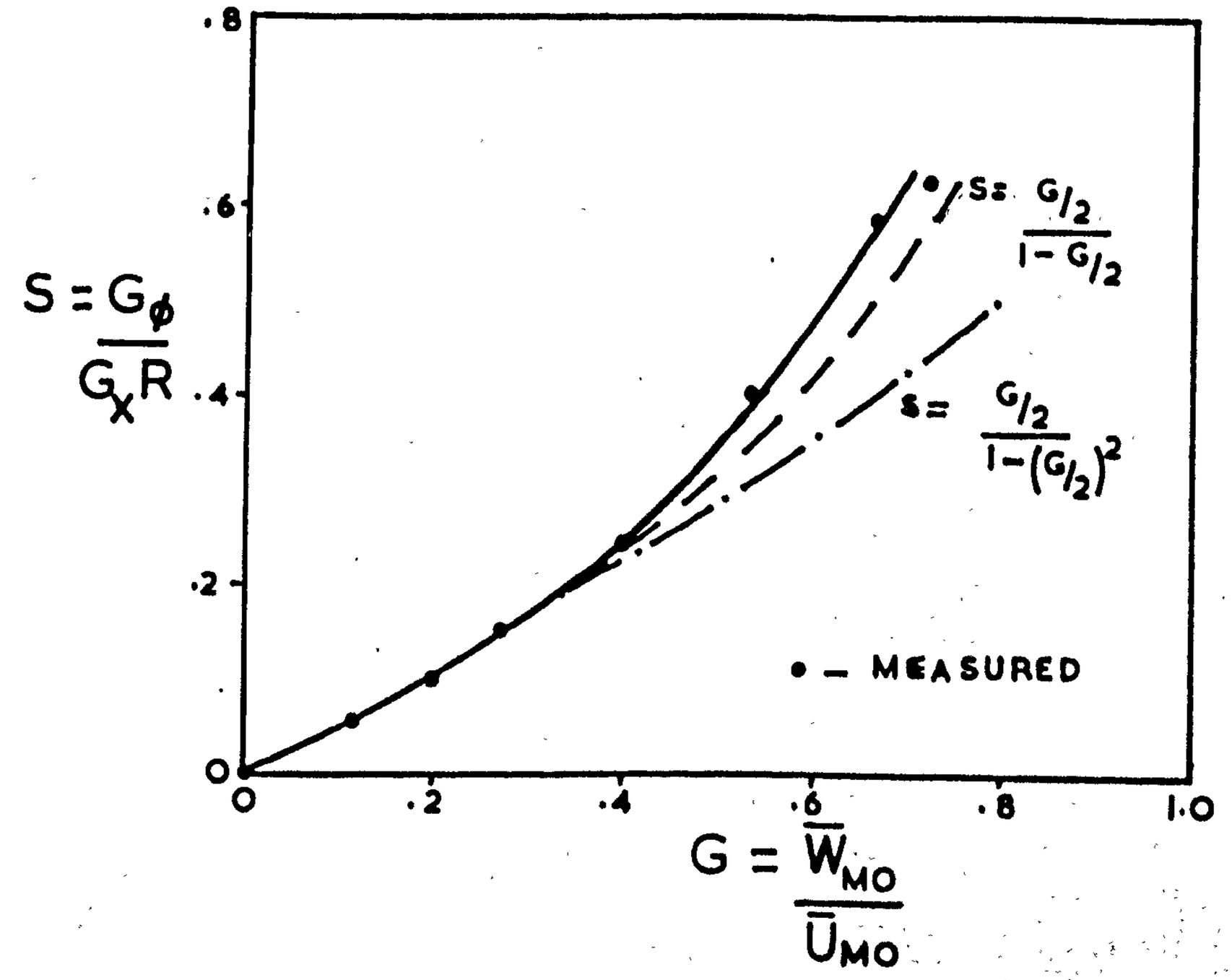

Fig. 2.3 Swirl parameters (Chigier & Chervinsky)

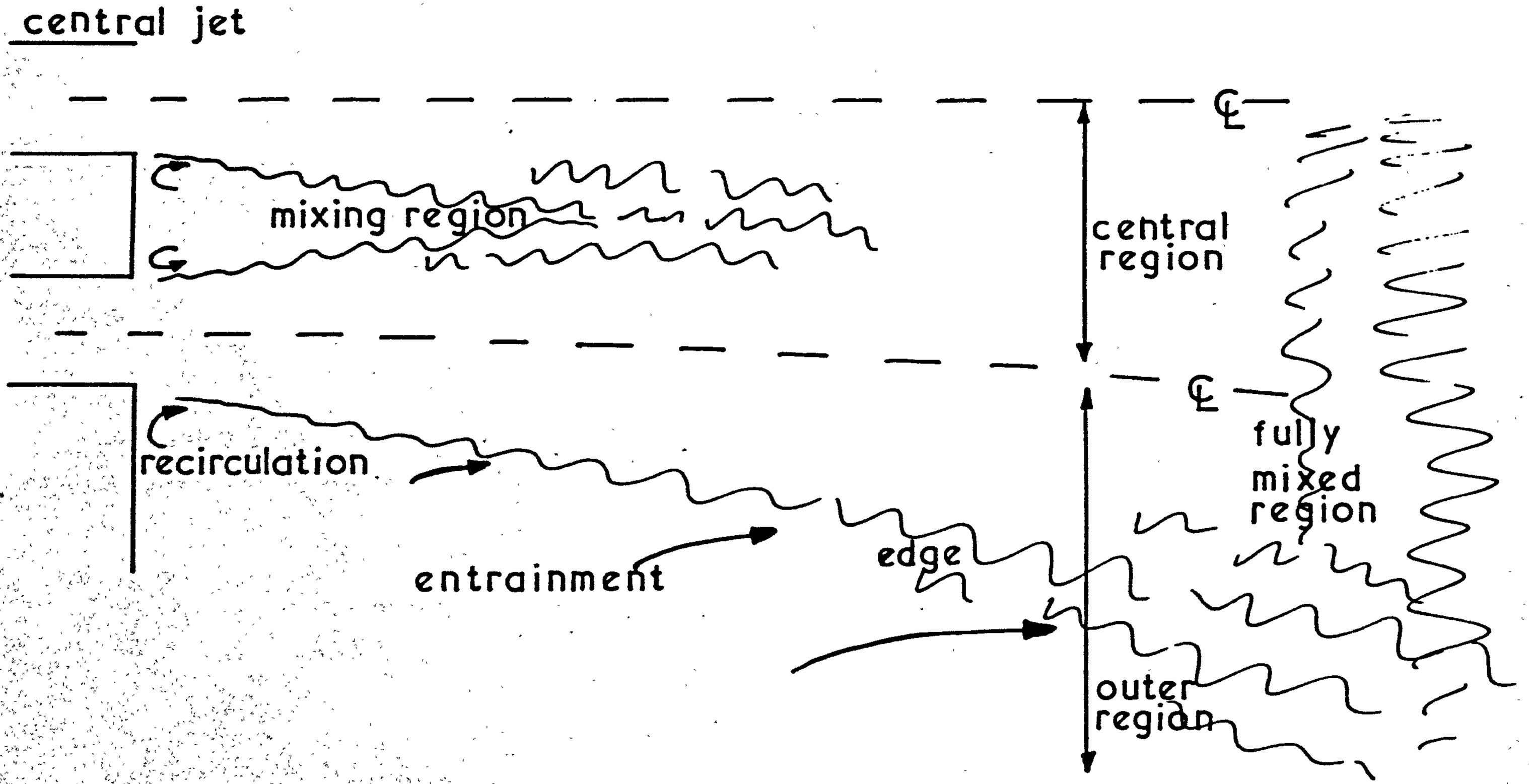

Fig. 2.4 Diagrammatic representation of regions associated with multiple jets

CHAPTER 3

Summary Of Contents

The chapter lists the general requirements of the apparatus with the fabrication details of each particular piece of the apparatus.

The method and importance of the supply and monitoring of clean air at a steady temperature, pressure, and flowrate for use with a hot-wire anemometer is reported, with the mode of operation of the hot wire probe and traversing mechanism.

The principles and mode of operation of a 5 hole pitot probe is also included.

CHAPTER 3

DESIGN AND DESCRIPTION OF THE EXPERIMENTAL APPARATUS

3.1. General Requirements Of The Apparatus

Fig.(3.2) shows a schematic flow diagram of the apparatus. The apparatus was designed such that :-

(a) 3 swirling or non-swirling jets placed horizontally could be used of variable pitch from 1.25 to 2.0 diameters.

(b) Each jet was fitted with a separate air monitoring device such that identical quantities of air could be fed to each jet, sufficient to give velocities of up to 20 metres/sec.

(c) The jets issued from a flat wall, into an enclosure open at the opposite end.

(d) The box and end walls were fabricated from perspex to facilitate easy probe positioning.

(e) The air supply was steady, clean and at a constant temperature.

3.2 Specific Design Of The Apparatus

3.2.1 The Perspex Box

The box was fabricated from $\frac{1}{4}$ inch thick perspex and was of 16" cube interior dimensions, with interchangeable nozzle support plates spaced 6 inches apart to ensure accurate alignment of the jets. Fig.(3.3) shows a schematic diagram of the box with the probing mechanism. ~~and plate (P3.1) shows a general view of the apparatus with the hot wire probe in position.~~ Enclosing the jets served two main purposes, namely preventing outside draughts from affecting the hot wire measurements, and promoting recirculation within the enclosure.

3.2.2 Air Jets

The jets were of the two swirling and non-swirling types as detailed below:-

Non-Swirling Jets

The non-swirling jets consisted of a one inch I.D. $1\frac{1}{8}$ inch O.D., 12 inch long brass tube with a sharp right angle bend at the air entry end. The use of a sharp bend was found necessary to destroy the upstream flow patterns formed in the delivery tubing to the jets. It was found that an asymmetric flow distribution was obtained without

the right angle bend due to crowding of the flow to the outer periphery of the delivery tubes, (which were necessarily bowed). The introduction of a fine wire mesh gauze immediately after the right angle bend helped to produce a flat (turbulent) velocity profile over the jet exit.

Swirling Jets.

In order to ensure that close packing of the jets was obtainable, and at the same time to be able to introduce the air into an inner annulus tangentially to produce the rotational motion, it was found necessary to design jets with a divergence before the mouth of the jet. Experience has shown that the most convenient and successful way of producing a swirling vortex motion type of jet was to introduce the air from an outer annulus tangentially into an inner annulus, which would normally restrict the close packing of the jets without a divergence (Ref.2 and 3). Fig. 3.1 shows a cross section through the swirl chamber which has 4 tangential entries for the air from the outer to inner annulus, and two tangential supply pipes for the air into the outer annulus. The resultant exit dimensions of the jet are identical to those of the non-swirling jets. It was found necessary to use two supply pipes for the air

into the outer annulus to overcome slight asymmetric flow distribution of the resultant swirling jet when only one supply was used.

Swirling jets with an opposite swirl direction were made to be able to investigate the effects of swirling "in mesh" and "out of mesh". The design was exactly similar to the above jets with the tangential entries and supply pipes altered. The total volume of air fed to the non-swirling and swirling jets was identical for all conditions.

3.31. Air Supply And Monitoring

The air supply needed to be of constant temperature, and of a constant pressure sufficient to overcome the pressure drop encountered along the lines to the nozzle exit. It was decided to use rotameters to meter each individual air supply, this being the quickest and easiest form of air flow monitor. To overcome the pressure drop associated with the valves, pipes, rotameters, and jets it was decided to use air from the compressed air line in the laboratory. The air supply was at 75 - 85 p.s.i.g. and fluctuated between these limits as the compressor cut in and out. The air from the compressor contained a relatively large amount of oil and water vapour and so it was found necessary to clean the air by means of filters before use. (It is necessary to have clean air when using a hot wire anemometer since

grease or particles adhering to the wire seriously affect its heat loss characteristics, and cleaning and recalibration of the wires would be necessary at very frequent intervals). The air was passed to a pressure regulator after the filters and the pressure maintained constant at 20 p.s.i.g. A throttle valve after the pressure regulator controlled the total flow of air to the manifold which in turn distributed the air through separate valves to each rotameter and jet.

The system once set would maintain a constant flow-rate of clean air at a steady temperature to each jet. No detectable variation occured over long intervals, and the filters were kept clean by regular maintenance.

One particular disadvantage of using a blower as opposed to the above system is the fact that generally the temperature of the air rises for some considerable time, and since the hot wire works on the principle of forced convection to the wire (see Appendix 1) the hot wire is as sensitive to temperature changes as to velocity changes, and any changes in temperature would necessitate corrections being applied to the constants of calibration (Ref.4).

The filters are designed to remove grit, water vapour and oil vapour down to 0.5 microns. A schematic flow diagram of the system is shown in Fig.(3.2).

3.3.2 Air Supply To The Jets And Production Of A Free Swirling Jet Of Variable Swirl Number.

Each non-swirling jet was fed from a single rotameter supplying the full volumetric flow for each jet. For the case of the swirling jets, each jet was supplied with the same total volumetric flowrate as the non-swirling jets, split up equally between two rotameters, each feeding one of the tangential air supply pipes fitted to the jets.

In order to produce a jet of variable swirl number, it was found satisfactory to introduce a proportion of the air to the jet along its inner annulus, the proportion depending upon the degree of swirl required. Each of the 3 air supplies to such a swirling jet were again fed from individual rotameters, the total volumetric flowrate being the same as used in the non-swirling jets. A long extension (16 diameters) was fitted to the nozzle for the latter case in order that the tangential and axial mass flows could have time to mix thoroughly before the nozzle exit, it also served the purpose of extending the jet outside the region of the box. It was found that the long extension helped to improve the uniformity of the resulting jet, and did not reduce the resultant exit swirl velocity or axial velocity profiles.

3.4 Probe Traversing Mechanism.

The hot wire probes were used from the open end of the box, and the 5 hole pitot probe was used with the same mechanism from the side of the box, probing through holes drilled into the side.

The mechanism consisted of a small lathe bed with facilities for traverse in each of the 3 mutually perpendicular directions corresponding to the 3 axes. Typical positions of measurement for radial traverses from the centre line are shown in Fig.(3.8).
The hot wire probes, and the 5 hole pitot probe were rotatable about their axes fitted with a protractor and pointer.

3.5 Measuring Instruments

3.5.1 The 5 Hole Pitot Probe

Construction

The probe consists of a tube with several pressure tappings drilled into the tip. One is drilled on the axis of the probe and 4 more drilled equidistant from the first hole symmetrically around the probe. The way in which these are positioned is shown in Fig.(3.4). The dimensions of the probe tip are small in comparison to the flow field, and the disturbance of the flow is assumed to be negligible.

Principle and Mode Of Operation

When the probe is positioned in a flow field such that the total velocity vector is at some angle to the probe tip, but in the plane of holes 5 and 4 only, then a pressure differential will be set up between holes 5 and 4 and the pressure differential between holes 3 and 2 will be zero. By calibration (see Appendix 3) the magnitude and direction of the total velocity may be determined. The technique of operation of the probe was as follows.

i) The probe was rotated until $P_2 - P_3 = 0$ and the yaw angle θ was recorded directly from the protractor on the pitot probe body.

ii) The pressure readings P_1, $P_4 - P_5$, $P_1 - P_{2/3}$ were recorded (where $P_{2/3}$ is the average of P_2 and P_3).

The orientation of the probe, the total velocity vector and the 3 resultant component velocities in the 3 mutually perpendicular axes is shown in Fig.(3.5).

Measurement Of Pressure Differentials

The pressure differential $P_2 - P_3$ was monitored continuously on a Beaudoin pressure transducer and quick sensitive response was achieved for minimum reading corresponding to zero pressure differential.

The yaw angle could be determined to within 1° accuracy by this method. For the pressure differential $P_4 - P_5$, $P_1 - P_{ambient}$, $P_1 - P_{2/3}$ three inclined tube manometers were used with an accuracy of $\pm$ .005 mm H_2O.

The calibration graphs Figs. (3.6 and 3.7), were used in conjuction with the computer programme (see Appendix 3 and 5) for determination of the 3 component average velocities $\bar{u}, \bar{v}, \bar{w}$, and the static pressure P_s.

The correlation between measurements taken with the 5 hole pitot probe and the hot wire anemometer are shown in Appendix 5.

A full description of the principles of operation of a 5 hole pitot probe are described in (Ref.1) and the calibration procedure used are detailed in Appendix 3.

3.5.2 The Constant Temperature Hot Wire Anemometer Mode Of Operation

The principles of operation are detailed in Appendix 1. The equipment used was made by D.I.S.A. and was the 55D00 Universal Anemometer Unit including a D.C. Voltmeter and R.M.S. (root mean square) Voltmeter. The technique used to take measurements was as follows (6 pt. technique - see Chapter 4 and Fig.4.1).

(i) Traverse probe type (a) into the desired position and rotate to orientation No.1, record position.

(ii) Read $\bar{E}$, and $\tilde{E}'$, at that orientation (wait for the meters to come to rest - use of high damping for $\bar{E}$ measurements in highly turbulent conditions).

(iii) Rotate probe to orientation No.2 and read E_2, $\tilde{E}'_2$.

(iv) Repeat for orientations 3 and 4.

(v) Change to probe type (b) and rotate to orientation No.5, read $\bar{\bar{E}}_5$, $\tilde{E}'_5$.

(vi) Rotate to orientation No.6, read $\bar{\bar{E}}_6$ and $\tilde{E}'_6$.

(vii) Traverse to new position and perform readings vi)→ i) in reverse. Repeat i)→vii) for new positions.

For the 3 point technique a similar procedure for measuring is adopted. The positions of the wire supports in orientations 1→ 8 inclusive are fixed and it is necessary to assume that the flow over the wire supports, that may occur in any of the 8 positions, does not affect the readings too much. For orientation No.9 the wire supports may be rotated in any desired position without altering the position of the wire since the axis corresponds to the probe axis of rotation. It is sometimes necessary to discard a set of readings when flow hits a wire support before the wire,

since obvious erroneous results are obtained, usually indicated by a very high $\tilde{E}'$ reading.

A full electrical specification, construction and description of each unit of the Universal Anemometer is given in (Ref.5.).

3.5.3 Choice Of The Prime Measuring Instrument

All the results quoted within this thesis were taken with the hot wire anemometer, which was chosen as the prime measuring instrument. The purpose of the 5 hole pitot readings was to check the accuracy of the mean flow measurements taken with the hot wire anemometer under widely different conditions, and to establish the positions at which the swirl velocity changed sign from +ve to -ve when traversing a jet system. A typical correlation between the two instruments is shown in Fig. (A4.1)

REFERENCES - CHAPTER 3

(1) Lee J.C. and Ash J.E.
"A Three-Dimensional Spherical Pitot Probe"
Trans. A.S.M.E. Vol.78 (1956)

(2) Chigier N.A. and Chervinsky A.
"Experimental Investigation Of Swirling Vortex Motion In Jets"
Jnl. Appl.Mech., Trans. A.S.M.E. (June 1967)

(3) Chigier N.A. and Chervinsky A.
"Aerodynamic Study Of Turbulent Burning Free Jets With Swirl"
11th Symposium On Combustion (1967)

(4) Davies T.W.
"A Study Of The Aerodynamics Of The Recirculation Zone Formed In A Free Annular Air Jet"
Ph.D. Thesis, University Of Sheffield (Jan 1969)

(5) D.I.S.A. 5500 Hot Wire Anemometer Manual.

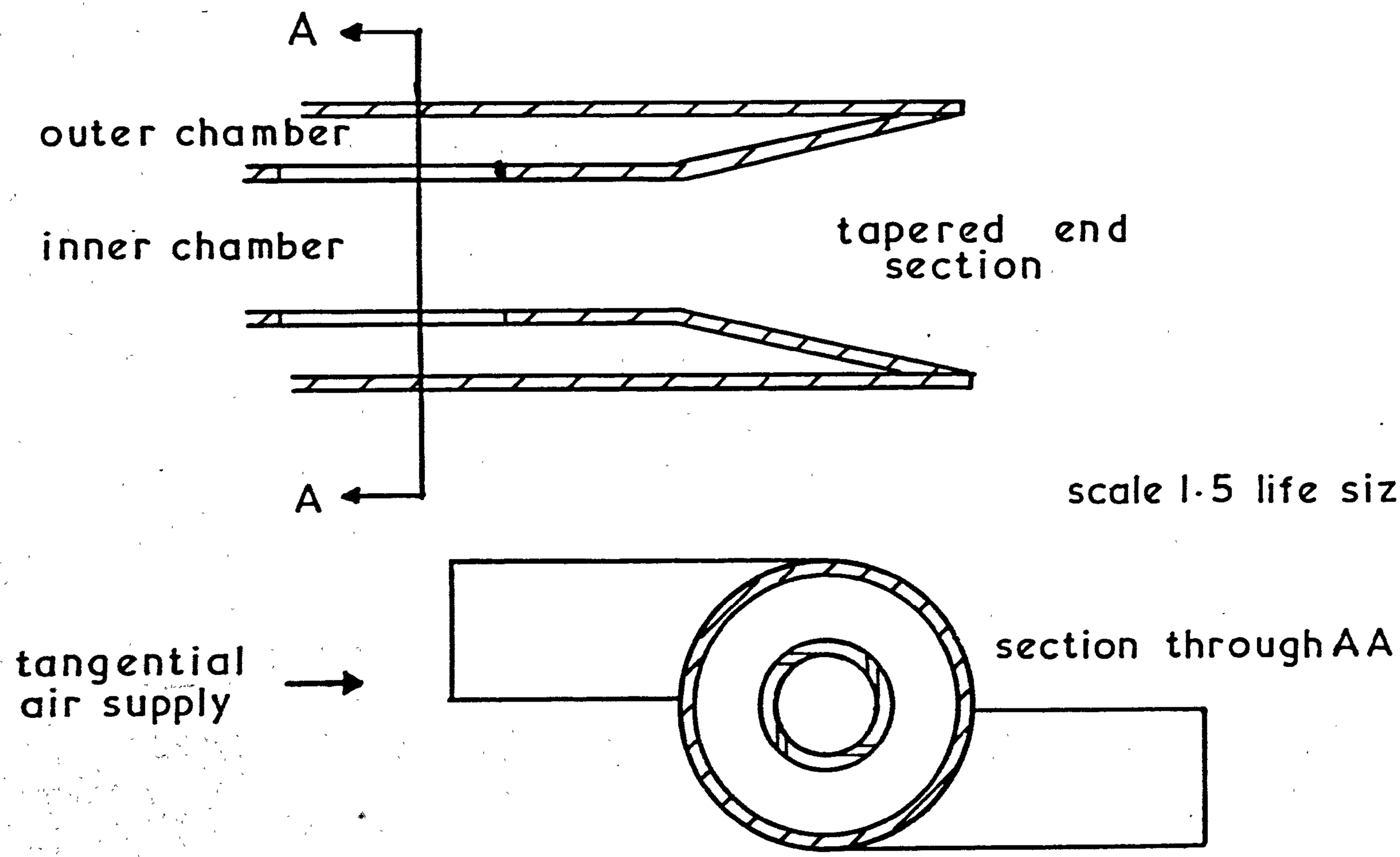

Fig. 3.1 Design of a swirling jet nozzle

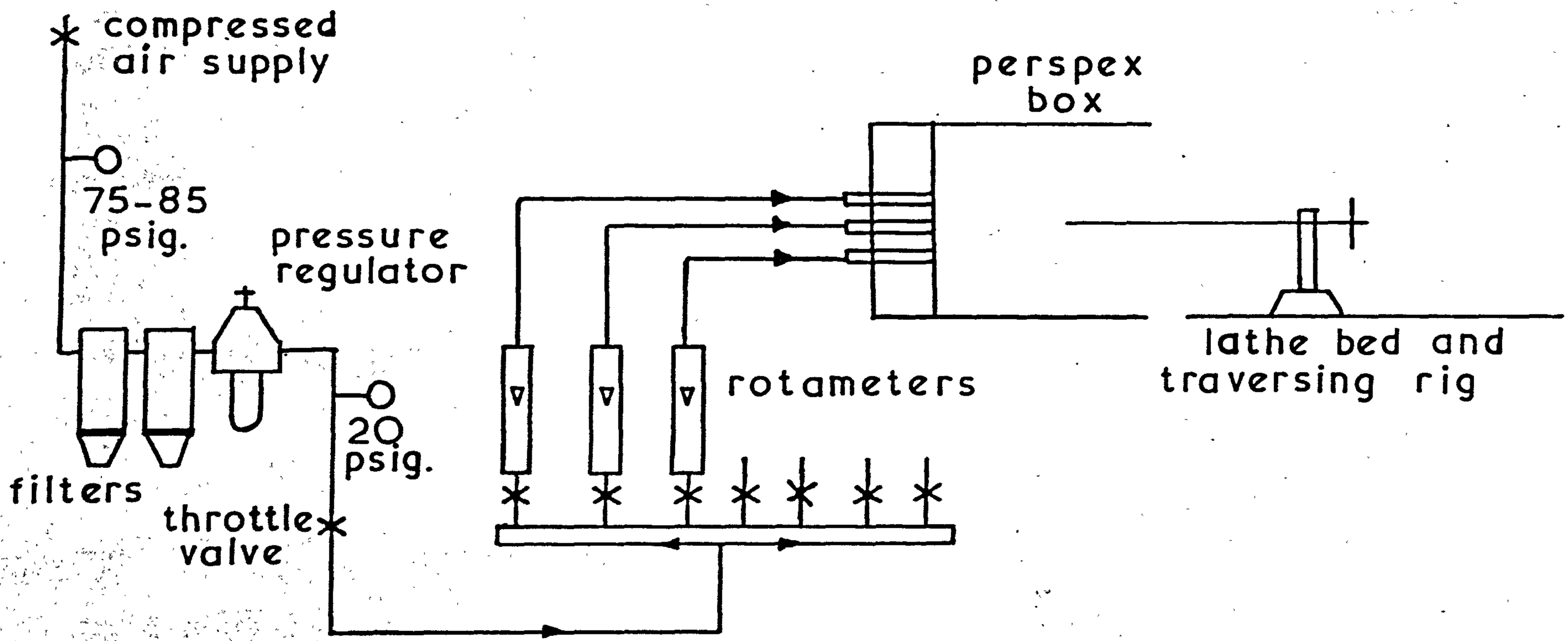

Fig. 3.2 Schematic flow diagram of equipment showing 3 nozzle set up

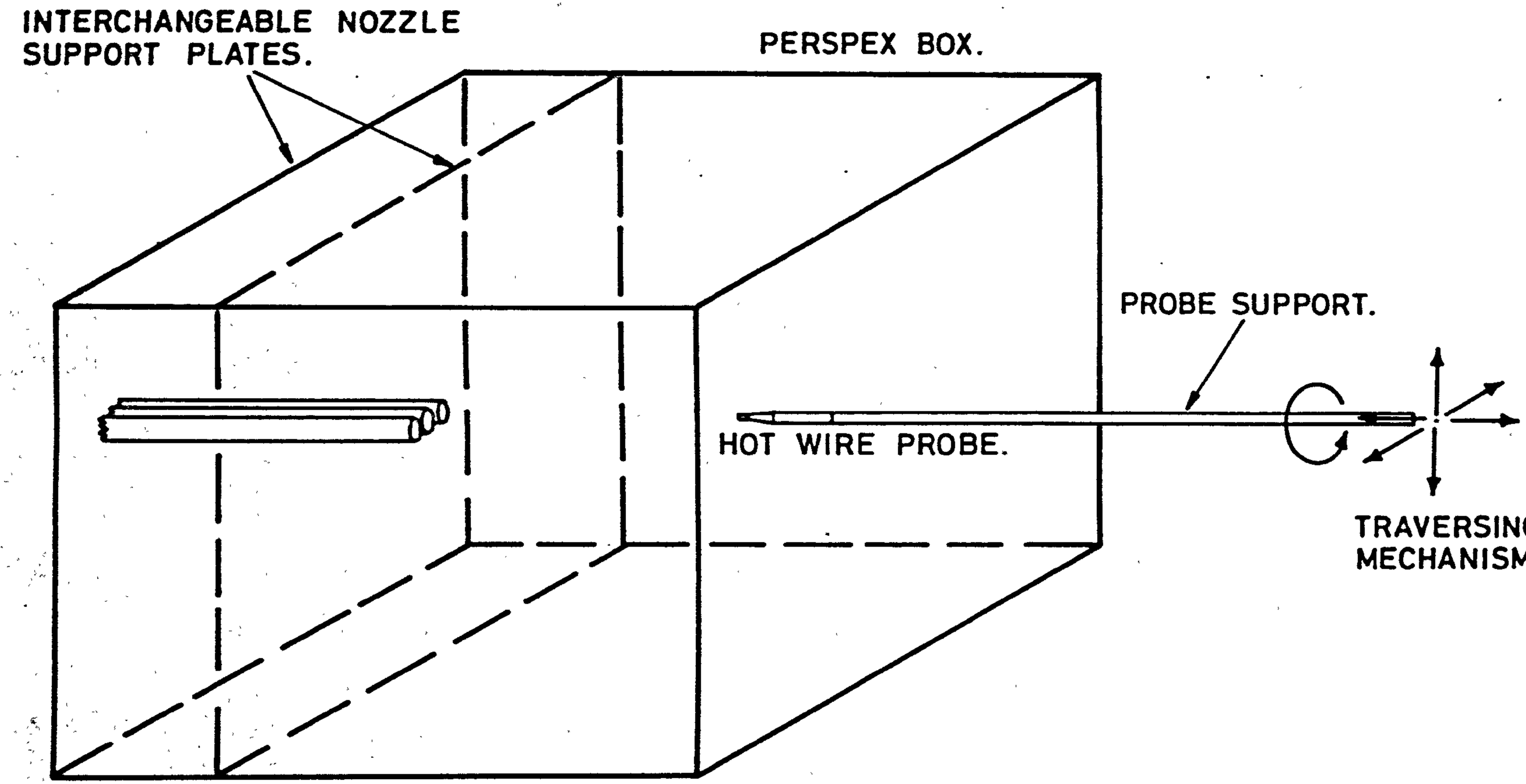

FIG. 3.3 AIR RIG SHOWING MULTIPLE AIR JETS AND HOT WIRE PROBE TRAVERSING DIRECTIONS.

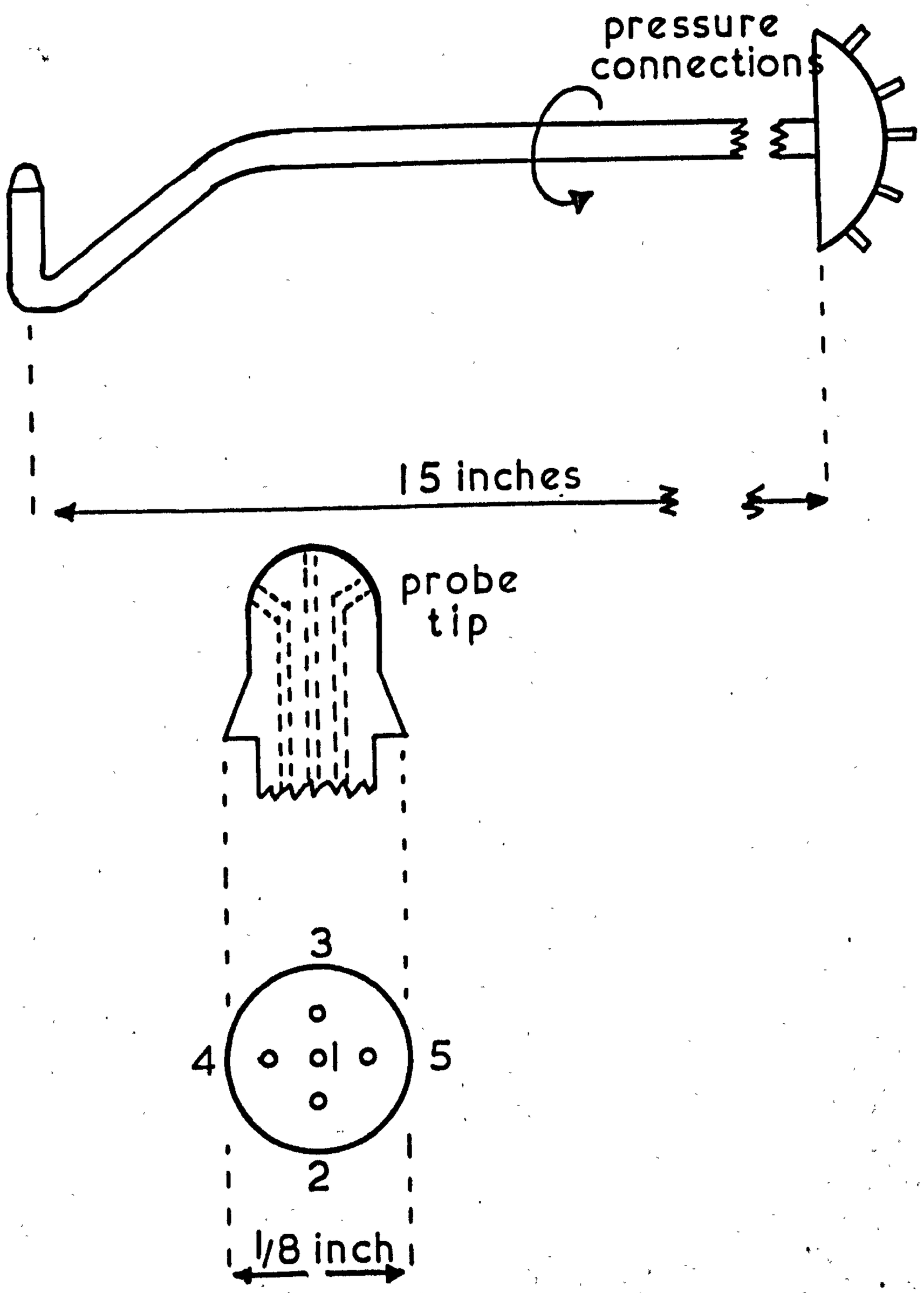

Fig. 3.4 Construction of 5-hole pitot pressure probe

Θ _ yaw angle

β _ pitch angle

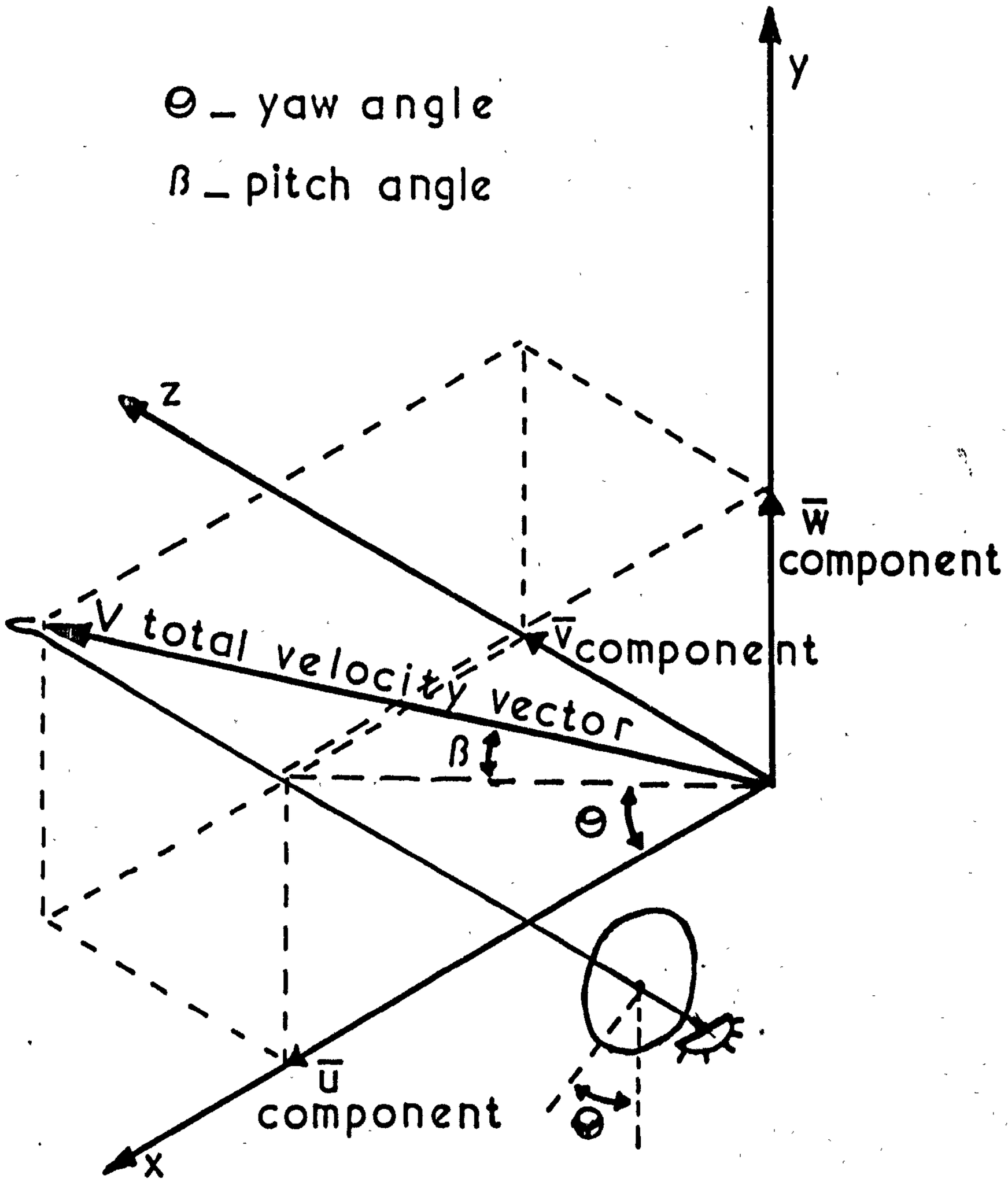

$\bar{u} = V\cos\beta.\cos\Theta$

$\bar{w} = V\cos\beta.\sin\Theta$

$\bar{v} = V\sin\beta$

Fig. 3.5 Definition of yaw and pitch angles, total velocity vector, and component velocities

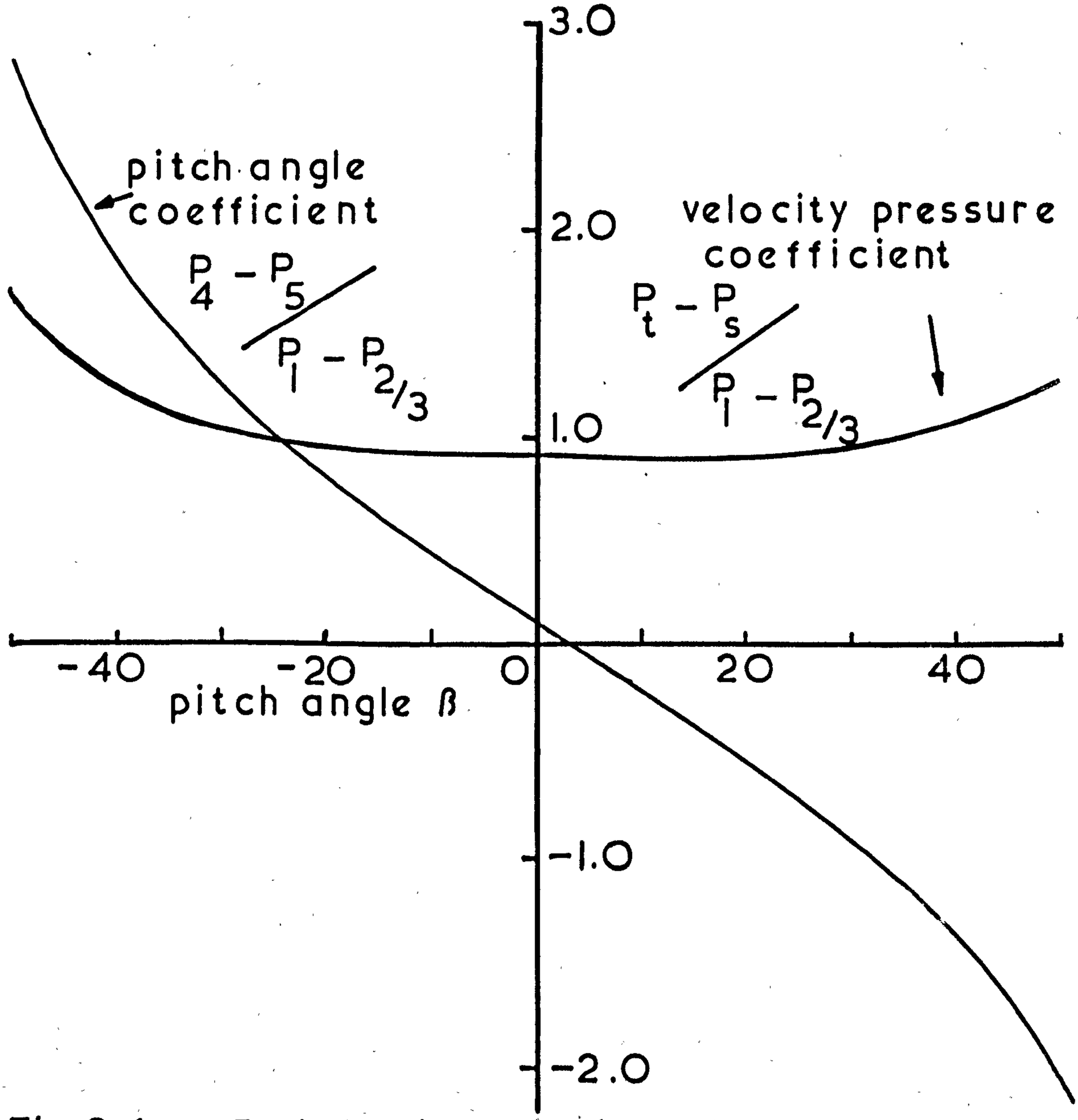

Fig. 3.6 5 - hole pitot calibration data

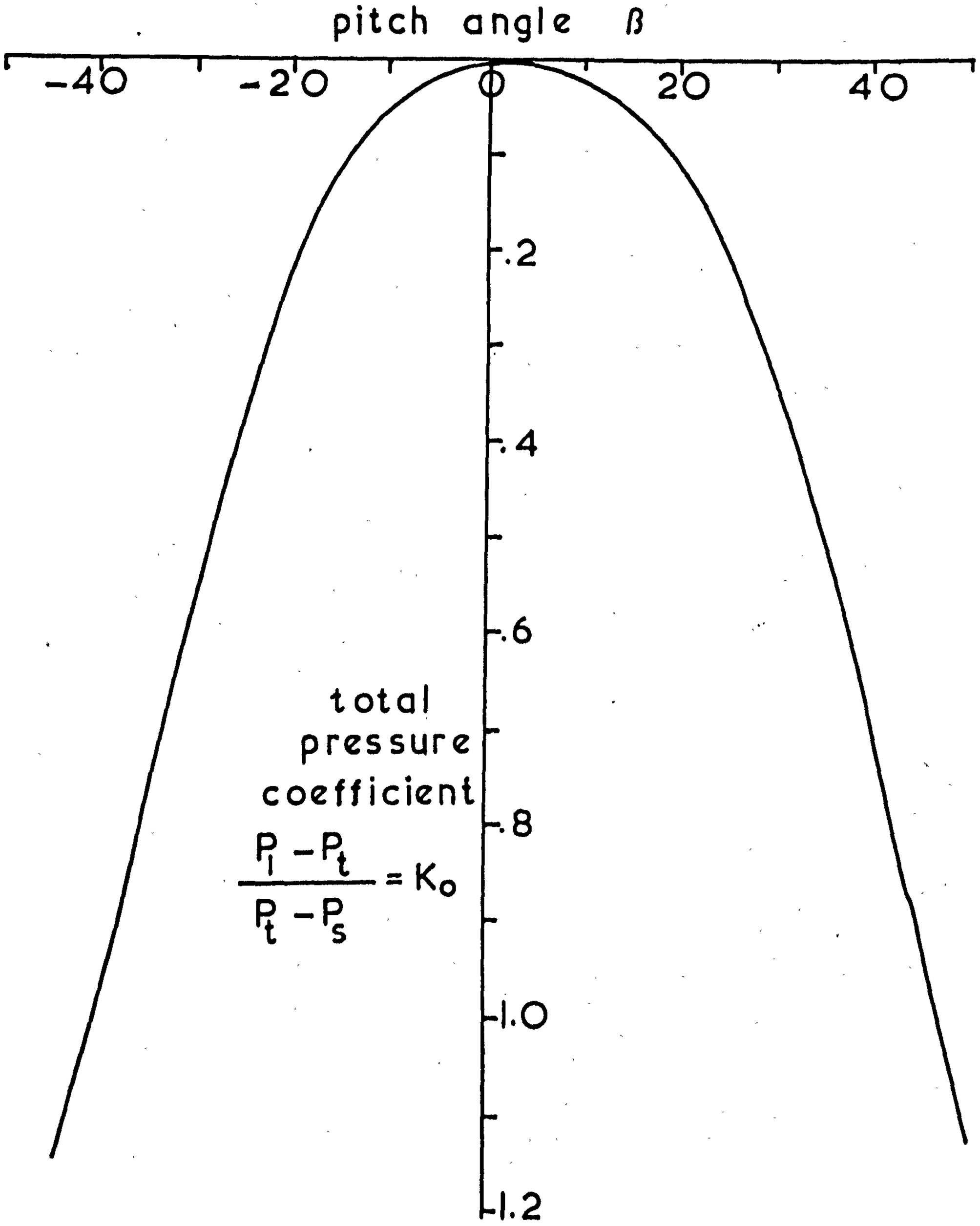

Fig.3.7 5 – hole pitot calibration data

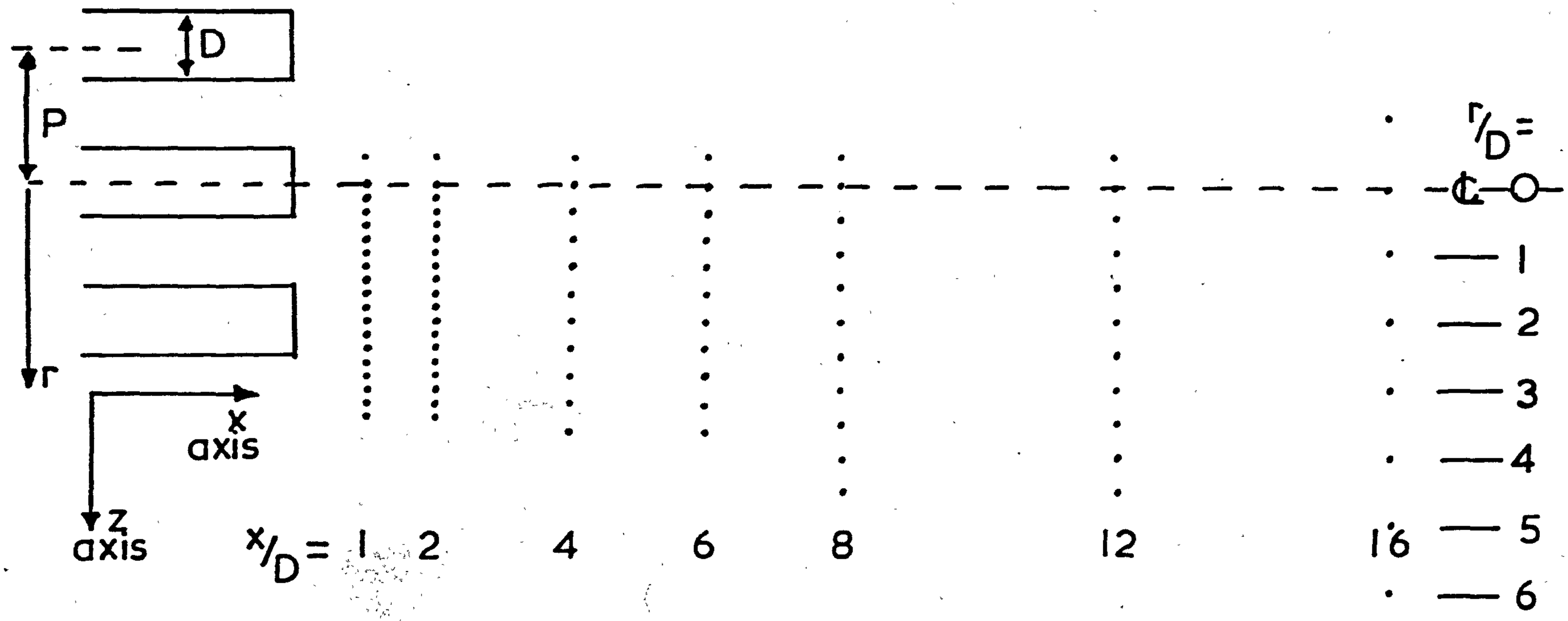

Fig.3.8 Typical positions of measurement for radial traverses from centre line

CHAPTER 4

Analysis Of The Signals From The Hot Wire Anemometer

4.1 Technique Of Probe Orientation

In order to investigate the aerodynamic interaction of the multiple jets a method was needed which would be able to separate and identify each average and fluctuating velocity component in the 3 mutually perpendicular axes and to be able to identify each shear stress term associated with the above. The separation of each term was necessary because no one term was considered small enough to neglect, as is the case in (Ref.1) and a technique of probe orientation similar to that used in (Ref.2) was adopted. The following method was developed and may be used in two ways, the choice of the way adopted being governed by whether the shear stress terms are required. The principles of each method are the same but the time involved in taking the measurements may be halved when shear stress terms are not required.

The two choices are:-

(a) A 3 Position Technique

Where a wire is positioned in turn in the direction of each of the 3 mutually perpendicular axes (x, y, z) when

the 3 component average velocities and normal stresses may be evaluated.

(b) A 6 Position Technique

Where a wire is positioned in turn at $\pm 45^{\circ}$ to the direction of each of the 3 mutually perpendicular axes when the 3 component average velocities, normal stresses, and shear stresses may be evaluated.

To be able to accurately orientate the wire in the 3 mutually perpendicular directions or at $\pm 45^{\circ}$ to these it was found necessary to use two different probes for each technique. The configuration of the probes and the way that they are orientated w.r.t. the axes is shown in fig.(4.1). Positions 1→6 are used for the 6 pt. technique and positions 7→9 are used for the 3 pt. technique respectively.

Care must be taken to ensure that accurate positioning of one probe with respect to the other probe is achieved, so that the wire mid point is in the same position in space for each orientation.

4.2 The 6 Position Technique

The voltage and velocity may be related by

$$\bar{E}^2 = A + B\bar{U}_N^{\frac{1}{2}} + C\bar{U}_N \qquad \text{(see Appendix 1)} \qquad (4.1)$$

Where $\bar{E}$ = D.C. Voltage, A,B,C are constants

$\bar{U}_N$ = Cooling velocity normal to the wire

(Initially we shall neglect the effect of cooling velocity along the wire. The way that this is accounted for will be shown later).

A,B,C are obtained by calibration using the method reported in Appendix 2.

Equation (4.1) is assumed to hold instantaneously to give:-

$$E^2 = A + BU_N^{\frac{1}{2}} + CU_N \qquad (4.2)$$

Hinze (Ref. A1.1 3) has shown that the instantaneous total velocity (U) may be split up into an average velocity ($\bar{U}$) and an instantaneous fluctuating velocity (U') which at any time may be -ve or +ve such that :-

$$U = \bar{U} + U'$$

It follows that since $\bar{U}'=0$, (time average of U')

then $\overline{U^2} = \bar{U}^2 + \overline{U'^2}$ (4.3.)

Similarly we can split up the instantaneous total voltage (E) into an average voltage ($\bar{E}$) and an instantaneous voltage (E') such that:-

$$E = \bar{E} + E' \qquad \text{and}$$
$$\overline{E^2} = \bar{E}^2 + \overline{E'^2} \qquad (4.4)$$

It is further assumed that we can split any flow field, at a particular point into its 3 mutually perpendicular component velocities, see fig.(4.2) such that:-

$$\bar{U}^2 = \bar{u}^2 + \bar{v}^2 + \bar{w}^2$$

$$\overline{U'^2} = \overline{u'^2} + \overline{v'^2} + \overline{w'^2}$$

hence $\bar{U}^2 + \overline{U'^2} = \overline{U^2} = \bar{u}^2 + \overline{u'^2} + \bar{v}^2 + \overline{v'^2} + \bar{w}^2 + \overline{w'^2}$

The way in which the wire responds to the flow field when placed in the plane of two axes and at $\pm 45^{o}$ to ~~the~~ other axis is shown by the following equations, neglecting in the first instance the flow component along the wire, (that is to say considering the total normal cooling velocity only). The technique is to position the wires in turn in each of the 6 orientations whilst maintaining the mid point of each wire in the same position in space (ie. flow field).

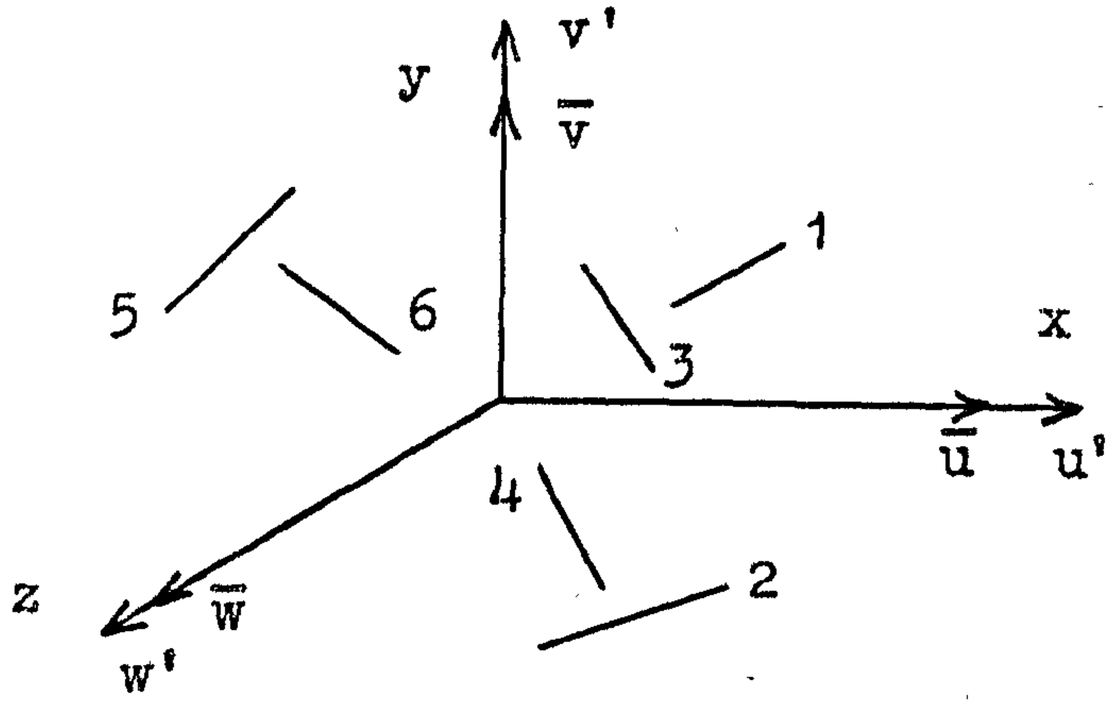

Wire Type (b) used for positions 1 → 4

Wire type (a) used for positions 5 and 6

If we define:-

U_1 - Instantaneous Cooling velocity on wire in position 1

$\bar{U}_1$ - Average Cooling velocity on wire in position 1

Then-

$$U_1^2 = (\bar{w} + w')^2 + \tfrac{1}{2}\left((\bar{u} + u') - (\bar{v} + v') \right)^2$$

$$U_2^2 = (\bar{v} + v')^2 + \tfrac{1}{2}\left((\bar{u} + u') + (\bar{w} + w') \right)^2$$

$$U_3^2 = (\bar{w} + w')^2 + \tfrac{1}{2}\left((\bar{u} + u') + (\bar{v} + v') \right)^2$$

$$U_4^2 = (\bar{v} + v')^2 + \tfrac{1}{2}\left((\bar{u} + u') - (\bar{w} + w') \right)^2$$

$$U_5^2 = (\bar{u} + u')^2 + \tfrac{1}{2}\left((\bar{w} + w') + (\bar{v} + v') \right)^2$$

$$U_6^2 = (\bar{u} + u')^2 + \tfrac{1}{2}\left((\bar{w} + w') - (\bar{v} + v') \right)^2 \qquad (4.5)$$

Also -

$$\overline{U}_1^2 = \overline{w}^2 + \tfrac{1}{2}\,(\overline{u} - \overline{v})^2, \quad \overline{U}_2^2 = \overline{v}^2 + \tfrac{1}{2}\,(\overline{u} + \overline{w})^2$$

$$\overline{U}_3^2 = \overline{w}^2 + \tfrac{1}{2}\,(\overline{u} + \overline{v})^2, \quad \overline{U}_4^2 = \overline{v}^2 + \tfrac{1}{2}\,(\overline{u} - \overline{w})^2$$

$$\overline{U}_5^2 = \overline{u}^2 + \tfrac{1}{2}\,(\overline{w} + \overline{v})^2, \quad \overline{U}_6^2 = \overline{u}^2 + \tfrac{1}{2}\,(\overline{w} - \overline{v})^2 \qquad (4.6)$$

Now we have said that we can represent the voltage at any time (Instantaneous Voltage E) by

$$E = \overline{E} + E' \qquad \text{hence} \qquad \overline{E^2} = \overline{E}^2 + \overline{E'^2}$$

Similarly

$$U = \overline{U} + U' \qquad \text{hence} \qquad \overline{U^2} = \overline{U}^2 + \overline{U'^2}$$

Now from equations of type (4.5) and (4.6) using a time averaging technique putting $\overline{u'}$ terms =o, etc., we obtain -

$$\overline{U_4^2} = \overline{v}^2 + \overline{v'^2} + \tfrac{1}{2}\,(\overline{u}^2 + \overline{u'^2} - 2\overline{uw} - \overline{2u'w'} + \overline{w}^2 + \overline{w'^2}) \qquad (4.7)$$

$$\overline{U_2^2} = \overline{v}^2 + \overline{v'^2} + \tfrac{1}{2}\,(\overline{u}^2 + \overline{u'^2} + 2\overline{uw} + 2\overline{u'w'} + \overline{w}^2 + \overline{w'^2}) \qquad (4.8)$$

So by addition -

$$\overline{U_4^2} + \overline{U_2^2} = 2\overline{v}^2 + 2\overline{v'^2} + \overline{u}^2 + \overline{u'^2} + \overline{w}^2 + \overline{w'^2}$$

Also -

$$\overline{U}_4^2 = \overline{v}^2 + \tfrac{1}{2}\left(\overline{u}^2 - 2\overline{uw} + \overline{w}^2\right) \qquad (4.9)$$

$$\overline{U}_2^2 = \overline{v}^2 + \tfrac{1}{2}\left(\overline{u}^2 + 2\overline{uw} + \overline{w}^2\right) \qquad (4.10)$$

Therefore -

$$\overline{U}_4^2 + \overline{U}_2^2 = 2\overline{v}^2 + \overline{u}^2 + \overline{w}^2$$

Now -.

$$\overline{U_4^2} - \overline{U}_4^2 = \overline{U'^2_4} \qquad (4.11)$$

Therefore from (4.7), (4.8), (4.9), (4.10), (4.11)

$$\overline{U_4^2} - \overline{U}_4^2 + \overline{U_2^2} - \overline{U}_2^2 = \overline{U_4'^2} + \overline{U_2'^2} = 2\overline{v'^2} + \overline{u'^2} + \overline{w'^2} \qquad (4.12)$$

By similar manipulation we obtain the 3 equations :-

$$\begin{aligned}
\overline{U_4'^2} + \overline{U_2'^2} &= 2\overline{v'^2} + \overline{u'^2} + \overline{w'^2} \\
\overline{U_1'^2} + \overline{U_3'^2} &= 2\overline{w'^2} + \overline{u'^2} + \overline{v'^2} \\
\overline{U_5'^2} + \overline{U_6'^2} &= 2\overline{u'^2} + \overline{v'^2} + \overline{w'^2}
\end{aligned} \qquad (4.13)$$

Which are 3 solvable simultaneous equations.

Similarly we also have :-

$$\overline{U}_4^2 + \overline{U}_2^2 = 2\overline{v}^2 + \overline{u}^2 + \overline{w}^2$$

$$\overline{U}_1^2 + \overline{U}_3^2 = 2\overline{w}^2 + \overline{u}^2 + \overline{v}^2$$

$$\overline{U}_5^2 + \overline{U}_6^2 = 2\overline{u}^2 + \overline{v}^2 + \overline{w}^2 \qquad (4.14)$$

Which again are 3 solvable simultaneous equations.

From (4.9), (4.10)

$$\overline{U}_2^2 - \overline{U}_4^2 = 2\overline{uw}$$

From (4.7), (4.8)

Also :-

$$\overline{U_2^2} - \overline{U_4^2} = 2(\overline{uw} + \overline{u'v'})$$

Hence :-

$$\overline{U_2^2} - \overline{U_4^2} - (\overline{U}_2^2 - \overline{U}_4^2) = \overline{U_2'^2} - \overline{U_4'^2} = 2\overline{u'w'}$$

Hence by similar manipulation we obtain :-

$$\overline{U_2'^2} - \overline{U_4'^2} = 2\overline{u'w'}$$

$$\overline{U_3'^2} - \overline{U_1'^2} = 2\overline{u'v'}$$

$$\overline{U_5'^2} - \overline{U_6'^2} = 2\overline{v'w'} \qquad (4.15)$$

Hence from equations of the type (4.13), (4.14), (4.15) we can deduce $\bar{u}$, $\bar{v}$, $\bar{w}$, $\overline{u'^2}$, $\overline{v'^2}$, $\overline{w'^2}$, $\overline{u'v'}$, $\overline{u'w'}$, $\overline{v'w'}$ knowing the values of $\bar{U}^2_{1\to6}$ $\overline{U'^2}_{1\to6}$ by solution of the simple simultaneous equations.

The solution to these equations give :-

$$\bar{u}^2 = \tfrac{1}{4}\left(3(\bar{U}_5^2 + \bar{U}_6^2) - (\bar{U}_4^2 + \bar{U}_3^2 + \bar{U}_2^2 + \bar{U}_1^2)\right)$$

$$\bar{v}^2 = \tfrac{1}{4}\left(3(\bar{U}_2^2 + \bar{U}_4^2) - (\bar{U}_6^2 + \bar{U}_5^2 + \bar{U}_3^2 + \bar{U}_1^2)\right)$$

$$\bar{w}^2 = \tfrac{1}{4}\left(3(\bar{U}_3^2 + \bar{U}_1^2) - (\bar{U}_6^2 + \bar{U}_5^2 + \bar{U}_4^2 + \bar{U}_2^2)\right) \qquad (4.16)$$

$$\overline{u'^2} = \tfrac{1}{4}\left(3(\overline{U_5'^2} + \overline{U_6'^2}) - (\overline{U_4'^2} + \overline{U_3'^2} + \overline{U_2'^2} + \overline{U_1'^2})\right)$$

$$\overline{v'^2} = \tfrac{1}{4}\left(3(\overline{U_2'^2} + \overline{U_4'^2}) - (\overline{U_6'^2} + \overline{U_5'^2} + \overline{U_3'^2} + \overline{U_1'^2})\right)$$

$$\overline{w'^2} = \tfrac{1}{4}\left(3(\overline{U_3'^2} + \overline{U_1'^2}) - (\overline{U_6'^2} + \overline{U_5'^2} + \overline{U_4'^2} + \overline{U_2'^2})\right) \qquad (4.17)$$

$$\overline{u'v'} = \tfrac{1}{2}\left(\overline{U_3'^2} - \overline{U_1'^2}\right)$$

$$\overline{u'w'} = \tfrac{1}{2}\left(\overline{U_2'^2} - \overline{U_4'^2}\right)$$

$$\overline{v'w'} = \tfrac{1}{2}\left(\overline{U_5'^2} - \overline{U_6'^2}\right) \qquad (4.18)$$

4.3 The 3 Position Technique

To represent the cooling effect of the velocity component along the wire we shall include it in the 3 position analysis and then show how it affects the 6 position analysis.

For the 3 position technique we have the 3 wire orientations coincident with the 3 axes.

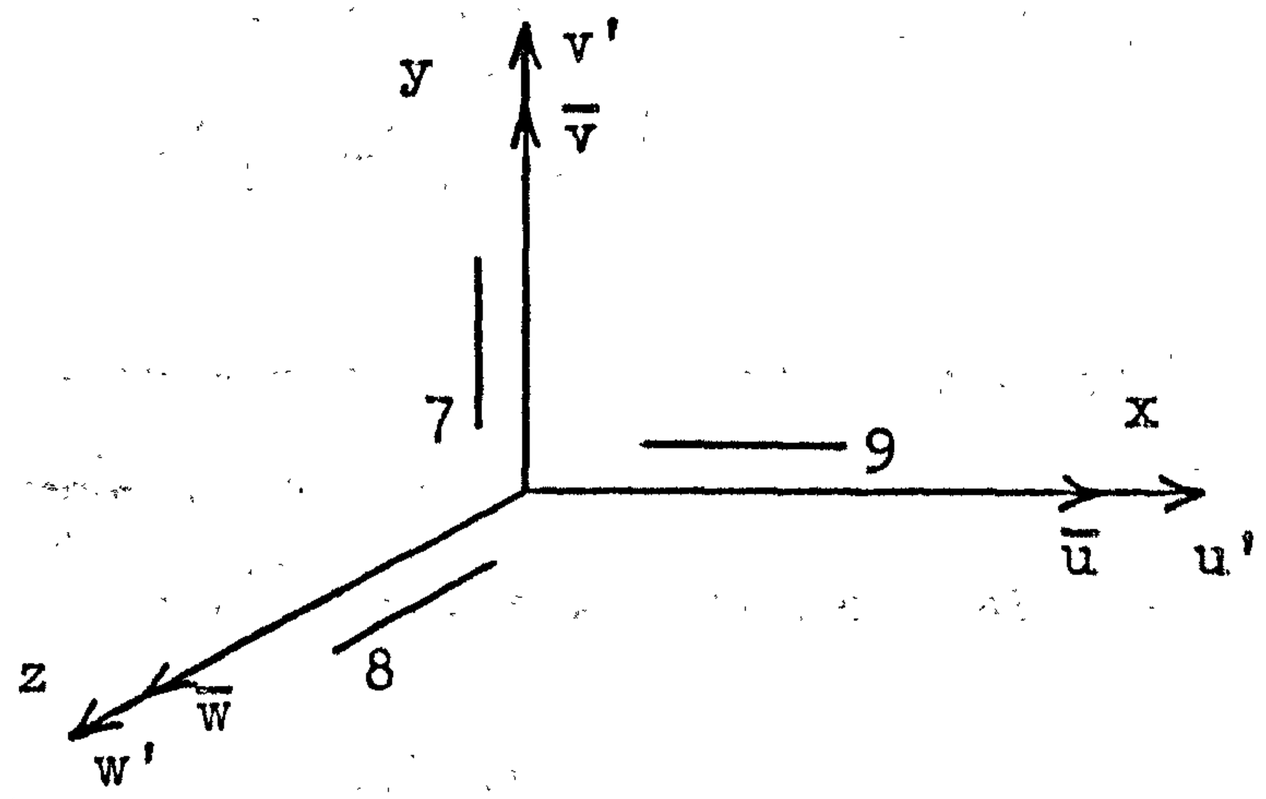

Wire type (a) is used for positions 7 and 8.

Wire type (c) is used for position 9.

If we call these wire positions 7,8 and 9, so as not to confuse them with the 6 pt. technique we have the following:-

$$U_7^2 = (\bar{u} + u')^2 + (\bar{w} + w')^2 + K1^2(\bar{v} + v')^2$$

$$U_8^2 = (\bar{u} + u')^2 + (\bar{v} + v')^2 + K1^2(\bar{w} + w')^2$$

$$U_9^2 = (\bar{v} + v')^2 + (\bar{w} + w')^2 + K3^2(\bar{u} + u')^2 \qquad (4.19)$$

Where K1 refers to the K value for wire (a) placed in position 7 or 8.

Where K3 refers to the K value for wire (c) placed in position 9.

Similarly:-

$$\overline{U}_7^2 = \overline{u}^2 + \overline{w}^2 + K1^2\overline{v}^2$$

$$\overline{U}_8^2 = \overline{u}^2 + \overline{v}^2 + K1^2\overline{w}^2$$

$$\overline{U}_9^2 = \overline{v}^2 + \overline{w}^2 + K3^2\overline{u}^2 \qquad (4.20)$$

Again by applying a time averaging technique to equations of type (4.14) to find $\overline{U^2}$ values, and putting $\overline{U'^2} = \overline{U^2} - \overline{U}^2$ again, we obtain the following :-

$$\overline{U_7'^2} = \overline{u'^2} + \overline{w'^2} + K1^2\overline{v'^2}$$

$$\overline{U_8'^2} = \overline{u'^2} + \overline{v'^2} + K1^2\overline{w'^2}$$

$$\overline{U_9'^2} = \overline{v'^2} + \overline{w'^2} + K3^2\overline{u'^2} \qquad (4.21)$$

Then by manipulation of these equations we obtain:-

$$\overline{u'^2} = (\overline{U_7'^2} + \overline{U_8'^2} - \overline{U_9'^2}(1 + K1^2)) / Z$$

$$\overline{v'^2} = (\overline{u'^2}(1 - K2^2) + \overline{U_9'^2} - \overline{U_7'^2}) / (1 - K1^2)$$

$$\overline{w'^2} = (\overline{u'^2}(1 - K2^2) + \overline{U_9'^2} - \overline{U_8'^2}) / (1 - K1^2) \qquad (4.22)$$

and -

$$\overline{u}^2 = (\overline{U}_7^2 + \overline{U}_8^2 - \overline{U}_9^2 (1 + K1^2)) / Z$$

$$\overline{v}^2 = (\overline{u}^2 (1 - K2^2) + \overline{U}_9^2 - \overline{U}_7^2) / (1 - K1^2)$$

$$\overline{w}^2 = (\overline{u}^2 (1 - K2^2) + \overline{U}_9^2 - \overline{U}_8^2) / (1 - K1^2) \qquad (4.23)$$

Where $Z = 2 - K3^2 (1 + K1^2)$

Again by knowing $\overline{U}^2_{7\to9}$, $\overline{U'^2_{7\to9}}$ values the above equations are solvable.

4.4 The 6 Position Technique With The Flow Component Alorg The Wire.

If we now consider the flow component along the wire for the 6 pt. technique equations of the type (4.5) become :-

$$U_1^2 = (\overline{w} + w')^2 + \tfrac{1}{2} ((\overline{u} + u') - (\overline{v} + v'))^2 + \frac{K1^2}{2} ((\overline{u} + u') + (\overline{v} + v'))^2$$

$$U_2^2 = (\overline{v} + v')^2 + \tfrac{1}{2} ((\overline{u} + u') + (\overline{w} + w'))^2 + \frac{K1^2}{2} ((\overline{u} + u') - (\overline{w} + w'))^2$$

$$U_3^2 = (\overline{w} + w')^2 + \tfrac{1}{2} ((\overline{u} + u') + (\overline{v} + v'))^2 + \frac{K1^2}{2} ((\overline{u} + u') - (\overline{v} + v'))^2$$

$$U_4^2 = (\bar{v} + v')^2 + \tfrac{1}{2}\left((\bar{u} + u') - (\bar{w} + w')\right)^2 + \frac{K1}{2}^2 \left((\bar{u} + u') + (\bar{w} + w')\right)^2$$

$$U_5^2 = (\bar{u} + u')^2 + \tfrac{1}{2}\left((\bar{w} + w') + (\bar{v} + v')\right)^2 + \frac{K2}{2}^2 \left((\bar{w} + w') - (\bar{v} + v')\right)^2$$

$$U_6^2 = (\bar{u} + u')^2 + \tfrac{1}{2}\left((\bar{w} + w') - (\bar{v} + v')\right)^2 + \frac{K2}{2}^2 \left((\bar{w} + w') + (\bar{v} + v')\right)^2 \qquad (4.24)$$

Clearly equations of type (4.24) reduce to those of (4.5) when K1 = K2 = 0, (where K2 is the K value for wire (b).

Manipulation of these equations results in the following equations which are modified versions of (4.16), (4.17), (4.18).

$$\bar{u}^2 = \left((\bar{U}_5^2 + \bar{U}_6^2)(H+2) - J(\bar{U}_4^2 + \bar{U}_3^2 + \bar{U}_2^2 + \bar{U}_1^2)\right) / 2(2+H(1-J))$$

$$\bar{v}^2 = \left((\bar{U}_4^2 + \bar{U}_2^2)(4-HJ) + H((J-2)(\bar{U}_3^2 + \bar{U}_1^2) + (H-2)(\bar{U}_5^2 + \bar{U}_6^2))\right) / 2(4-2HJ+H^2(J-1))$$

$$\bar{w}^2 = \left((\bar{U}_3^2 + \bar{U}_1^2)(4-HJ) + H((J-2)(\bar{U}_4^2 + \bar{U}_2^2) + (H-2)(\bar{U}_5^2 + \bar{U}_6^2))\right) / 2(4-2HJ+H^2(J-1)) \qquad (4.25)$$

$$\overline{u'^2} = \left((\overline{U_5'^2} + \overline{U_6'^2})(H+2) - J(\overline{U_4'^2} + \overline{U_3'^2} + \overline{U_2'^2} + \overline{U_1'^2}) \right) /$$

$$2(2+H(1-J))$$

$$\overline{v'^2} = \left((\overline{U_4'^2} + \overline{U_2'^2})(4-HJ) + H((J-2)(\overline{U_3'^2}+\overline{U_1'^2}) + (H-2)(\overline{U_5'^2}+\overline{U_6'^2})) \right) /$$

$$2(4-2HJ+H^2(J-1))$$

$$\overline{w'^2} = \left((\overline{U_3'^2} + \overline{U_1'^2})(4-HJ) + H((J-2)(\overline{U_4'^2}+\overline{U_2'^2}) + (H-2)(\overline{U_5'^2}+\overline{U_6'^2})) \right) /$$

$$2(4-2HJ+H^2(J-1)) \qquad (4.26)$$

$$\overline{u'v'} = (\overline{U_3'^2} - \overline{U_1'^2}) / 2(2-H)$$

$$\overline{u'w'} = (\overline{U_2'^2} - \overline{U_4'^2}) / 2(2-H)$$

$$\overline{v'w'} = (\overline{U_5'^2} - \overline{U_6'^2}) / 2(2-J) \qquad (4.27)$$

Where $H = 1 + K1^2$, $J = 1 + K2^2$

Putting $K1=K2=0$, equations (4.25), (4.26), (4.27) reduce to equations (4.16), (4.17), (4.18).

4.5 Evaluation Of The Time Mean Average Velocity Terms $\bar{U}^2$, $\overline{U'^2}$

The problem now is to deduce the $\bar{U}^2$, $\overline{U'^2}$ readings for each particular orientation of the wire.

Since $\overline{U'^2} = \overline{U^2} - \bar{U}^2$ then knowing $\bar{U}^2$ terms if we could evaluate $\overline{U^2}$ terms we could then directly obtain the $\overline{U'^2}$

terms. Another method of analysis using $\overline{U^2}$ terms has also been developed (Ref.34), the correlation between the methods is shown in Appendix 4, the method does not depend upon differentiation of the velocity-voltage expression, (as does one of the following methods), but assumes some wave-form for E', and then uses the relationship.

$$f.(\overline{E^2}) = {}^1/t \int_o^t f.(E^2).\,dt$$

Very close correlation exists between the 3 (see Appendix 4) methods up to the validity limits of the analysis.

Knowing $\overline{U}$ and $\overline{U'^2}$ terms all equations of the type (4.25). (4.26) and (4.27) are solvable.

Two methods of evaluating the $\overline{U}$ and $\overline{U'^2}$ terms are possible one which is very simple and another which is slightly more complicated. The two methods give close agreement as shown in fig. (A4.4).

4.5.1 Method (1)

From fig.(A1.3) for unlinearised response we have assumed that from 4.2

$$E^2 = A + BU^{\frac{1}{2}} + CU$$

holds instantaneously,

whence, $$(\overline{E} + E')^2 = A + B\,(U + U')^{\frac{1}{2}} + C\,(\overline{U} + U')$$

for any instant of time.

Differentiation of the above response equation yields

$$2E\,\partial E/\partial t = \tfrac{1}{2}BU^{-\frac{1}{2}}\partial U/\partial t + C\,\partial U/\partial t$$

So for a maximum or minimum value $\partial E / \partial t = 0$ which is coincident with $E' = E'_{max}$ solution of the above differential equation gives

$$\partial U / \partial t = 0 \text{ when } \partial E / \partial t = 0$$

which means that E'_{max} and U'_{max} are coincident in time.
This means that we may write

$$(\bar{E} + E'_{max})^2 = A+B\ (\bar{U} + U'_{max})^{\frac{1}{2}} + C\ (\bar{U} + U'_{max})$$

similarly

$$(\bar{E} - E'_{max})^2 = A + B(\bar{U} - U'_{max})^{\frac{1}{2}} + C(\bar{U} - U'_{max})$$

Now in order to be able to solve the above equations for $\tilde{U}'$ and $\bar{U}$ in terms of the measured $\bar{E}$ and $\tilde{E}'$ we need to know the relationship between U'_{max} and $\tilde{U}'$ and E'_{max} and E'.
If we assume that E' and U' fluctuate with the same type of waveform then generally we may write :

$$(\bar{E} + n\tilde{E}')^2 = A + B(\bar{U} + n\tilde{U}') + C(\bar{U} + n\breve{U}') \qquad (4.28)$$

where

$n = +1.0$ for a square waveform ($\breve{U}' = U'_{max}$)
$n = \pm \sqrt{2}$ for a sinusodial waveform ($\hat{U}' = U'_{max}/\sqrt{2}$)
$n = \pm \sqrt{3}$ for atriangular waveform ($\hat{U}' = U'_{max}/\sqrt{3}$)

Equation (4.28) is a quadratic in $(\bar{U} \pm n\tilde{U}')$ which simply gives the values of $\tilde{U}'$ and $\bar{U}$ knowing A, B C, $\tilde{E}'$ and $\bar{E}$, and assuming a value of n based on the assumed type of waveform.

Comparative results are shown in fig. (A4.4) between different methods of analysis. The results quoted for method (1) are those assuming an n value of 1.0. The difference in the results obtained by using different values of n (ie different assumptions about the waveform) make very little difference to the calculated turbulence values of up to 50% turbulence intensity.

For a $\tilde{U}'/_U$ value of approximately 0.5 the difference in the calculated value of $\tilde{U}'/_U$ when n takes the value of $\sqrt{3}$ instead of 1.0 is approximately 3%.

4.5.2 Differentiation Method (2)

The $\bar{U}$ term may be evaluated by solution of the calibration equation (4.1) using the measured $\bar{E}$ value. The $\tilde{U}'$ term may then be evaluated by a procedure based upon differentiation of the velocity-voltage equation of type (4.2) and putting

$$\frac{E'}{U'} = \frac{dE}{dU}$$

So from (4.2)

$$E^2 = A + BU^{\frac{1}{2}} + CU \qquad (4.30)$$

diffn. w.r.t. U

$$2E\frac{dE}{U} = \tfrac{1}{2} B\bar{U}^{-\frac{1}{2}} + C$$

hence by putting

$$\frac{dE}{dU} = \frac{E'}{U'}$$

then :-

$$\frac{4\ E\ E'\ U^{\frac{1}{2}}}{U'} = B + 2\ U^{\frac{1}{2}}\ C \qquad (4.31)$$

Squaring both sides of (4.31) and substituting for $U^{\frac{1}{2}}$ from (4.30) we obtain :-

$$\frac{16\ E^2\ E'^2\ U}{U'^2} = B^2 + 4C\ (E^2 - A) \qquad (4.32)$$

To be able to use equation (4.32) for evaluation of $\overline{U'^2}$ terms we need to be able to express all the quantities in the equation as time mean average (measurable) quantities, (ie $\overline{E}^2$, $\overline{E'^2}$, $\overline{U}$ terms).

Clearly a time averaging technique could be employed, such that :-

$$\left(\frac{\overline{16\ E^2\ E'^2\ U}}{U'^2}\right) = B^2 + 4C\ (\overline{E^2} - A) \qquad (4.33)$$

The L.H.S. of equation (4.33) may be evaluated by using the fact that by definition :-

$$\overline{Z} = {}^1/_t \int_0^t Z.dt \qquad (4.34)$$

If we know how each of the terms in (4.33) vary with time.

If we assume that $E = \overline{E} + E'$, $U = \overline{U} + U'$ then we can say that U and U' fluctuate in phase, and similarly that E and E' fluctuate in phase. Since E' is produced by

U', and if we assume that the response of the anemometer is instantaneous, then we can say that E' and U' fluctuate in phase and similarly E and U. Hence all the values of the L.H.S. of (4.33) are in phase. The problem is to say how E' and U' fluctuate with time.

If we consider 3 possibilities :

(1) Square waveform

(2) Sinusodial Waveform

(3) Triangular waveform

Then the L.H.S. of (4.33) works out to be identical for each waveform.

It is not considered necessary to detail the evaluation of the integral for each waveform, as this is quite lengthy, and of standard mathematical form, but the result is quoted.

So :-

$$\left(\frac{\overline{E^2\,E'^2\,U}}{U'^2}\right) = \frac{\overline{E'^2}}{\overline{U'^2}}\left(\overline{E^2U} + 2\overline{E}\;\overline{E'}\;\widetilde{U'}\right) \qquad (4.35)$$

The result is the same for a sine wave, square wave, or a triangular waveform. Hence with a certain degree of justification it may be assumed to be independent of the type of waveform. The type of waveform as seen on an oscilloscope approximates more closely to that of a triangular waveform.

The analysis is considered valid until the onset of flow reversal at any one position, since at the onset of flow reversal the anemometer cannot differentiate between negative velocity and positive velocity and automatically reads any flow reversal as positive flow. If the following waveform is considered where E is the consequence of U, then E will follow U until the position where U = 0, but when U < 0, E increases until U = Minimum, decreases until U = 0 again and then follows U for the remainder of tne cycle until U = 0 again.

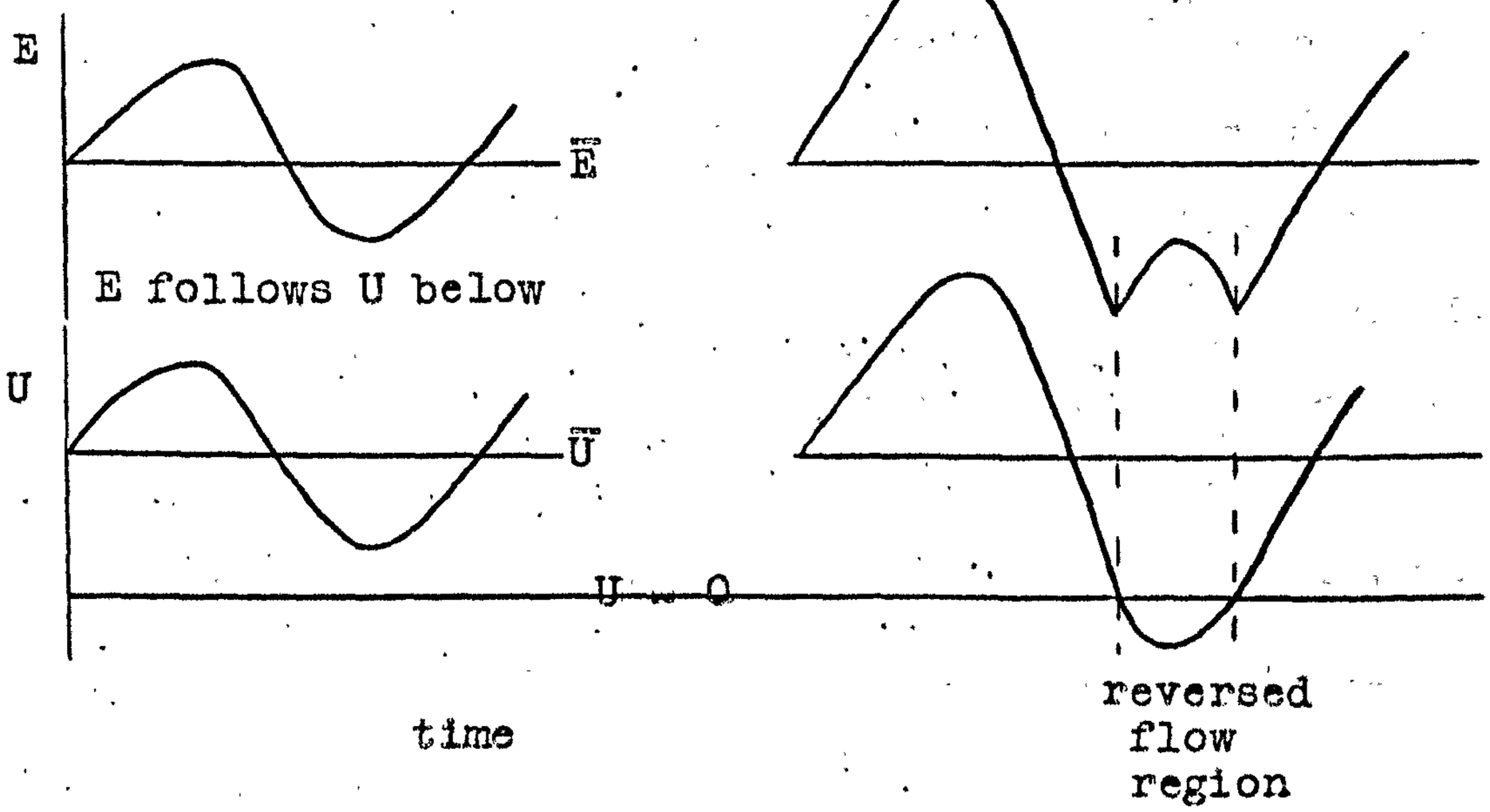

The onset of flow reversal puts a limit on the maximum turbulence intensity that may be measured, this maximum depends upon the type of waveform assumed for the fluctuating velocity, because flow reversal occurs when

$\bar{U} - U' < 0$, hence the limit occurs just when $U'max = \bar{U}$.

(a) For a square wave $(\overline{U'^2})^{\frac{1}{2}} = U'max$

and turbulence intensity limit = 1.0

(b) For a sine wave $(\overline{U'^2})^{\frac{1}{2}} = \frac{U'max}{\sqrt{2}}$

and turbulence intensity limit = .708

(c) For a triangular wave. $(\overline{U'^2})^{\frac{1}{2}} = \frac{U'max}{\sqrt{3}}$.

and turbulence intensity limit = .577

If we assume that the fluctuating velocity takes a triangular waveform then the maximum turbulence intensity is 57.7% that can be measured assuming the technique to be accurate. To be able to measure intensities greater than this it should be possible to correlate the R.M.S. and D.C. reading with the required R.M.S. and D.C. reading.

The use of a digital computer to work out the results is considered necessary to facilitate the speed and accuracy required. Programmes written in FOCAL for both 6 pt. and 3 pt. are included in Appendix 5.

The results quoted within the body of this thesis were those evaluated by method (2). The correlation between the two methods is shown in fig.(A4.4).

REFERENCES - CHAPTER 4.

(1) D.I.S.A. 55D00 Anemometer Handbook.

(2) Escudier M.P.
"The Turbulent Incompressible Hydrodynamic Boundary Layer"
Ph.D. Thesis Imperial College
London University (1967)

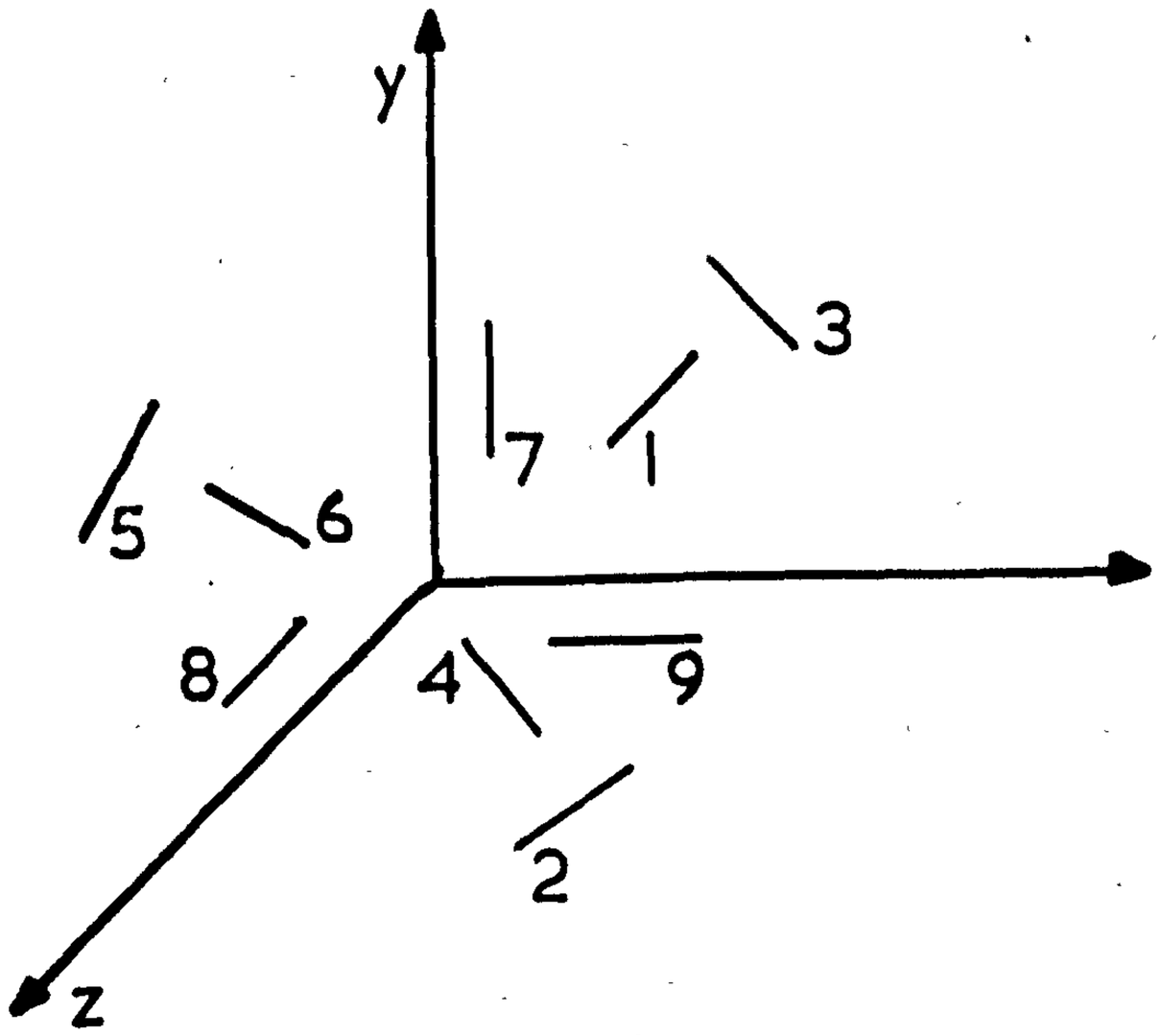

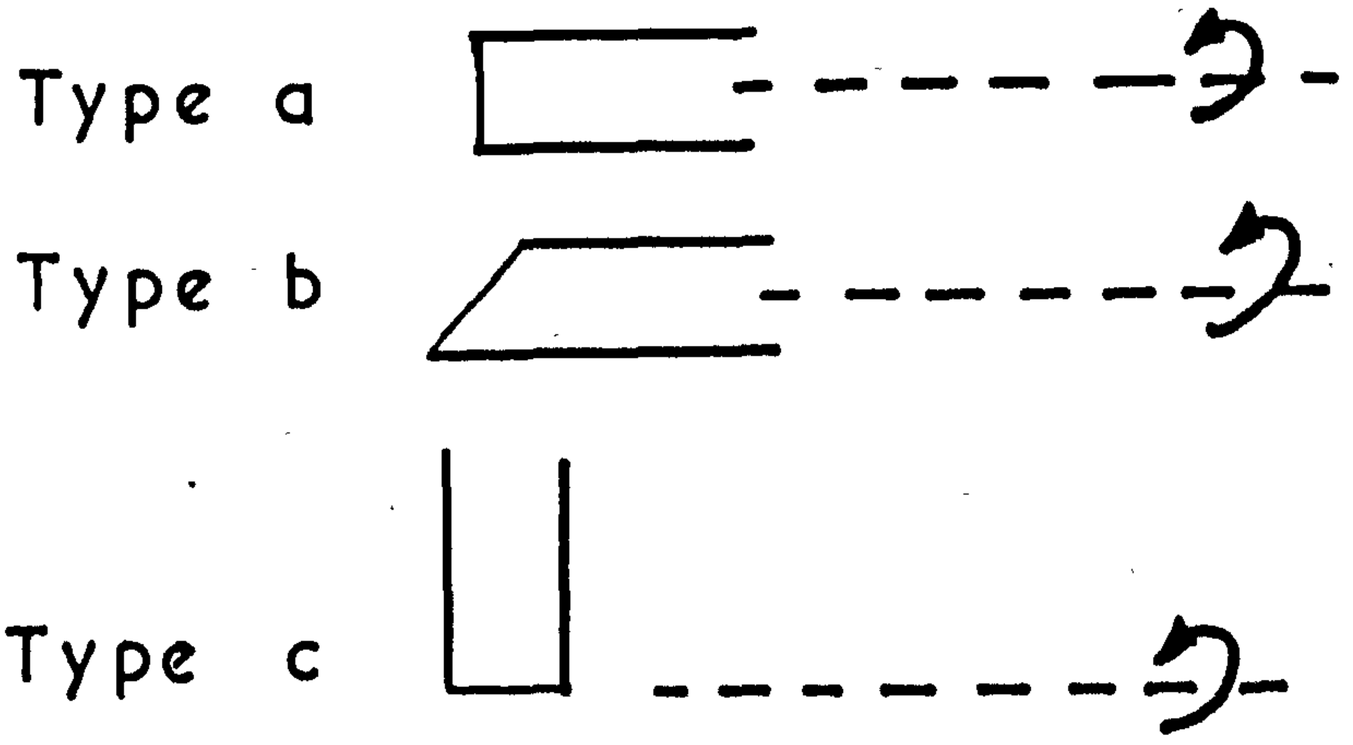

Type a - wire 90° to probe axis of rotation used for positions 5,6 & 7, 8

Type b - wire 45° to probe axis of rotation used for positions 1, 2, 3.4

Type c - wire coincident with probe axis of rotation used for position 9

Fig. 4.1 Hot wire probes and wire orientations

$$\tilde{u}' = \left[\overline{u'^2}\right]^{1/2} \quad \text{etc.}$$

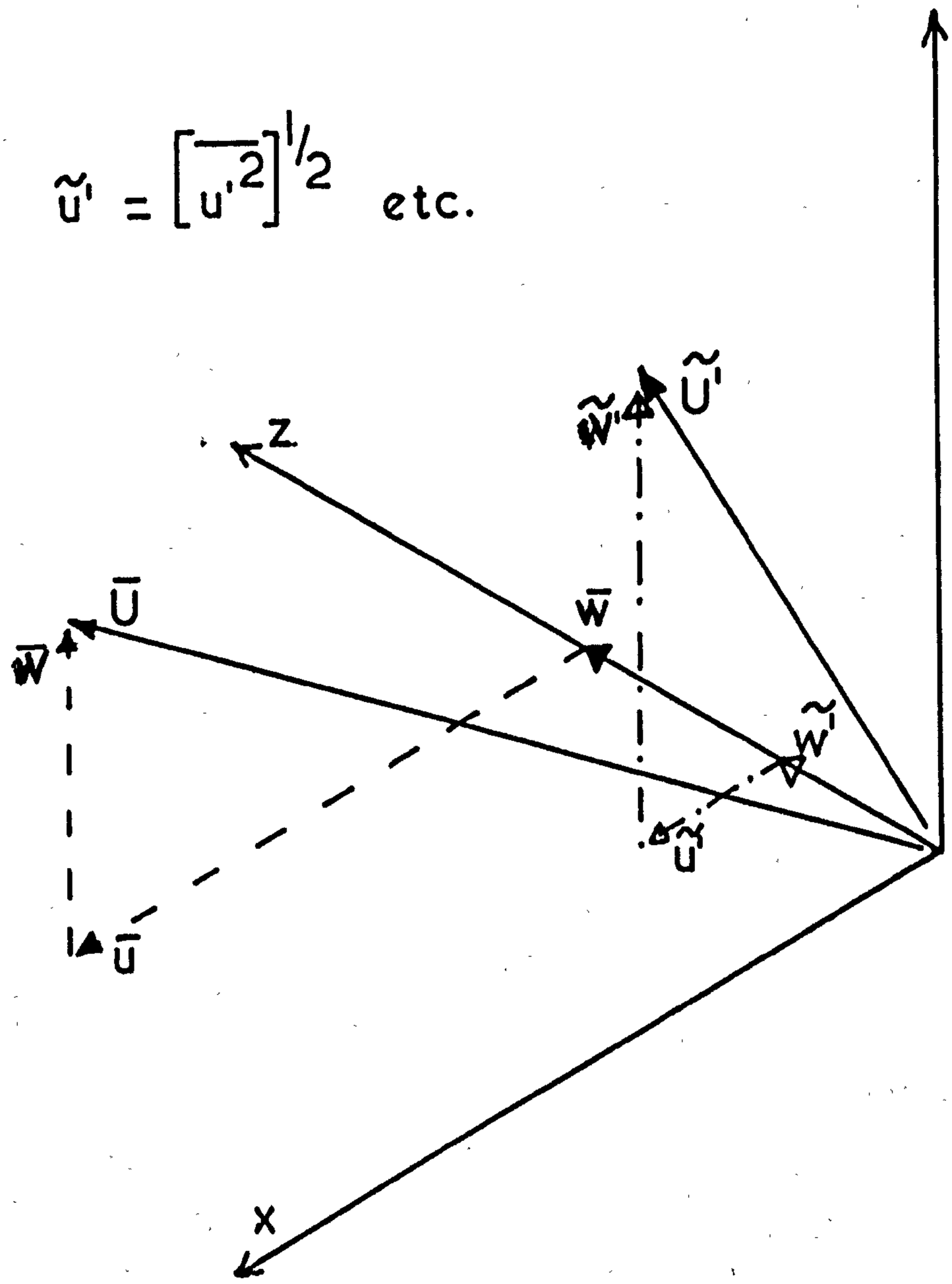

$\bar{U}$ - Total average velocity

$\tilde{U}'$ - Total r.m.s. fluctuating velocity

$\bar{U}^2 = \bar{u}^2 + \bar{v}^2 + \bar{w}^2$, $\tilde{U}'^2 = \tilde{u}'^2 + \tilde{v}'^2 + \tilde{w}'^2$

Fig. 4.2 Relationship between total and component velocities

CHAPTER 5

Results And Conclusions

5.1 Introduction

In order to mix one fluid with another fluid the designer often introduces the one fluid into the other fluid as a single jet. The particular application may be in order to burn a fluid within another, to mix two differant fluids as in a reactor or may be formed by flow through or round an obstacle. The system may be contained within a definite volume, and it is often desirable to obtain very high mixing rates between the two fluids in order to restrict the volume of the system, or the time taken to mix.

One method of increasing the rate of mixing between the two fluids is to rotate the jetting fluid thereby increasing the jet angle, increasing the turbulent motion of the jetting fluid, and decreasing the time and distance required to mix. Another method is to increase the number of jets whilst maintaining the same total volumetric flowrate. The process of splitting a jet up into a series of smaller jets increases the available "surface area per unit volume" of the jetting fluid enabling the mixing process to be completed in a shorter time. The individual jets are

correspondingly smaller and shorter and providing that each individual jet is turbulent (MMMMMMM) the subsequent rate of mixing of the two fluids will be greater. Until now the effect of rotation and the number and spacing of the jets upon the resulting turbulence and mixing characteristics has not been known, with the view to optimum design of the system.

The turbulent mixing of a single fluid stream with the surrounding fluid is greatly influenced by the close proximity of another fluid stream and the results of the aerodynamic investigation of multiple jet streams shows that the mixing is increased the further apart the individual fluid streams are, which again may be explained by the fact that the jetting fluid has a greater "surface area per unit volume" with which to perform the mixing processes, since as soon as the jets coalesce to form a combined jetting fluid the total surface area per unit volume is necessarily decreased. A series of jets in a line closely spaced soon become a single two dimensional jet whose mixing rate is less than that of the sum of the individual jets.

Much higher mixing rates may be achieved by rotation of each of the individual fluid streams. This fact becomes increasingly important when one considers that the volume of the system may be so restricted that close packing of the jets is essential. The direction of rotation of each

individual fluid stream also has an effect on the subsequent mixing rate and it is found that rotation of each individual jet in the same direction leads to greater mixing rates than jets having alternate directions of rotation.

5.2 Single And Multiple Jet Flames. Qualitative Results

5.2.1 Central Argument Concerning Observed Flame Interactions

It has been shown that flame interactions may occur when 3 identical flames are brought close together such that firstly the overall visible flame length is increased and secondly on bringing the flames closer together the central flame becomes unstable and lifts off the burner rim and is either stabilised further downstream, or causes the system as a whole to 'blow off.' These effects are shown to occur both for swirling and non-swirling jet flame systems, and may be explained from a purely aerodynamic interaction point of vie by consideration of the mixing entrainment, velocity and turbulence quantities contained in the experimental results and their relevance to flame stability.

From consideration of the effect of the pitch of the jets upon the resulting jet velocities, turbulence intensity, mixing rates and entrainment rates in the region between adjacent jets, and also in the outer regions of the jet system, it may be seen that the aerodynamic factors which determine flame stability are affected in such a manner as to reduce and eventually destroy the flame stability in these regions. The result is that the central flame either lifts off the burner rim and is stabilised further downstream, or the system

as a whole 'blows off' depending upon the severity of the interaction. The fact that the central jet is stabilised further downstream is mainly due to the fact that the adjacent jets, which themselves are stable, provide the heat source to combust the gases in a region where the velocity has reduced to that of the flame velocity for the gas mixture.

5.2.2 Observed Multiple Jet Flame Interactions

Simple flame interactions were observed for systems of 3 swirling and non-swirling free jet flames. The nozzles were the same ones used for the cold aerodynamic study and were positioned vertically at 1.25 and 2.0 diameters apart. Each nozzle was fed with a separately monitored premixed propane air gas mixture.

A horizontal enclosed system of 2 swirling jet flames 1.25 diameters apart was also observed. The flames could be fed with either propane/air or kerosine/air mixtures by using a pressure jet atomiser for the kerosine. The fuel and air was again individually metered to each jet.

Non-Swirling Propane/Air Flames

Plate (P5.1) shows three adjacent non-swirling jet flames in a stable condition 1.25 diameters apart. On increasing the total flowrate to each jet a condition is reached where the central flame lifts off the burner rim and burns further downstream - see Plate (P.5.2). On further

increase of the total mass flowrate the whole flame system 'blows off' completely. These two stable burning conditions were similarly observed for flames placed 2.0 diameters apart though higher flowrates were necessary to promote lift off of the central jet flame, and 'blow off' of the whole system. The combined visible flame lengths were some 40% greater than the single flame length and was correspondingly greater for the 1.25 diameter apart condition.

The lift off of the central flame may be explained by the destruction of the flame stabilising effect associated with the low velocity regions on the edge of the jet flame close to the nozzle as mentioned in the central argument and detailed in section 4 of this chapter. In these regions the stability is dependant upon the fact that low velocities, and high velocity gradients giving high shear and high degrees of mixing and entrainment, give conditions where the flame is stabilised.

Due to the close proximity of an adjoining jet flame the local velocity is increased with a corresponding decrease in velocity gradients, shear stress, mixing and entrainment terms to conditions where the flame is no longer stabilised and the central flame tends to 'blow off'. The flame system may however be stabilised by the adjacent outer jet flames which

are themselves being stabilised by the low velocity regions associated with their outer edges. The system of flames may 'blow off' as a whole on further increase of the total mass flowrate in the same manner as a single jet flame 'blows off' when the flowrate is too large. (See section on flame stabilisation, 'blow off' and 'flash back' in chapter 2).

The combined jet flame lengths are longer for the same reason that the reduced mixing and entrainment leads to higher velocities, lower combustion intensities and consequently longer flames.

As stated previously the interaction effects are more severe the closer together the jets are and so the velocities which promote 'lift off' and 'blow off' of a jet flame system are lower the nearer together the flames are positioned. Similarly the overall flame length is greater the nearer together the flames are positioned.

Swirling Propane/Air Flames

Plate (P5.3) shows three adjacent swirling jet flames in a stable condition 1.25 diameters apart. On increasing the total flowrate the central flame lifts off the burner rim as observed previously for the non-swirling jet flames (Plate P5.4). The velocities necessary to promote lift off were very much greater than those for the non-swirling jets and on further increase of the total flowrate the combined jets did not 'blow off' at the maximum flowrate obtainable which was some 500% greater than that which produced blow off of the non-swirling jet flames. The overall combined flame lengths were again some 40% greater than the single flame length. Very much higher flowrates were necessary to lift off the central flame for the flames placed 2.0 diameters than for those placed 1.25 diameters apart.

Clearly the stability of the swirling jet flames is very much greater than those of the non-swirling jet flames due partly to the fact that the mixing and turbulence quantities close to the nozzle exit are very much greater for swirling jet flames than for non-swirling jet flames, (see section 3 of this chapter), and partly to the presence of the of the low velocity region on the axis of the jet and close

to the nozzle exit associated with swirling type flames.

The system was operated for jets swirling with the same direction of rotation "out of mesh" and for alternate jets having different directions of rotation "in mesh". The results were qualitatively the same but higher velocities were required to promote lift off of the central jet flame with jets swirling "out of mesh" which again supports the results of the aerodynamic investigation where greater mixing rates, turbulence quantities and lower velocities were obtained for jets swirling 'out of mesh' which indicates greater flame stability (see section 5 of this chapter).

Two Enclosed Swirling Jet Flames

The metal flame box was of the same dimensions as the perspex box used for the cold aerodynamic study. The system was set up to view the visible overall flame length of one jet flame and to compare these with the visible flame length of two adjacent jet flames spaced 1.25 diameters apart. The type of fuel could be changed from gas (propane) to kerosine (pressure jet atomiser) to see if the type of fuel had any effect on the result. The propane/air is essentially a premixed air fuel system whereas the kerosine/air is not and is considered more representative of Marine Boiler practice

The results were identical for both types of fuel, the combined flame lengths being some 30-40% greater in each case.

5.2.3 Conclusions For Observed Multiple Jet Flame Interactions

The close proximity of one flame to another affects the flame stability of both flames and the effect increases the nearer together the flames are. In the region between the jets the jet flames interact and combine to give velocity gradients which are reduced, with a corresponding reduction in the mixing and entrainment rates, which in turn gives rise to less intense combustion higher velocities and longer flame lengths.

For a jet flame positioned in between two similar jet flames these factors destroy the stability of the central flame with the result that the central flame tends to blow off.

Rotation of each of the individual jets greatly increases the flame stability and combustion intensity of each jet, with the result that very much higher flowrates are necessary to obtain flame interactions for any set configurations. Systems in which adjacent jets rotate 'out of mesh' are more stable than those where adjacent jets rotate 'in mesh' the reason being attributable to the fact that adjacent jets swirling 'out of mesh' have higher shear terms because the swirl velocities of adjacent jets are opposed.

The change in flame length can be considerable and the type of fuel (propane or kerosine) had no effect upon the results.

5.3 Single Swirling Free Jet Of Variable Swirl

5.3.1 Central Argument For Single Swirling Free Jets Of Variable Swirl

The turbulent mixing of a single jet with the surrounding fluid is greatly influenced by the degree of rotation of the jet. The degree of rotation has been characterised by the swirl No.S which varies from zero for a non-swirling jet to 0.6 for a strongly swirling jet. Higher swirl numbers correspond to jets having a very high degree of rotation often with reversed flow on the axis and close to the nozzle exit of the jet.

Increase of the swirl number for a single swirling jet increases the angle of spread of the jet thereby increasing the total"surface area per unit volume" of the jet for mixing with the surrounding fluid. The velocity gradients close to the nozzle outlet are increased to such an extent that much higher shear occurs in these areas giving rise to shear stress terms which are higher than those found for the non-swirling jet. The intensity and length scale of turbulence is so increased that mixing of the jetting fluid proceeds at a much more rapid speed than that of the non-swirling jet, and coupled to the fact that the available surface area of the jet is increased the resulting rate of mixing is greatly increased. The resulting swirling jet dissipates its turbulent

energy much more rapidly and after a few diameters downstream the mixing has been so accomplished that the velocity, velocity gradients, and resulting shear terms are now reduced to values less than those found with a non-swirling jet which is still mixing with the surrounding fluid. The changeover point at which these turbulence or mixing parameter change from being larger to smaller for a swirling jet is typically between 3 and 5 diameters downstream from the nozzle exit for the range of swirl numbers encountered.

5.3.2 Results For Single Swirling Free Jets Of Variable Swirl

The flow conditions mentioned in Chapter 3 gave a jet of variable swirl corresponding to swirl numbers (S) of 0, 0.2, 0.5 and 0.6. The axial velocity profiles were measured for these jets and compared favourably with those obtained by Chigier and Chervinsky (ref.32) (see fig.5.1). At x/D values greater than 8.0 all jets have the $\bar{u}_{max}$ value on the axis of the jet, and provided the $\bar{u}_{max}$ value is on the axis of the particular jet considered the axial velocity profiles may be characterised by equations of the type (2.17). For the axial decay of $\bar{u}_{max}$ equations of the type (2.19) may be used.

It is found that the turbulent velocity fluctuations close to the nozzle exit are greater, the greater the swirl number this being due partly to the fact that the fluid has to take a more tortuous route out of the nozzle exit, and partly to the fact that very high axial and swirl velocity gradients exist in the nozzle exit giving rise to high shear. Fig.5.2 shows that each of the 3 normal stress terms $\tilde{u}'$, $\tilde{v}'$, $\tilde{w}'$ have higher values as S increases for regions of $x/D < 3$. All graphs show a cross over point in the region of $x/D = 3.5$ beyond which the increase in S results in a decrease in the normal stress terms. A similar trend is shown for the shear stress terms for which one term $\overline{u'v'}$ is quoted (see fig.5.3). The decrease in the shear stress values with increase in S for $x/D > 4$ is attributable to the lower velocity gradient terms as mentioned in the central argument. The maximum relative kinetic energy KE_{max} $(=I^2_{max})$ contained by the fluctuating velocity is some ten times greater for a swirl No. of 0.6 and $x/D = 1$ than for a non-swirling jet.

In general the turbulence characteristics are anisotropic with $\tilde{u}'$ terms having higher values than $\tilde{w}'$ are $\tilde{v}'$.

It can be seen clearly that the high shear rates ascribed to swirling jets can only be found in the region $x/D < 3.0$. At $x/D = 1.0$ the shear stress is increased by a

factor of 3 when S increases from zero to 0.6.

Figure 5.3 also shows that the rate of entrainment in swirling jets is higher than that of non-swirling jets in the region $^{x}/_{D} < 6.0$ but subsequently the rate is the same for both cases. The total amount of entrained fluid at any axial station will however be greater for swirling jets than for non-swirling jets. The reduction in the rate of entrainment of swirling jets with increasing axial distance may be explained by the fact that the swirl velocity decays at a very much faster rate than the axial velocity, and hence the slope of the curve (rate of entrainment) decreases with the decreasing swirl until the swirl component is negligible ($^{x}/_{D} > 6$) and then the jet entrains at the same rate as that of a non-swirling jet. These results do not agree with the empirical equation put forward by Chigier and Chervinsky (Ref.1.):-

$$\frac{M_e}{M_o} = (0.32 + 0.8\ S)\ {}^{x}/_{D}$$

A comparison of the experimental data obtained by the Author and that of Chigier and Chervinsky shows that they are in general agreement, whereas that of Kerr and Fraser (Ref.2) does not agree to the same extent and there is no justification in considering that the rate of entrainment

is constant with axial distance for any swirling jet.

The radial position at which the axial velocity is a maximum is shown also in fig.5.3. For non-swirling jets the maximum is always on the axis of the jet. As the degree of swirl is increased the position of $\bar{u}_{max}$ is pushed further away from the axis. Once the swirl velocity ($\bar{w}$) has decayed with axial distance to a value which is negligible w.r.t. that of the axial velocity ($\bar{u}$) so the position of $\bar{u}_{max}$ coincides with the axis of the jet as with a non-swirling jet.

Comparison of fig. 5.3 with fig. 5.1 shows the greater decay of swirl velocity with axial distance than that of the axial velocity.

The fluctuating components of velocity are shown in fig.5.4 for 3 axial stations with a swirl number S of 0.6. The $\overline{u'^2}$ and $\overline{w'^2}$ are of similar magnitude but greater than $\overline{v'^2}$. The maximum values of $\overline{u'^2}$ and $\overline{w'^2}$ are found in the regions of maximum axial velocity ($\bar{u}$) (see fig.5.1) and swirl velocity ($\bar{w}$) respectively. The shear stress components are (fig.5.5) are seen to have values which are approximately one half those of the normal stresses, but have a totally different form. It is seen that for a strongly swirling jet all the components of the stress tensor are important. The $\overline{u'w'}$ term is always +ve whereas the $\overline{u'v'}$ and $\overline{v'w'}$ terms display both -ve and +ve values.

The rapid decay of I with $^{x}/_{D}$ is shown in fig.(5.6). At values of $^{x}/_{D} > 4.0$ the kinetic energy ($KE = I^2$) is evenly spread throughout the central region of the jet, whereas for $^{x}/_{D} < 4.0$ the maximum energy is situated close to the regions of maximum axial velocity and in the case of $^{x}/_{D} = 1$ the energy at $^{r}/_{D} = 0.5$ is some 4 times that on the axis. The maximum I value of 0.36 found at $^{x}/_{D} = 1.0$ is three times the maximum value of 0.12 found for a non-swirling jet.

For non-swirling jets where the effective viscosity does not vary greatly throughout the jet there is a simple relation between the shear stress $\overline{u'v'}$ and the mean velocity gradient $\frac{d\bar{u}}{dr}$. This is shown clearly in fig.5.7. For the strongly swirling jet the relation between $\overline{u'v'}$ and $\frac{d\bar{u}}{dr}$ is is more complex and account needs to be taken of other terms in the equation of motion which now become significant. The comparison shows that there still is a relation between the forms of the distribution of the curves.

The Boussinesq Eddy Viscosity (ε) for the non-swirling jet has a value close to $(\frac{\rho R \bar{u}_0}{100})$ up to $^{x}/_{D}$ values of 12 and is fairly constant throughout the jet, but for the strongly swirling jet the turbulence models of Boussinesq and Prandtl break down and are no longer useable. From measurements of normal and shear stress terms, and knowing the velocity

gradients it is possible to calculate the effective viscosity terms in equations of the type 2.21. The distribution of these effective viscosity terms are difficult to measure in such a small system as a 1 inch diameter swirling jet, but the radial variation of μ_{zz}, μ_{oo} and μ_{rr} for one particular case is shown in fig.5.8. In making predictions for swirling jet systems Spalding and Pun (Ref.3) have assumed that the effective viscosity is isotropic whereas fig.5.8 shows that the effective viscosity must be considered to have components which vary in each of the equations relating stress to velocity gradients.

A comparison of the spatial distributions of $\bar{u}$, I and $\overline{u'v'}$ contained in the appendix in figs (A6.1), (A6.2), (A6.6) and (A6.7), show the considerable changes brought about in a single jet as a consequence of swirl. The magnitudes of the turbulence quantities I and $\overline{u'v'}$ are higher in the swirling jet particularly close to the nozzle exit. The mean velocity gradients and the associated shear stresses give rise to $\overline{u'v'}$ terms which are +ve and -ve in single swirling jets, and for $^{x}/_{D}$ values greater than 8.0 the $\overline{u'v'}$ terms are much lower than those found in the non-swirling jet. These spatial distributions help the reader to visualise the overall distribution of the turbulence and

mean flow characteristics in a system and are particularly useful for comparison with the multiple jet data presented later.

5.3.3. Conclusions For Single Swirling Jet Of Variable Swirl

The introduction of swirl greatly modifies the velocity and turbulence distributions with a jet. On introduction of swirl the jet widens out and the maximum velocity close to the nozzle exit moves to a position away from the centre line. The velocity gradients within the jet are greatly increased along with the corresponding shear terms. The mixing rates are thereby increased close to the nozzles and the resulting jet entrains and mixes a greater rate than the non-swirling jet with the result that the length of the je and time required to mix is reduced. This gives rise to the fact that after about 4 diameters downstream the jet has exhausted its relatively higher turbulence and mixing properties and the mixing and entrainment rates fall off to values close to that of the non-swirling jet. Although the normal and shear stress terms are now less in magnitude than those found in the non-swirling jet, the area over which the jet has spread is much greater and for the case of a strongly swirling jet (S = 0.6) a cross section of the jet

at $^{x}/_{D}$ = 8.0 shows a uniform well stirred distribution.

There appears to be a well defined change-over position where the maximum turbulence values found in a swirling jet become less than those found in a non-swirling jet. This position occurs at about 3 to 4 diameters downstream and is attributed to the fact that the swirl velocities in a jet decay at a very much greater rate than the axial velocity, with a correspondingly rapid decrease in turbulence quantities. Because the axial velocity, in a swirling jet also decreases faster than that of a non-swirling jet, a position is reached where the velocity gradients and corresponding turbulence quantities are less than those found in a non-swirling jet, but are distributed over a greater cross sectional area.

Study of the turbulence distributions in a swirling jet should aid the designer of swirling jet flames to be able to introduce the fuel in the region of maximum shear to promote greater mixing rates since although a swirling jet flame is capable of burning a much higher quantity of fuel than a corresponding non-swirling jet, some difficulty is found sometimes in completing combustion if most of the fuel is not burnt in these regions close to the nozzle exit.

5.4 Multiple Non-Swirling Jets

5.4.1 Central Argument For Multiple Non-Swirling Jets.

The turbulent mixing that occurs between adjacent jets and the surrounding fluid is greatly influenced by the distance apart of the jets.

The close proximity of one jet upon another produces an interaction in the regions between the jets, which gives rise to a damping of the turbulent motion of the fluid particles. The high velocity gradients and high shear associated with the outer edges of single jets are destroyed due to the higher velocity of the adjacent fluid stream and resulting regions of high axial velocity and lower velocity gradient give mixing rates and turbulence quantities which are reduced compared to the single jet values.

The decrease in the length scale of turbulence and the associated lower mixing rates means that the rate of entrainment into the jetting fluid is reduced giving higher velocities and longer jet lengths. The close proximity of one jet to another produces a pushing apart effect which gives rise to jet deflection of the outer jets, but in regions far enough downstream the jets coalesce to form a combined jet system.

5.4.2 Results For Multiple Non-Swirling Jet Systems

The interaction between multiple non-swirling jets is greatly affected by the variation in the pitch between the jets. Maximum interaction occurs when the jets are adjacent to each other (ie. the jet centres are 1 diameter apart; P = 1) and the effect of interaction diminishes. rapidly as the jets are moved apart. A comparison of mean velocity and turbulence characteristics are given for 2 cases of 3 jets with pitch (P) of 1.25 and 2.0 in figs. (5.9) and (5.10). These figures show radial distributions at $x/D = 2,4,8,16$. The way in which the jets merge can be follo by observing the mean velocity distribution $\bar{u}/\bar{u}_{max}$.
Shear stress distributions follow closely the mean velocity gradients with points of inflection in the mean velocity curve associated with zero shear stress, and the positions of maximum shear coincide with regions of maximum mean velocity gradient. As the jets merge the turbulence intensities are reduced in the region between the jets, and the position of maximum velocity on the outer jet is seen to move outwards, these effects being greater the smaller the value of P. At $x/D = 16$ the 3 jets have practically combined and are forming a single jet with its axis on the centre line of the central jet. Measurements show that by $x/D = 30$ the jet system is

practically symetrical in the horizontal and vertical planes. The local turbulence intensity I_{loc} and the mean velocity $\bar{u}/\bar{u}_{max}$ show the "mirror image" effect common to all non-swirling jet systems where low velocity corresponds to high turbulence and vice versa.

Interaction causes the jet axis of the outer jet to be deflected. This deflection is shown in fig.(5.11) for two values of P = 1.25 and 2.0. The deflection is greater the smaller the value of P (ie. the nearer the jets are). Interaction also results in a slower decay of mean velocity and a lower intensity of turbulence as shown in fig.(5.12), the value of P = 2.0 lies practically mid-way between the P = 1.25 and P = ∞ value. This graph illustrates clearly the "mirror image" effect shown previously, and for the case of P = 1.25 and x/D = 2.0 the $\bar{u}_{max}$ is increased by some 25% over that of a single jet (P = ∞). This increase in jet length is attributable to the reduction in the entrainment of the central jet due to the close proximity of the outer jets. The reduced entrainment is due in turn to the reduction of the mixing rates (shown by the reduction in I values) in the region between the jets. In fact one may say that adjacent non-swirling jets tend to 'damp out' the turbulent mixing in these regions.

The turbulence models put forward by Prandtl and Boussinesq vary slightly throughout a multiple jet system and fig.(5.13) shows a typical variation for 3 jets 1.25 D apart 4.0 diameters downstream.

The effect of variation of pitch upon the velocity and turbulence intensity values is summarised in fig.(5.14). The maximum interaction effect of reduced decay of axial velocity, and reduced turbulence intensity is at P = 1 when the jets are adjacent. Beyond P = 3 the interaction effects are small and P = ∞ corresponds to a single free jet. The turbulent damping is greater for the central regions between jets than for the outer region of the jet system, and fig. (5.15) shows how the predominent shear stress $\overline{u'v'}$ is reduced in this region. The reduction of the shear stress terms is due to the interference of the jets and beyond $^{x}/_{D}$ = 12 the maximum shear stress in the central jet region is reduced by over 50% as P is reduced from ∞ to 1.

Spatial distributions (A6.3) (A6.4) and (A6.5) for multiple non-swirling jets when compared with figs. (A6.1) and (A6.2) for single non-swirling jets show visually how the turbulence and mean flow characteristics are greatly affected and should be referred to by the reader.

5.4.3 Conclusions For Multiple Non-Swirling Jet Systems

The results show that interference causes a damping of the turbulent motion of the fluid particles particularly in the region between the jets. In order to obtain maximum mixing rates and minimum jet lengths it is desirable to have the jets as far apart as possible. Since it is desirable for flame stabilisation to have high I values (increased flame speed) and low $\bar{u}$ values for each individual jet flame, and for flame length considerations to have low $\bar{u}$ values and high I and $\overline{u'v'}$ values which give rise to higher mixing rates and consequently shorter flames, it is clearly shown to be advantageous to have the value of P as large as possible, (which is also shown to be the case in the results of the Multiple Non-Swirling Jet Flames).

For non-swirling jet systems high $\bar{u}$ values generally correspo to low I values and vice versa a fact which helps the designe to visulise the overall turbulence and mixing characteristics of multiple jet systems.

5.5 Multiple Swirling Jets

5.5.1 Central Argument For Multiple Swirling Jets

The turbulent mixing that occurs between adjacent swirling jets and the surrounding fluid is influenced by the distance apart of the jets and the direction of rotation of the individual jets.

The effect of bringing together two swirling jets is to reduce the turbulence quantities and mixing rates. For regions close to the nozzle exit the turbulence quantitie are still very much higher in value than those found in the non-swirling jet systems, and although interaction leads to a damping of the turbulent fluid motion between adjacent jets the effect is less than that experienced in non-swirling jet systems. The reduction in the turbulence quantities is more marked for jets swirling "in mesh" than "out of mesh" due mainly to the fact that the swirl velocity gradients and corresponding shear terms are very much greater for jets swirling "out of mesh" since the swirl velocity directions are opposed in the region between adjacent jets.

Jets in line swirling 'out of mesh' are more symmetrical about a horizontal line drawn through their centres than jets swirling 'in mesh' which show asymmetric distribution in the vertical plane.

5.5.2 Results For Multiple Swirling Jets

In most practical systems swirl is introduced with rotation in the same sense in each burner so that at the poin of contact adjacent jets are 'out of mesh' which means that their swirl velocities are going in the opposite direction. It was considered of interest to investigate the effect of variation in the sense of the direction of the swirl for adjacent jets and typical comparative results are shown in fig.(5.16). The difference between the two systems is clearly seen in the tangential velocity distributions. For the 'in mesh' system the jets attempt to combine whereas with the 'out of mesh' system the jets tend to push each other apart. This may be seen by comparison of the $\bar{u}$ distributions of fig (A6.8) and (A6.9). Intensities of turbulence are high in both systems and there is some increase in the turbulence with the 'out of mesh' system. The fact that the 'in mesh' jets tend to combine more readily than the 'out of mesh' jets leads to higher maximum $\bar{u}$ values in the central regions.

It is particularly interesting to note that the $\bar{u}$ distributions for the 'in mesh' system has two peaks as shown in the graph whereas the 'out of mesh' system has 3 peaks. The shear stress in the 'out of mesh' system is typically higher than that of the 'in mesh' system.

The differences between the 'in mesh' and 'out of mesh' systems are most marked when P = 1 and in the region close to the nozzle ($^{x}/_{D} < 3.0$). Beyond $^{x}/_{D} = 3.0$ there is little effect of variation of pitch and meshing sense. These results are summarised in fig. (5.17) and (5.18). As mentioned previously the intensities of turbulence in swirling jets is so high in the regions close to the nozzle exit that variation in pitch and meshing sense have far less effect than for the non-swirling jet systems, what effect there is occurs at low values of P and is more marked for velocity than turbulence terms.

Taking figs. (5.18) and (5.19) together the advantage of swirling "out of mesh" over "in mesh" for conditions of high intensity combustion (as may be found for example in a marine boiler) are clearly seen especially in the regions close to the nozzle exit and for values of P less than 2.0.

Figs. (A6.8) (A6.9) (A6.10) and (A6.11) show the spatial distributions of $\bar{u}$ and I for swirling jets "in mesh" and "out of mesh" 1.25 and 2.0 diameters apart. The results are more complex than the non-swirling multiple jet data presented previously, but help to show particularly the greater spread of the "out of mesh" system and the increased velocity terms of the "in mesh" system.

5.5.3 Conclusions For Multiple Swirling Jets

By the introduction of swirl it is possible to obtain high mixing rates and relatively low velocities close to the nozzle exit for multiple jet systems which gives conditions which are still favourable for stable flames and rapid combustion when multiple jet flame systems are considered. There are still marked interaction effects which vary with the distance apart of adjacent swirling jets but the interference is not as great as experienced in the multip non-swirling jet systems. The direction sense of the swirl velocity to each jet also has an affect upon the degree of interaction, and it is found that adjacent jets each having the same direction sense for the swirl velocity (termed "out of mesh") display less interaction affects, greater stability and uniformity, and give conditions which are much more suitable to multiple jet flame systems.

5.6 General Conclusions And Recommendations For Further Work

5.6.1 General Conclusions

For the specific conclusions relevant to each aspect of the research, the reader is referred to the particular conclusions at the end of each section in this Chapter. The general conclusions may be briefly summarised as follows :

(a) Swirl greatly increases the turbulence and mixing characteristics of a single jet particularly in region close to the nozzle. After about 4 diameters downstream the maximum turbulence values are less than those found in non-swirling jets but the overall mixing is still greater.

(b) Aerodynamic interaction between adjacent jets in a multiple jet system produces a 'damping' of the turbulent motion of the fluid particles within this region, giving a reduction in the value of turbulence and mixing characteristics.

(c) Non-swirling jets show markedly more interaction effects than the corresponding swirling jet configurations.

(d) The effect of interaction decreases with increasing distance apart of the jets (Pitch - P) and swirl $N^c(S)$ and beyond P = 4.0 very little interaction was observed for

distances up to 12 diameters downstream.

(e) The aerodynamic interaction effects go a long way to explain and predict flame interactions particularly flame length, mixing and stability characteristics.

(f) Multiple and particularly swirling jet systems show that simple relationships between the velocity gradients and the shear stress terms are no longer valid, and that effective viscosity terms may vary significantly throughout a flow field.

5.6.2 Recommendations For Further Work

The method of analysis for the hot wire anemometer contained within this thesis may be used to separate out the 9 components of the average and fluctuating velocity terms in any cold isothermal aerodynamic system, into which it is possible to place a hot wire probe without interferring too much with the flow field. The information may then be used to calculate the spatial distribution of related properties such as effective viscosity. The Author has shown how such a property may vary from position to position within a flow field and for the particular case of prediction proceedures aimed at predicting the behaviour of rotating or recirculating fluid flow systems, a knowledge of the variation of these effective viscosity terms would be useful.

The above investigation would necessitate very many careful readings in a flow field that was very large in relation to the probe size since large errors in interpolation may otherwise be incurred.

It would be possible to use the analysis and probing technique to measure velocity and turbulence characteristics of swirling jets which have reversed flow (ie. recirculation) within the jet, or indeed of any recirculating flow system. Here the problems associated with the interpretation of the sign (ie. + ve or - ve) of the velocities within such a jet could be overcome by firstly probing with a 5 hole pitot probe to find the positions at which the velocity changed sign from - ve to + ve and vice versa, and subsequently using these changeover positions to reverse the probing direction of the hot wire probes to eliminate interference of the probe supports on the hot wire itself. It would be interesting to know how multiple jet interactions affect the size and position of this recirculation zone, particularly from the stability viewpoint of multiple jet flames.

A detailed study of the velocity and mixing processes contained within two identical burning and non-burning multiple jet systems would be interesting to relate the predicted and observed flame stability, interaction and

and mixing rates with a view to accurate prediction of flame interactions.

A study of the aerodynamic shear stress and turbulence distribution close to the nozzle of a burner used to burn atomised fuel oil with a view to design of the atomiser and position of introduction of the atomised fuel within such a flow field to obtain maximum air/fuel mixing and complete combustion.

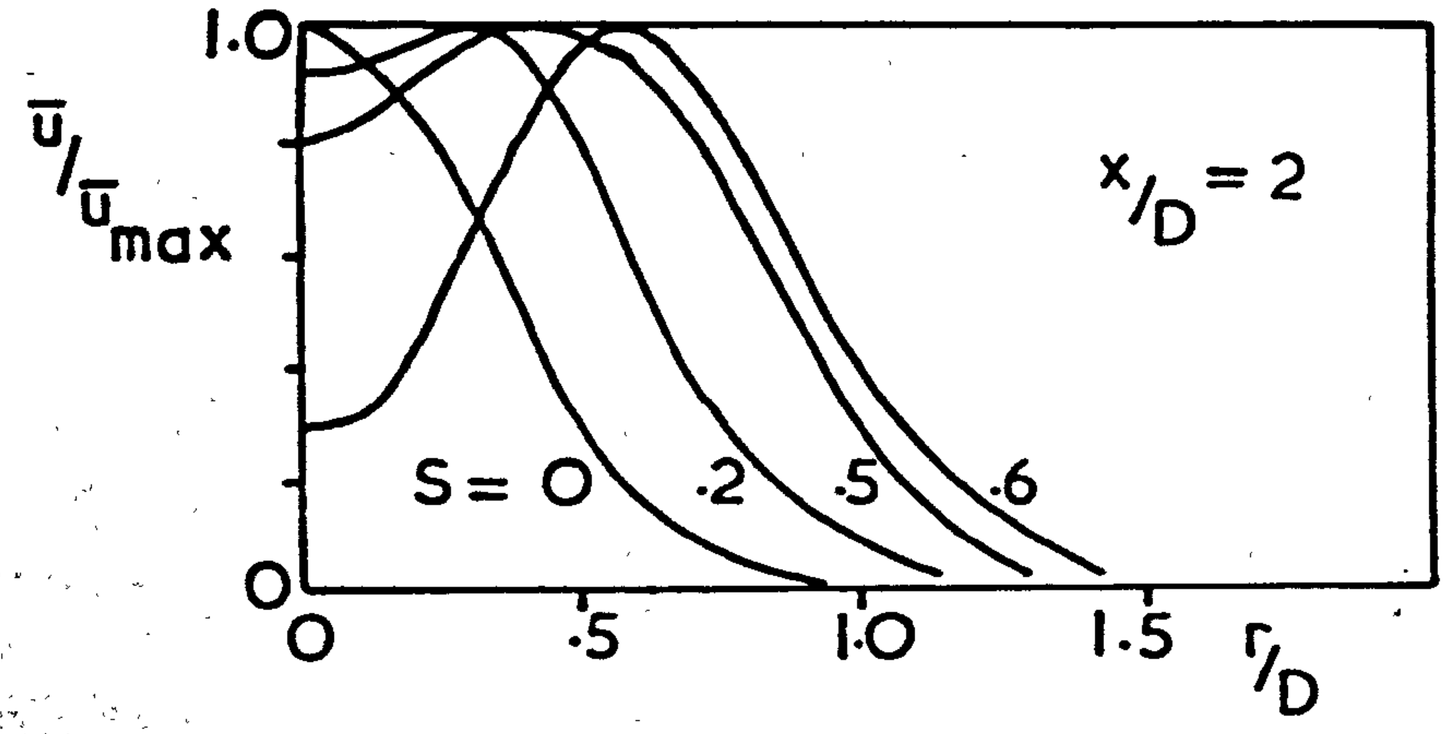

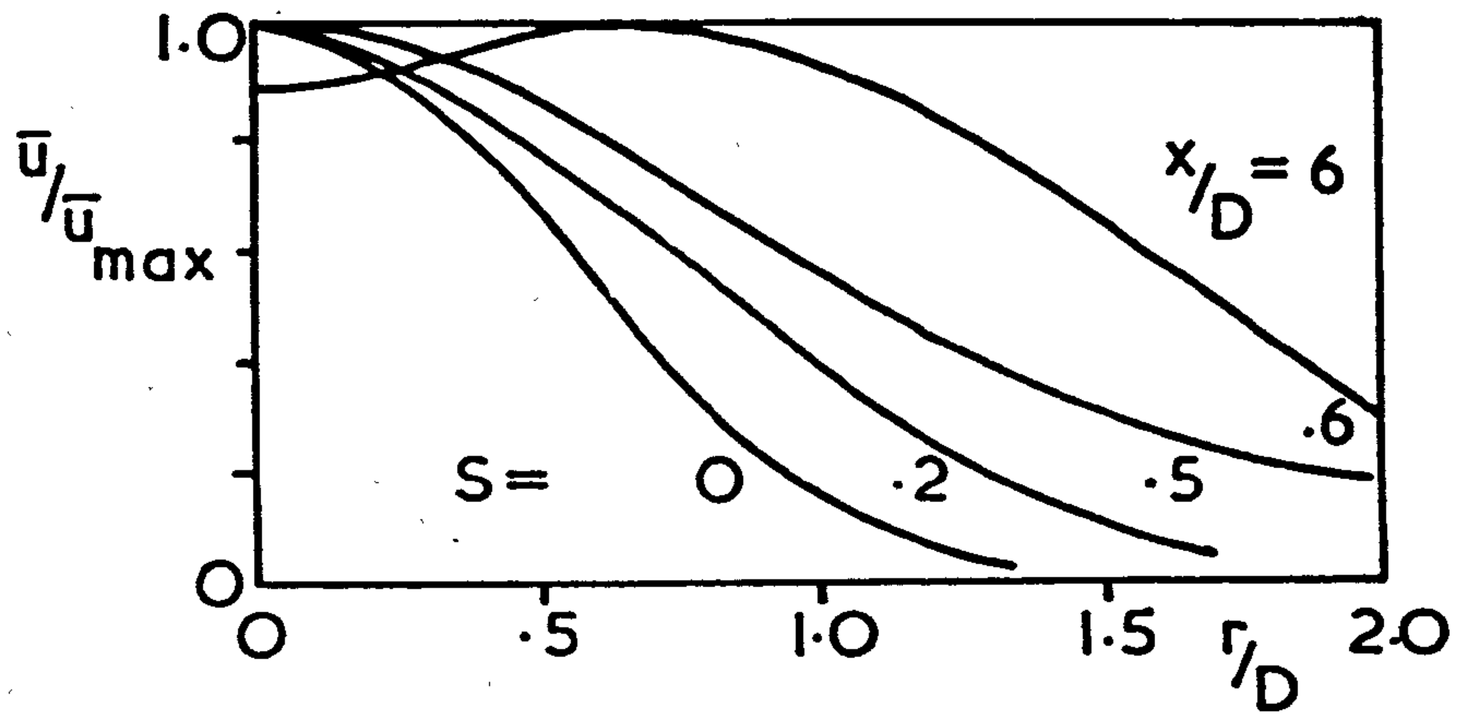

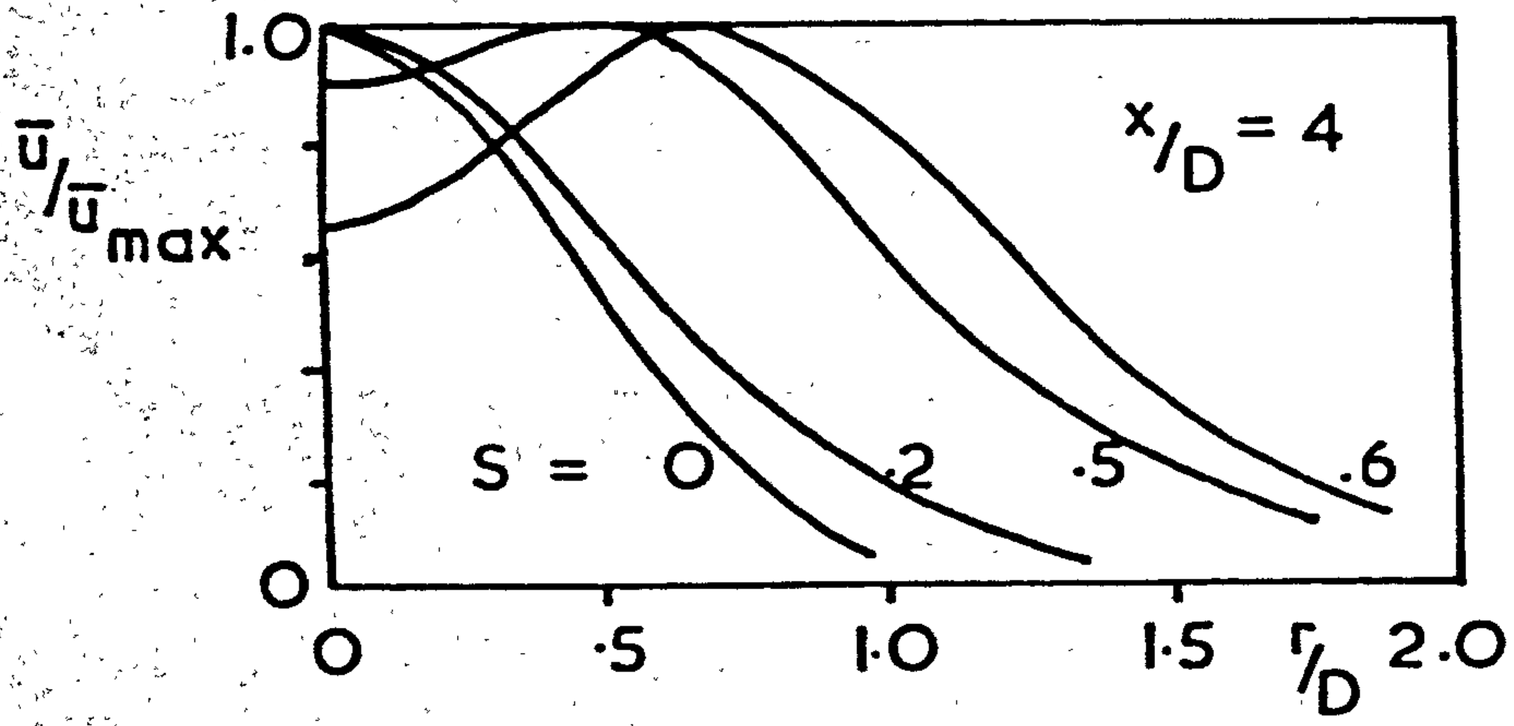

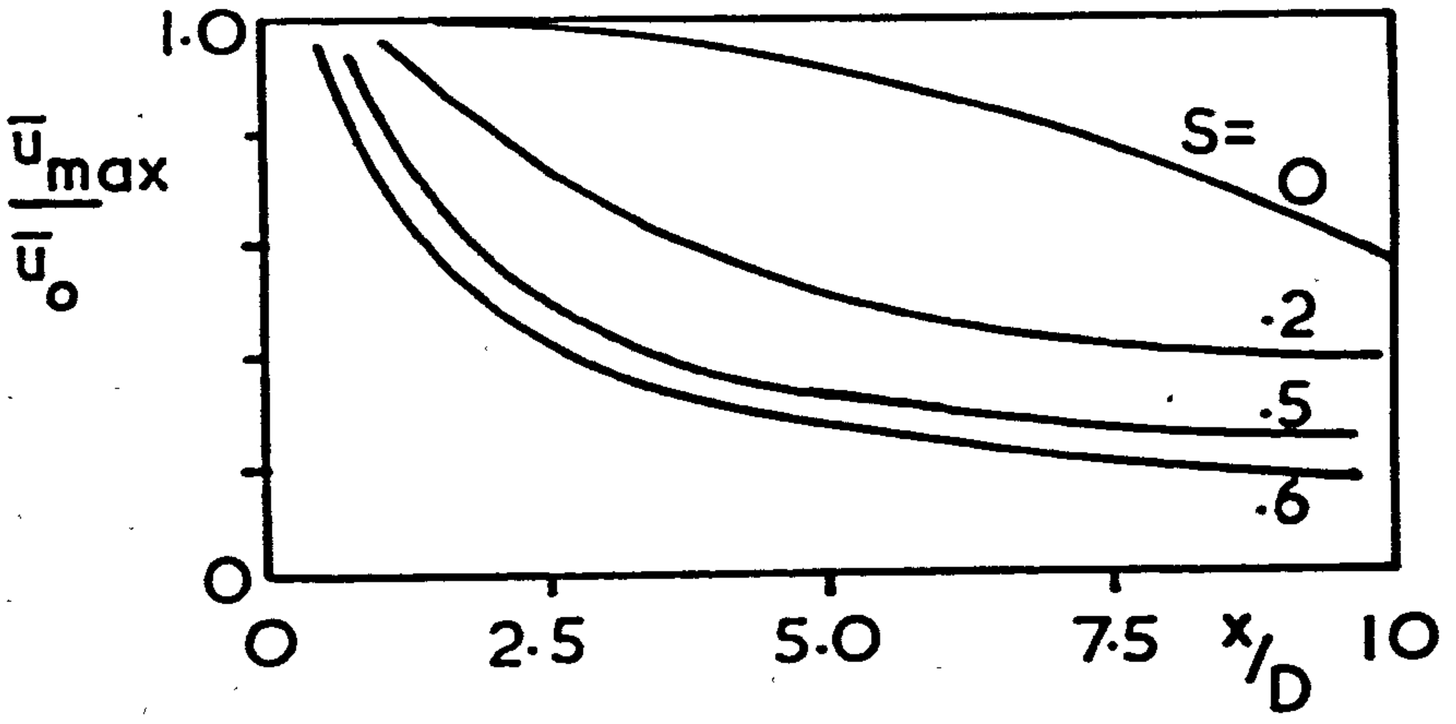

Fig. 5.1 Radial and axial $\bar{u}/\bar{u}_{max}$, $\frac{\bar{u}_{max}}{\bar{u}_o}$ distribution for a single free swirling jet of variable swirl

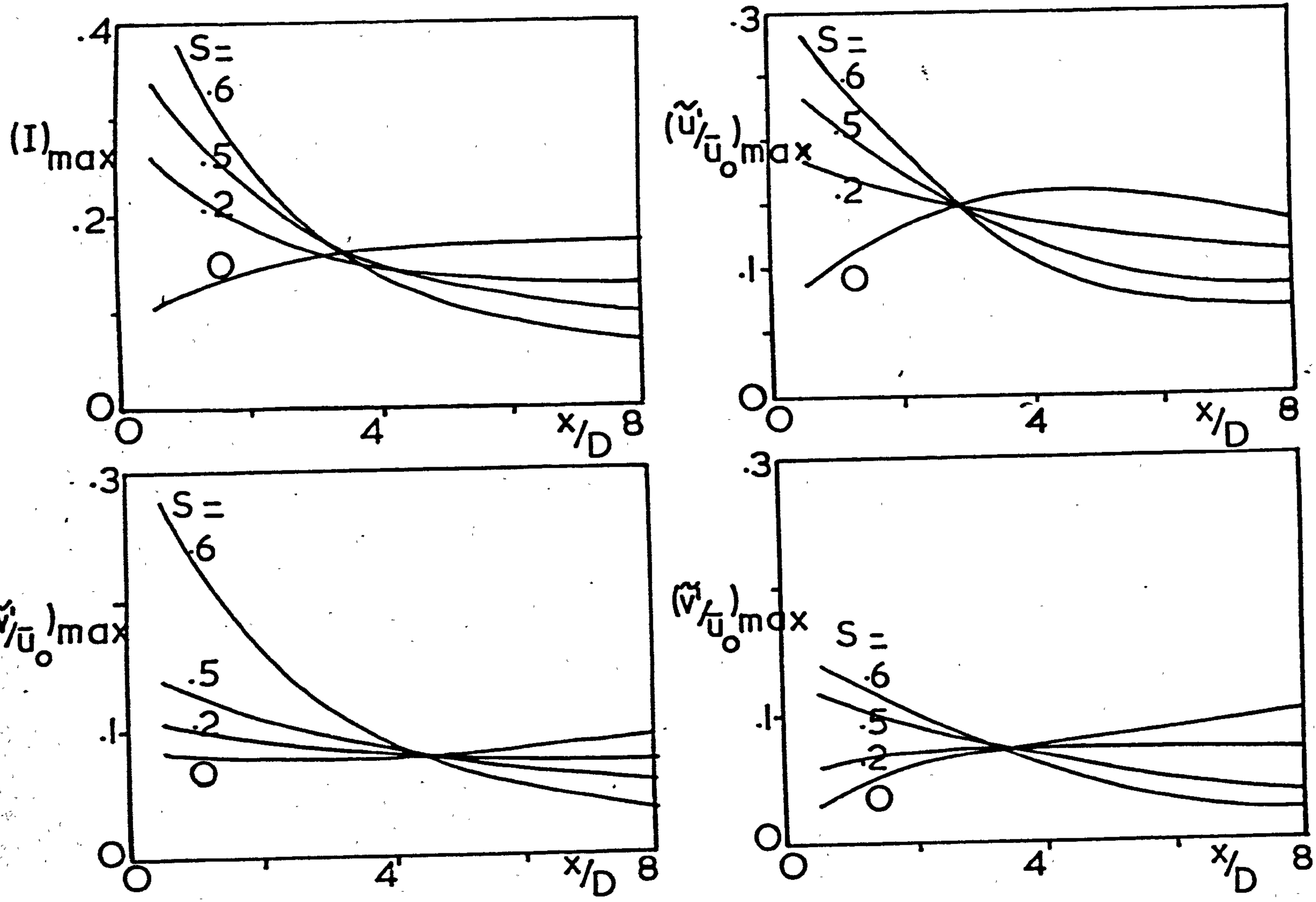

Fig. 5.2 Comparative axial $(I)_{max}$, $(\tilde{u}'/\bar{u}_o)_{max}$, $(\tilde{w}'/\bar{u}_o)_{max}$, $(\tilde{v}'/\bar{u}_o)_{max}$ values for a single swirling free jet of variable swirl

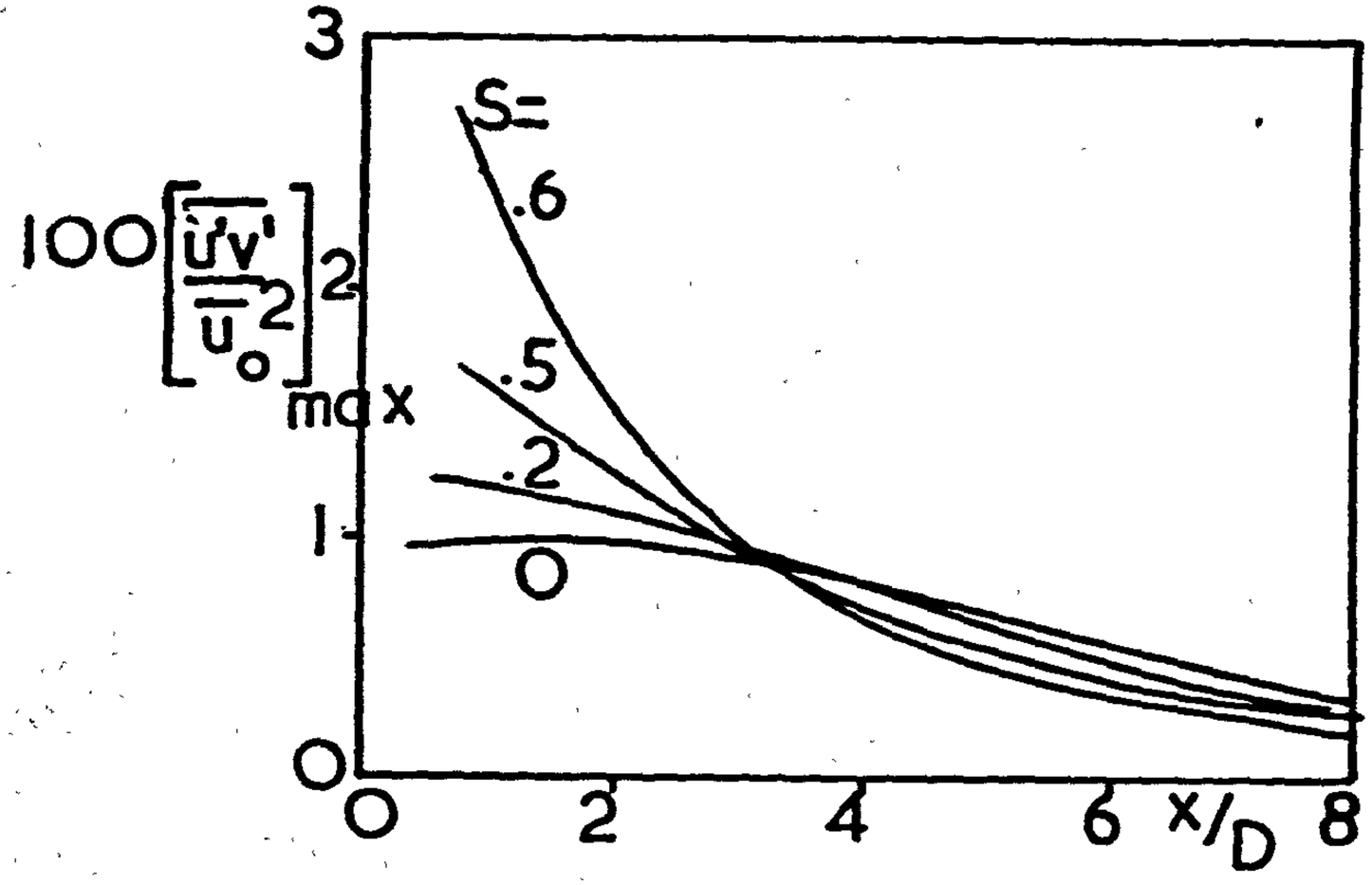

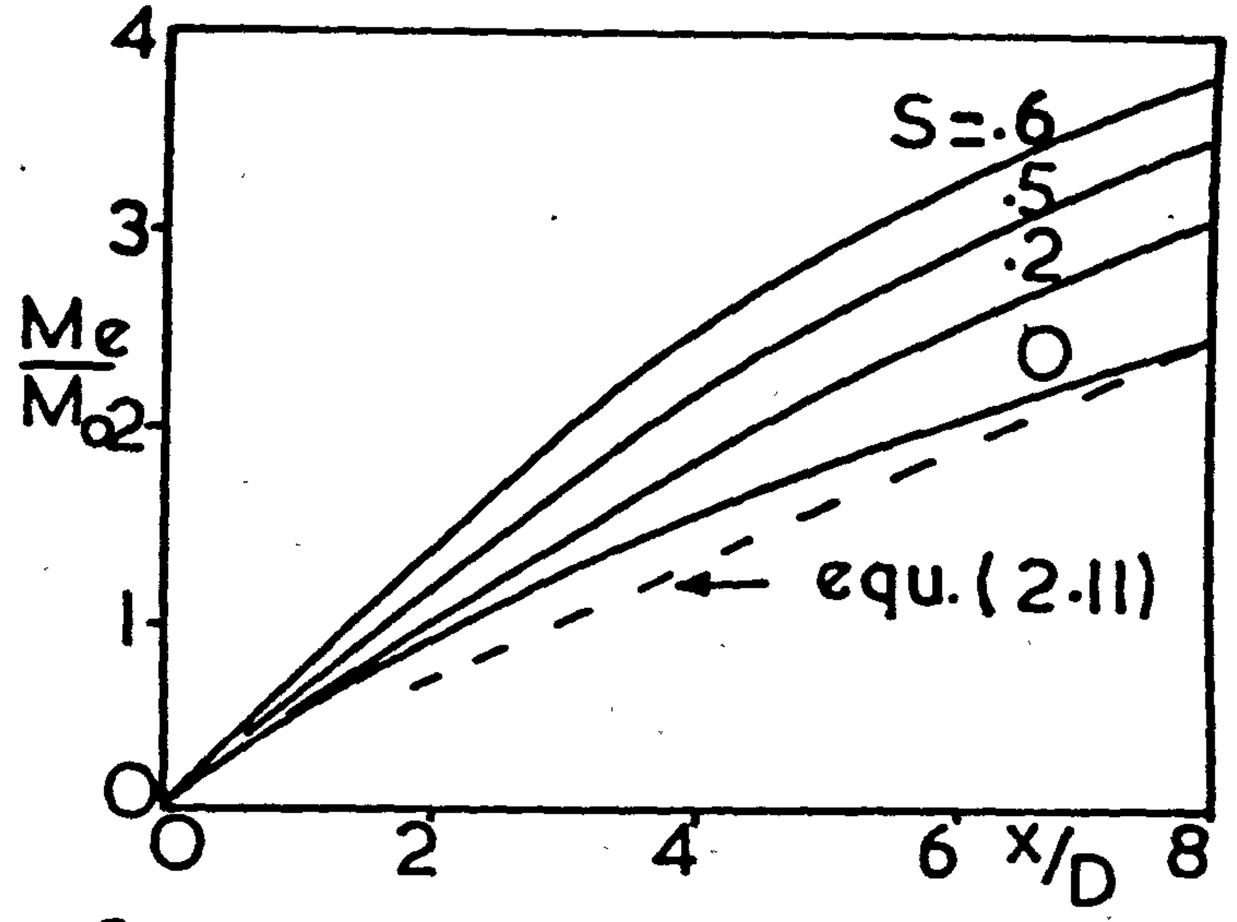

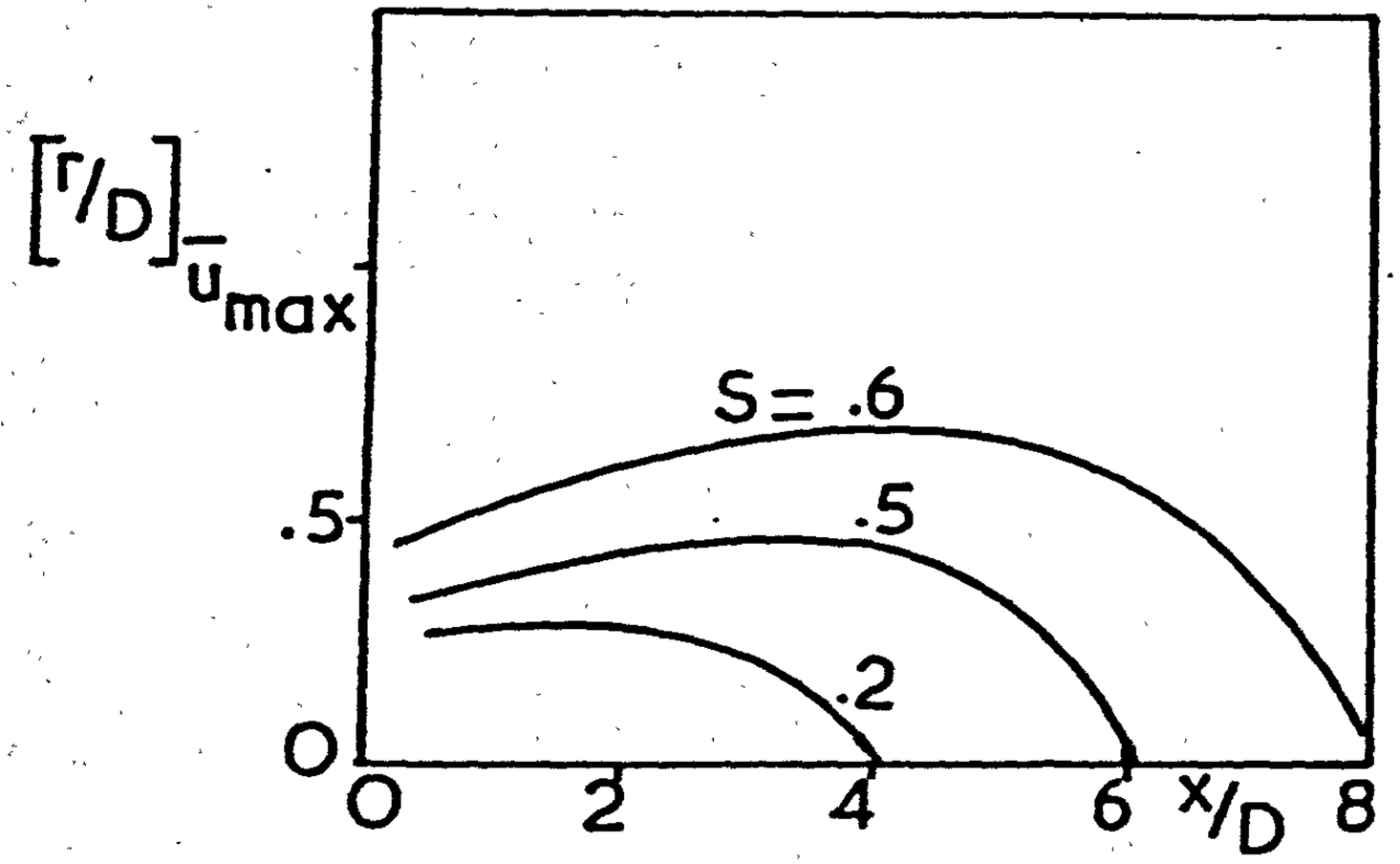

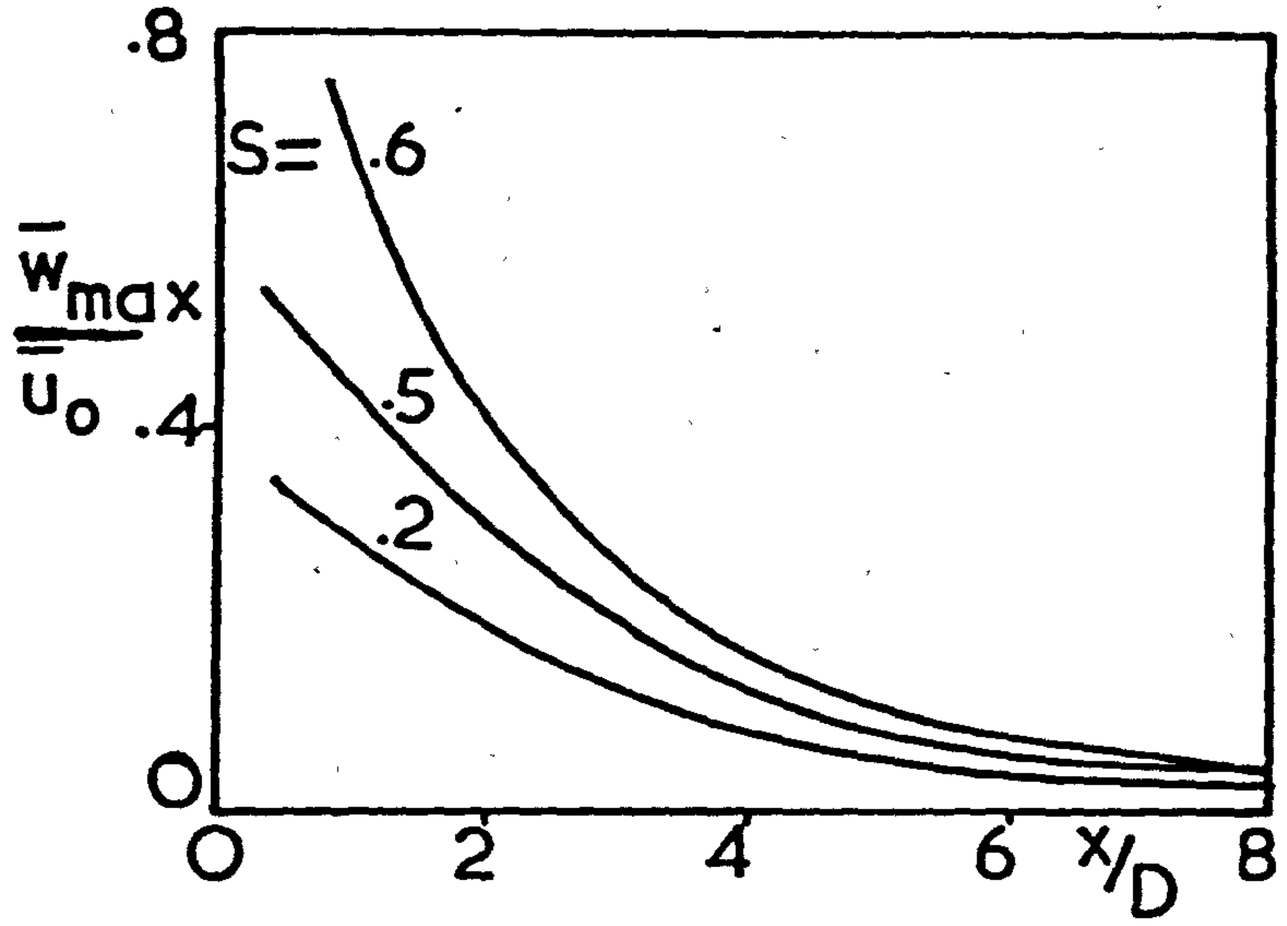

Fig. 5.3 Axial $100\left[\frac{\overline{u'v'}}{\overline{u}_o^2}\right]_{max}$, $\frac{M_e}{M_o}$, $[r/D]_{\bar{u}_{max}}$, $\frac{\bar{w}_{max}}{\bar{u}_o}$ values for a single swirling free jet of variable swirl

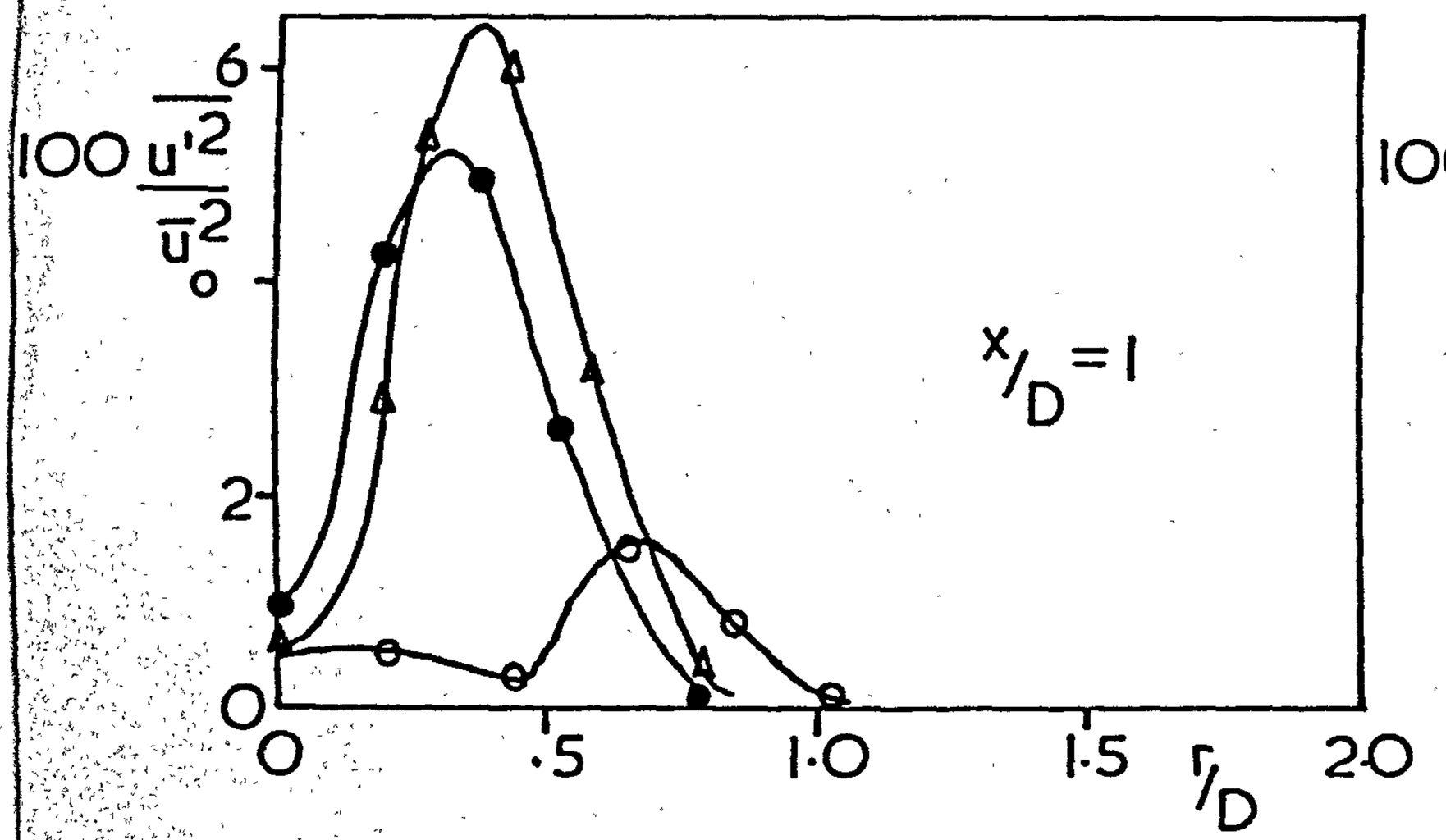

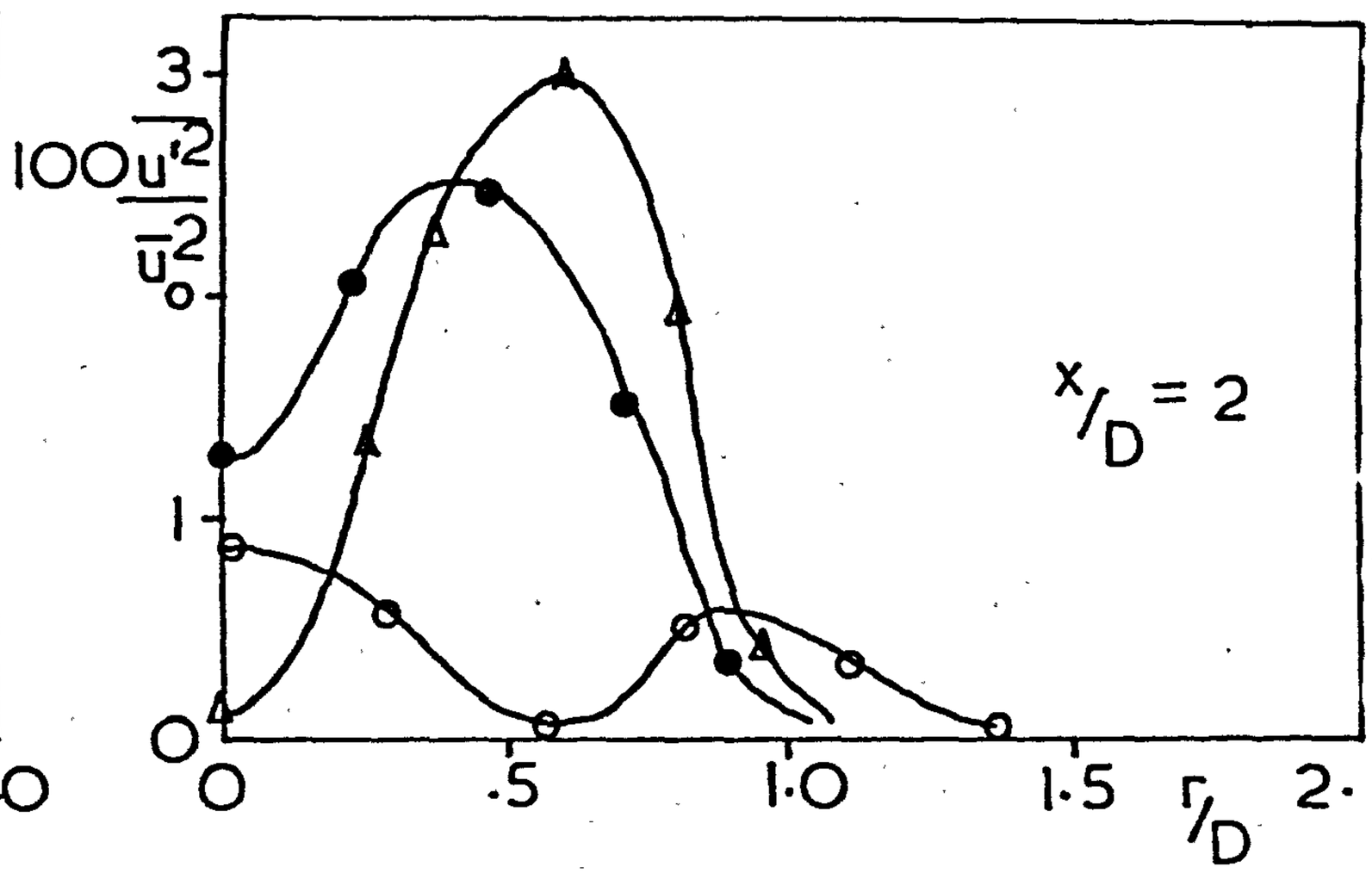

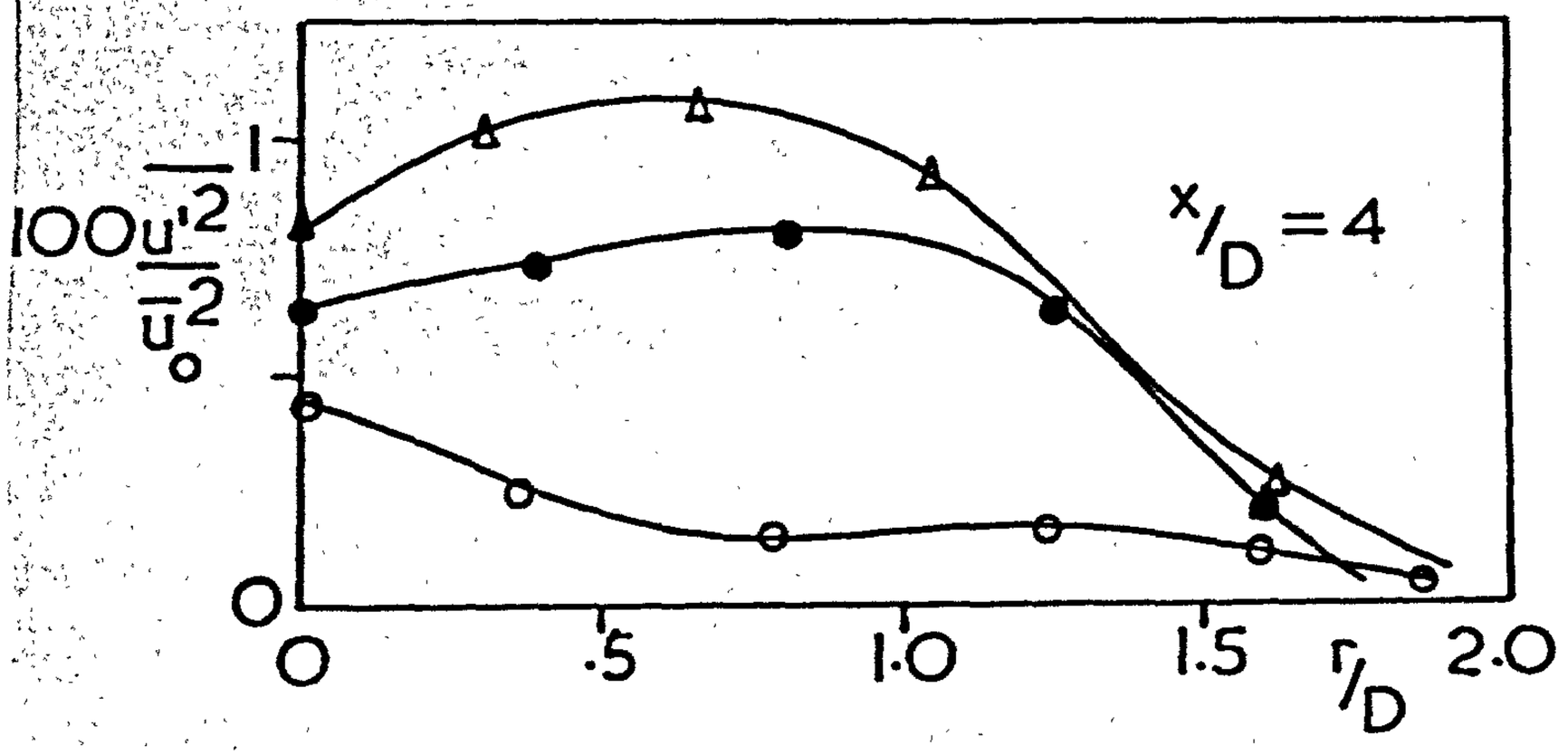

Δ — $\overline{u'^2}$ values

● — $\overline{w'^2}$ "

○ — $\overline{v'^2}$ "

S = 0.6

Fig. 5.4 Radial fluctuating velocity terms for a strongly swirling j (normal stress terms)

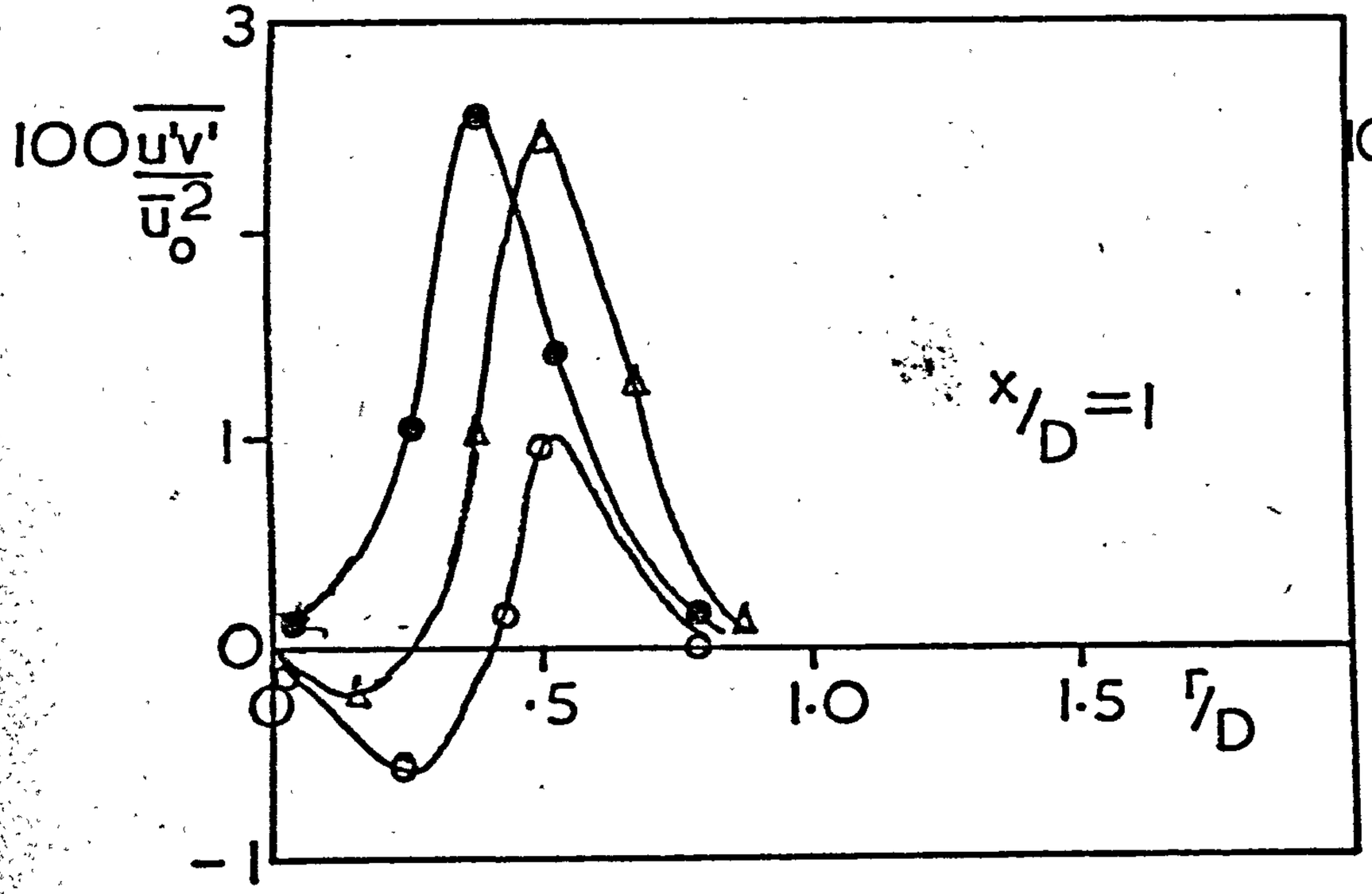

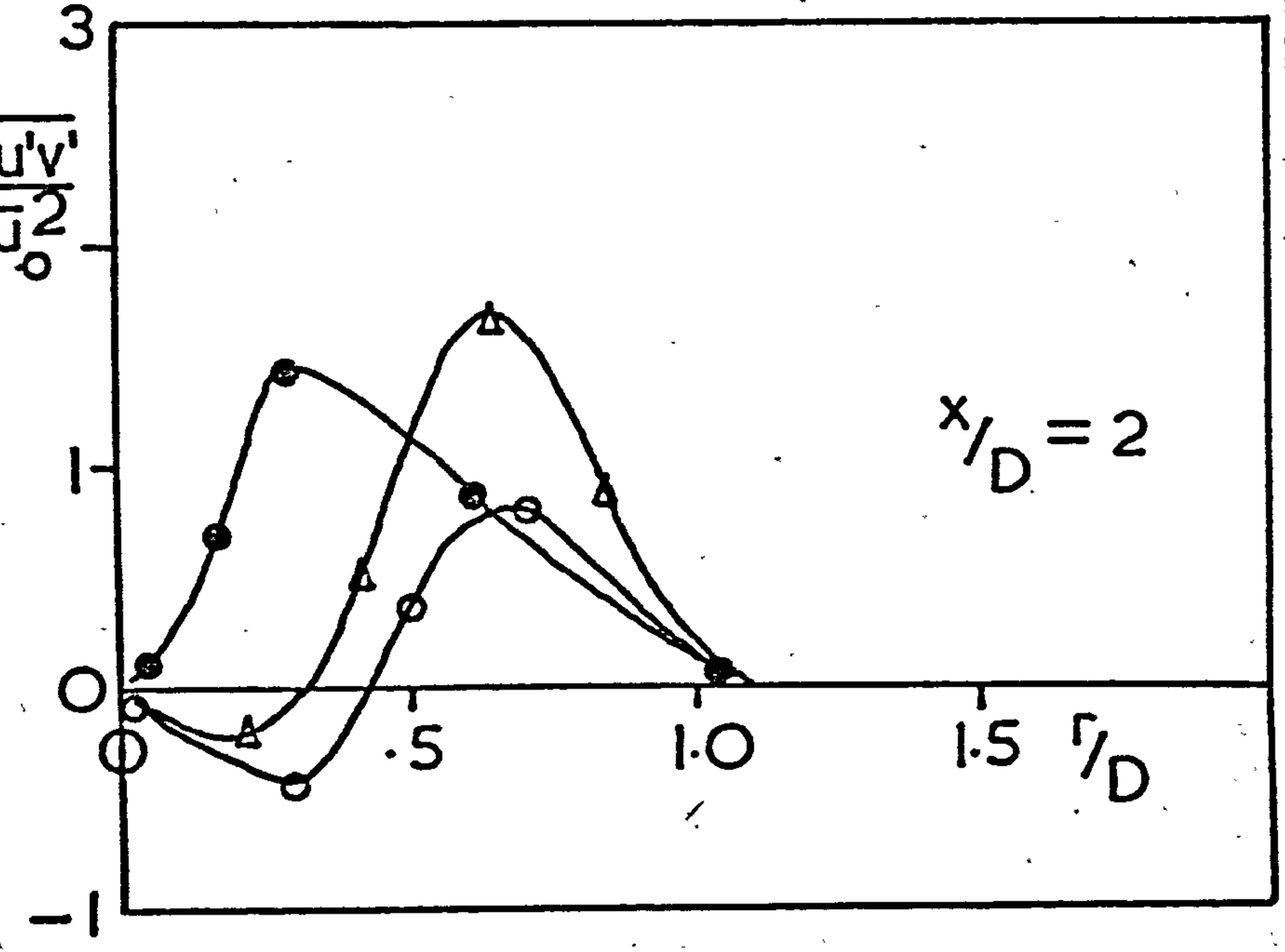

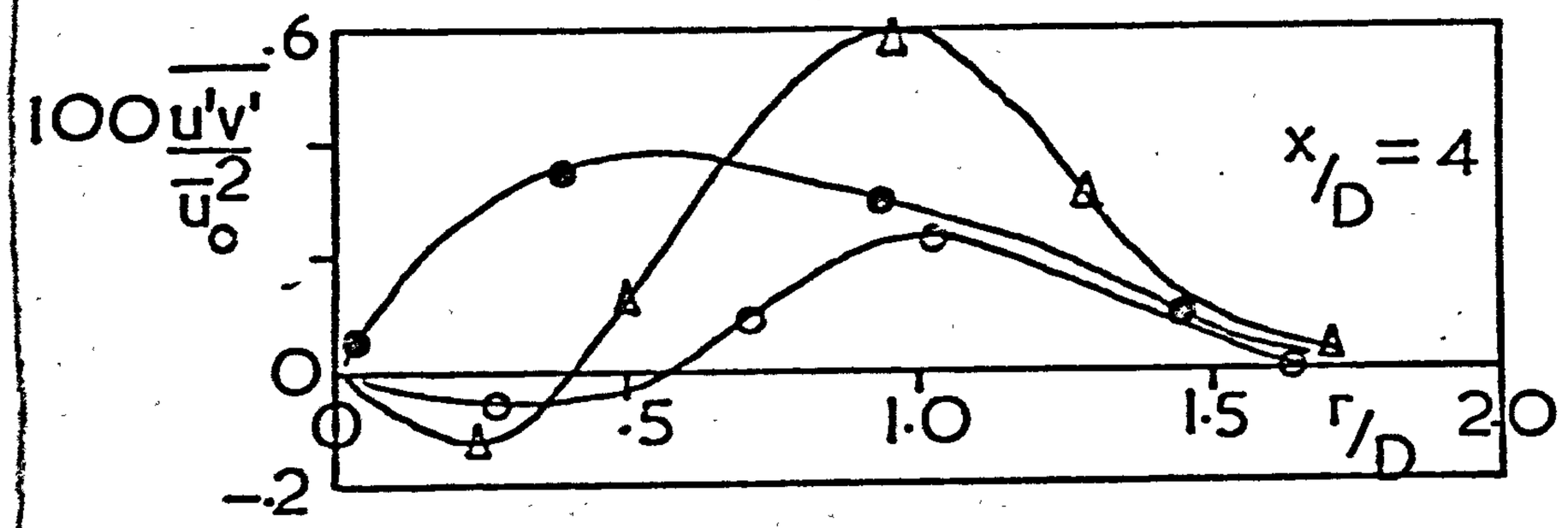

Δ — $\overline{u'v'}$ values

● — $\overline{u'w'}$ "

o — $\overline{v'w'}$ "

S = 0.6

Fig. 5.5 Radial shear stress terms for a strongly swirling jet

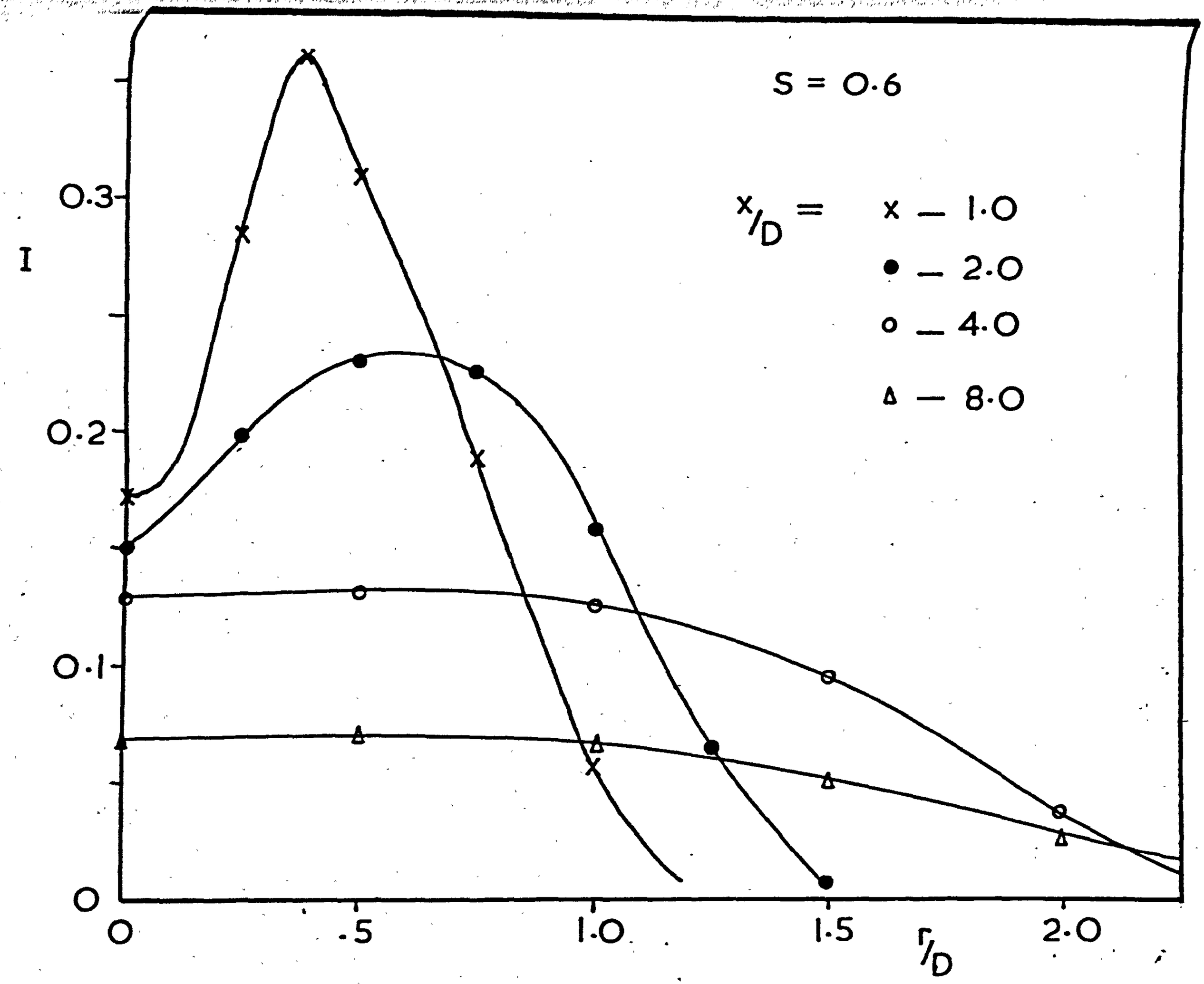

Fig. 5.6 Radial I distribution for a single free swirling jet

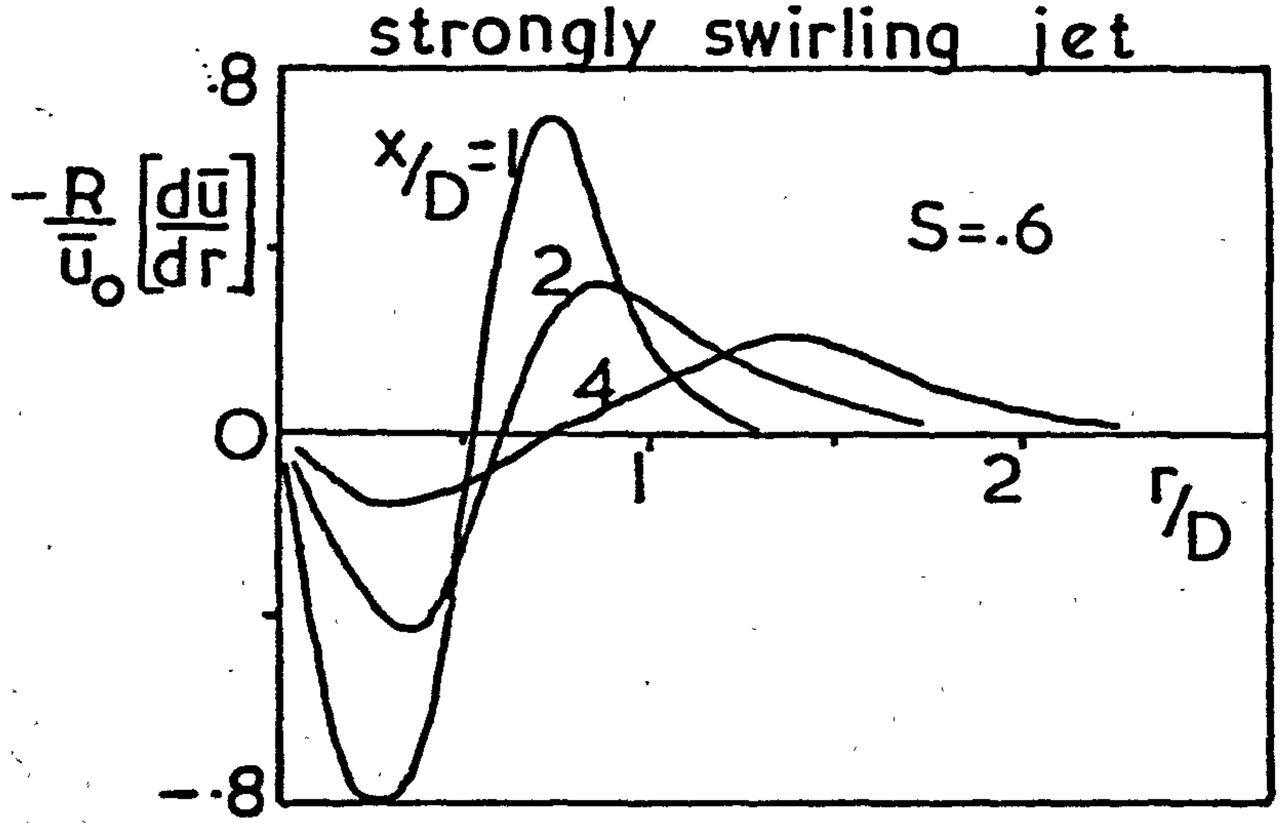

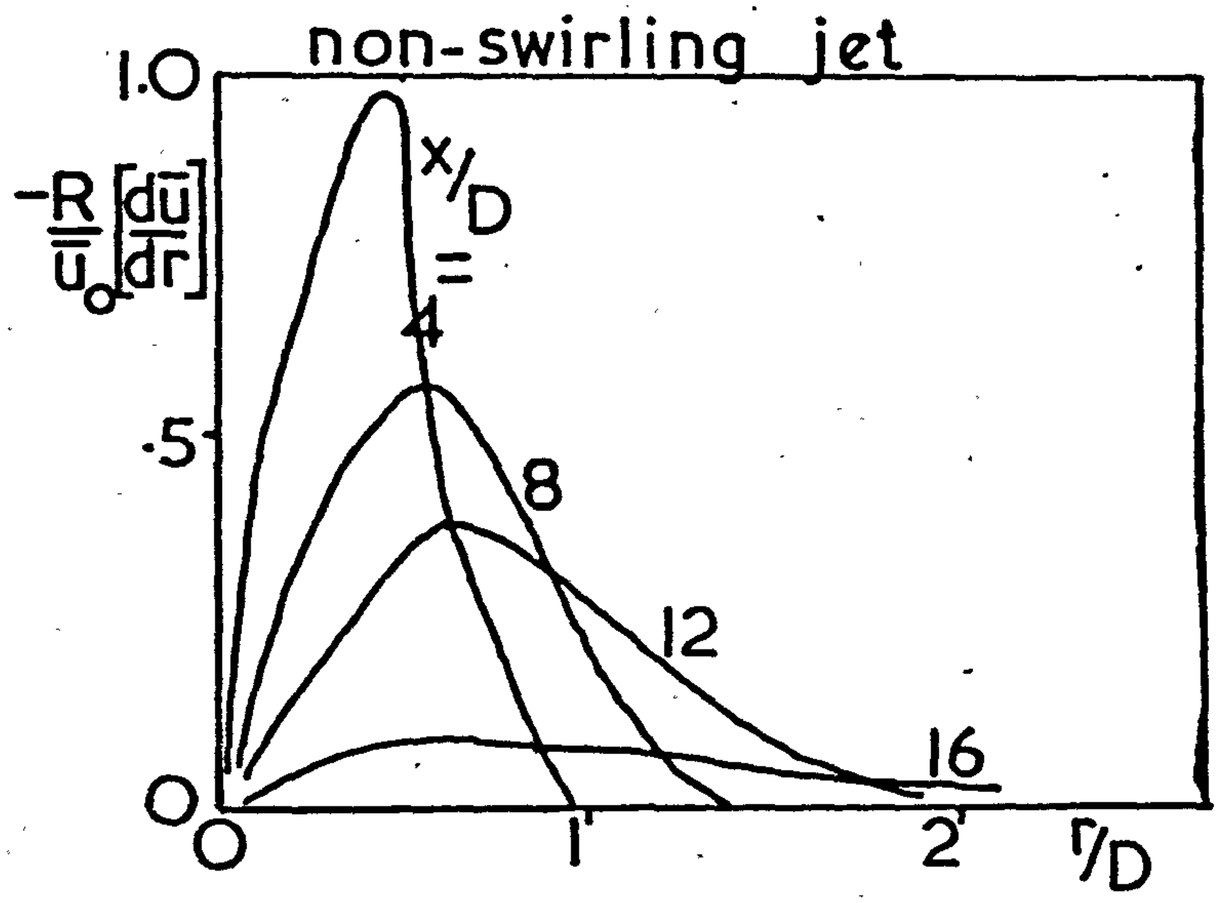

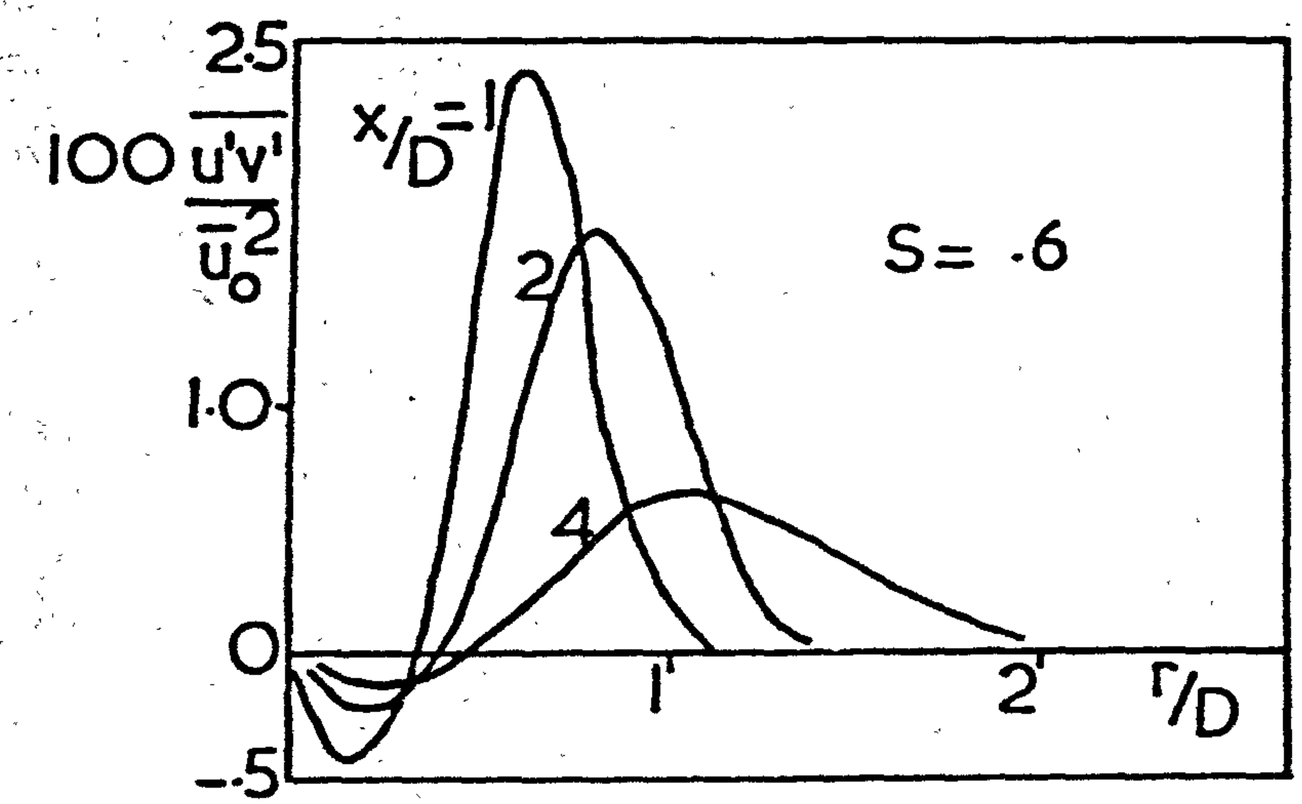

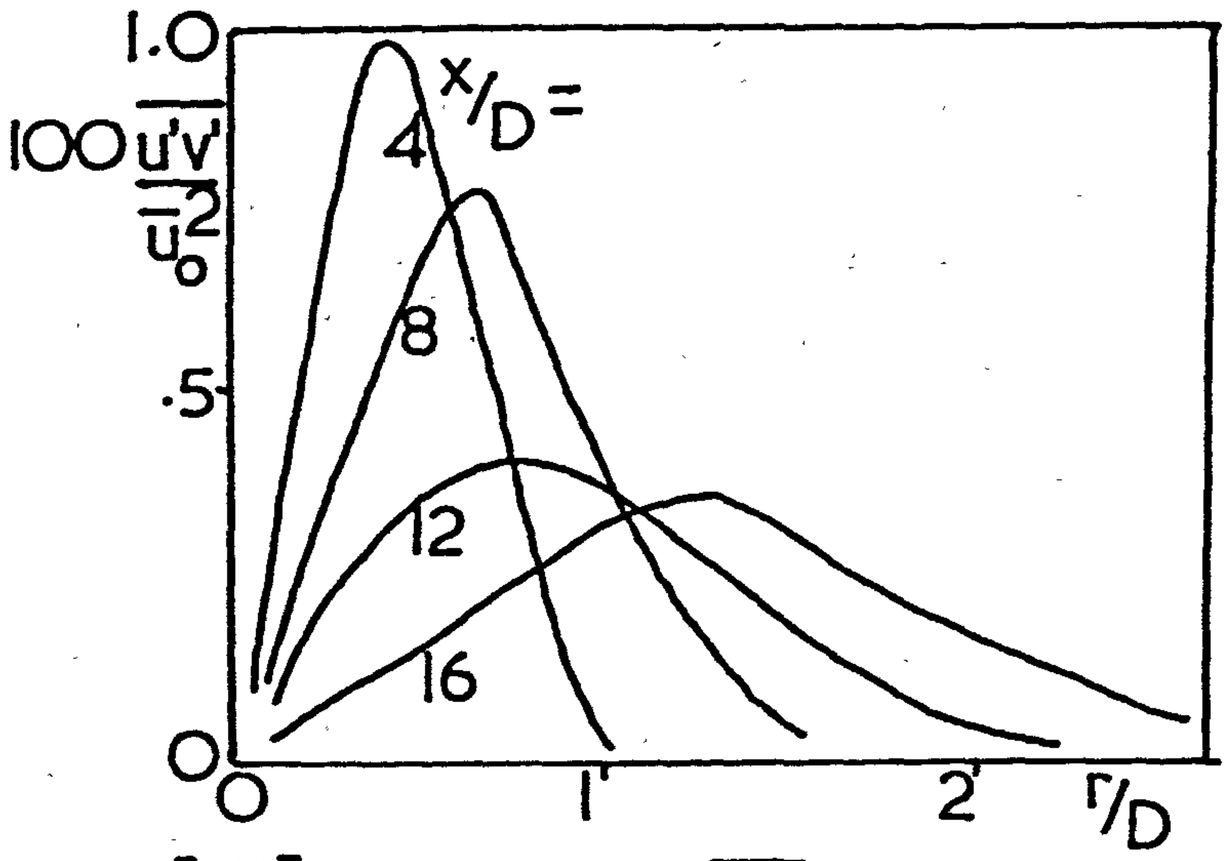

Fig. 5.7 Relation between $-\frac{R}{\bar{u}_o}\left[\frac{d\bar{u}}{dr}\right]$ and $100\frac{\overline{u'v'}}{\bar{u}^2}$ distribution for a non-swirling and strongly swirling jet

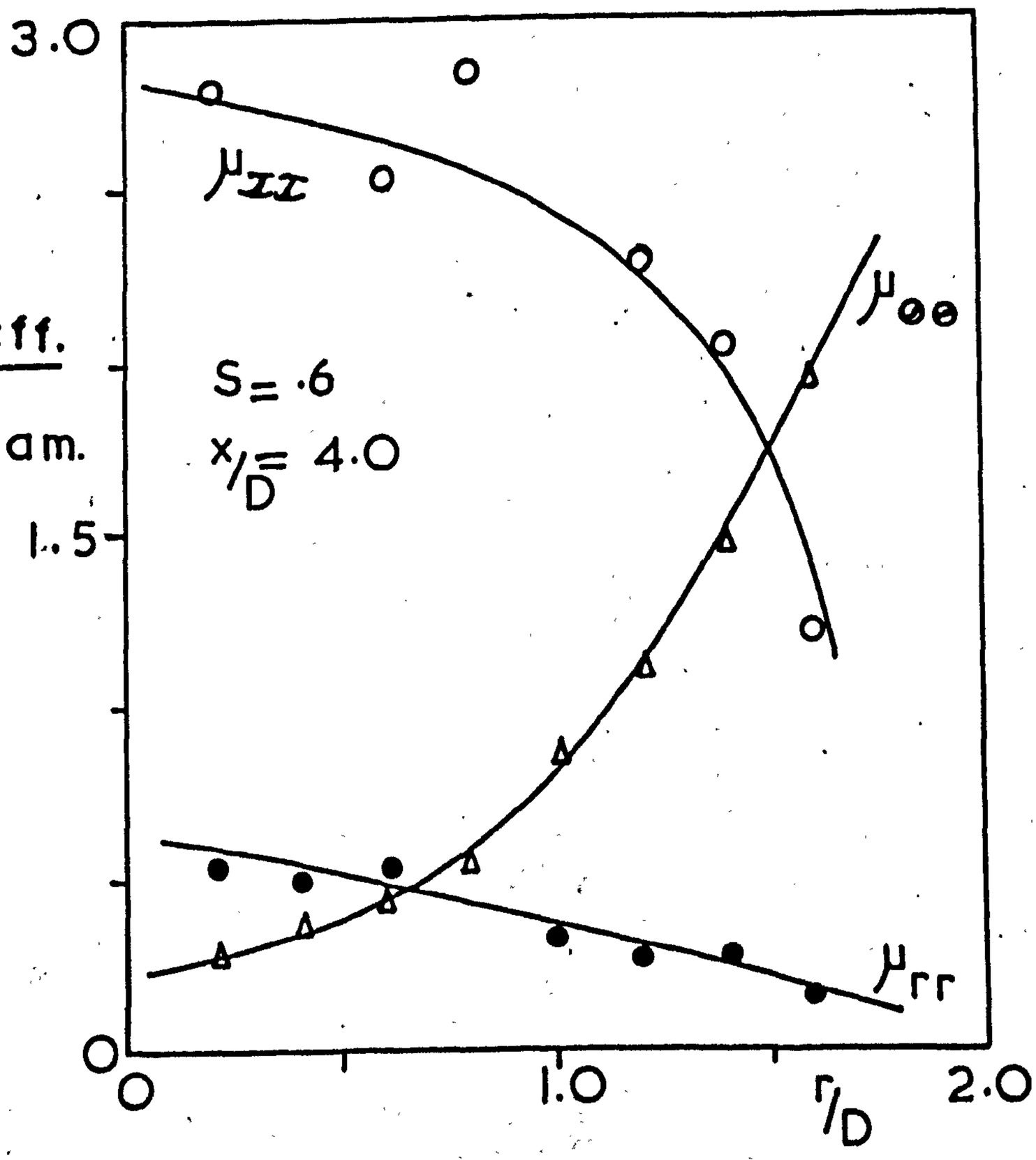

Fig. 5.8 Radial variation of measured effective viscosity terms for a strongly swirling jet 4 diameters downstream

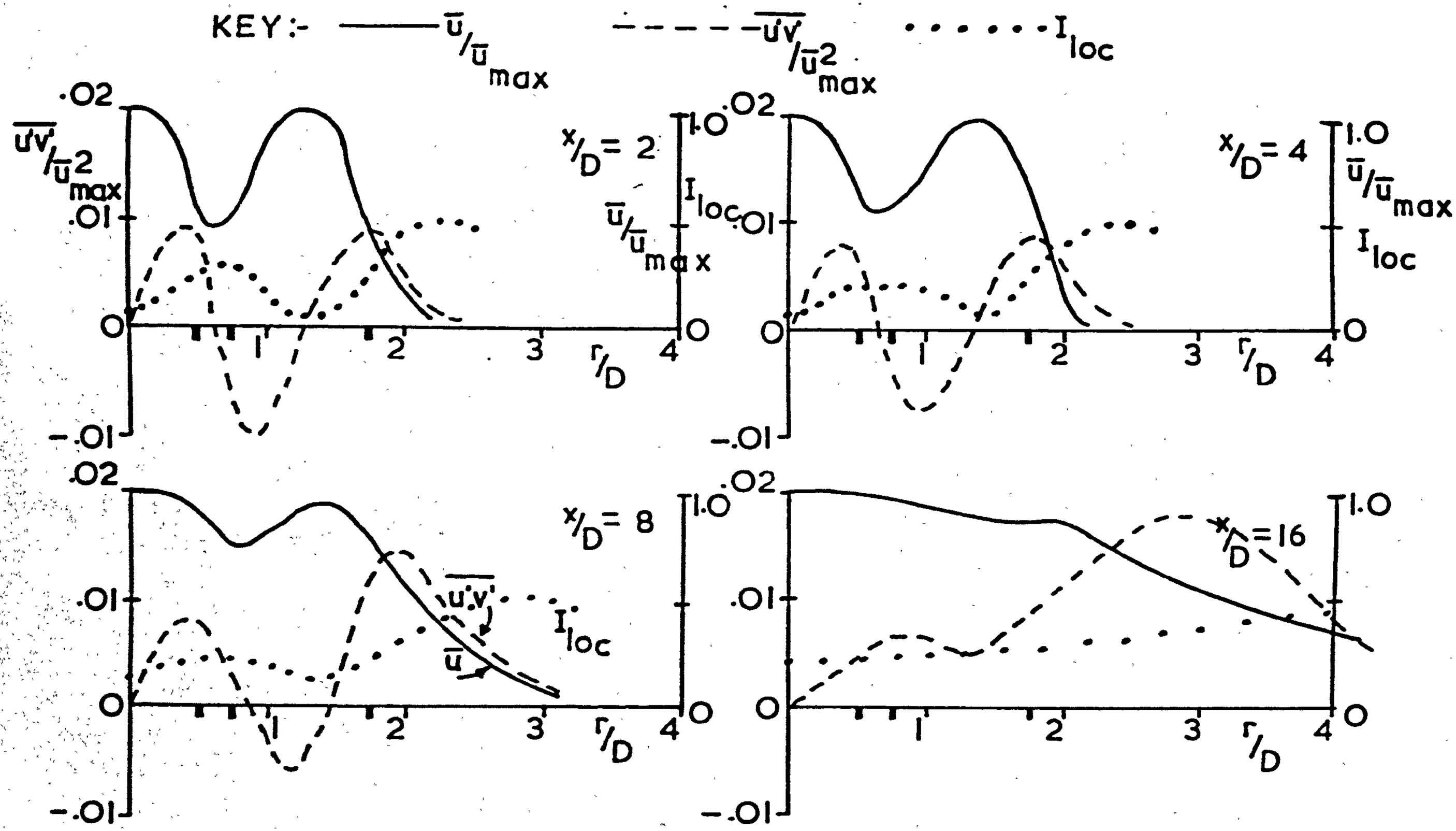

Fig. 5.9 Radial $\overline{u'v'}/\bar{u}^2_{max}$, $\bar{u}/\bar{u}_{max}$, I_{loc}-distributions for 3 non-swirling jets 1.25 diameters apart. (P 1-25)

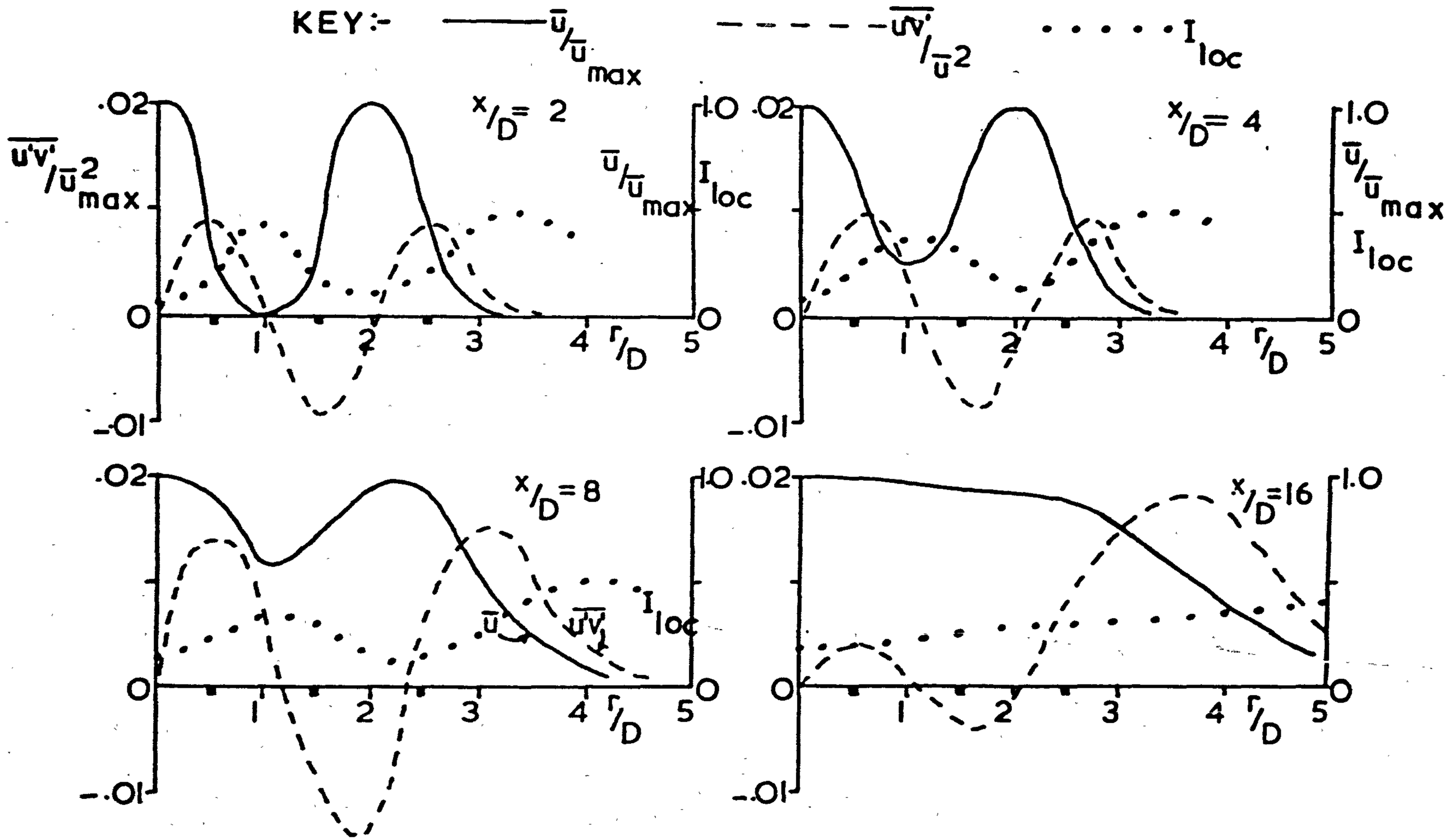

Fig. 5.10 Radial $\overline{u'v'}/\bar{u}^2_{max}$, I_{loc}, $\bar{u}/\bar{u}_{max}$ distributions for 3 non-swirling jets 2·0 diameters apart (P=20)

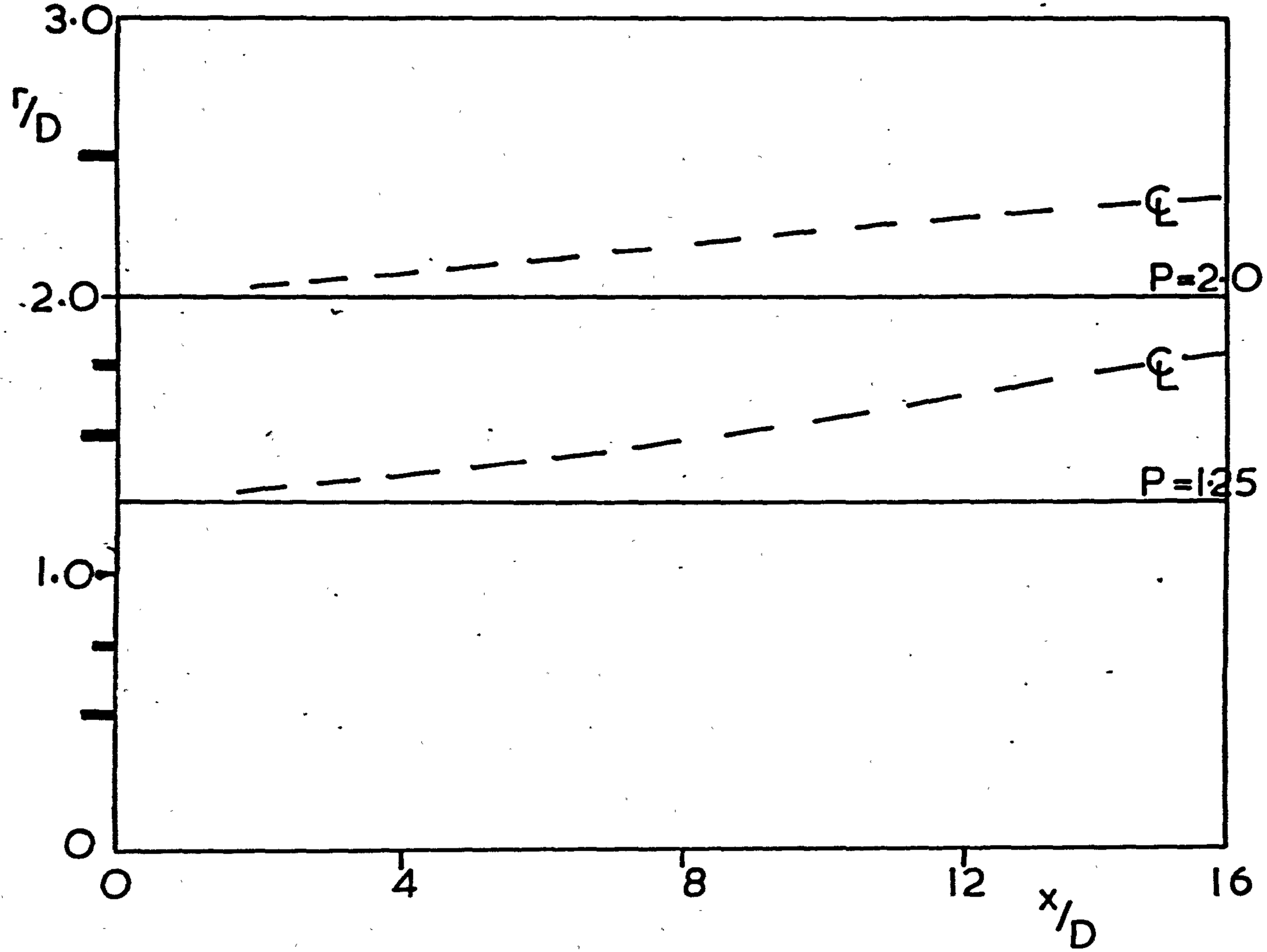

Fig. 5.11 Deflection of outer jet axis for 3 non-swirling jets 1·25 & 2·0 Dia. apart

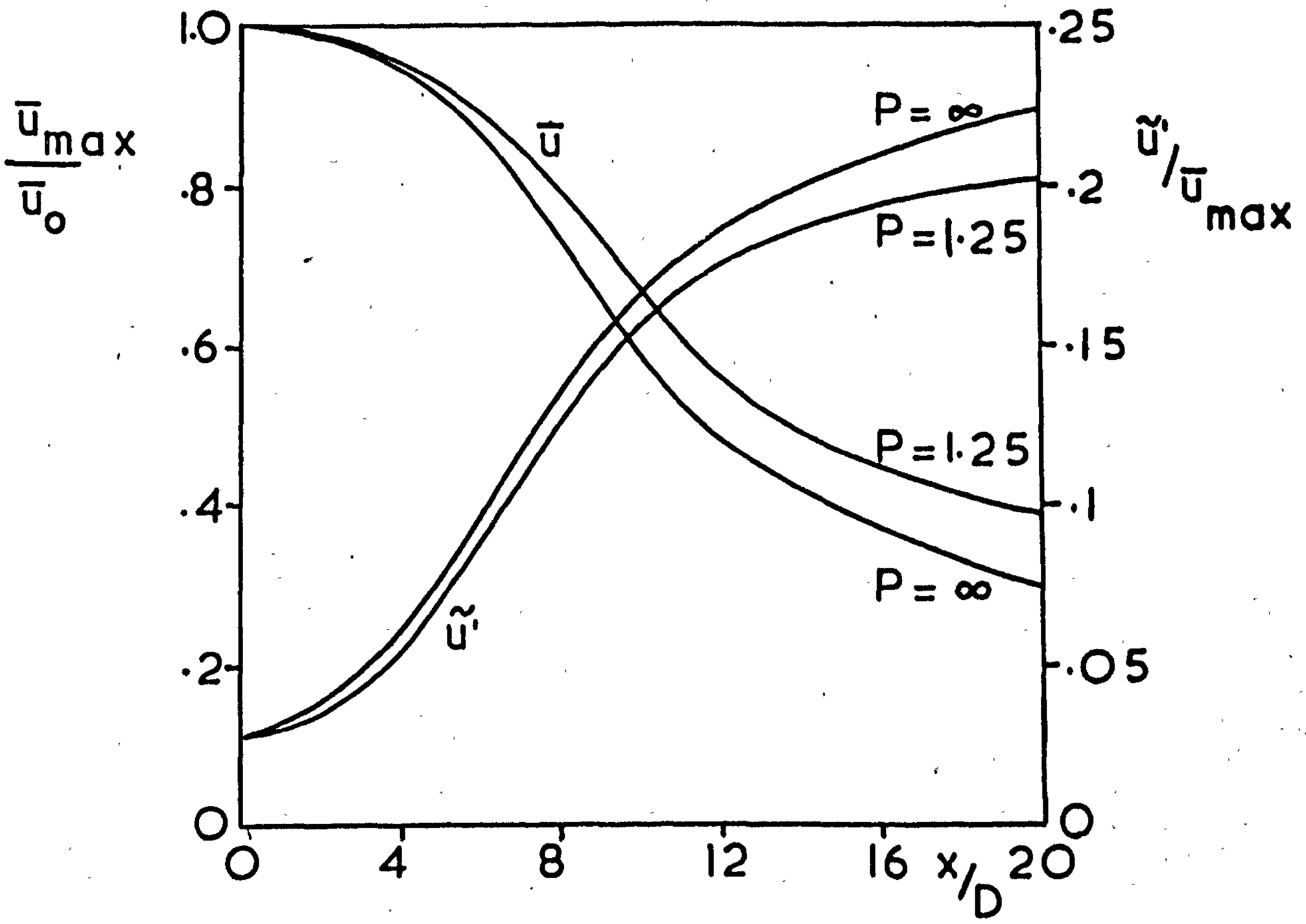

Fig. 5.12 Axial $\frac{\bar{u}_{max}}{\bar{u}_o}$ and $\tilde{u}'/\bar{u}_{max}$ for 3 non-swirling jets (values on centre line of central jet)

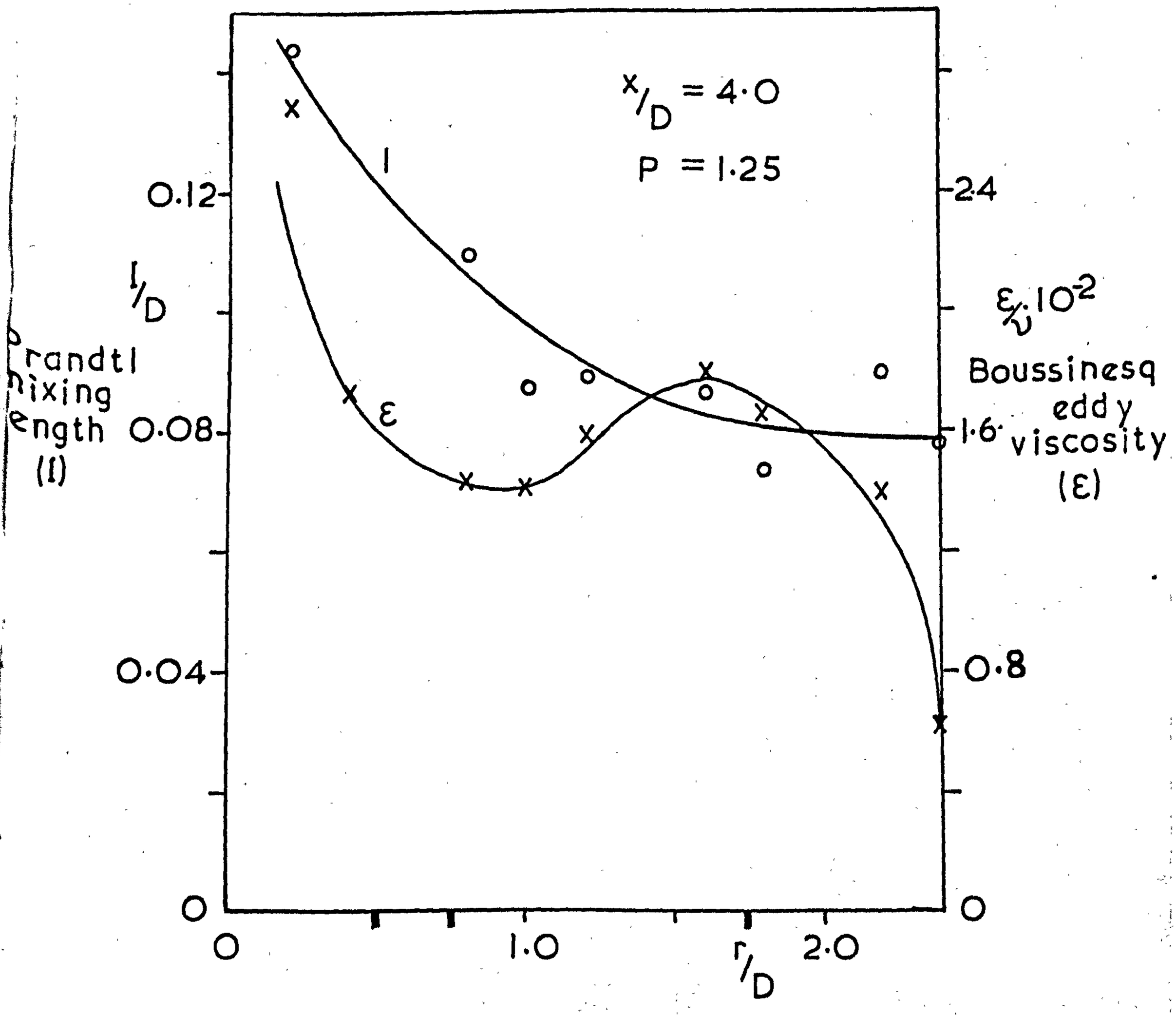

Fig. 5.13 Typical ε/ν and l/D distribution for 3 non-swirling jets 1.25 D apart

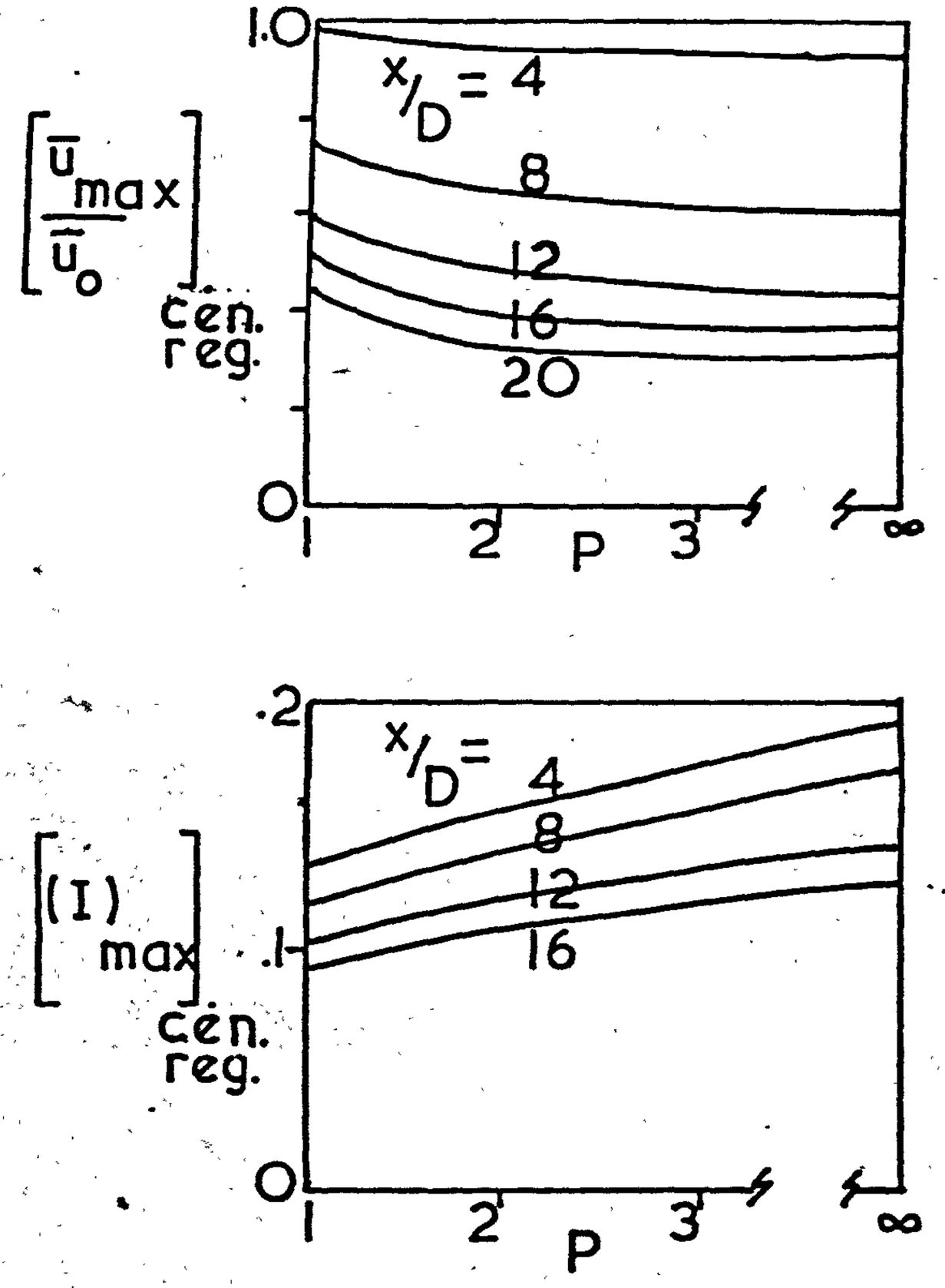

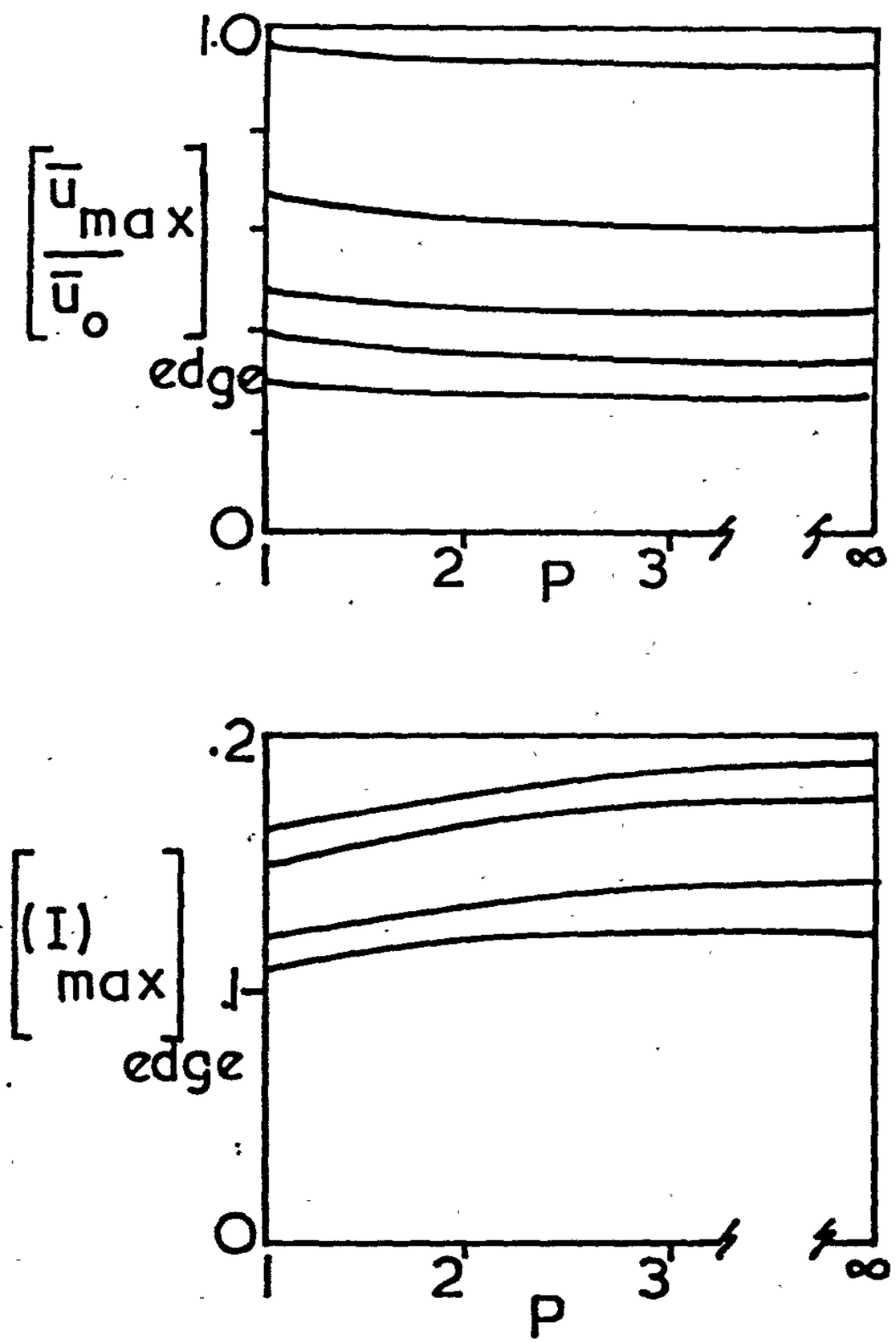

Fig. 5.14 Comparative $\left[\frac{\bar{u}_{max}}{\bar{u}_o}\right]_{\text{cen. reg.}}$ & edge, $\left[(I)_{max}\right]_{\text{cen. reg.}}$ & edge vs. pitch (P) values for multiple non-swirling jets

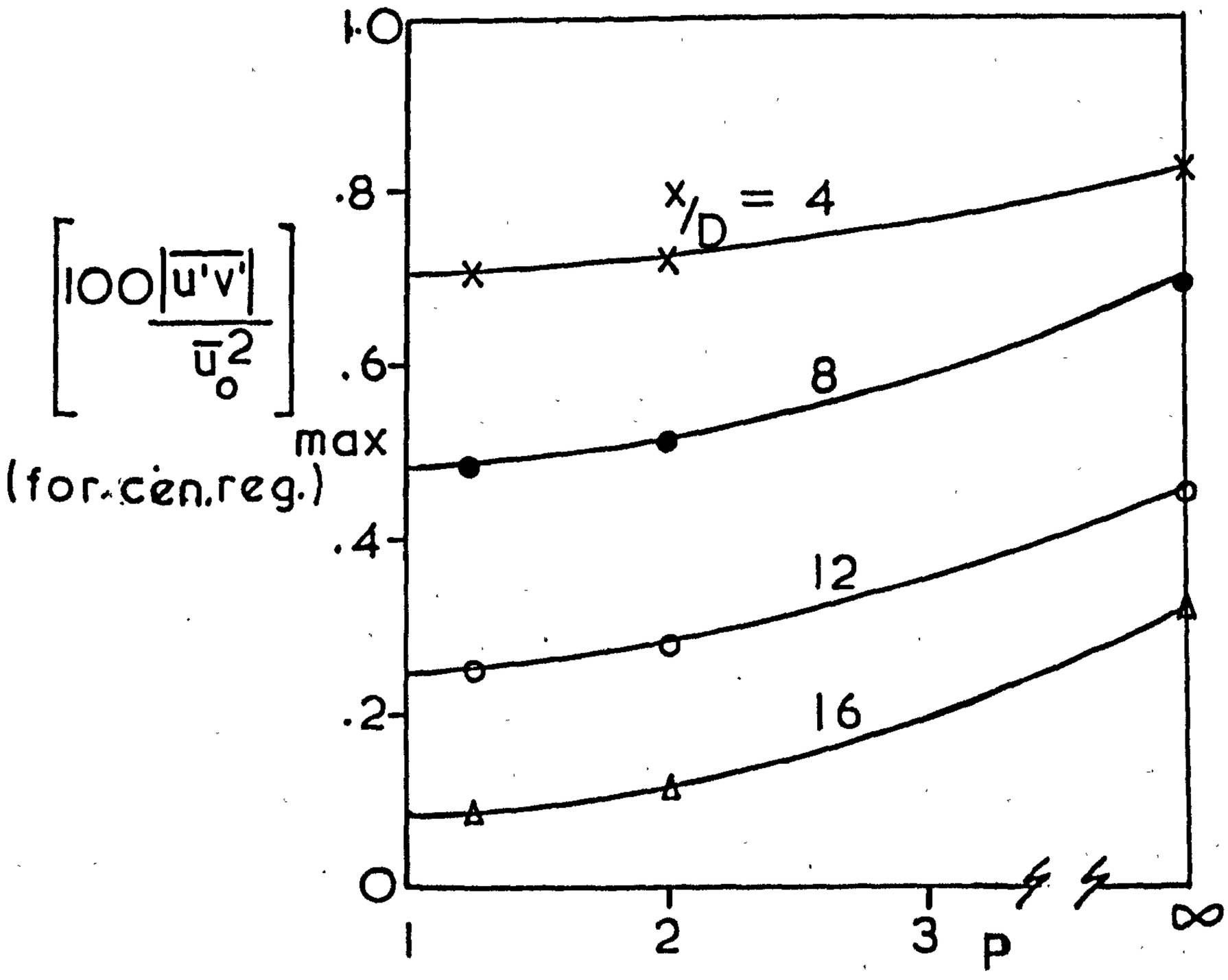

Fig. 5.15 $\left[100\frac{|\overline{u'v'}|}{\overline{u}_o^2}\right]_{max}$ values

(for the mixing region between jets)

for multiple non-swirling jets

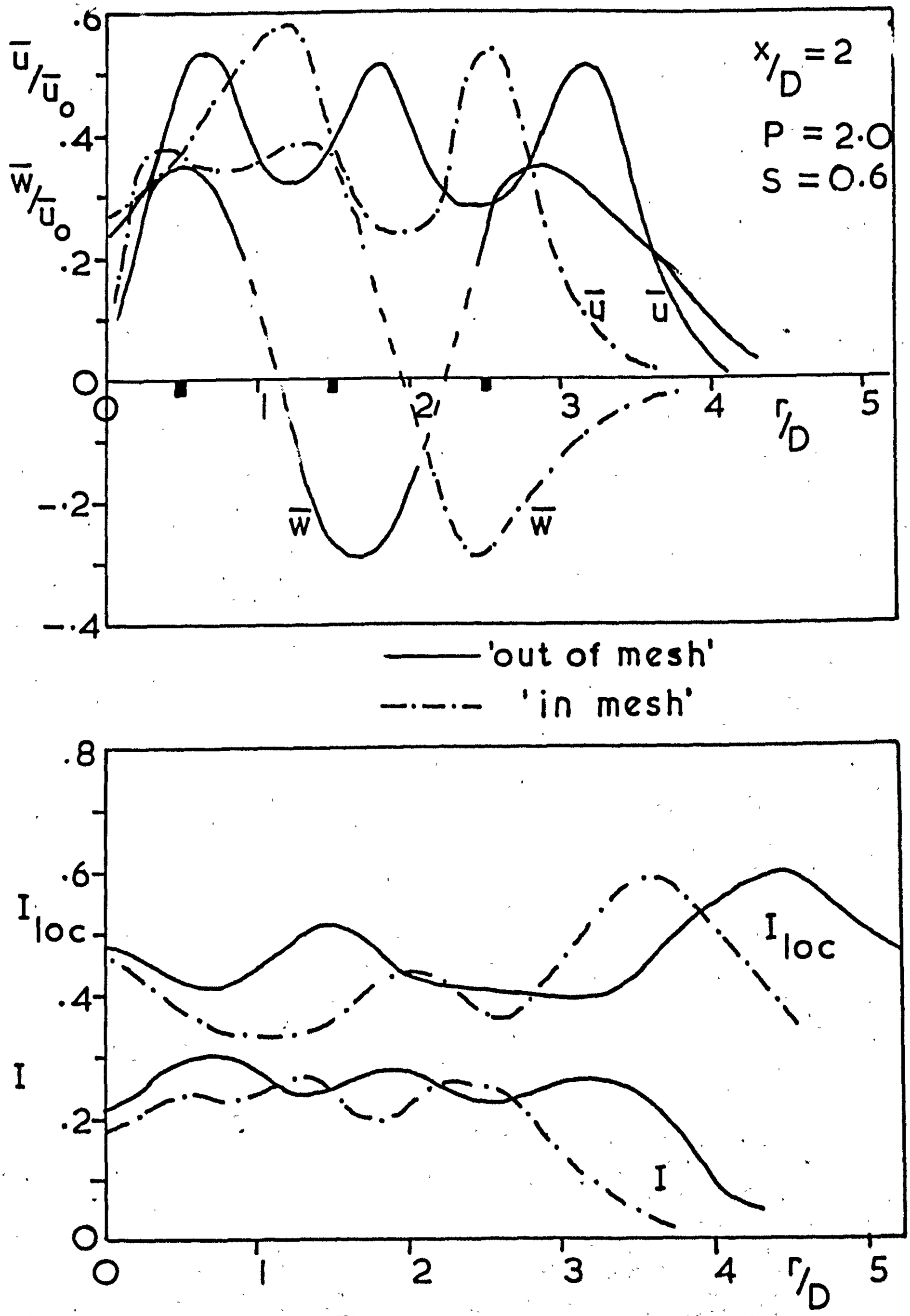

Fig. 5.16 Typical $\bar{u}/\bar{u}_o$, $\bar{w}/\bar{u}_o$, I_{loc}, & I distributions for 3 swirling jets

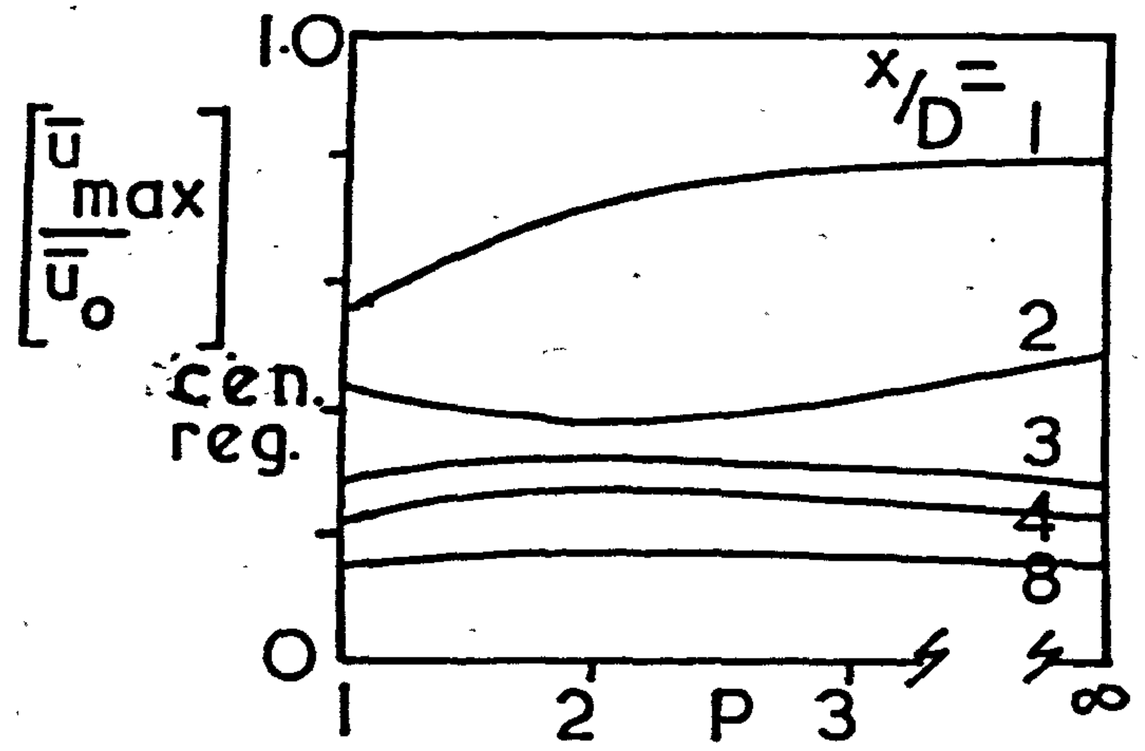

jets 'out of mesh'

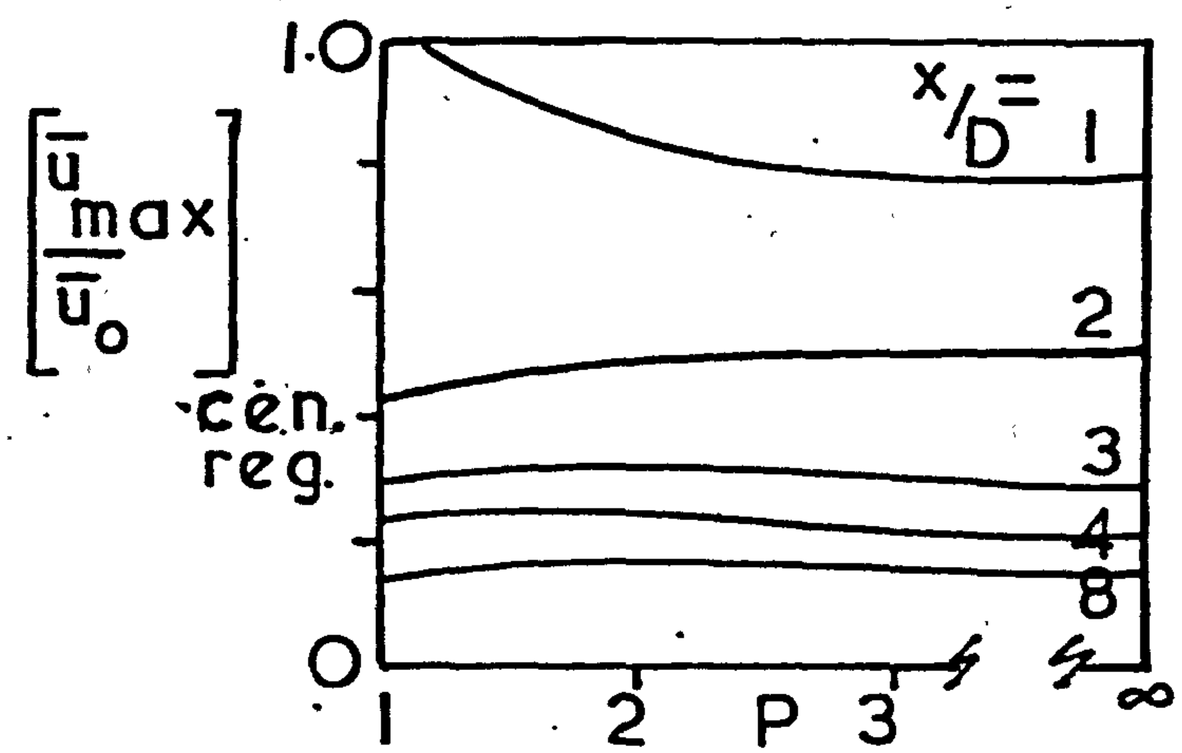

jets 'in mesh'

Fig. 5.17 Comparative $\left[\frac{\bar{u}_{max}}{\bar{u}_o}\right]_{\substack{cen.\\reg.}}$ values vs. pitch(P) & edge for multiple swirling jets 'in mesh' and 'out of mesh'

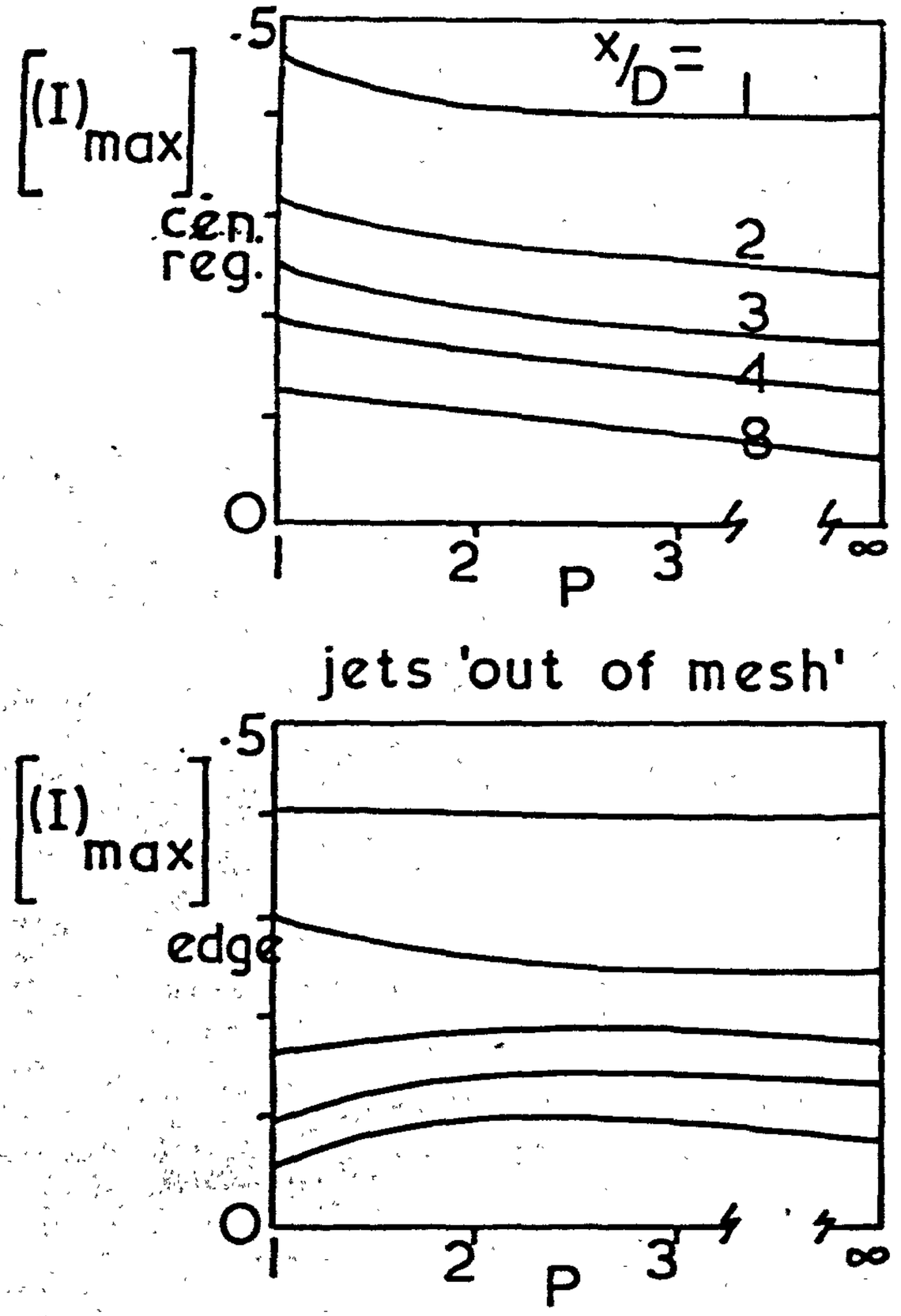

Fig. 5.18 Comparative $\left[(I)_{max}\right]_{\substack{cen.\\reg.}}$ & edge values vs. pitch(P) for multiple swirling jets 'in mesh' and 'out of mesh'

P5.1

P5.2

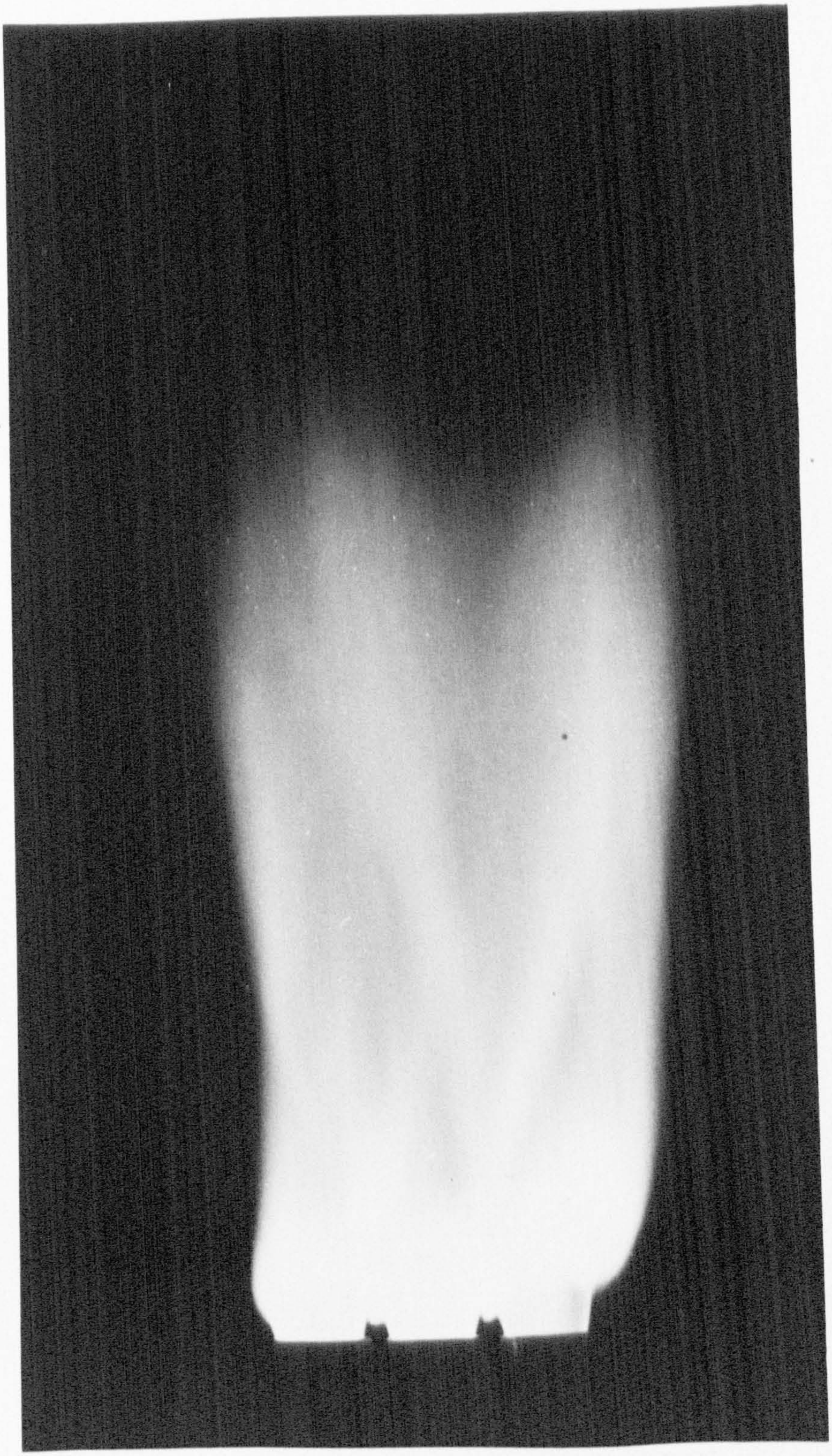

P5.3

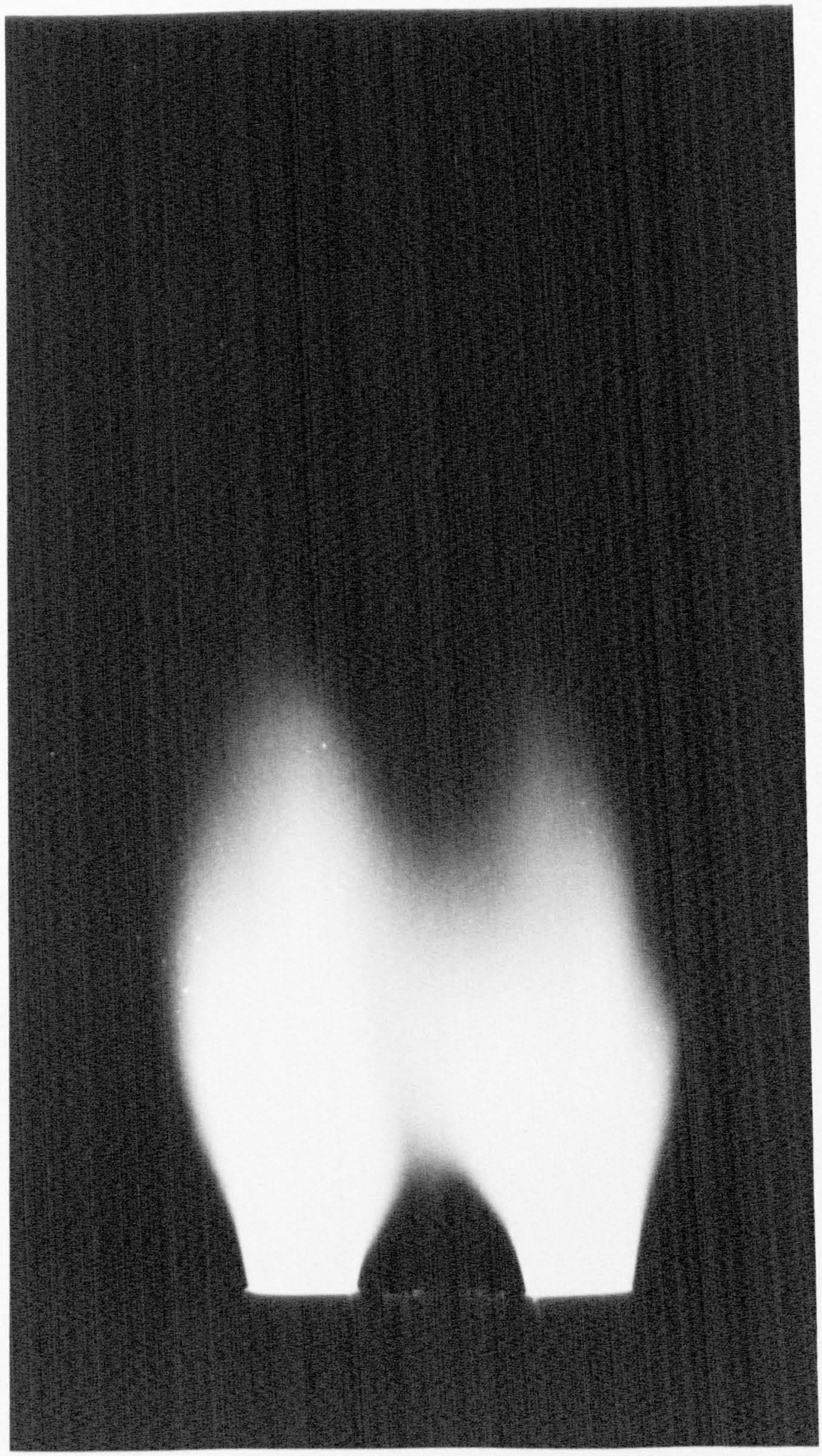

PS.4

APPENDIX 1

The Principles of the Constant Temperature Hot Wire Anemometer and Development of a New Velocity Voltage Relationship

A.1.1 The Constant Temperature Hot Wire Anemometer

The constant temperature hot wire anemometer (sometimes referred to as the constant resistance hot wire anemometer), is used to measure the instantaneous mass flow or velocity of gases or liquids, using either a hot wire or hot film probe as transducer. The instrument gives instantaneous readings of mean flow velocity, and the root mean square of the instantaneous velocity fluctuations. The anemometer is especially suited to high frequency flow fluctuation measurement, and is extremely sensitive to low speed flow. In principle the anemometer consists of a wheatstone bridge using the hot wire probe as part of the bridge, and a D.C. amplifier.

Electric current from the anemometer flows through the probe heating the wire to a predetermined temperature suitable to the conditions of flow measurement. A small change in the temperature of the wire, corresponding to

a small change in the flow conditions over the wire, causes a slight unbalance voltage of the bridge, which is greatly amplified and used to rebalance the bridge voltage by means of a servo control system built into the anemometer. The instantaneous value of the electrical power applied to the probe may be assumed to equal the instantaneous heat loss to the surrounding fluid. The actual thermal loss depends on the physical properties of the fluid under measurement, and if all the physical properties are kept constant, but the velocity is varied, then the probe current and consequently the voltage across the wire, are a measure of the velocity.

The anemometer has two voltmeters, the D.C. meter reads the time average of the fluctuating voltage fed to the wire, and the R.M.S. meter reads the root mean square of the fluctuating part of the voltage fed to the wire. The relationship between the D.C. voltage fed to the wire and the flow velocity is non-linear, the exact form of the relationship is found empirically by careful calibration of each particular probe. The measurement of velocity and turbulence is performed by manipulation of the above empirical equation explained in detail in chapter 4.

A full description the principles of operation of the constant temperature hot wire anemometer is found in reference 1.

The equipment used was the D.I.S.A. 55D00 Universal Anemometer with wires of 5 micron diameter and 1mm length.

A.1.2. Development Of A Velocity-Voltage Relationship

Before any measurements can be performed with the anemometer the form of the velocity - voltage relationship for the probe must be known.

Heat transfer from a cylinder to a flowing gas, may be described in terms of the Nusselt (Nu) Prandtl (Pr) and Reynolds (Re) numbers. A satisfactory form of this relationship was proposed by Kramers (Ref. 1, 2) where

$$Nu = 0.42\ Pr^{0.2} + 0.57\ \ Pr^{0.33}Re^{0.5} \qquad (A1.1)$$

when free convection terms are neglected.

For thermal equilibruim on the wire (Ref. 1) we have

$$I_w^2 R_w = e.\pi.K_f.l.(\theta_w-\theta_g)\ (0.42\ Pr_f^{0.2} + 0.57\ Pr_f^{0.33}\ Re_f^{0.5}) \qquad (A1.2)$$

Where f refers to the film temperature $(\theta_w+\theta_g)/2$

From the above equation if all the gas properties remain constant and the velocity is varied then by putting

$$I_w^2 R_w = E_w^2 / R_w$$

(where R_w is constant at constant temperature)

$$E_w^2 = \bar{E}^2 = A' + B' \bar{U}^{0.5} \qquad (A1.3)$$

Where A' and B' are constants for constant gas properties and are determined by calibration.

At zero flow $\bar{U}^{0.5} = 0$ and $\bar{E} = \bar{E}_o$

So $A' = \bar{E}_o^2$. The equation (A1.3) is often referred to as Kings law (Ref.3).

An improvement upon equation (A1.3) was proposed by Collis and Williams (Ref.4) and Bradshaw and Johnson (Ref.5) where

$$\bar{E}^2 = A'' + B'' \bar{U}^{0.45} \qquad (A1.4)$$

where $A'' = \bar{E}_o^2$

This fits the calibration data better than (A1.3) above, but is still not considered to be accurate enough especially at the lower velocity regions. Comparisons of the two forms are shown in fig. (A1.1). Here it may be seen the $\bar{E}_o$(zero flow voltage) does not lie upon the 'best fit' curve through the calibration points, and for this reason it is considered to be in error, probably due to free convection and conduction terms present when the wire is situated in still air. Hence this point is not considered when the new velocity voltage

relationship is deduced.

This new calibration technique is performed by placing the wire in a region of known velocity and recording the voltage and velocity as the velocity is varied. This is explained in Appendix (A.2).

Davies and Bruun (Ref.6) put forward an empirical voltage-velocity relationship where

$$\bar{E}_{\phi}^{2} - \bar{E}_{o}^{2} = K'' \bar{U}^{N} . \cos^{M}(90-\phi) \qquad (A1.5)$$

Where E_{ϕ} = Wire voltage at yaw angle ϕ to mean flow direction. K'', N, M are all functions of the flow velocity and remain constant only over small velocity ranges. For velocities over 1 metre/sec $M \simeq N-0.05$, and the relationship between K", N and $\bar{U}$ are shown in fig. (A1.2).

Schauber and Klebanoff (Ref.7) have shown that the effective cooling velocity $\bar{U}_E$ is given by

$$\bar{U}_E = \bar{U}_{TOTAL} \cdot \cos(\theta) \qquad (A1.6)$$

where θ is the yaw angle between the wire and the total velocity vector $\bar{U}_{TOTAL}$. Equations (A1.3), (A1.4) (A1.5) and (A1.6), assume that the cooling of the wire is performed by the velocity vector resolved normal to the wire. There is however a cooling effect of the velocity vector resolved along the wire. This is also shown in fig. (A2.1) where

typically K has a value of 0.2. To allow for this heat loss due to the component of the velocity along the wire.

Champagne and Sleicher (Ref.8) put forward the expression

$$\bar{U}_E^2 = \bar{U}_O^2 (\cos^2\theta + K^2 \sin^2\theta) \qquad (A1.7)$$

Where $\bar{U}_E$ = effective cooling velocity

$\bar{U}_\theta$ = total velocity at yaw angle θ to wire.

Many of the above expressions are summarized by Delleur (Ref.12). Clearly it would be advantageous if an empirical expression could closely fit the calibration data and be able to take into account the velocity component along the wire as well as the component normal to the wire.

A.1.3. A New Velocity-Voltage Relationship

The proposed expression which fits the calibration data better than those mentioned above and is convenient for further analysis is based upon a least squares fit for a second order polynomial on the calibration data. This gives

$$\bar{E}^2 = A + B\bar{U}^{\frac{1}{2}} + C\bar{U} \qquad (A1.7)$$

See figure (A1.1) for comparison of fit.

Equation (A1.7) is a quadratic in $\bar{U}^{\frac{1}{2}}$ and it may be readily seen is similar to Kings law (A1.3) with an extra term $C\bar{U}$.

If Kings law was found to hold exactly, then C would take a value of zero. In fact C is almost invariably negative and small, and since A, B, C, are 'best fit' constants $A \neq \bar{E}_o^2$ but is numerically less ($\bar{E}_o^2 > A$) which shows the importance of discarding $\bar{E}_o^2$ from any calibration data.

This much improved empirical velocity-voltage relationship provides the basis for the analysis of the signals obtained from a hot wire anemometer, reported in chapter 4, developed by the author. The results obtained are compared (in appendix 4) to those reported in literature (Ref.1) and to a similar method developed independantly using the same velocity-voltage expression (Ref.9). The last method shows remarkable agreement with the authors despite the fact that different assumptions are made to arrive at the answers.

A.1.4. Linearisation Of The Output From The Anemometer

Many workers favour a linear velocity-voltage relationship which may be obtained by electrical linearisation of the output from the anemometer. In practice it is impossible to obtain a truly linear calibration and in the authors experience creates more problems than non-linearisation. If it was possible to obtain a linear response easily such that two wires could be used alternatively, then the method would be preferred. At present the

disadvantages outweigh the advantages. The differance between linear and non-linear response and subsequent evaluation of the fluctuating velocity terms is shown in fig. (A1.3).

For true linearisation using a differentiation technique and putting $dE/dU = \Delta E/\Delta U$

$$\tilde{E}' \text{ measured} = \tilde{E}' \text{ actual}$$

$$\tilde{U}, \text{ computed} = \tilde{U}' \text{ actual}$$

for non-linear response

$$\tilde{E}' \text{ measured} = \tilde{E}' \text{ actual}$$

$$\tilde{U}' \text{ computed} \simeq \tilde{U}' \text{ actual}$$

$$\text{actually } U' \text{ computed} < U' \text{ actual}$$

$$\text{and the \% error} = \frac{100\,(\tilde{U}' \text{ actual} - \tilde{U}' \text{ computed})}{\tilde{U}' \text{ actual}}$$

The error increases with increasing turbulence intensity. Some of the drawbacks of linearisation are reported in Refs.(10 and 11).

The important procedure for accurate calibration of the hot wire probes, developed by the author, is reported in Appendix 2.

REFERENCES - APPENDIX 1

1 - Hinze J.O. "Turbulence" Mcgraw Hill Book Co.,

2 - Kramers H. Physica 12, 61 (1946)

3 - King L.V. "On The Convection Of Heat From Small Cylinders in a Stream of Fluid". Proc. Royal Soc., Vol. 214A No.14 (1914)

4 - Collis D.C. and Williams M.J. "Two Dimensional Forced Convection From Cylinders At Low Reynolds Numbers". Jnl. Fluid Mech., Vol.6 (1959).

5 - Bradshaw P. and Johnson R.F. "Turbulence Measurements With Hot Wire Anemometers" N.P.L. Notes on Appl. Sci., No.33 (1963)

6 - Davies P.O.A.L. and Bruun H.H. "The Performance of a Yawed Hot Wire" Proceedings of a Symposium on Instrumentation and Data. Processing for Industrial Aerodynamics N.P.L. Nov. 1968.

7 - Schauber G.B. and Klebanoff P.S. "Theory and Application of Hot Wire Instruments in the Investigation of

REFERENCES - APPENDIX 1 CONTINUED

Turbulent Boundary layers"

N.A.C.A. WR 86 (1946)

8 - Champagne F.H. Sleicher C.A. and Wehrmann O.H. "Turbulence Measurement's with Inclined Hot Wires"
Jnl. Fluid Mech., Vol 28 (1967)

9 - Davies T.W. "A Study of the Aerodynamics of the Recirculation Zone formed in a Free Annular Air Jet".
Ph.D. Thesis University of Sheffield (Jan. 1969).

10 - Parthasarathy S.P. and Tritton D.J. "Impossibility of Linearizing a Hot Wire Anemometer for Measurements in Turbulent Flows".
AIAA Jnl. Vol. 1 No. 5 (1963)

11 - Rose W.G. "Some Corrections to the Linearized Response of a Constant-Temperature Hot Wire Anemometer Operated in a Low Speed Flow".
Jnl. Appl. Mech. 29, (1962 also Erratum)

REFERENCES - APPENDIX 1 CONTINUED

12 - Delleur J.W. "Flow Direction Measurement by Hot Wire Anemometry". Jnl.Eng.Mech.Div. Proc.A.S.C.E. EM4 (1966)

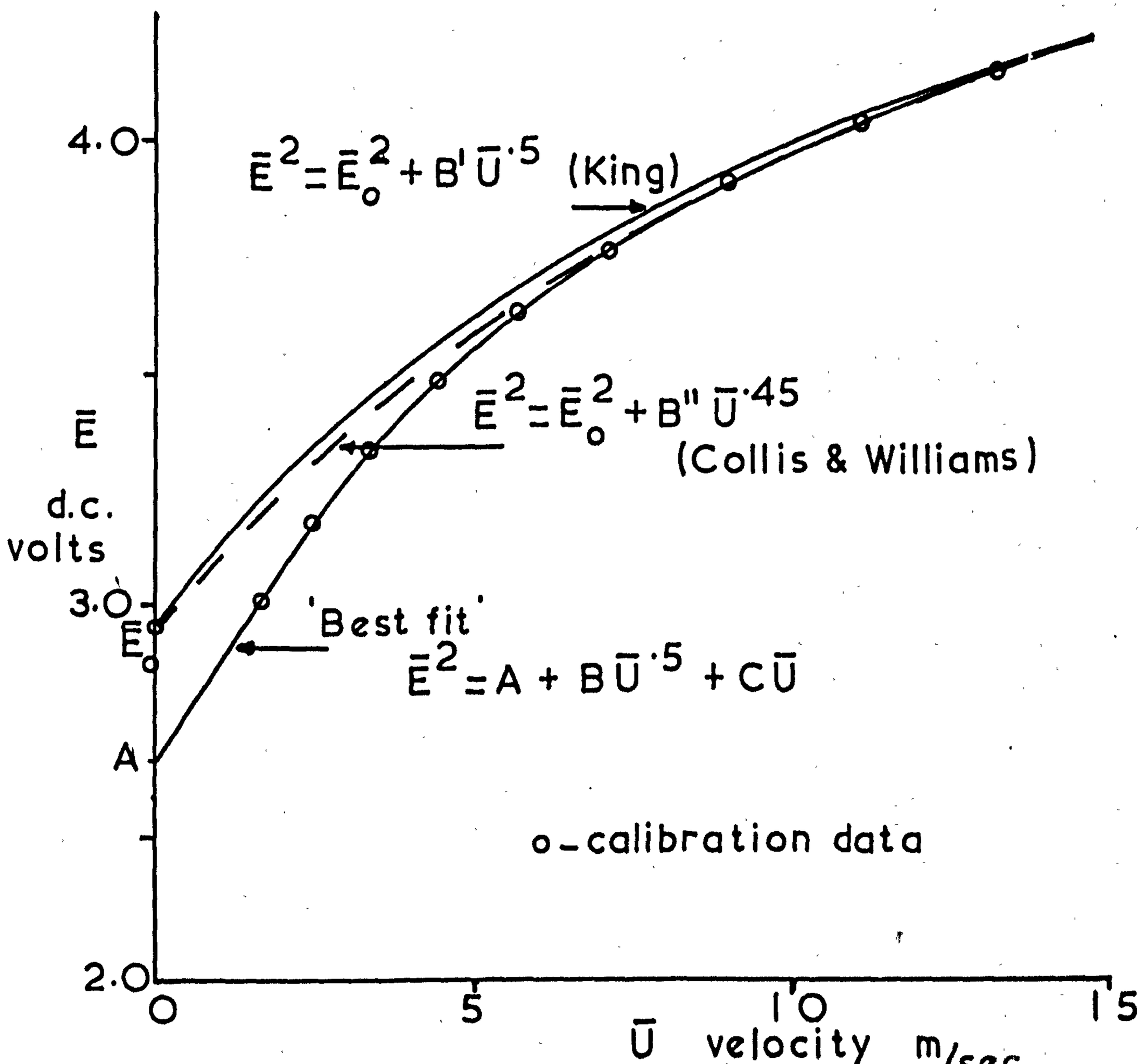

Fig. A1.1 Typical velocity-voltage relationship

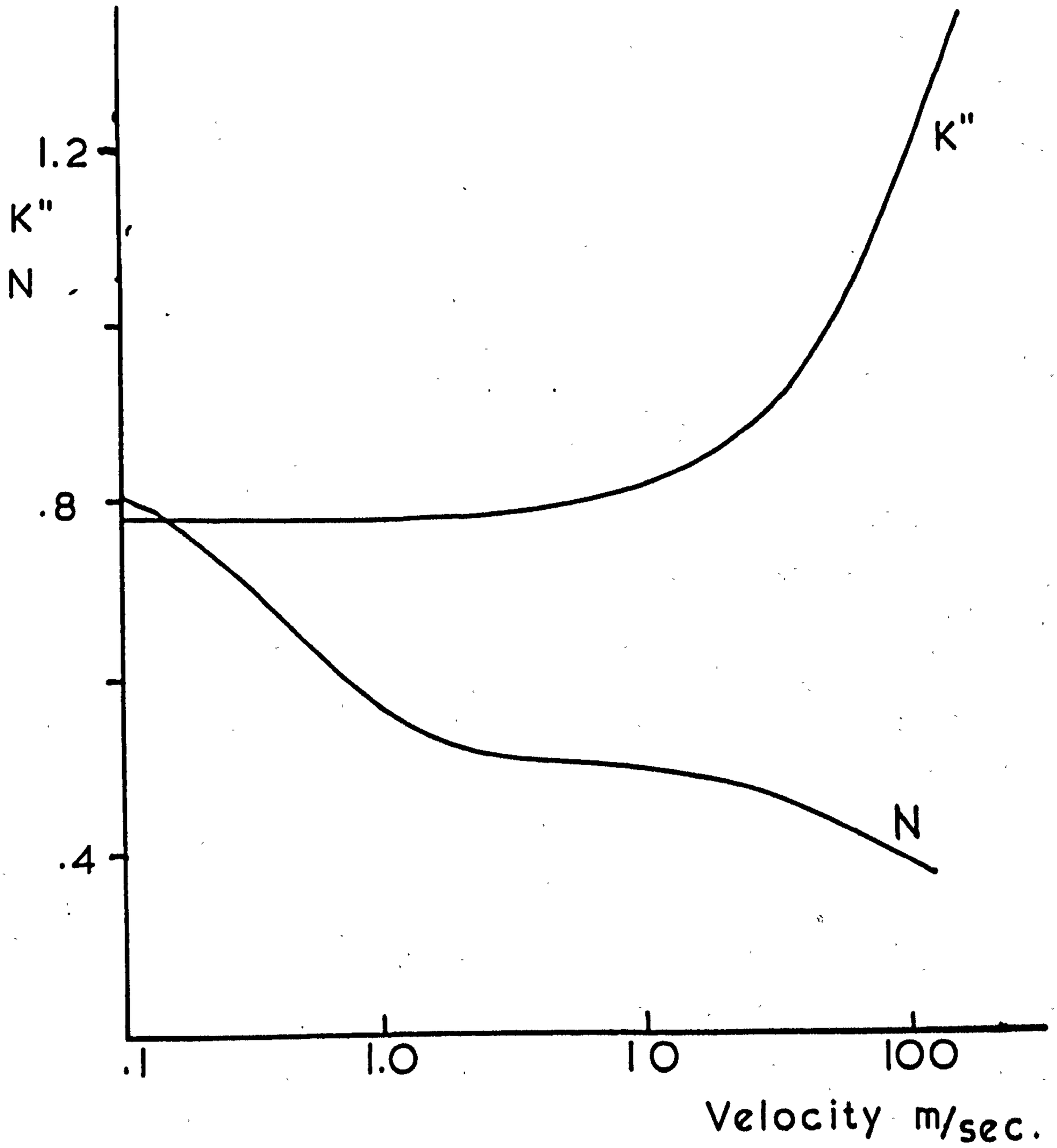

Fig. A1.2 Variation of K" and N with velocity

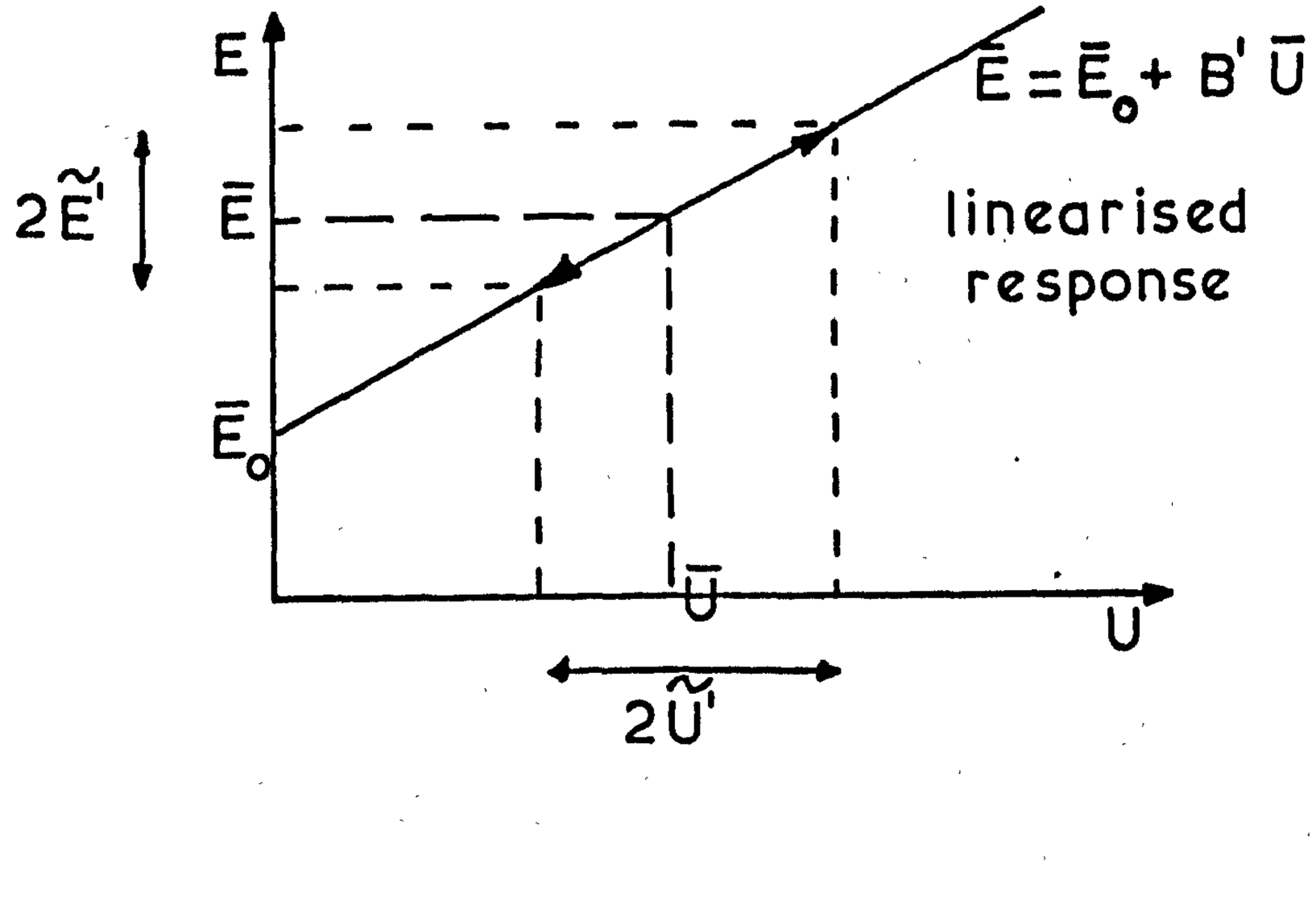

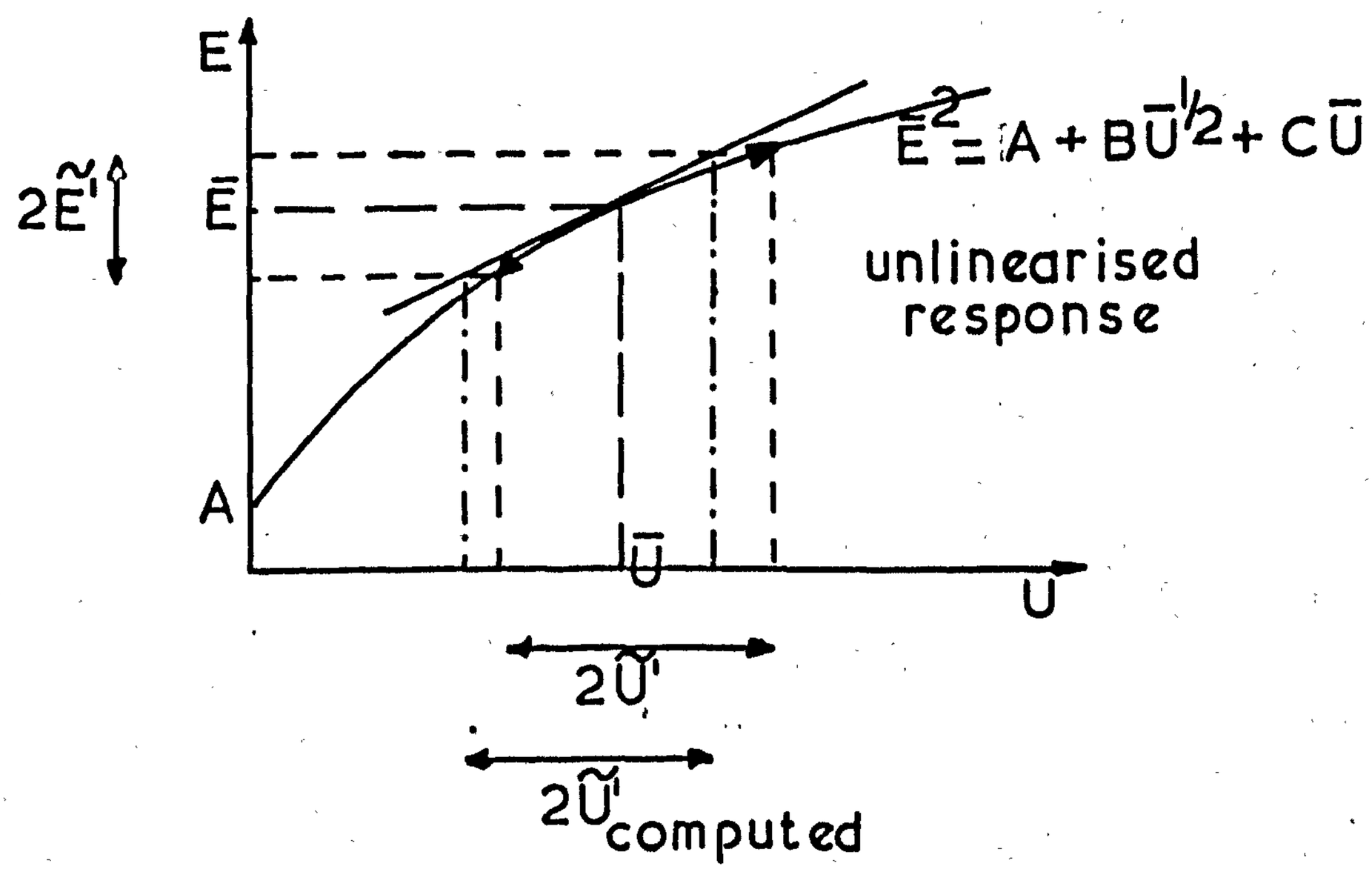

Fig. A1.3 Difference between linearised and unlinearised response, with subsequent evaluation of r.m.s. fluctuating velocity ($\tilde{U}'$) terms for differentiation technique.

APPENDIX - 2

Calibration Technique For The Hot Wire Anemometer Probes.

For accurate measurements it is necessary to accurately calibrate the wire before each run. Calibration of the wire is performed to be able to fit the second order polynomial:-

$$\bar{E}^2 = A + B\bar{U}^{\frac{1}{2}} + C\bar{U} \qquad (A2.1)$$

to the calibration data.

The wire voltage is compared to the pressure drop on an N.P.L. type pitot pressure probe placed along-side the wire on the axis and in the nozzle exit of a round free jet of low turbulence intensity (Typically 3%). The wire is placed normal to the flow and the flow is varied throughout and slightly beyond the flow velocities to be encountered in practice. The D.C. voltage is recorded against the pressure drop for about 10 to 15 points throughout the velocity range. Here it is important to note that the zero flow voltage $\bar{E}_o$ is not recorded as one point for the reasons stated in Appendix 1.

From these readings the velocity-voltage expression may be determined by fitting the second order polynomial, to the data by the method of least squares. The use of a

digital computer in working out all results is necessary to facilitate speed and accuracy. Computer programs written in FOCAL are included in Appendix 5.

To be able to allow for the cooling component of the velocity along the wire, K, and since this value varies from wire to wire, it is necessary to evaluate K either at the mid velocity point, or throughout the whole velocity range depending upon the degree of accuracy required. This is performed by rotating the probe until the flow is along the wire, which coincides with a minimum $\bar{E}$ reading on the anemometer. Graphs similar to those shown in Fig. (A2.1) may then be constructed and the K value determined. As stated above the value of K may be assumed constant over a limited velocity range, but for greater accuracy a value of K obtained from the K vs. $\bar{E}$ plot would be more accurate and takes into account the change of K with velocity. K may also vary from run to run due to ageing of the wire, distortion and dirt or grease adhering to the wire, and K may take a value within the range 0.175 to 0.3. The importance of K is shown in fig. (A4.1)

When using two different wires at each position to be measured, it is necessary to calibrate the wires before and after each run to minimise the effect of the change of

the calibration constants A,B and C with time and fluid properties. It is essential to have a clean steady air supply for the use of hot wires, and the calibration should be performed using the same air, as to be used for the measurements, or corrections must be apllied to A, B, C to allow for temperature differences.

In practice it has been found that it is not possible to supply perfectly clean air under constant temperature, pressure, humidity, conditions and any one calibration is found to hold good for periods up to two hours when re-calibration must be performed.

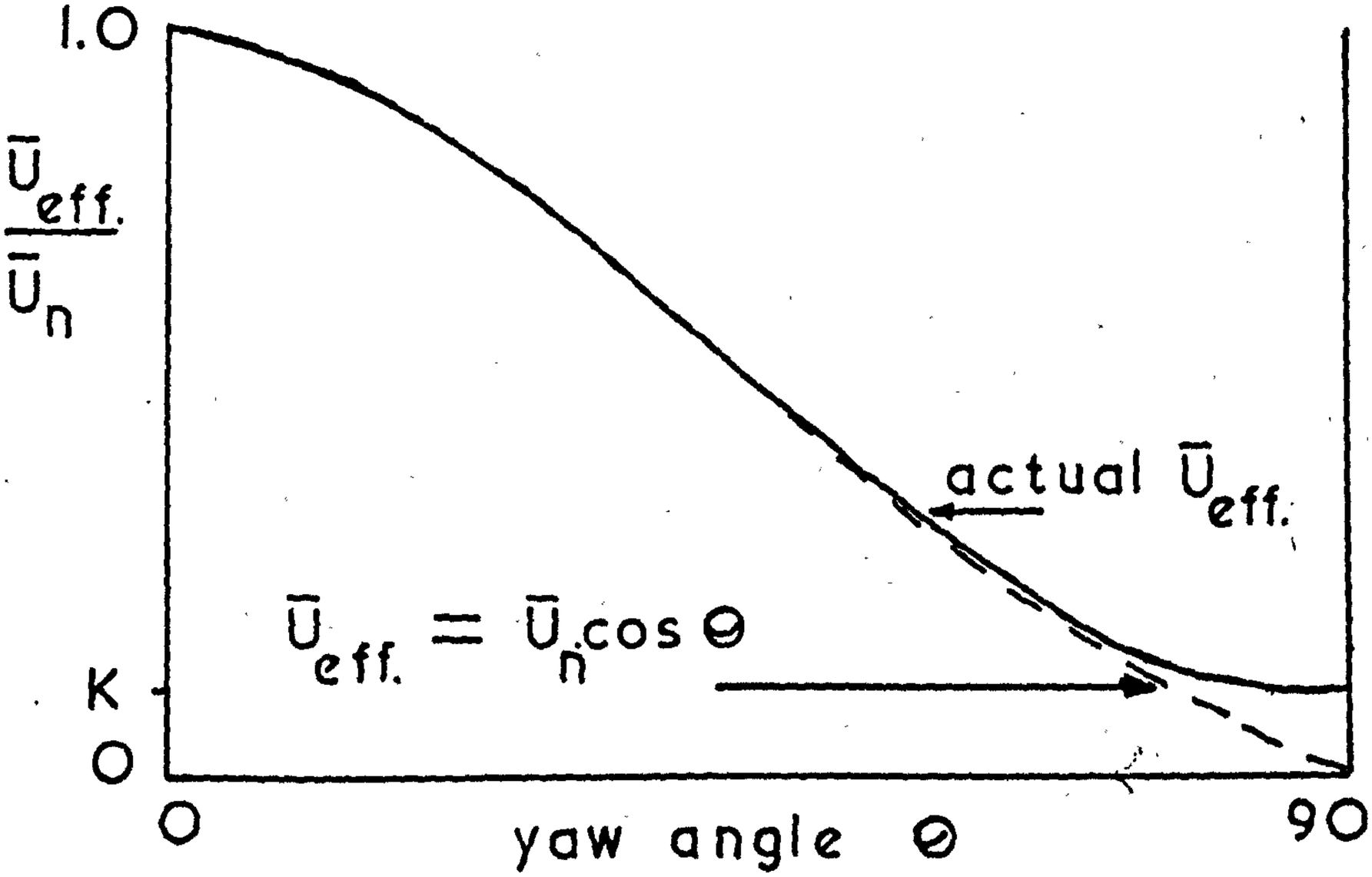

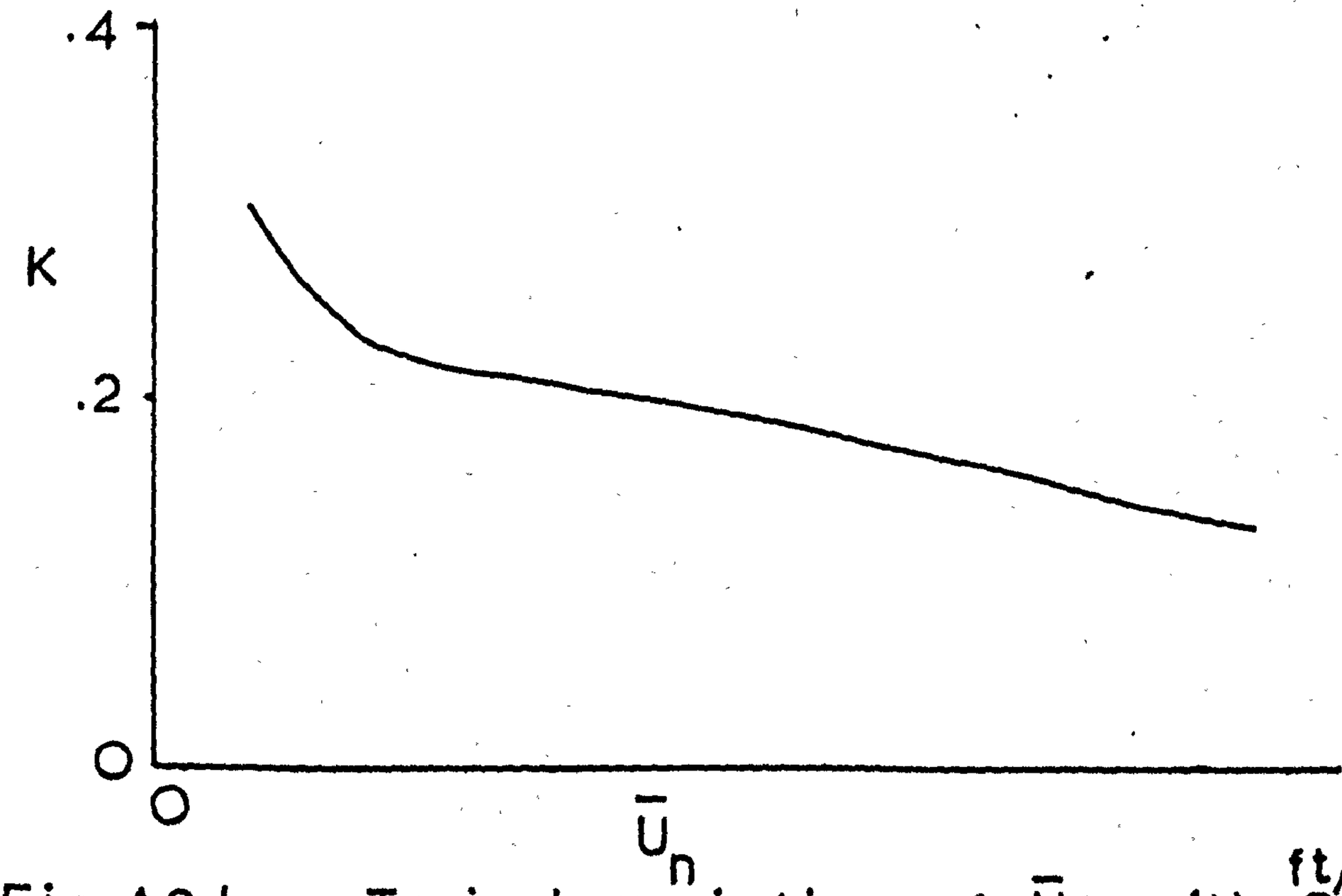

Fig. A2.1 Typical variation of $\bar{U}_{eff.}$ with Θ, and K with $\bar{U}_n$

APPENDIX 3

The Multi-Directional 5 Hole Pressure Probe (5 Hole Pitot)

A.3.1 Calibration

The probe was calibrated in a uniform velocity field which was large in relation to the probe dimensions, and of low turbulence. The probe was rotated in 2 degree intervals in the plane of holes 4 and 5 whilst maintaining (P2 - P3) = 0, (which was continuously monitored). This means that the total velocity vector was in the plane of holes 4 and 5. The total velocity was continously checked by use of an N.P.L. type pitot and was found to remain constant throughout the calibration. The rotation of the probe was arranged so that the tip of the probe remained in the same position in space relative to the flow field.

The pressure differentials P2-P3, P4-P5, $P1-P^2/_3$. $P1-P_{ambient}$, were measured as in chapter 3. From the above measurements at each 2^o interval, the graphs shown in figs.(3.6 and 3.7) were constructed.

A.3.2 Evaluation Of Velocity And Static Pressure

The relationship between the total velocity vector and the yaw, and pitch angles is shown in fig.(3.5).

After reading the yaw angle on the protractor on the probe body, the pitch angle is determined by evaluating the pitch angle coefficient $(\frac{P4-P5}{P1-P2/3})$ and then β (pitch angle) is read from the graph fig.(3.3).

(P_t-P_s) is evaluated from the velocity pressure coefficient on the same graph and the total velocity vector (V) is determined from $\frac{1}{2}\rho V^2=(P_t-P_s)$ where ρ = air density. The three component velocities are given by:-

$$\bar{u} = V \cos\beta.\cos\theta$$

$$\bar{v} = V \sin\beta$$

$$\bar{w} = V \cos\beta.\sin\theta$$

Fig.(3.4) is used to calculate the static pressure (P_s) by reading the value of the total pressure coefficient KO at the value of β, evaluating P_t from:-

$$P_t = P_1 - K_0(P_t-P_s)$$

and P_s from

$$P_s = P_t - (P_t-P_s)$$

It was assumed that the effect of turbulence present on the pressure readings was negligible.

A.3.3. The Computer Programme

There are two ways in which the computer programme may be arranged:-

(a) Graphs of figs. (3.6 and 3.7) expressed in table form for small intervals, or the graphs expressed in the form of an equation. For each of the above the only data necessary at each point to be fed to the computer would be $P_1 - P_{ambient}$, $P_1 - P_{2/3}$ $P_4 - P_5$, yaw angle 0. In fact it is fairly easy to fit expressions to the curves, but usually one has to use tables which take up a lot of memory space and an alternative method is given below.

(b) At each point it is possible for the computer to ask for the values obtained from the graphs. The computer programme in Appendix 5 is of this form and asks for values of pitch angle β, velocity pressure coefficient K, and total pressure coefficient K_0 at each point, after the initial data has been fed in and the pitch angle coefficient value typed out.

The choice of (a) or (b) above depends on the size of computer, availability for personal use, and the number of times the programme is to be used.

A programme using method (b) above is shown in Appendix 5.

APPENDIX 4

Correlation Of Turbulence Measurements And Other Data

The purpose of this appendix is to show the correlation between various methods of working out data and the relative significance of the data measured. The presentation is in the form of graphs.

Fig.(A.41) shows the correlation between measurements taken using a 5 hole pitot probe and the hot wire anemometer, on a single swirling jet 6 diameters downstream. The 3 component average velocities are plotted and the K values for the two particular wires are quoted. The importance of the K values may be readily seen when the $\bar{w}$ (swirl) component is plotted neglecting the flow component along the wire (ie. K1 = K2 = 0). The relative sizes of the wire and pitot probe tip to the flow field are also shown.

Fig.(A4.2) shows the correlation between the measurements taken by the Author on a single non-swirling jet, and those obtained by Corrsin (Ref.1) on a similar system. The radial distribution of $\bar{u}/\bar{u}_{max}$, $\overline{u'v'}/\bar{u}^2_{max}$ and $(\overline{u'^2})^{\frac{1}{2}}/\bar{u}$ are plotted at $x/D = 16$.

Fig.(A.4.3) shows the correlation between $(\overline{u'^2})^{\frac{1}{2}}/\bar{u}$ and I_{loc} (= $\frac{(\overline{u'^2} + \overline{u'^2} + \overline{w'^2})^{\frac{1}{2}}}{(\bar{u}^2 + \bar{u}^2 + \bar{w}^2)^{\frac{1}{2}}}$) terms for a non-swirling jet 16 diameters downstream, and for a strongly swirling jet 4 diameters downstream.

Fig.(A.4.4) shows the correlation between the authors methods of analysis and a similar method, developed by a co-worker (Ref.2).

Fig.(A4.5) shows typical $\bar{u}/\bar{u}_{max.}$ and $u'/\bar{u}$ measurements on free swirling jets by Rose, Craya and Darrigol and Chigier and Chervinsky having similar swirl number (S).

Fig. (A4.6) shows computed $\overline{u'v'}$ terms by Craya and Darrigol, (the measured distributions are said to have the same form, but slightly weaker), and measured $\bar{u}/\bar{u}_{max.}$ and I_{loc} distributions for jets having a very strong swirl. (The values for I_{loc} were quoted as $u'/\bar{u}$ terms, but since Johansen O.N. used only a single position technique for measuring local turbulence intensities as shown in (Ref.7), the actual measured values were considered to be too high and more closely resembled

$$\frac{\left(\overline{u'^2} + \overline{v'^2} + K^2 \overline{w'^2} \right)^{\frac{1}{2}}}{\left(\overline{u}^2 + \overline{v}^2 + K^2 \overline{w}^2 \right)^{\frac{1}{2}}}$$

Because a single vertical wire picks up all the above component fluctuating terms (see 3 pt. technique Chapter 4.)).

REFERENCES - APPENDIX 4

(1) Hinze J.O. "Turbulence"
M^cGraw Hill Book Co.,

(2) Davies T.W.
"A Study Of The Aerodynamics Of The Recirculation Zone Formed In A Free Annular Air Jet."
Ph.D. Thesis University Of Sheffield : (Jan 1969)

(3) Rose W.G.
"A Swirling Round Turbulent Jet"
Jnl. Appl. Mech. (Dec.1962)
Trans. A.S.M.E.

(4) Craya A and Darrigol M.
"Turbulent Swirling Jet"
Physics Of Fluids Supplement (1967)
Vol.10 pt.9.

(5) Chigier N.A. and Chervinsky A.
"Experimental Investigation of Swirling Vortex Motion In Jets".
Jnl.Appl. Mech. (June 1967) Trans A.S.M.E.

REFERENCES - APPENDIX 4 Cont.

(6) Johansen O.N.
"Investigation Of The Flow-Pattern In An Oil Burner With Varying Degree Of Swirl On The Combustion Air"
Ph.D. Thesis Heat Eng.Lab. Mech.Dept. N.T.H. Trondheim (July 1967).

(7) D.I.S.A. 55D00
Universal Anemometer Manual.

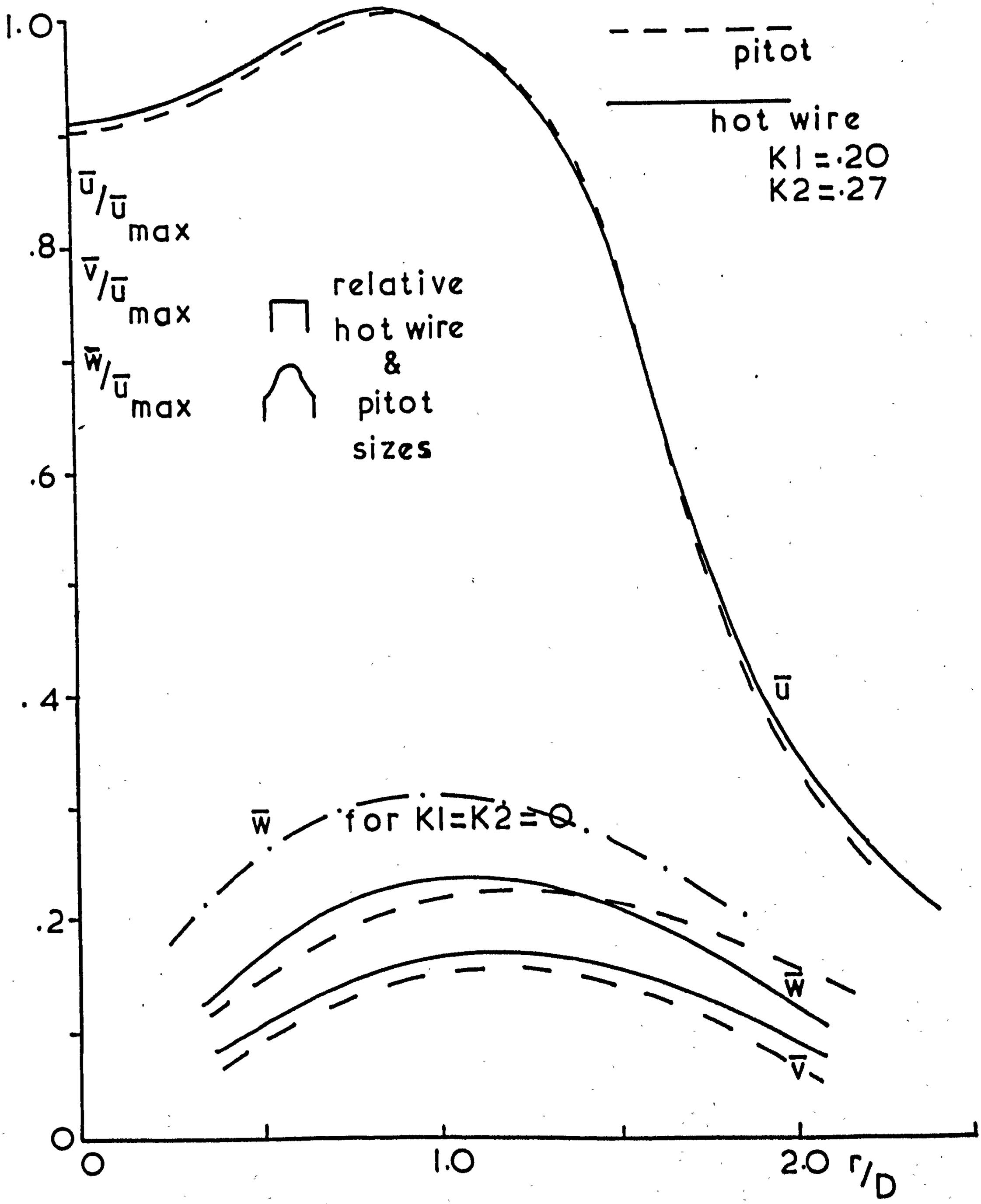

Fig. A4.1 Correlation between pitot and hot wire data for single swirling jet 6 dia. downstrec

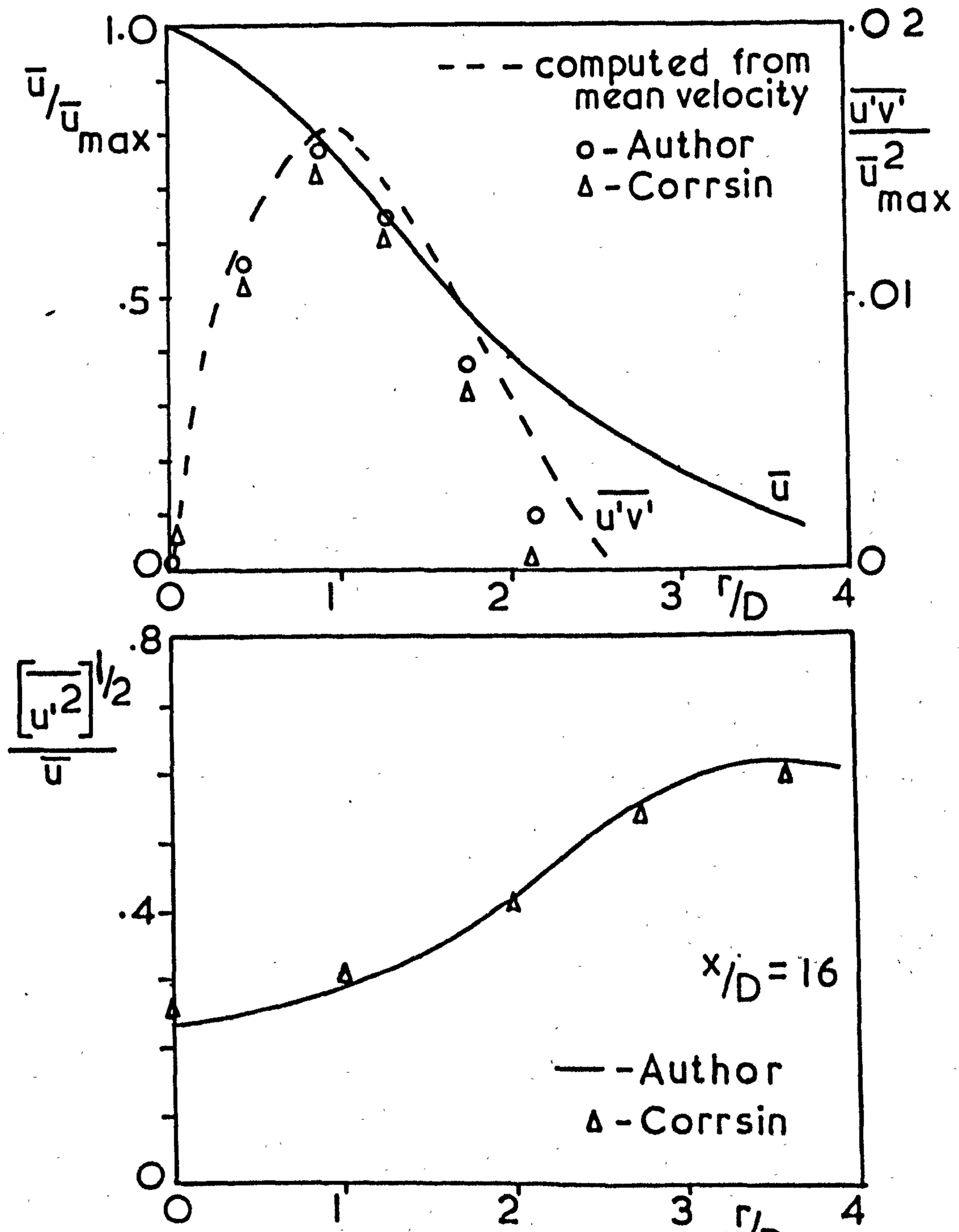

Fig. A4.2 Radial distribution of turbulence quantities in a round free jet

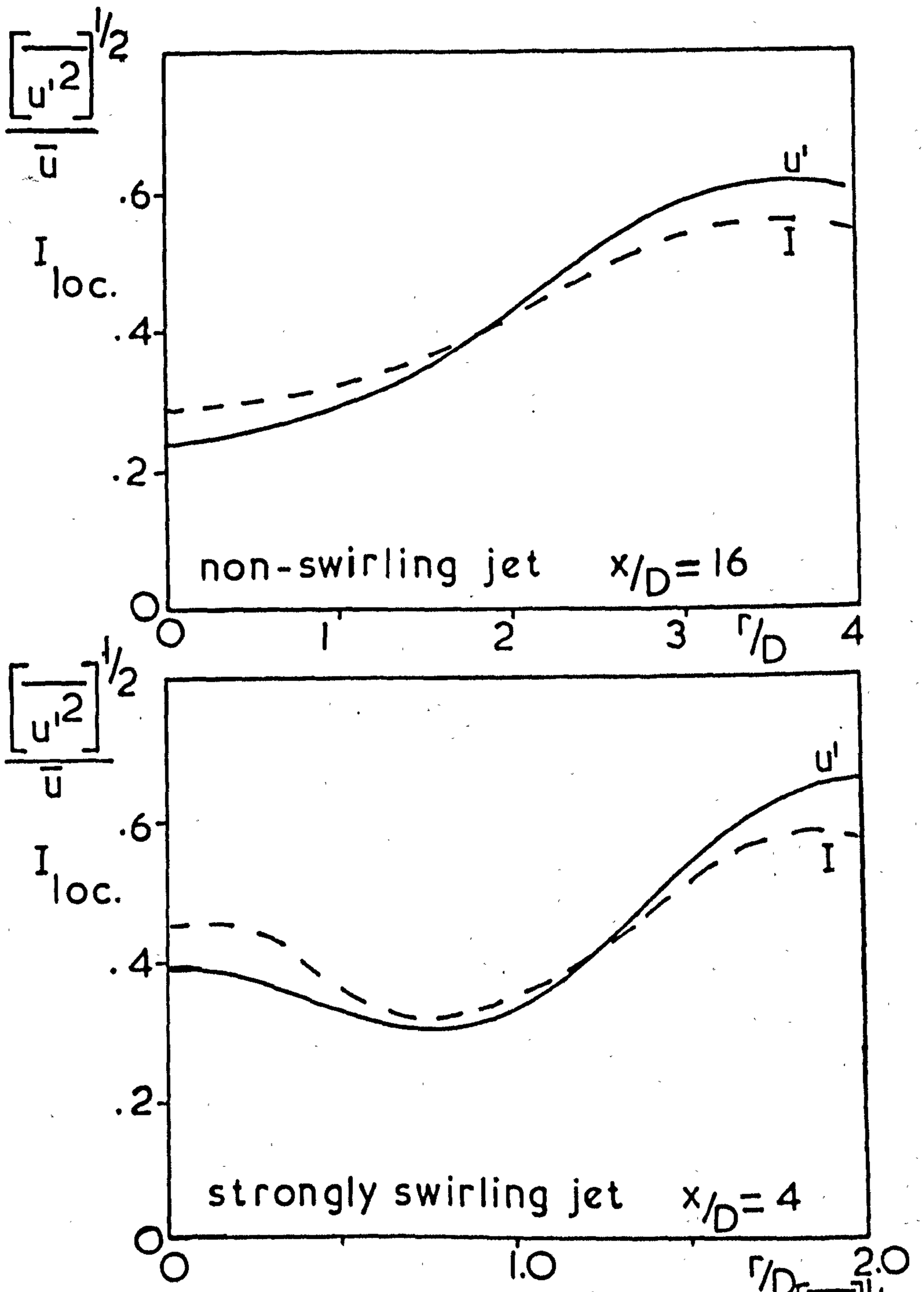

Fig. A4.3 Correlation between $\frac{[\overline{u'^2}]^{1/2}}{\bar{u}}$ and $I_{loc.}$ terms for a non-swirling and strongly swirling jet

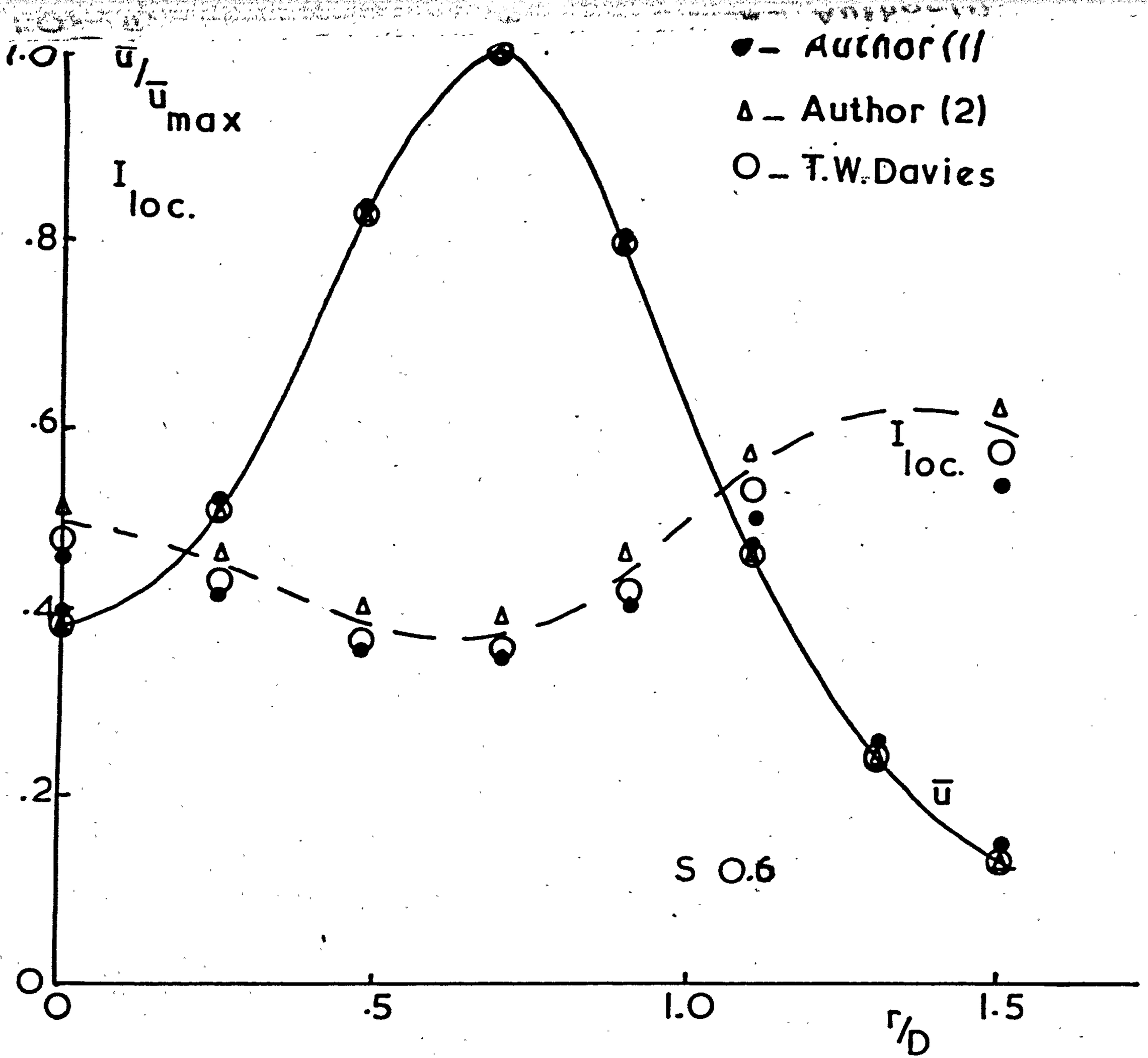

Fig. A4.4 Correlation between author's methods of analysis and co-worker's method, (T.W. Davies) for single swirling jet 2 diameters downstream

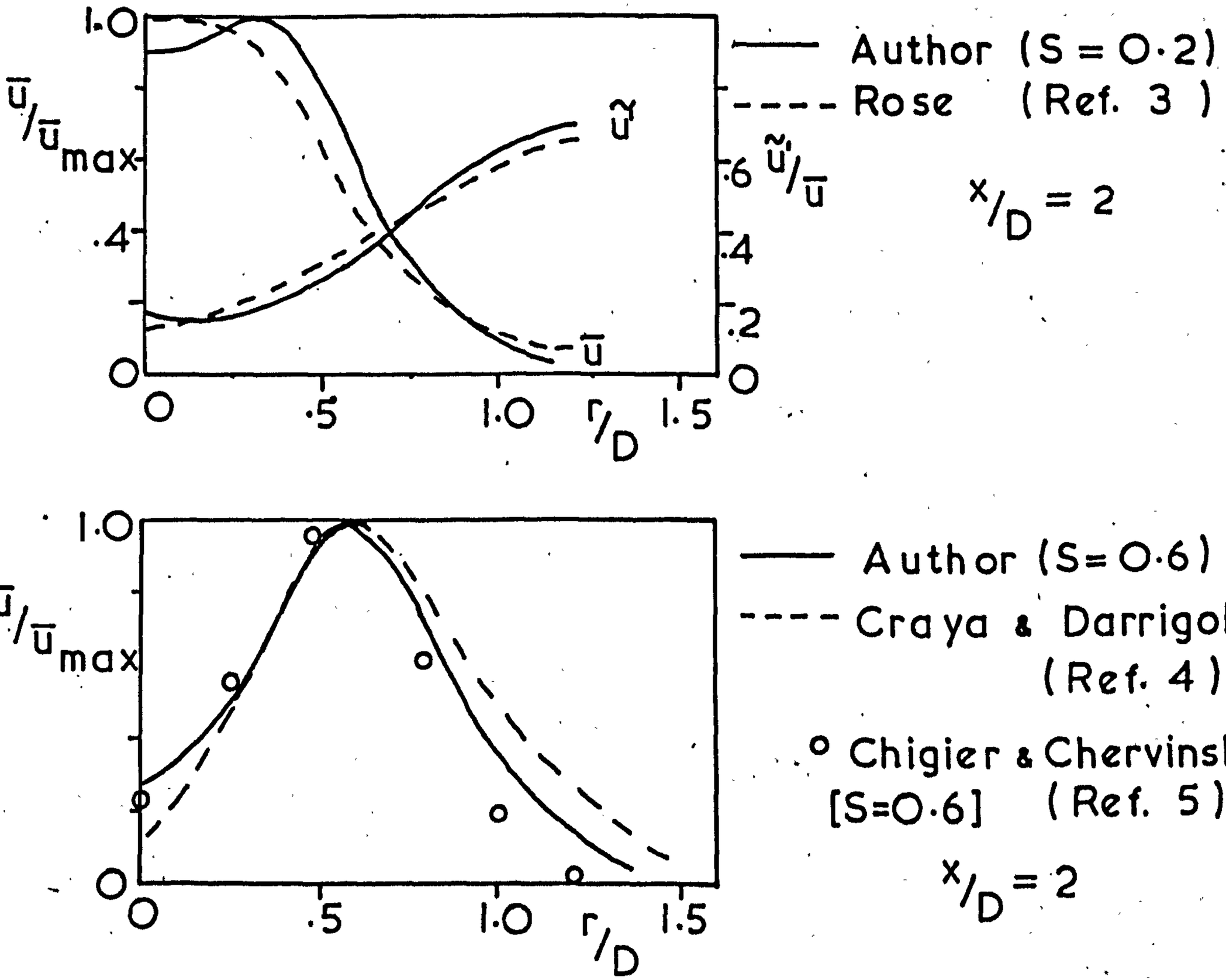

Fig: A4.5 Comparative swirling jet data (i)

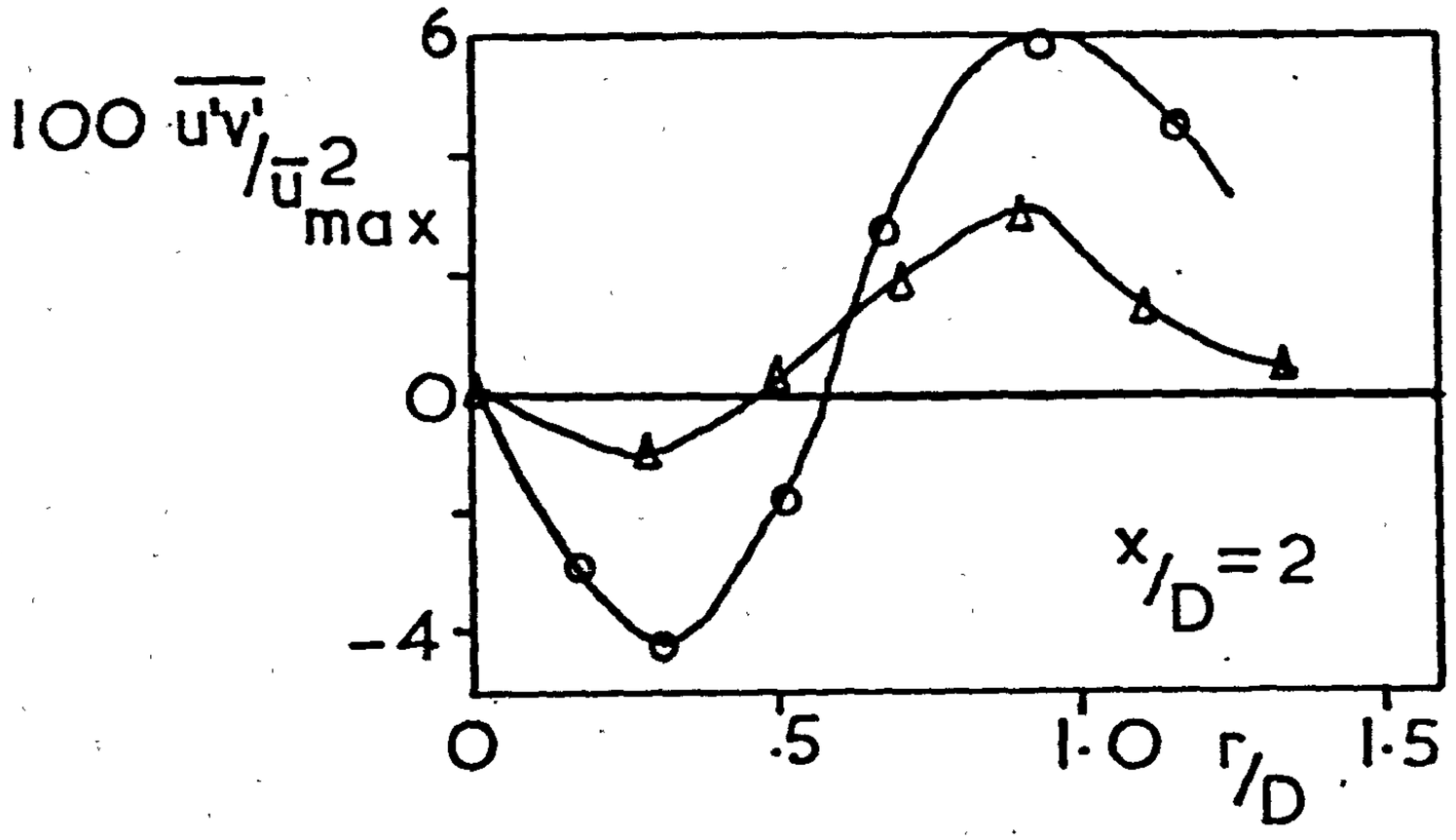

Δ — Author (measured for S=0·6)

o — Craya & Darrigol (computed for a very strongly swirling jet — ref. 4) [S≈0·8]

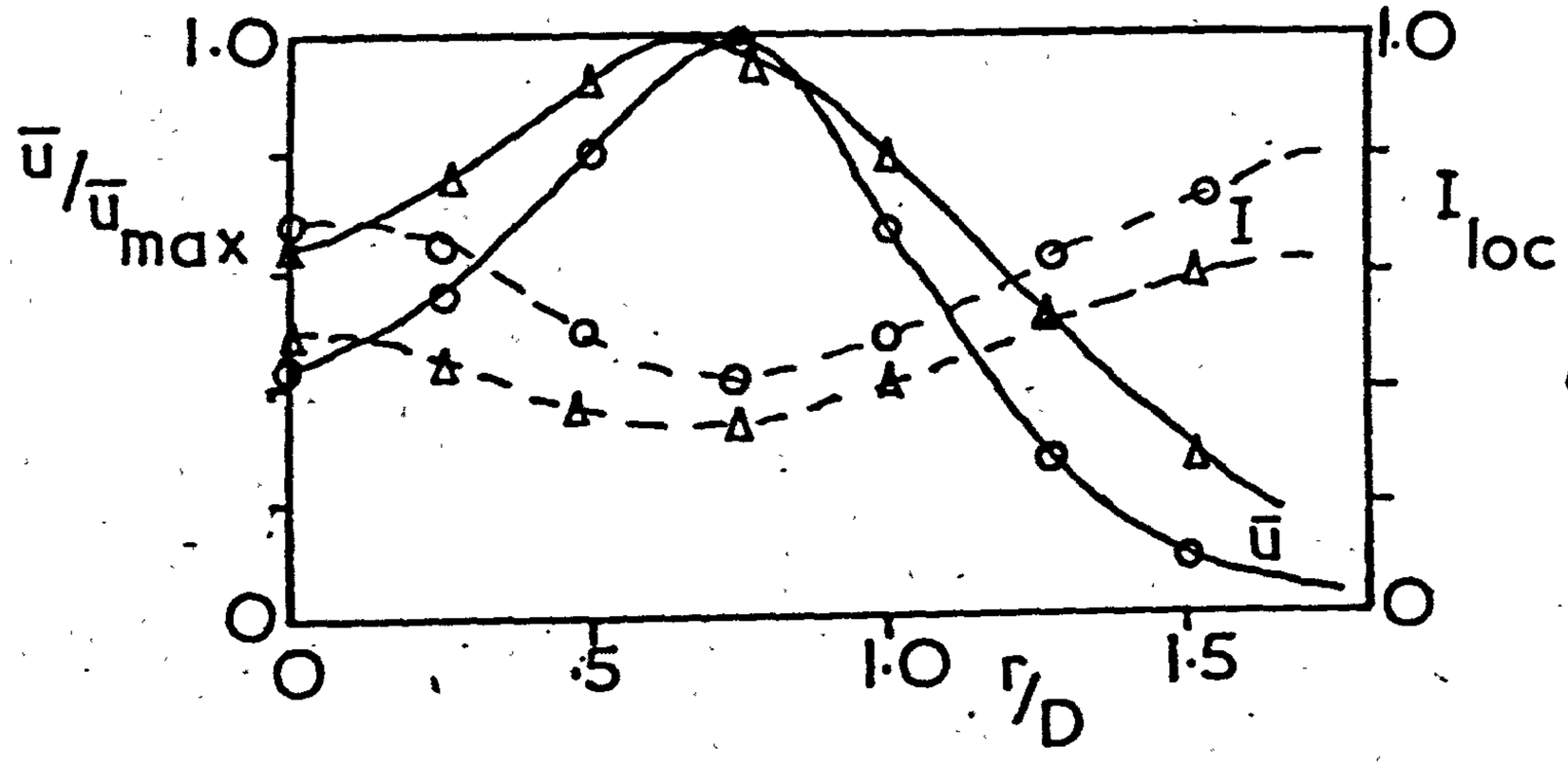

Δ — Author (measured for S=0·6, $x/D = 4$)

o — Johansen O.N. (for strongly swirling jet $x/D = 3.3$) [Ref. 6] (S≃0·6)

Fig.A4·6 Comparative swirling jet data (ii)

APPENDIX 5

Computer Programmes

This appendix gives worked examples of the computer programmes written in FOCAL used to evaluate the data.

Programme No.1

This programme is used to evaluate the constants A,B,C in the calibration equation (A1.7). The atmospheric conditions of temperature (^{o}C) pressure ("H_g) and the number of sets of calibration data (in this case 11) are fed in first, with the corresponding anemometer D.C.Voltage ($\bar{E}$) and pitot pressure readings ("H_2O) later.

The computer does a least squares fit on the data and types out the corresponding constants A,B,C. The computer then types out the value of the anemometer D.C. Voltage fed in (E) and the corresponding voltage (P) obtained from the calibration equation. Comparison of (E) and (P) shows the very close fit of the calibration equation throughout the whole velocity range; which usually agrees to the third significant figure.

Programme No.2

This programme is used for the 3 position technique of analysis with the hot-wire anemometer.

The values of the factors K1, K2 allowing for cooling along the wire are fed in first with the calibration data A,B,C, for each wire immediately afterwards.

For each position measured the 3 values of $\bar{E}$ and $\tilde{E}'$ are fed in and the computer types out the values of $\overline{u'^2}$, $\overline{v'^2}$, $\overline{w'^2}$, $\bar{u}$, $\bar{v}$, $\bar{w}$, total velocity, I_{loc}, $\tilde{u}'/\bar{u}$, etc., (Note in these programmes the v and w terms are interchanged ie. $\bar{v}$ = swirl velocity etc.)

Programme No.3

This programme is used for the 6 position technique of analysis with the hot-wire anemometer. This programme is similar to the 3 pt. programme but gives $\overline{u'v'}$, $\overline{u'w'}$, $\overline{v'w'}$ terms, after the $\bar{E}$ and $\tilde{E}'$ correspond/ing to all the 6 measurement positions have been fed in after the calibration data.

Programme No.4

This programme is used for the 5 hole pitot probe in conjunction with the calibration charts (Figs.(3.6 and 3.7)).

The atmospheric temperature and pressure are fed in first, followed by the radial position (R) and the values of (P_4-P_5), $(P_1-P_{2/3})$, yaw angle (O) and (P_1-P_o). The computer then types out the value $(P_4-P_5) / (P_1-P_{2/3})$

and asks the value of the pitch angle (A), the velocity pressure coefficient (K) and the total pressure coefficient (K_O).

The computer then types out the values of $\bar{u}$, $\bar{v}$, $\bar{w}$, static pressure, total velocity.

Programme No,1

Hot wire calibration

```
C-FOCAL., 1968

01.01 A "T"T,"P"RP,"N"N; S S=0; S L=0; S V=0; S K1=(273+T)*30/293*RP
01.04 S O=0; S A=0; S I=0; S Q=0; S J=0; F M=1,N; A E(M); A P(M); D 2
01.07 G 3.10

02.01 S X(M)=FSQT(66.5*FSQT(P(M)*K1))
02.11 S A=A+E(M)↑2; S I=I+X(M); S S=S+X(M)↑2; S L=L+X(M)*E(M)↑2
02.16 S V=V+X(M)↑3; S O=O+X(M)↑2*E(M)↑2; S J=J+X(M)↑4

03.10 S U=N*(S*J-V↑2)+I*(V*S-I*J)+S*(I*V-S↑2)
03.20 S W=N*(S*O-L*V)+I*(L*S-I*O)+A*(I*V-S↑2)
03.30 S G=N*(L*J-V*O)+A*(V*S-I*J)+S*(I*O-L*S)
03.40 S H=A*(S*J-V↑2)+I*(V*O-L*J)+S*(L*V-S*O)

04.11 T %8.06, "A"H/U,!; T "B"G/U,!; T "C"W/U,!
04.20 F M=1,N; S R(M)=H/U+G*X(M)/U+W*X(M)↑2/U; T "E"E(M),"  P"FSQT(R(M))
*G

T:18.0 P:29.295 N:11

:3.522 :.010 :3.628 :.017 :3.711 :.0265 :3.841 :.047 :3.957 :.0775
:4.055 :.1155 :4.138 :.159 :4.233 :.2245 :4.303 :.29 :4.377 :.368
:4.433 :.446

A=+ 7.128440
B=+ 2.155680
C=- 0.042650
E=+ 3.522000   P=+ 3.524910
E=+ 3.628000   P=+ 3.623530
E=+ 3.711000   P=+ 3.712880
E=+ 3.841000   P=+ 3.837710
E=+ 3.957000   P=+ 3.955580
E=+ 4.055000   P=+ 4.055590
E=+ 4.138000   P=+ 4.139500
E=+ 4.233000   P=+ 4.233780
E=+ 4.303000   P=+ 4.306150
E=+ 4.377000   P=+ 4.375270
E=+ 4.433000   P=+ 4.432260
*
```

Programme No. 2

Hot wire —3 Point

```
C-FOCAL., 1968

01.01 A ?K1?,?K2?; S K1=K1↑2; S K2=K2↑2; S Z=2-K2-K1*K2
01.02 F Q=1,2; A A(Q),B(Q),C(Q)

02.01 F N=1,2; S Q=1; A E(N),V(N); D 3
02.03 S N=3; S Q=2; A E(N),V(N); D 3
02.04 G 5.02

03.01 S U(N)=(-B(Q)+FSQT(B(Q)↑2-4*C(Q)*(A(Q)-E(N)↑2)))/2*C(Q)
03.02 S J=16*V(N)↑2/(B(Q)↑2+4*C(Q)*((E(N)↑2+V(N)↑2)-A(Q)))
03.03 S W(N)=J*V(N)*E(N)+FSQT(J↑2*V(N)↑2*E(N)↑2+J*(E(N)↑2+V(N)↑2)*U(N)↑2
03.04 S W(N)=W(N)↑2

05.02 S U'=(W(1)+W(2)-W(3)*(1+K1))/Z; S V'=(U'*(1-K2)-(W(1)-W(3)))/(1-K1
05.03 S W'=(U'*(1-K2)-(W(2)-W(3)))/(1-K1); S KE=U'+V'+W'
05.04 S U=FSQT((U(1)↑4+U(2)↑4-U(3)↑4*(1+K1))/Z)
05.05 S V=FSQT((U↑2*(1-K2)-(U(1)↑4-U(3)↑4))/(1-K1))
05.06 S W=FSQT((U↑2*(1-K2)-(U(2)↑4-U(3)↑4))/(1-K1)); S G=FSQT(U↑2+V↑2+W2

06.01 T %8.04,?U'?,!?V'?,!?W'?,!?U?,!?V?,!?W?,!"TOTV"G,!
06.03 T "ILOC"FSQT(KE)/G,!"U'/U"FSQT(U')/U,!; G 2.01
*G

K1:.16 K2:.24
:8.17432 :1.75041 :-.006523 :7.73749 :2.00727 :-.020415
:4.251 :.250 :4.482 :.251 :4.435 :.232

U'=+ 187.6210
V'=+ 188.0350
W'=+  34.9177
U=+  30.6825
V=+  37.9506
W=+  11.6860
TOTV=+  50.1819
ILOC=+   0.4038
U'/U=+   0.4464
:
```

Programme No, 3

Hot wire — 6 Point

C-FOCAL., 1968

```
01.01 A "K"P; S P=1+P↑2; F Q=1,2; A A(Q),B(Q),C(Q)

02.01 F N=1,4; S Q=1; A E(N),V(N); D 3
02.03 F N=5,6; S Q=2; A E(N),V(N); D 3
02.04 G 5.01

03.01 S U(N)=(-B(Q)+FSQT(B(Q)↑2-4*C(Q)*(A(Q)-E(N)↑2)))/2*C(Q)
03.02 S J=16*V(N)↑2/(B(Q)↑2+4*C(Q)*((E(N)↑2+V(N)↑2)-A(Q)))
03.03 S W(N)=J*V(N)*E(N)+FSQT(J↑2*V(N)↑2*E(N)↑2+J*(E(N)↑2+V(N)↑2)*U(N)↑2
03.04 S W(N)=W(N)↑2

05.01 S U=((2+P)*(W(5)+W(6))-P*(W(1)+W(2)+W(3)+W(4)))/2*(2+P*(1-P))
05.02 S V=(U*(2-P)+W(4)+W(2)-W(5)-W(6))/(2-P);S W=.5*(W(1)+W(3)-P*(U+V))
05.03 S X=FSQT(U+V+W); T %8.04,"U'"U,!"V'"V,!"W'"W,!; S Z=U
05.04 S U=((2+P)*(U(5)↑4+U(6)↑4)-P*(U(1)↑4+U(2)↑4+U(3)↑4+U(4)↑4))
05.05 S U=FSQT(U/2*(2+P*(1-P)))
05.06 S V=FSQT((U↑2*(2-P)+U(4)↑4+U(2)↑4-U(5)↑4-U(6)↑4)/(2-P))
05.07 S W=FSQT(.5*(U(1)↑4+U(3)↑4-P*(U↑2+V↑2)))
05.08 T ?U?,!?V?,!?W?,!"U'/U"FSQT(Z)/U,!; S Z=FSQT(U↑2+V↑2+W↑2)
05.09 S U=(W(3)-W(1))/2*(2-P);S V=(W(2)-W(4))/2*(2-P)
05.10 S W=(W(5)-W(6))/2*(2-P); T "U'V'"U,!"U'W'"V,!"V'W'"W,!"TOTV"Z,!
05.11 T "ILOC"X/Z,!"I"X/50,!; G 2.01
*G

K:.18 :7.62302 :2.27890 :-.044775 :7.16625 :2.55744 :-.070992

:4.334 :.112 :4.346 :.127 :4.330 :.107 :4.312 :.081
:4.528 :.105 :4.529 :.107
U'=+  48.4155
V'=+   4.1346
W'=+   7.0860
U=+  39.1212
V=+   7.9089
W=+   8.9065
U'/U=+   0.1779
U'V'=-   1.8227
U'W'=+  15.6645
V'W'=-   1.1546
TOTV=+  40.8943
ILOC=+   0.1888
I=+   0.1544
:
```

Programme No. 4

5 - hole pitot

C-FOCAL., 1968

```
01.01 A "TEMP"T,"PRESSURE"P,!; S Z=(273+T)*30/293*P
01.03 A "R="R,"P4-P5"P4,"P1-P2/3"P1,"YAW ANGLE"J; S O=J*.0174533
01.04 A "P1-P0"P0,!

02.01 S DP=P4/P1; T "P4-P5/P1-P2/3"DP; A "   PITCH ANGLE"A,"   K"K
02.02 S PT=K*P1; A ?K0?,!; S PS=P0-PT-K0*PT; S Q=.0174533*A
02.03 S V=66.5*FSQT(P1*Z*K/25.4); S U1=V*FCOS(O)*FCOS(Q)
02.05 S V1=V*FSIN(Q); S W1=V*FCOS(O)*FSIN(O)
02.06 T % 8.04,!"U"U1,!"V"V1,!"W"W1,!"P STATIC"PS,"  MM.H20",!
02.07 T "TOTV"V,!!
*G
```

```
TEMP:21.2 PRESSURE:29.68
R=:2.5 P4-P5:.425 P1-P2/3:.655 YAW ANGLE:18 P1-P0:.05
P4-P5/P1-P2/3=+   0.6489   PITCH ANGLE:-16    K:.89 K0:.13

U=+    9.2786
V=-    2.7975
W=+    3.0148
P STATIC=-    0.6087  MM.H20
TOTV=+  10.1493

*
```

APPENDIX 6

Experimental Results Presented As Spatial Distributions

This appendix gives most of the significant recorded data in a form which it is easy to understand, and which may be used for quick reference to enable the reader to visualise some of the observations and results detailed in Chapter 5.

The data is presented as spatial distributions of $\bar{u}/\bar{u}_o$, I, $\overline{u'v'}/\bar{u}_o^2$ for all the single and multiple swirling and non-swirling jet systems used. (Note that for most of the swirling jet systems the 3 pt. technique was used to reduce the time required for taking the measurements and hence the shear stress terms $\overline{u'v'}$, $\overline{u'w'}$, $\overline{v'w'}$ were not available. The values of these shear stress terms and also the swirl velocity terms change so many times and so rapidly from +ve to -ve during a single traverse that the spatial distributions are very comples and confusing, and for this reason were not recorded). The edge of the jets are shown in the r/D scale as black marks to help the reader to visualise the position of the jets w.r.t. the spatial distributions.

This appendix may be treated as part of the experimental results. As it was considered too confusing to include all the results in the main body of the thesis,

these spatial distributions were placed at the end of the thesis for ready reference.

Figs. (A6.1 and A6.2) show the spatial distributions of $\bar{u}/\bar{u}_o$, I, and 100 $\overline{u'v'}/\bar{u}_o^2$ for a single enclosed non-swirling jet for comparison with the multiple non-swirling jet distributions recorded immediately afterwards.

Figs. (A6.3, A6.4 and A6.5) show the spatial distribution of $\bar{u}/\bar{u}_o$, I, and 100 $\overline{u'v'}/\bar{u}_o^2$ respectively for 3 non-swirling jets 1.25 D and 2.0 D apart.

Figs. (A6.6 and A6.7) show the spatial distribution of $\bar{u}/\bar{u}_o$, I, and 100 $\overline{u'v'}/\bar{u}_o^2$, $W/\bar{u}_o$ respectively for a single enclosed swirling jet, for comparison with multiple swirling jets recorded immediately afterwards. (S = 0.6, for this and all the multiple swirling jet system).

Figs. (A6.8 and A6.9) show the spatial distribution of $\bar{u}/\bar{u}_o$ for 3 swirling jets "out of mesh" and "in mesh" respectively, 1.25 D and 2.0 D apart.

Figs. (A6.10 and A6.11) show the spatial distribution of I for 3 swirling jets "out of mesh" and "in mesh" respectively, 1.25 D and 2.0 D apart.

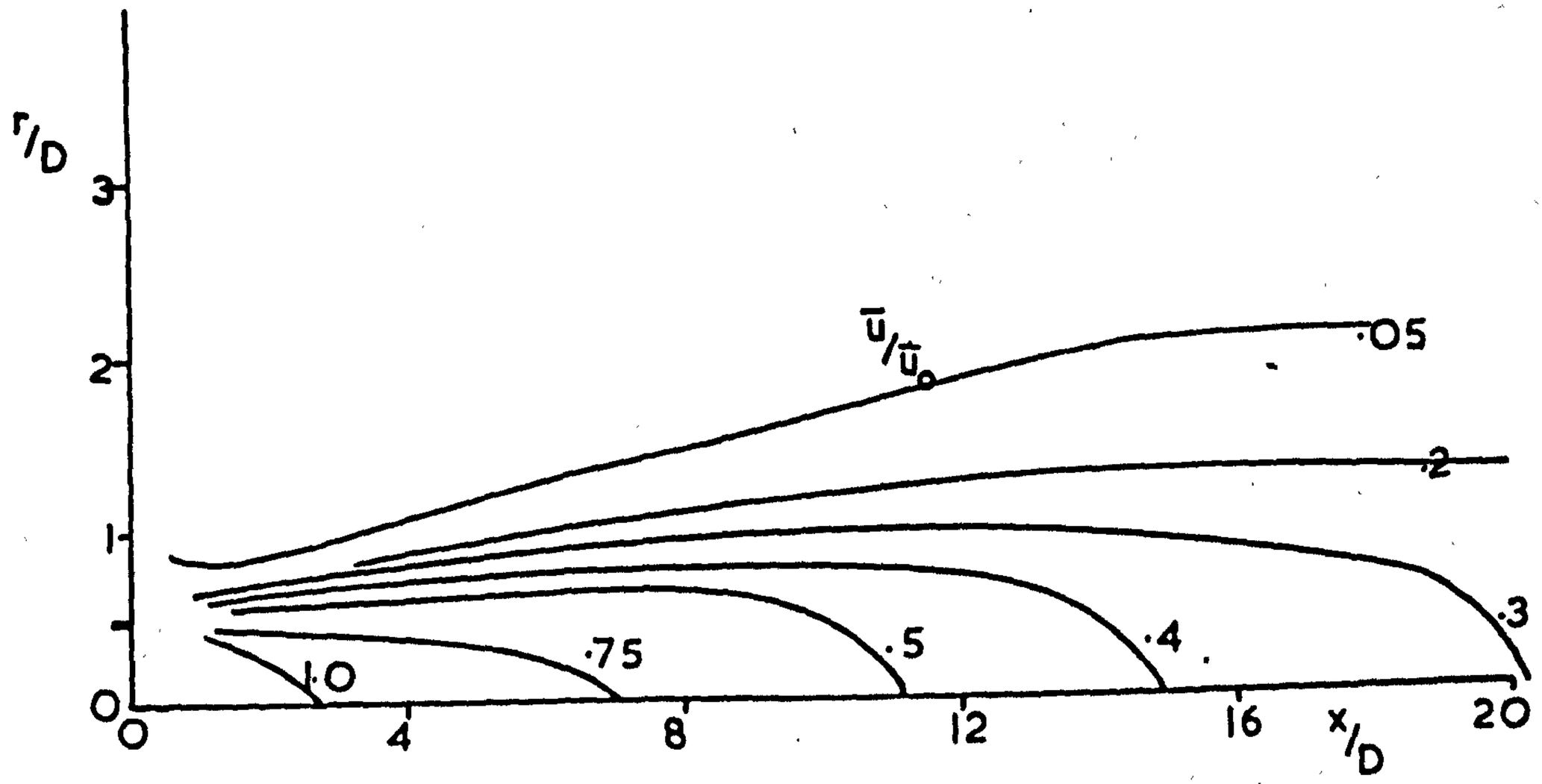

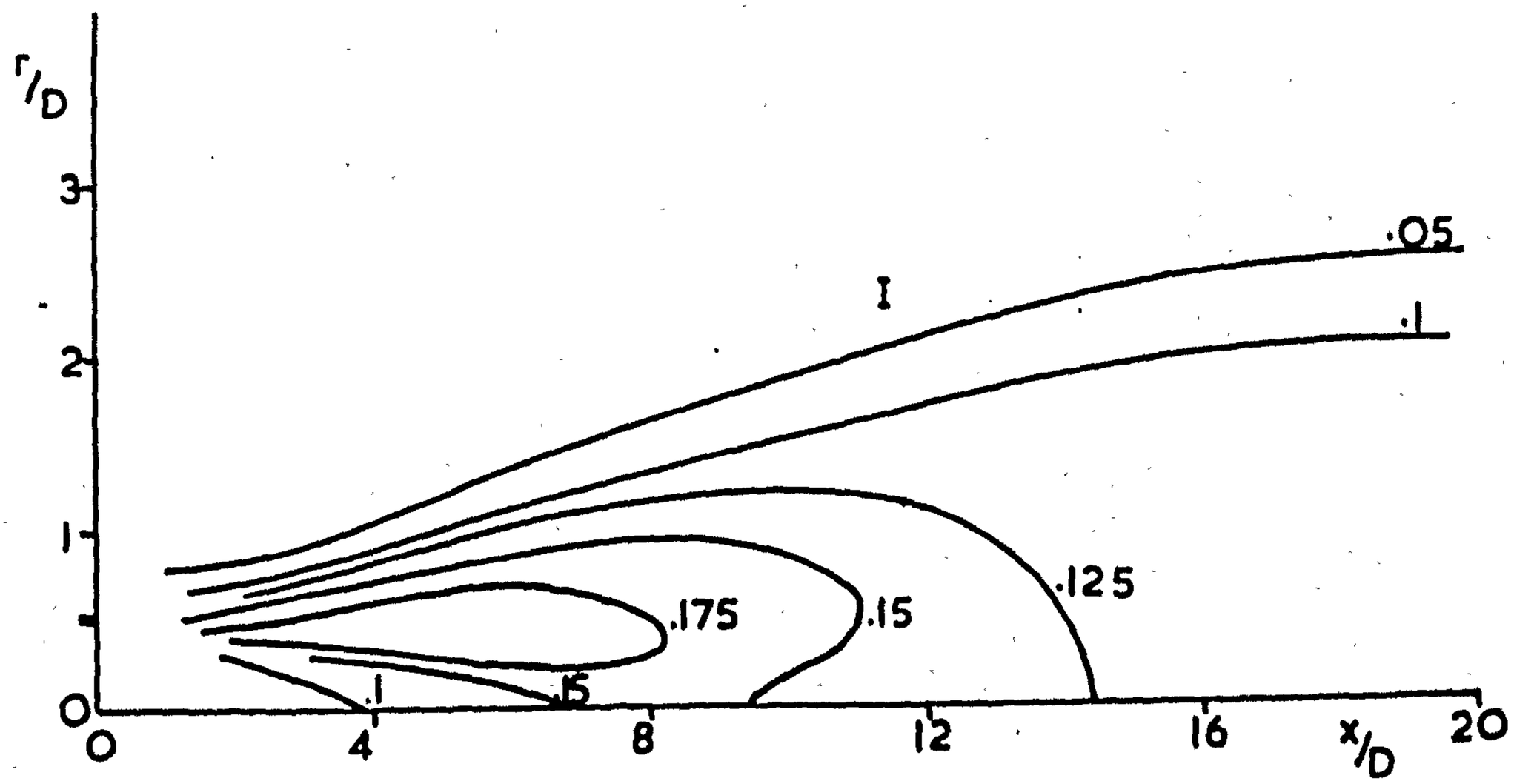

Fig. A6.1 Spatial $\bar{u}/\bar{u}_o$ & I distribution for a single non-swirling jet

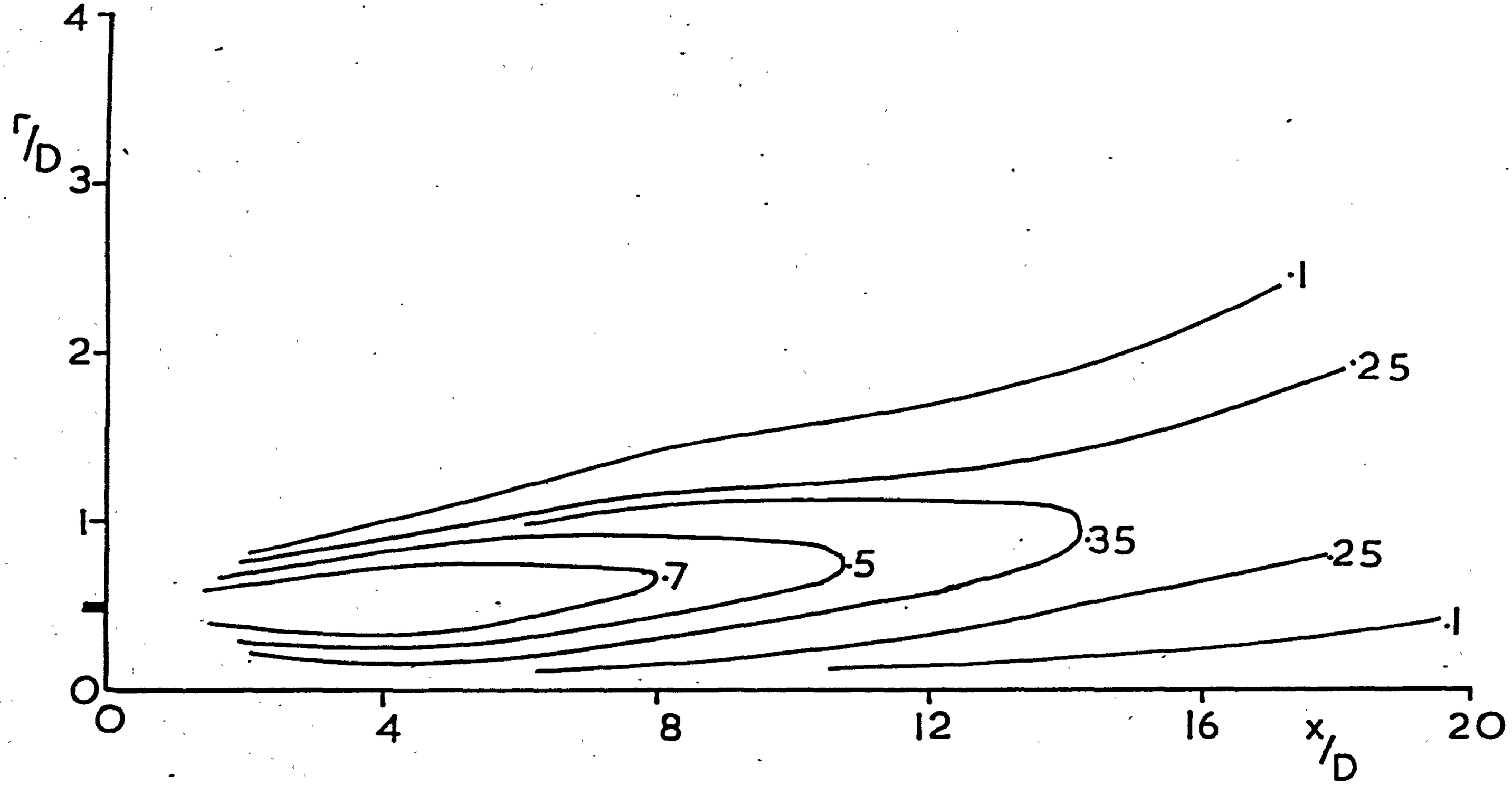

Fig. A6.2 Spatial $100\,\frac{\overline{u'v'}}{\bar{u}_o^2}$ distribution for a single non-swirling jet

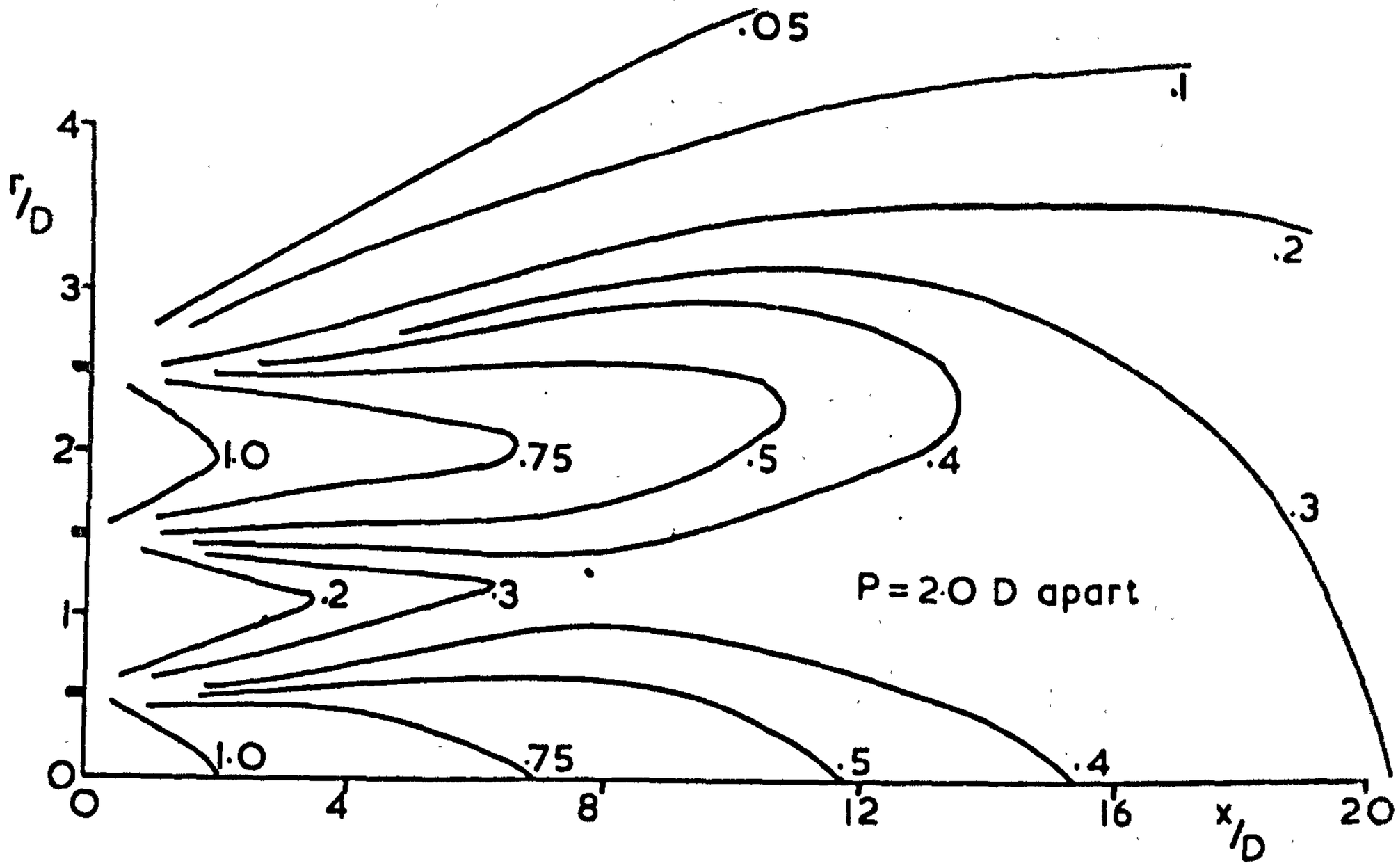

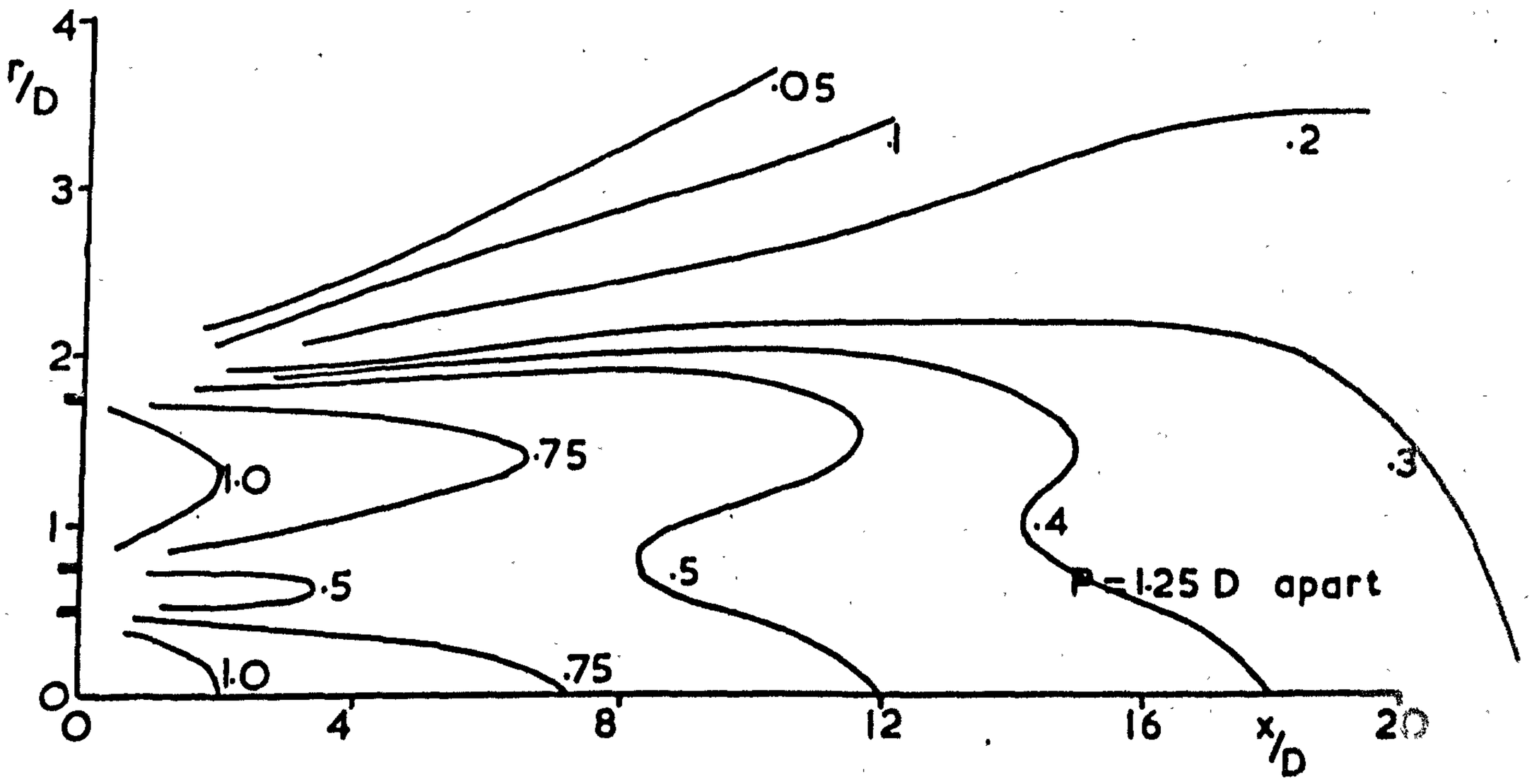

Fig. A6.3 Spatial $\bar{u}/\bar{u}_o$ distribution for 3 non-swirling jets 1.25 & 2·0 Dia. apart

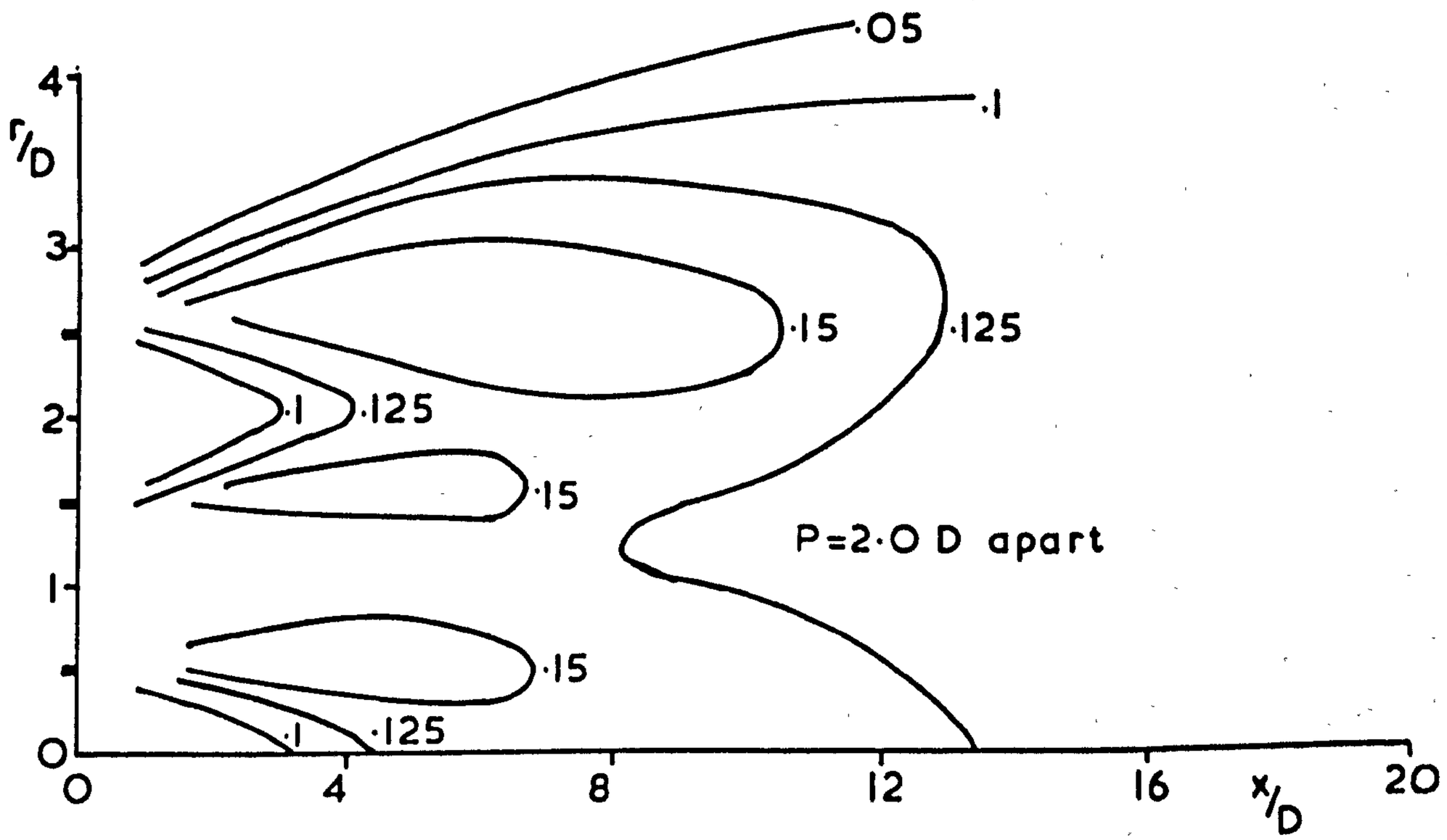

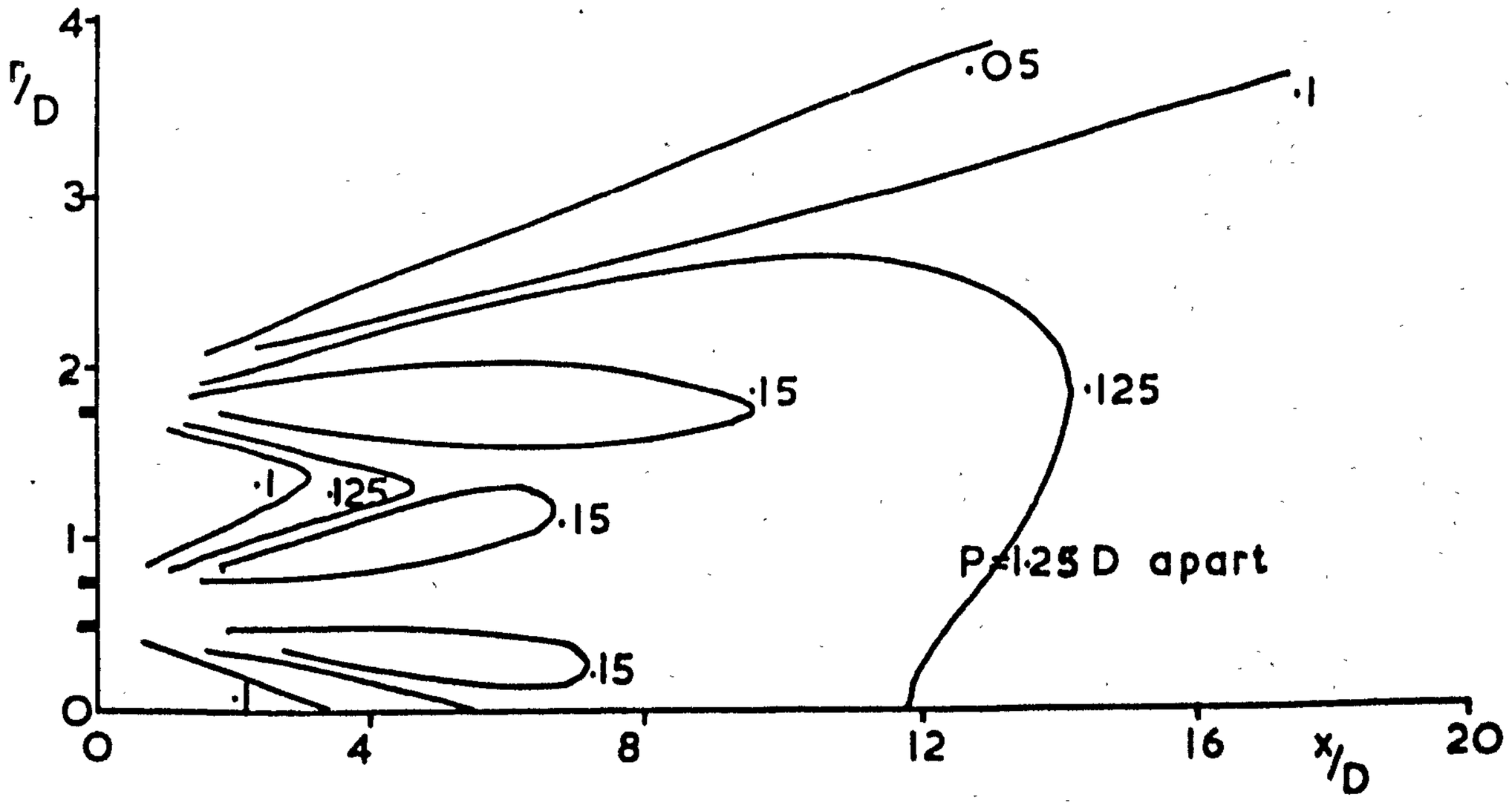

Fig. A6.4 Spatial I distribution for 3 non-swirling jets 1.25 & 2·0 Dia. apart

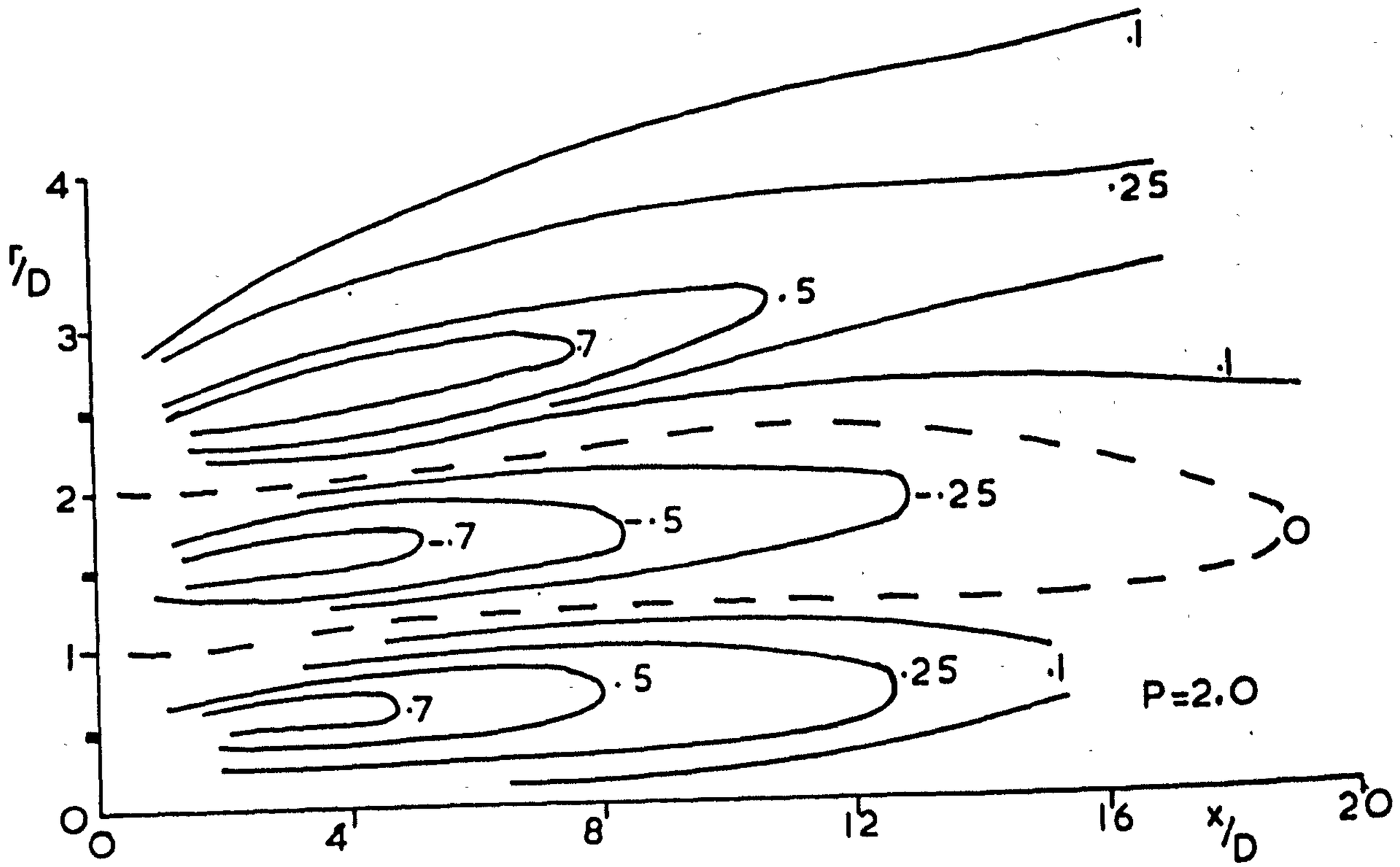

Fig. A6.5 Spatial $100\overline{u'v'}/U_0^2$ distribution for 3 non-swirling jets

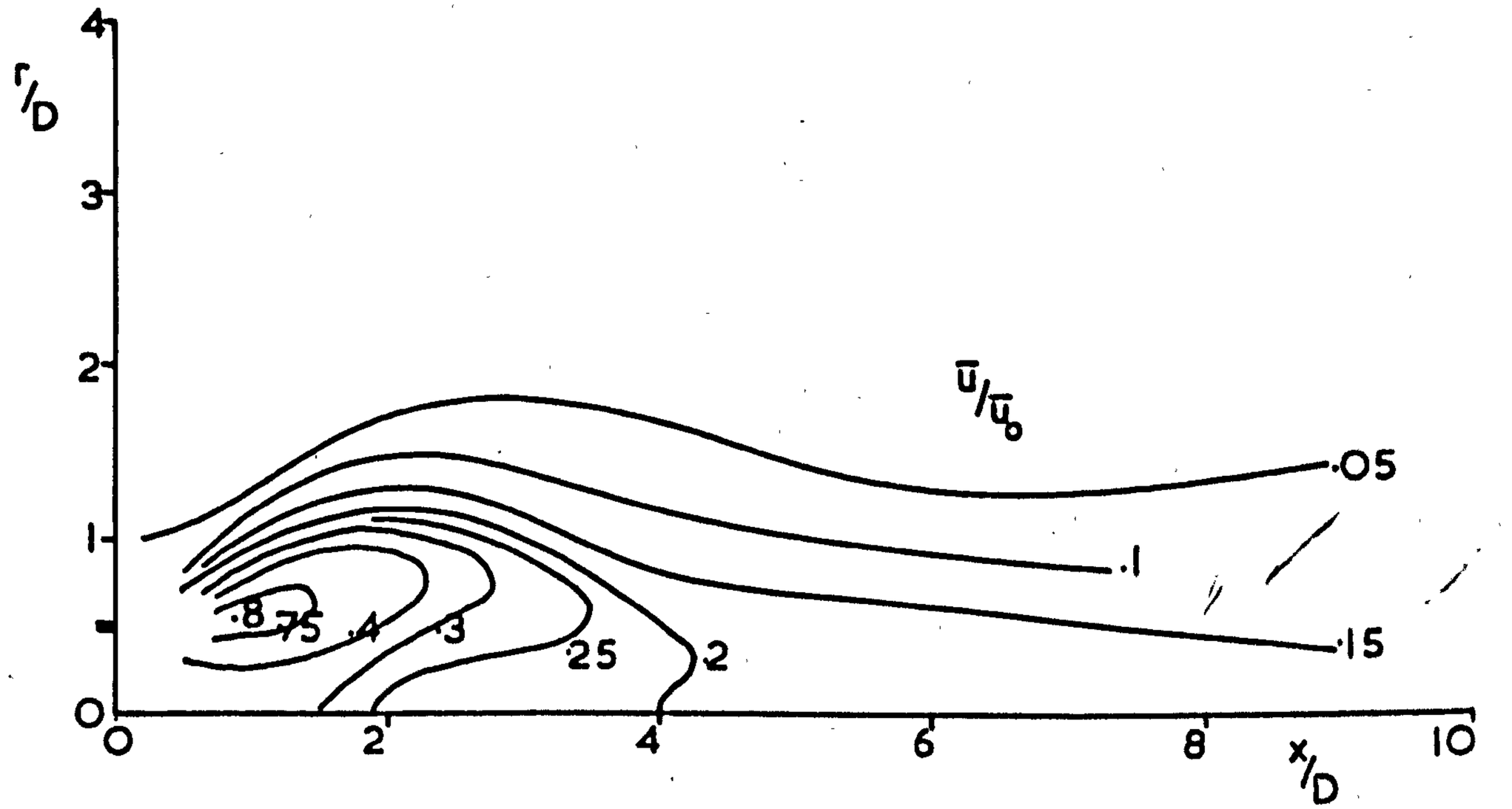

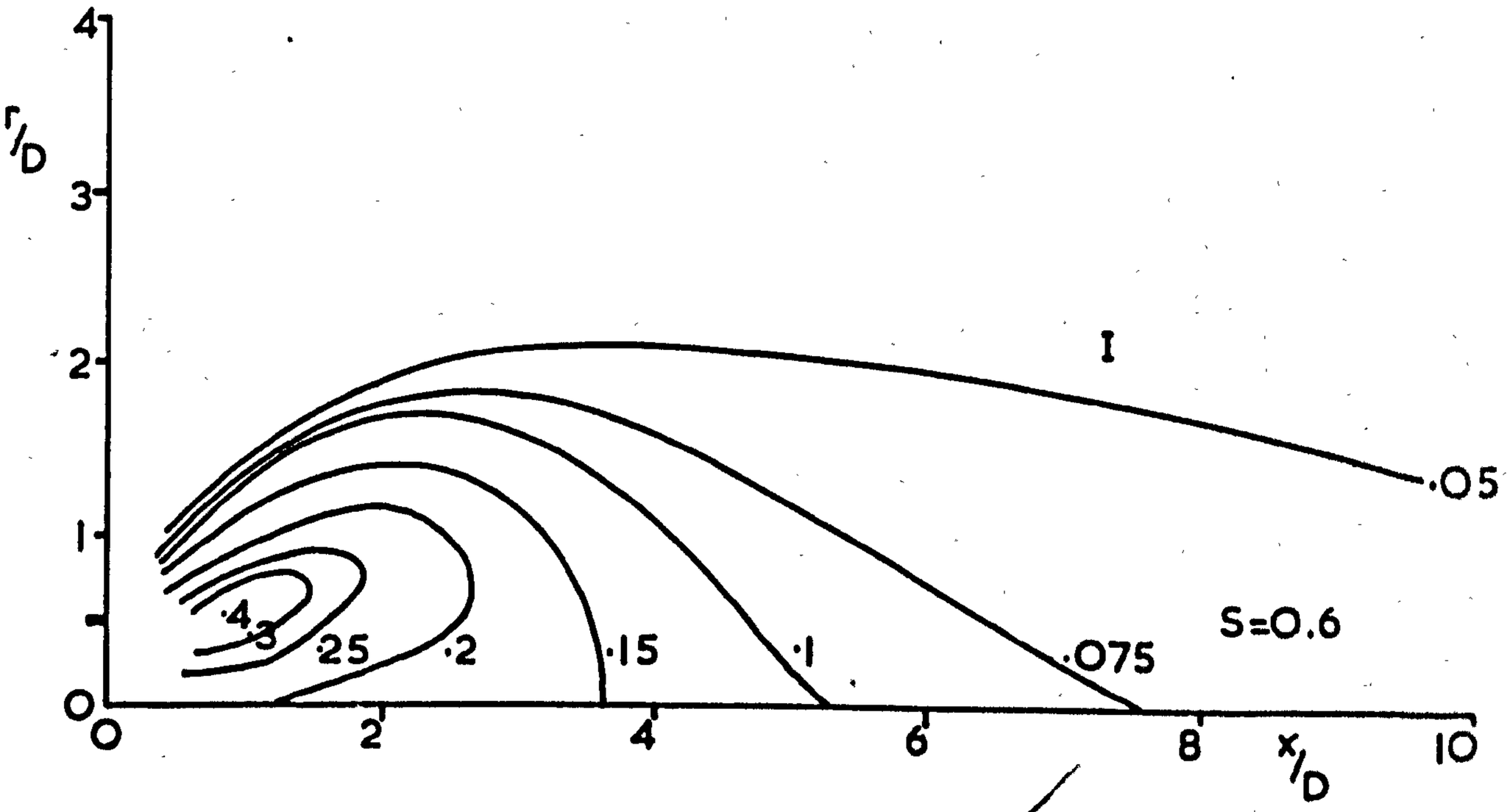

FIG. A6.6 Spatial $\bar{u}/\bar{u}_o$ & I distribution for a single swirling jet

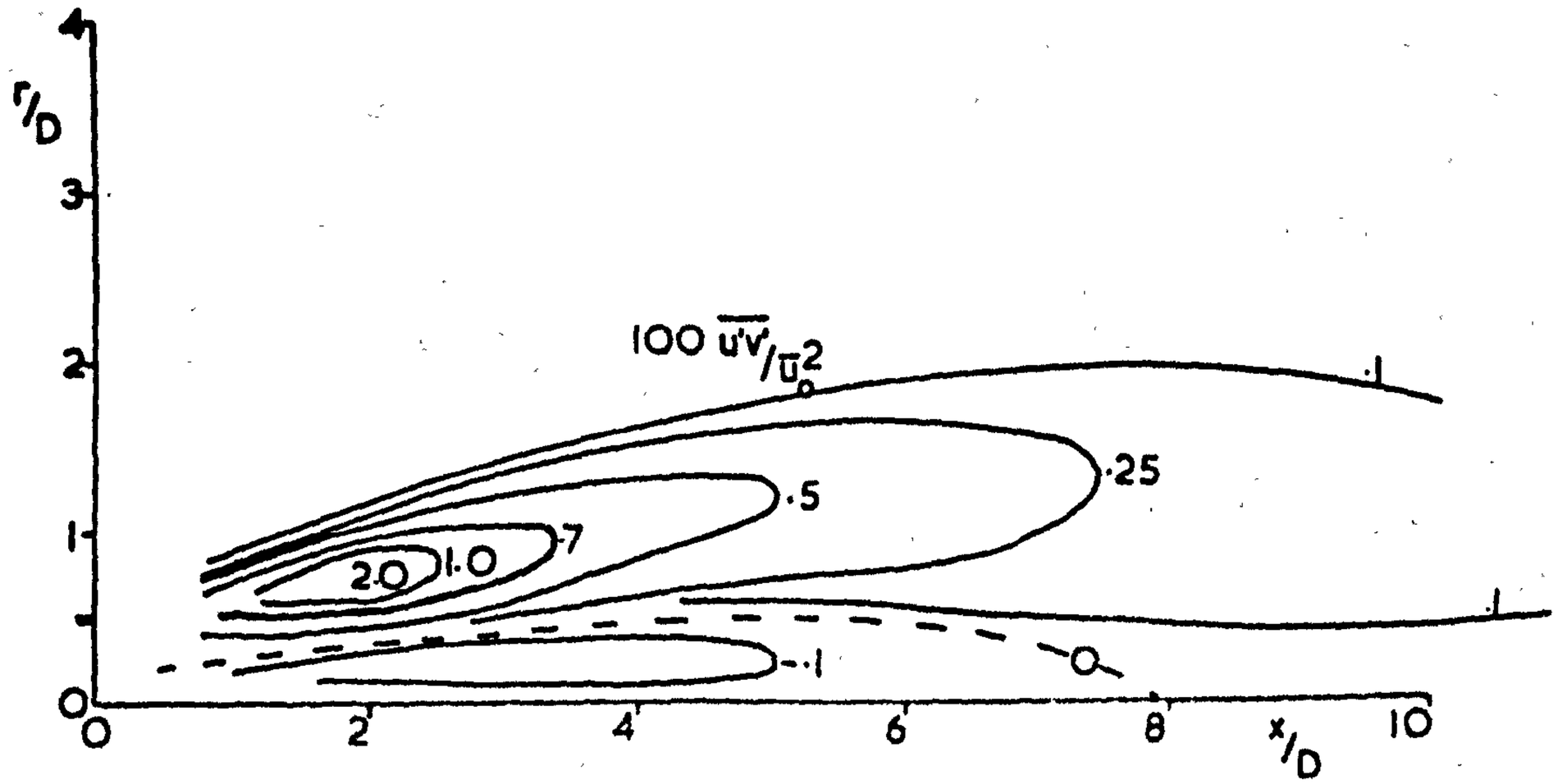

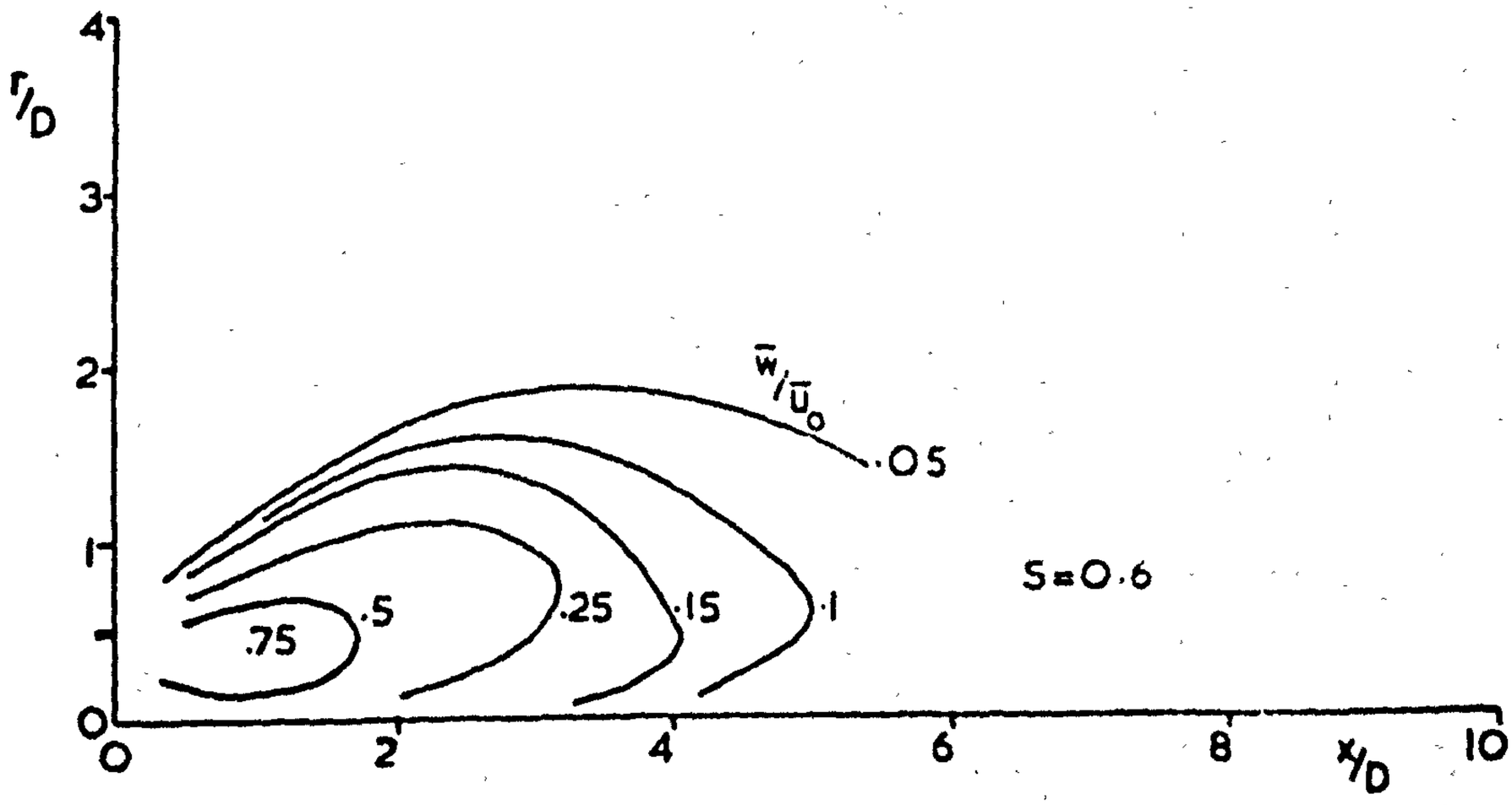

Fig. A6.7 Spatial $100\overline{u'v'}/\bar{u}_o^2$ & $\bar{w}/\bar{u}_o$ distribution for a single swirling jet

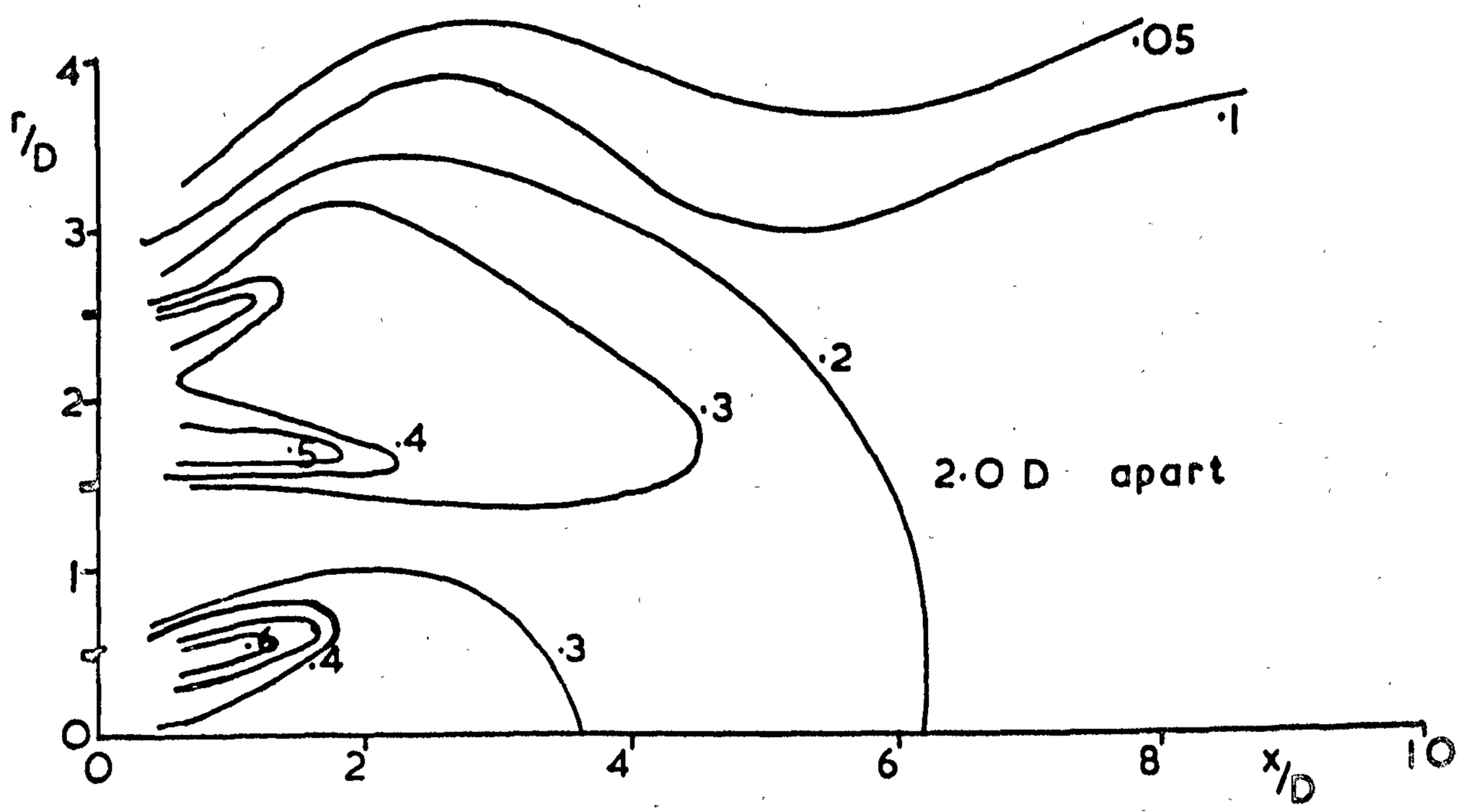

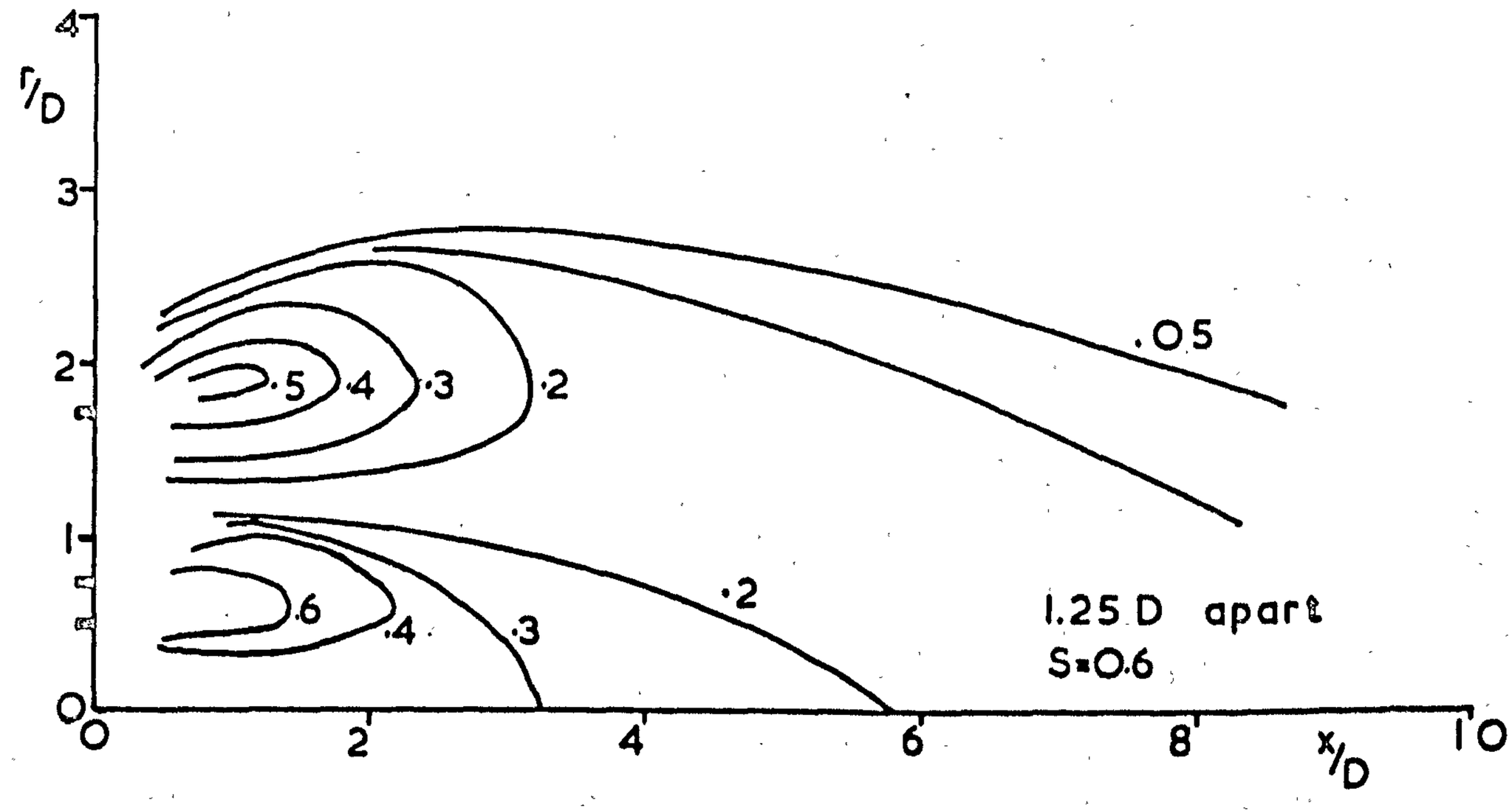

Fig.A6.8 Spatial $\bar{u}/\bar{u}_o$ distribution for 3 swirling jets 'out of mesh'

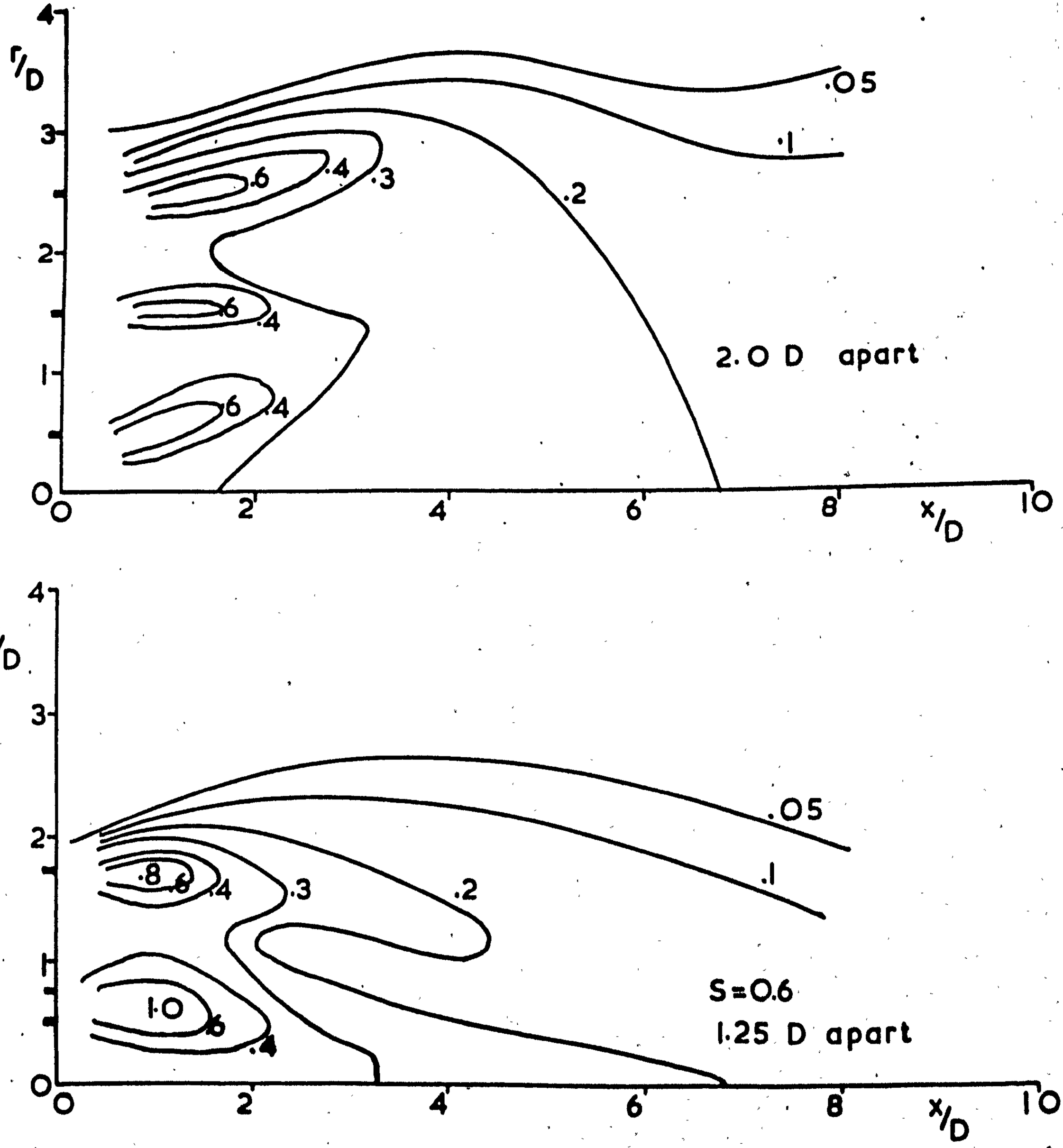

Fig. A6.9 Spatial $\bar{u}/\bar{u}_o$ distribution for 3 swirling jets 'in mesh'

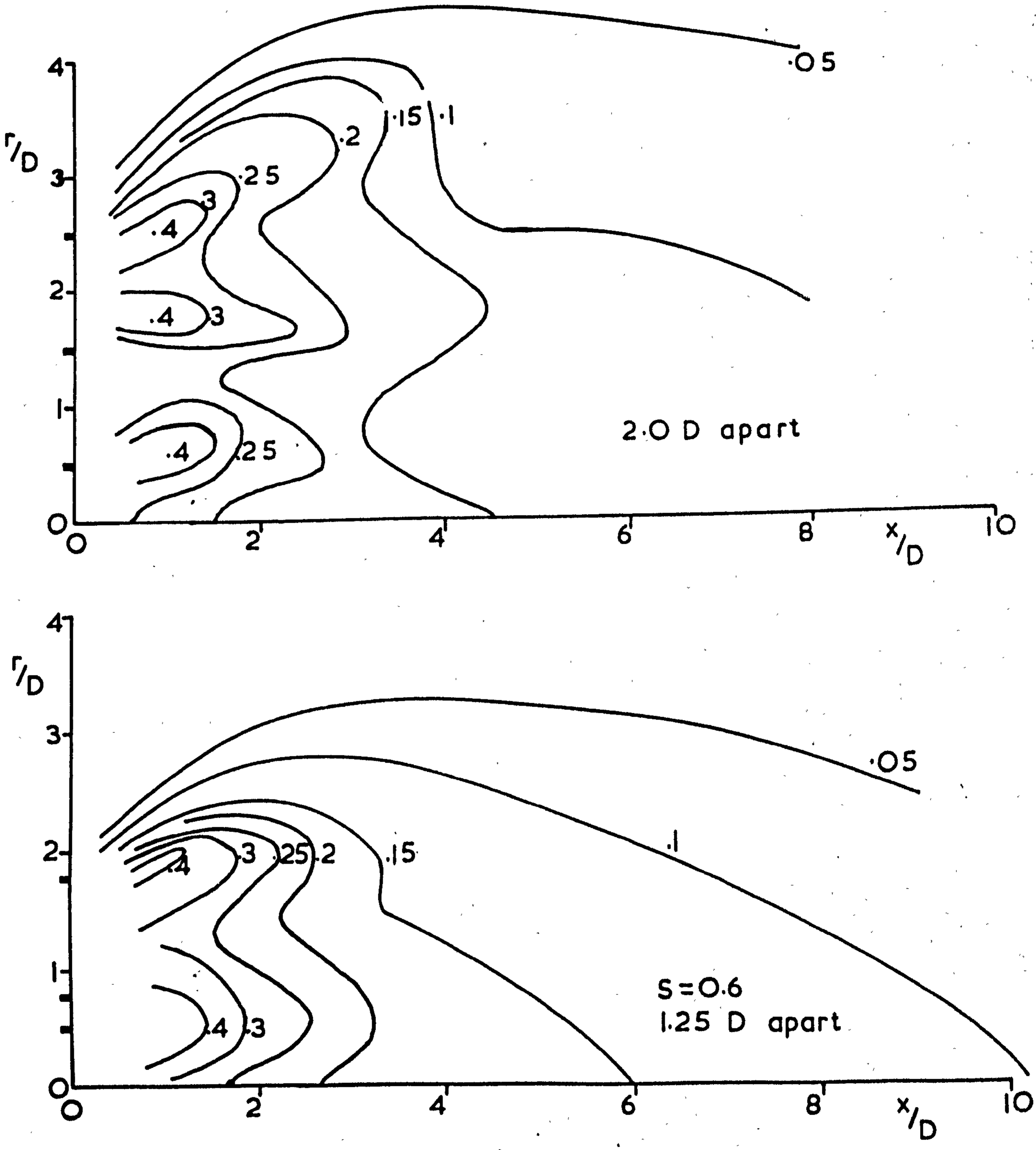

Fig.A6.10 Spatial I distribution for 3 swirling jets 'out of mesh'

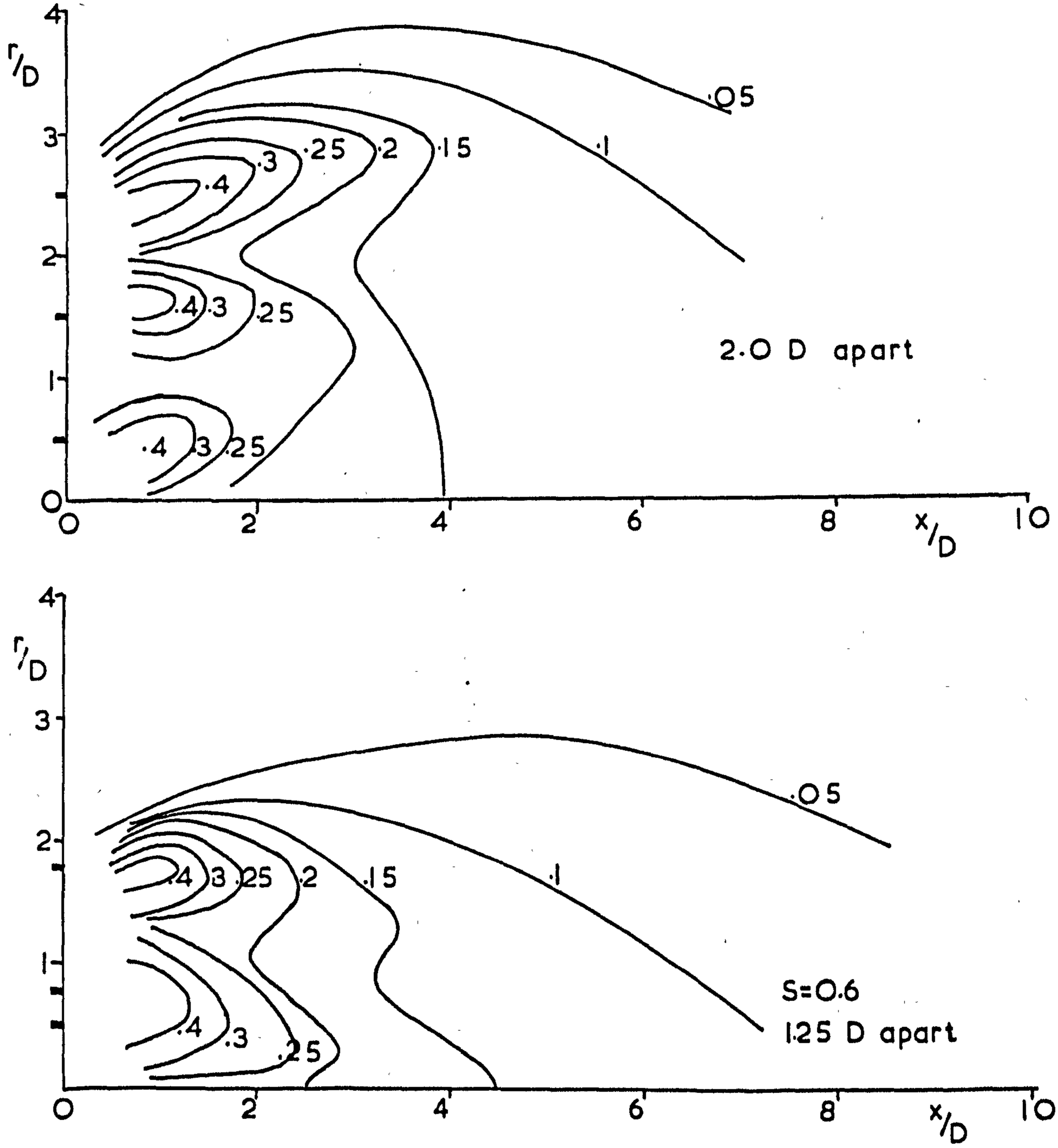

Fig.A6.11 Spatial I distribution for 3 swirling jets 'in mesh'

APPENDIX 7

Some Notes On The Design Of Multiple Jet Systems

The results contained within the body of this thesis should aid the designer, both from a theoretical and practical point of view, to design mixing or burning systems which contain multiple jet fluid streams. The designer has to consider what system will fulfill all of his requirements at the least cost. Many factors will affect the eventual cost and design and here are some notes intended to aid the designer to choose the correct system.

The designer must consider firstly the time, and consequently the mixing rate, which it is required to react the two, fluids and secondly the volume which will be required. The volume will be controlled by the number, type and configuration of the jets, and the length of the system or chamber. The mixing rate and length of the system should determine whether rotation of the individual fluid streams is necessary in order to obtain relatively short jet lengths. Cost of manufacture, pressure drop, and available area will generally restrict the number of jets that the total mass flowrate may be split up into, and it is upto the designer to space the jets such that optimum use

of available area is ensured.

The most important factors may be summarised :

1) Decide whether it is necessary or desirable to have rotating jets. This will generally be dictated by the size of the system in relation to the total mass flowrate or mixing, or residence time restrictions. If it is decided to rotate each jet then ensure that the jets each rotate in the same sense (ie."out of mesh") this will ensure greater uniformity and mixing rates.

2) Divide the total mass flowrate up into just as many jets as it is economical to do to achieve the desired mixing. This will usually be dictated by the cost of manufacture of the jets, pressure drop, considerations, and close packing restrictions.

3) Distribute the jets as unformally as possible throughout the system to ensure the maximum utilisation of space and separation of the jets. This may be dictated by impingement considerations and overall design or positioning of the system